Photoswitching Metal-Organic Frameworks: Towards Light Controlled Adsorptivity in Porous Materials

by

© **Brandon J. Furlong**

A thesis submitted to the School of Graduate Studies in partial fulfillment of the requirements for the degree of Master of Science.

Department of Chemistry

Memorial University

January 2023

St. John's, Newfoundland and Labrador, Canada

Abstract

Metal Organic Frameworks (MOFs) are porous material composed of metal nodes bridged by organic linkers. The resultant structures form porous 3-dimensional frameworks; the chemistry and applications of these materials is incredibly diverse. Through judicious choice of the metal coordination chemistry coupled with the imagination-limited organic linker design, MOFs have been tailored for numerous applications including gas storage, gas separations, and catalysis. While these properties are easily tuned, they are considered static (i.e., the properties do not change once the MOF is formed). For this reason, research into the design of stimuli-responsive MOFs has gained notoriety in the MOF literature. This is owed to changeable adsorptivity in response to introduced stimuli such as heat, pressure, and light.

This thesis discusses strategies to design PSZ-1, a new class of light-responsive MOFs that incorporates dithienylethene photoswitches into the pore lining. This new material behaves as a light controlled chemical filter and undergoes photoisomerization for a minimum of 5 times without degradation to the materials structure. Further work studied photophysical properties of a small family of structurally analogous DTEs, which are studied in order to understand the influence of 2-imidazoyl substituents on the thermal stability of these molecules. Finally, we report the synthesis of PSU-68, which has a controlled degrees of photoswitch incorporation and investigate the effect of linker loading on separation properties in the MOF.

To Everyone Who Supported Me
When I Felt Like Giving Up,
Thank You.

Acknowledgements

First and foremost, thank you to my supervisor Dr. Michael J. Katz, you have gone above, and far beyond the requirements of any PI or mentor. While there are many supervisors, you will always be "the boss."

Second, I want to thank my committee members Dr. Chris Kozak, and Dr. Chris Rowley for the fantastic advice, grant writing help, and directions I could take my research in. As well, I offer many thanks to Dr. Celine Schneider, Dr. Stefana Egli, Dr. Jian-Bin Lin and Nick Ryan for training and access to C-CART/CREAIT instrumentation, and helping with advanced characterization techniques.

Thirdly, I want to acknowledge my group mates who helped me through the years. You are all brilliant in your own respects and I will cherish our time working together.

Finally, I wish to acknowledge MUN School of Graduate Studies, NSERC for a PGS-D, and Dr. Liqin Chen Scholarship Fund for making my graduate studies financially possible.

Table of contents

List of tables

List of figures

Chapter 1

Introduction

1.1 The Sponge Analogy

Figure 1.1: Common washing sponges. Reproduced with permission under Public Domain. (www.publicdomain.net)

A porous material is a material that has a large internal space within its structure. The structure and periodicity of these pores are intrinsic to the material itself. There are many examples of porous materials that have found use in everyday life. Some basic examples include porous carbons that separate contaminants from drinking water, as well as concrete used in infrastructural development.

However, in the context of this work, a simple dish sponge is a great analogy to begin mentally envisioning porous materials. A dish sponge is perhaps one of the most common items that every person has encountered (or will encounter) and is a general example of a porous material, which is the theme of this thesis.

The porosity, elasticity, ductility, and flexibility of a dish sponge is one of the many practical reasons that dish sponges (Figure 1.1) have earned commonplace usage. A dry sponge that is soaked in water will readily retain water that the material is exposed to. Using a sponge as a conduit for low energy water retention allows us to transport, use, and separate water from multi-component mixtures easily (i.e., cleaning up a spill).

Inversely, when the water is no longer needed inside of the sponge, the activated sponge is regenerated by flushing the pores with fresh water, and/or by application of a low energy stimulus that promotes separation of the retained water from a sponge (i.e., wringing out of the sponge).

This simple and practical analogy illustrates the utility of free space inside of a material. With the utility of a sponge conveyed, it is easy to imagine how researchers may begin asking questions about systematically improving the sponge, or using it for alternative applications. For example, can the pores of this dish sponge be functionalized to have antibacterial properties, or tuned to specifically adsorb oil over water? If this analogy makes you wonder about what you can do with a sponge, then we are ready to embark on the work in this thesis.

The heart of this research project is to design porous materials that have controllable adsorption and separation properties that can be changed as a function of an external stimuli. The previous sponge analogy is an example of a mechanically responsive

porous material; the applied pressure of the wringing/squeezing of the material is the trigger that signals the release of water. The focus of this thesis is to design and understand how porous materials can be used to control uptake, retention, and release of internal guest molecules for more efficient chemical separations.

1.1.1 Models of Adsorption For Gas/Surface Interface in Porous Materials

Chemical separations using porous materials for purification of gas mixtures operate based on reversible non-covalent intermolecular forces between the gases and the active surface that the gas interacts with. This interaction is better known as adsorption, but can also be referred to as physisorption or non-covalent bonding interactions.[1] If an active and unoccupied surface is exposed to adsorbate (i.e., a gas) then equilibrium establishes, wherein part of the gas is adsorbed onto active surface sites.[2]

The Langmuir adsorption model[1] was originally derived to model adsorption of adsorbate on active surfaces in discrete monolayer formations (i.e., one layer at a time, independent of the other layer). This model operates under five assumptions:

1. The active surface is homogeneous (i.e., active sites are well dispersed periodically over the surface).

2. The adsorbate becomes immobile when interacting with the surface.

3. All active sites are equal and the energy of adsorption is the same for all active sites.

4. Each active site holds one molecule of gas (assuming monolayer coverage exclusively).

5. The behaviour of gas adsorbates is ideal (i.e., no intermolecular forces between gas molecules).

Using a kinetically-derived approach with these assumptions, Langmuir initially defined the rate of adsorption (r_{ad}) as being equal to the partial pressure of the adsorbing gas (p_{ad}) multiplied by the the number of available active surface sites, defined as [S] (active sites/m^2) as seen in Equation 1.1.

$$r_{ad} = k_{ad} \cdot p_{ad}[S] \tag{1.1}$$

The rate of desorption (r_d) from the surface is defined as being equal to the rate constant of desorption (k_d) and the area of adsorbed gas molecules ($[A_{ad}]$) in units of molecules/m^2 as seen in Equation 1.2.

$$r_d = k_d \cdot [A_{ad}] \tag{1.2}$$

At equilibrium, where r_{ad} and r_d are equal, the following relationship can be established by rearranging for $\frac{k_{ad}}{k_d}$, which for simplification is expressed as K_{eq}^A in Equation 1.3:

$$\frac{A_{ad}}{p_{ad}[S]} = \frac{k_{ad}}{k_d} = K_{eq}^A \tag{1.3}$$

The total concentration of all surface sites ($[S_0]$) is defined as being equal to the sum of all unoccupied sites ([S]) and occupied surface sites [A_{ad}] (Equation 1.4). By expressing [S] (Equation 1.5) as rearranged Equation 1.3, the equation for the

Langmuir adsorption isotherm (Equation 1.6) is obtained as such:

$$[S_0] = [S] + [A_{ad}] \tag{1.4}$$

$$[S_0] = \frac{[A_{ad}]}{K_{eq}^A p_A} + [A_{ad}] = \frac{1 + K_{eq}^A p_{ad}}{K_{eq}^A p_{ad}}[A_{ad}] \tag{1.5}$$

$$\theta_{ad} = \frac{[A_{ad}]}{[S_0]} = \frac{K_{eq}^A p_{ad}}{1 + K_{eq}^A p_{ad}} \tag{1.6}$$

The obtained equation (Equation 1.6) models the fractional adsorption of gases (θ_{ad}) to an active surface to form complete monolayers with an unoccupied surface. To model the intermolecular forces exhibited by the adsorbate with the surface and the next adjacent monolayer, an expansion of the Langmuir isotherm model known as the BET (Brunauer-Emmett-Teller) equation is used. A major difference between BET and Langmuir is that BET-modelled adsorption accounts for new monolayer formations before the previous monolayer is completed; Langmuir adsorption does not account for this since it assumes a new layer of adsorbate begins only after completion of the previous monolayer.

The usable form of the equation that models multi-layer gas adsorption is given in Equation 1.7:

$$\frac{1}{v} \cdot \frac{x}{[1-x]} = \frac{c-1}{v_m c} x + \frac{1}{v_m c} \tag{1.7}$$

$$\text{where } x = \frac{p}{p_0} \tag{1.8}$$

$$\frac{1}{v} \cdot \frac{1}{[1 - \frac{p_0}{p}]} = \frac{c-1}{v_m c}(\frac{p}{p_0}) + \frac{1}{v_m c} \tag{1.9}$$

Where v is the adsorbed gas quantity, x is a variable representing pressure of the gas (p) divided by saturation pressure (p_0), v_m is the volume occupied by a complete

monolayer, with c being the BET constant, which is a measure of the strength of adsorbant/monolayer interactions, and cannot be a negative number.

Plotting the left half of Equation 1.9 as a function of $(\frac{p}{p_0})$ yields a straight line. The equation of the line from plotting Equation 1.9 provides the valuable constants v_m, and c :

$$v_m = \frac{1}{\text{Slope} + \text{Y-intercept}} \tag{1.10}$$

$$S_{total} = \frac{v_m \cdot N_a \cdot S}{V} \tag{1.11}$$

$$S_{BET} = \frac{S_{total}}{m_{sample}} \tag{1.12}$$

Where N_a is Avogadro constant (6.223×10^{-23} mol^{-1}), S_{total} is the total surface area (m^2) and (S_{BET}) is the specific surface area of the material (m^2/g

BET theory differs from Langmuir theory by attempting to model adsorption and account for intermolecular interactions. However, the consistency of reporting surface areas with BET has its own limitations. The challenge with the above description is that it is not clear which part of the isotherm represents the region which can be modelled with BET Theory. Roquerol *et al.* have suggested the following criterion:

1. Regression criteria:
   (a) The linear range one intends to fit should be $\geq$ 10 points
   (b) The R^2 should be $\geq$ 0.995
2. Validity criteria:
   (a) Over the entire fitting range $N_a(1\text{-}\frac{P}{P_0})$ must increase monotonically with $\frac{P}{P_0}$

(b) The value of c obtained by linear regression must be positive (negative values correspond to imaginary energy)

3. Self-consistency criteria

   (a) The monolayer loading (N_m), when reported must correspond to a pressure that lies in the linear region established in the regression criteria.

   (b) The relative pressure corresponding to the monolayer loading as obtained from BET theory, $\frac{P}{P_0}$ (N_m BET), must be within 20 % of the expected/measured pressure obtained in criterion 3.

Although both models of adsorption have their respective drawbacks,[1,3] the use of these models for physisorptive interactions has been of great use in assessing the porosity of solid state materials and evaluating their potential performance in adsorption-based separations and an understanding of these models is a great tool for better understanding the scope of this work.

1.2 Chemical Separations Using Porous Materials

1.2.1 Energy Efficient Chemical Separations and Their Pertinence to Global Supply Chains

In 2019 at peak world energy consumption pre-pandemic, 14 billion toe (tonne of oil equivalence) was used, where 1 toe equals the amount of energy produced by burning one tonne of oil (11,630 kWh).[4] This is roughly equivalent to the amount of energy consumed by the average North American home (∼11,000 kWh as measured in 2017).[4] This energy expenditure, roughly equal to 12.5 billion homes was consumed worldwide in 2019. This steady growth in consumption and demand has raised questions by many

concerned scientists and activists about the environmental impact and sustainability of energy consumption.[5]

It is estimated that on average 15-20 % of our annual energy expenditures is dedicated to industrial processes for purifying chemicals. The primary technique by which gases are purified is cryogenic distillation, which is the separation of gas mixtures by the compression, and cooling of said mixture to liquefaction. The liquified fractions are then separated from the parent mixture by distillation of the liquified gas in the respective boiling point ranges of each gas. For example, the distillation of air, which is approximately 3:1 N_2/O_2 (with other trace gases comprising the remaining percentile) affords high purity N_2 and O_2 gas when distilled at 77 K and 90 K respectively. To summarize, for the production of high purity gases, cryogenic distillation is the industry standard; however, cryogenic distillation as a technique is very energy intensive, and requires cryogenic temperatures and strong thermal insulation for efficient thermal regulation throughout the complex assembly of valves and separation columns.

These energetically demanding processes in such a pertinent industry coupled with increased demand can lead to interruptions in vital supply chains.[6] When this happens, the ability to effectively perform routine, yet important tasks is greatly hindered. Referring back to chemical purifications, consider simple (yet significant) gases such as oxygen, nitrogen, and carbon dioxide. Oxygen is critical for cardio-pulmonary patient care, life support and medical procedures.[7] Meanwhile, nitrogen gas helps operate pneumatically powered medical equipment and is a vital precursor for cryogenics in diagnostic medical equipment.[8] Thirdly, carbon dioxide is another useful cryogen (as dry ice) and is also used in laser therapies for soft tissue procedures.[9] While these gases are structurally very simple their significance cannot be downplayed as they are

critical in vital industries such as healthcare.

1.2.2 Pressure/Temperature Swing Adsorption

As conveyed in the previous sections, adsorption is a reversible equilibrium process. By lowering pressure, or increasing the temperature in the system, adsorbed gas on a surface is expelled in response to the change in established equilibrium conditions; this is desorption (i.e., regeneration of the sorbent), the second step in purifying a gas stream.[2]

From a chemical/process engineering point of view, controlling surface adsorption in porous materials through pressure or temperature changes can be used to separate gases with different physical/chemical properties.[10] Figure 1.2 illustrates the general concept of swing adsorption, which is the process wherein a mixture of gas is separated by the selective adsorption of one adsorbate with the surface of a porous material.

A temperature/pressure swing adsorption system works as follows. Initially, the gas mixture of interest is flowed over the surface of the material. Assuming a two-component gas mixture, one of the gases is adsorbed more strongly than the other. Once the sorbent is saturated, which is indicated by the down-stream gas being similar in concentration to the upstream gas, then it is time to regenerate the material. By reducing the pressure in the chamber or increasing the temperature of the chamber, the adsorbed gas is desorbed. This produces exhaust streams of the adsorbed component, which is more pure relative to the input gas. Once the adsorbent is regenerated, it can be reused in another pressure/temperature swing cycle.

For example, in the case of a binary mixture of CO_2/N_2 gas, CO_2 adsorbs to an active surface at ambient temperatures better than N_2 gas. Thus, high purity CO_2 streams

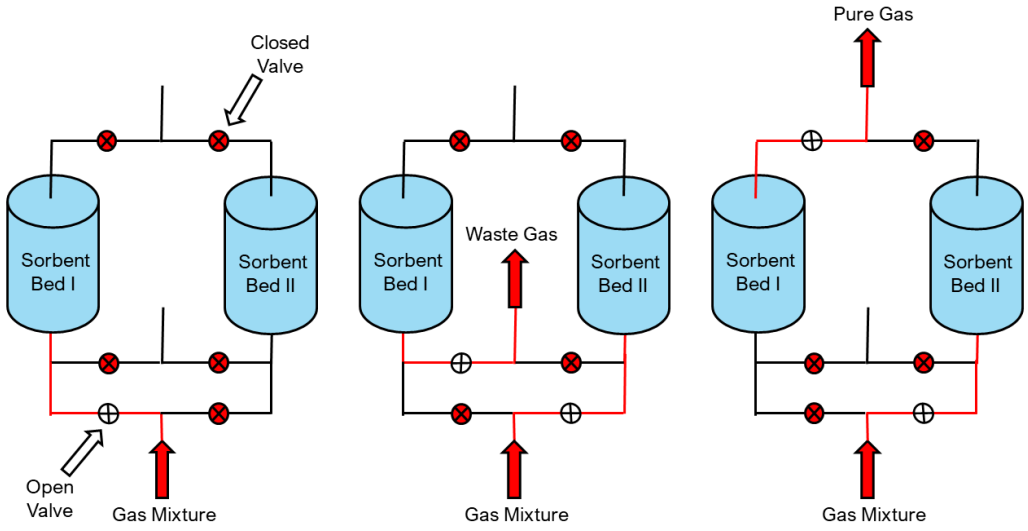

Figure 1.2: Simplified schematic of a dual sorbent PSA set up. One bed is pressurized under high pressures (5-10 bar) of a gas mixture, and when saturated with gas, it is sealed off from gas inlet. The second bed is then pressurized while the first bed desorbs purified gas. To avoid downtime, two beds enable one to always adsorb while the second is being regenerated.

can be obtained from impure mixtures of CO_2/N_2 streams when the separation is performed at room temperature. When the pressure is decreased, or temperature is increased the surface adsorbate, and active sites on the adsorbent are regenerated. Using two adsorber beds, one bed can be regenerated while the second bed adsorbs gases, which ensures little/no downtime during gas purification.

Given that adsorption is proportional to the amount of surface that adsorbates interact with (Equation 1.1), it is critical to maximize the amount of accessible surface sites for adsorptive applications. However, simply discussing the amount of surface is not sufficient. To be viable for applications such as emission control in vehicle and industrial settings, the mass of material being used is also important. With that in mind, we often report the surface area of a material as a gravimetric quantity in m^2/g, which is the amount of accessible active surface sites in m^2 in 1 g of material. This unit

emphasizes the importance of having many accessible surface sites to interact with, but also stresses the importance of keeping the weight of the material at a minimum. When the surface area is contextualized relative to the material being used as an adsorbent in m^2/g, this is known as the specific surface area (SSA).

For adsorption applications, the higher the SSA, the more gas a material can hold during storage and separation processes. As such, finding methods to produce high SSA materials is important. For example, an olympic hockey rink has an area of 61 m $\times$ 30 m ($\sim$ 1830 m^2). What if a gram of material could have the same surface area? To date, porous materials have been created with this level of SSA and greater. Materials such as porous carbon,[11] zeolites,[12] and metal-organic frameworks (MOFs)[13] are all porous materials that have potential to make industrial chemical separations more efficient.

1.3 Introduction to Metal-Organic Frameworks

1.3.1 Components of a MOF

Metal-Organic Frameworks (MOFs) are a hybrid class of porous materials composed of metal nodes and organic linkers.[14–16] Combining these components at elevated temperature (sometimes with other reagents as additives) creates a 3-D framework with empty space inside its large cage-like structure (Figure 1.3). Nodes can be metal ions from all over the periodic table; these include, but are not limited to, Al^{3+},[17] Mg^{2+},[18,19] $Cu^{1+/2+}$,[20–22] and Cr^{3+}.[23,24] To emphasize the diversity of metal centers and the versatility of MOF chemistry, porous structures have been previously reported that use non-transition metal centers such as Na^+, K^+, Ca^{2+} ions. Another

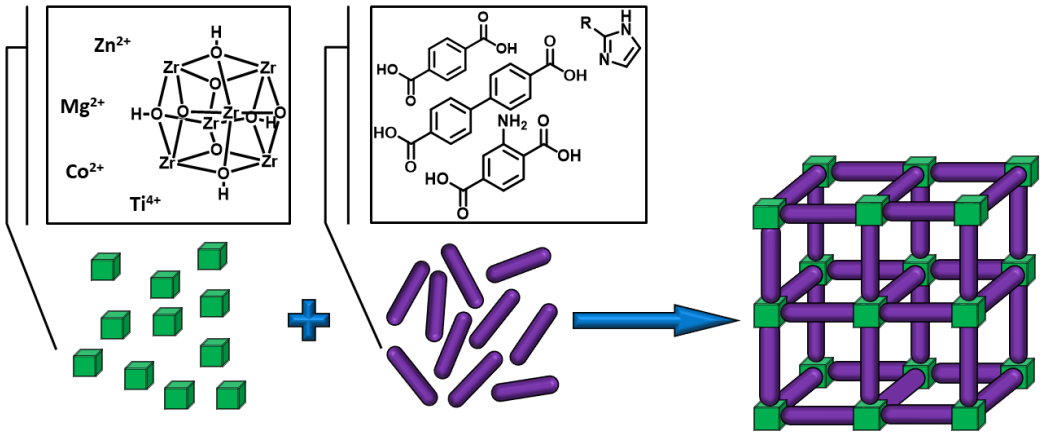

Figure 1.3: Inorganic clusters/metals (cubes) and organic linkers (sticks) combining to form a prototypical MOF (represented as the 3-D porous structure–right).

option is using metal-oxo clusters with predefined geometries such as the dodecavalent $[Zr_6O_4(OH)_4]^{12+}$ (Zr_6 node, Figure 1.3) and the hexavalent $[Zn_4O]^{6+}$ (Figure 1.4) clusters reported by Lillerud,[25] and Yaghi respectively.[26]

Linkers (Figure 1.3) are organic molecules that bridge two or more metal nodes to one another; these linkers contain functional groups such as carboxylate groups or basic nitrogen centers that space the nodes apart in 3-D space.[27] Linkers can have additional functional side groups such as amines,[28] hydroxyl groups,[29] or structurally complex side groups, which introduce new reactivity, or catalytic activity.[30–32] These functional groups decorate the internal pores of the MOF and are responsible for the reactivity and adsorptive changes associated with the pore.[33]

1.3.2 Isoreticular Theory For MOF Synthesis

To take a closer look at the core concepts of MOF chemistry, the iconic MOF-5 (Figure 1.4) is an excellent illustrative example. To synthesize MOF-5, $Zn(NO_3)_2$ and

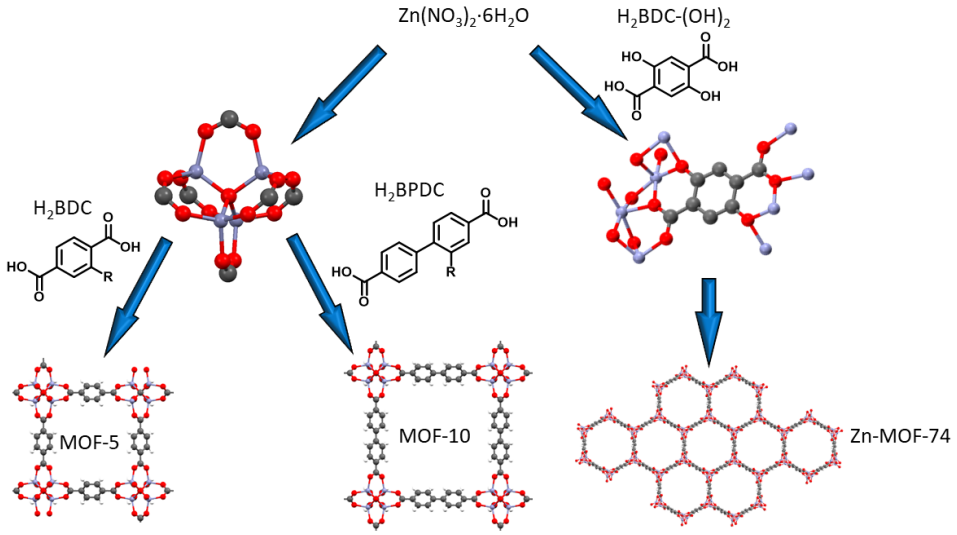

Figure 1.4: (A) Octahedral $[Zn_4O]^{6+}$ nodes generated *in-situ* bridged by 1,4-benzenedicarboxylic acid (H_2BDC) and 4,4'-biphenyldicarboxylic acid (H_2BPDC) to form MOF-5, and MOF-10 respectively. These MOFs are topologically equivalent and are therefore isoreticular with one another. Similar conditions using $H_2BDC-(OH)_2$ (2,5-dihydroxy-1,4-benzenedicarboxylic acid) produces Zn-MOF-74, which contains a 1-D chain of Zn nodes that form large hexagonal honeycomb grids when expanded in 3D space via the carboxylate groups and deprotonated hydroxy group of the linker chelating with the Zn^{2+} cation. (Zn = Grey Spheres, O = Red Spheres, C = Black Spheres, White Spheres = Hydrogens).

1,4-benzenedicarboxylic acid (H_2BDC) are heated in *N,N*-dimethylformamide (DMF) at 120 °C in a sealed vial.[26] MOF-5 contains octahedrally coordinating $[Zn_4O]^{6+}$ nodes (Figure 1.4), which are generated *in-situ*, and react with linear BDC linkers. This means that if the node connects to a linker, then the relative orientation of the linkers coming from the node will generate an octahedral shape.

One of the carboxylate groups of BDC connects to a node, while the other carboxylate group connects to a second node. This propagates 3-dimensionally, thereby generating the cubic topology of MOF-5. MOF-5 has been made with different functional groups on the BDC linker (e.g., amine, alkyl groups, halogens), which results in the same structure but with the pore presenting different groups to any guest

molecules that enter the pore.[34] This has led to MOF-5 being used in applications such as vapor sensing,,[35] heterogeneous catalysis,[36,37] and storage and separations.[38] One of the challenges with introducing larger functional groups into the pore is that the SSA often decreases or there is insufficient space inside the MOF for these larger groups. This leads to a decrease in the efficacy of the MOF for certain applications. Larger variants of the MOF-5 structure are possible by increasing the length of the linker from a single phenyl ring (BDC) to a biphenyl linker (BPDC) that makes MOF-10,[39] or even longer dicarboxylic acids for larger MOF-5 pore shape derivatives.[40] This allows more space in the pore for host-guest interactions to occur.

The concept demonstrated with MOF-5, MOF-10 and their derivatives is an example of isoreticular chemistry,[41,42] where keeping the orientation of the node attachment groups (carboxylates in the case of MOF-5/10) the same allows researchers to change the size and functionality of the pore without changing the shape of the overall 3-D structure. This is just one example of how a node and a linker can combine to form a MOF and how isoreticular chemistry can be used to exploit the pore properties.

The pore aperture size and shape are defined by node and the linker.[43] Different node geometries alter the MOFs pore shape and topology.[44] Ideally, the use of different functional groups to decorate the pore or longer linkers to expand the pores should not interfere with the formation of the respective MOF. However, this is not always the case. For example, if 2,5-dihydroxy-1,4-benzenedicarboxylic acid ($H_2BDC-(OH)_2$) is used as the linker with $Zn(NO_3)_2$ as the node precursor, then the $[Zn_4O]^{6+}$ cluster does not form (Figure 1.4B). Instead, the two carboxylate and the two hydroxyl units are deprotonated, making a tetra-anionic linker. The resultant MOF (Zn-MOF-74) has a hexagonal pore structure.[45] Furthermore, the pores are 1-D channels rather than the 3-D accessible pores of MOF-5. MOFs that are isoreticular with the MOF-74 topology

can be made with different metal nodes,[46] (which has not been reported with MOF-5) and longer linkers, so long as there are ortho-hydroxyl groups present on the terminal rings). The synthesis of Zn-MOF-74 illustrates that isoreticular theory is a powerful tool for predicting the resulting structures of MOFs, but possesses limitations to the scope of its predictions.[47]

1.3.3 Applications of MOFs

MOFs are frequently reported in gas storage/separation procedures,[48] such as pressure swing adsorption.[49] There are various examples of synthetically tailored MOFs performing volumetric uptake and storage of numerous gases.[50–52] For example, researchers in the Long group have developed MOFs for effective storage of H_2 for green fuel storage.[53] Many researchers have also reported MOFs that effectively adsorb and store light hydrocarbon fuels such as methane,[54] acetylene,[55] and propane.[56] Other reports for MOF based adsorption applications include more harmful gases that compose exhausts such as SO_2,[57] NO_x,[58] NH_3,[59] and H_2S.[60] These gases must be sequestered because of their corrosive properties, along with subsequent environmental and occupational hazards.[61]

MOFs not only adsorb gases proficiently, but they have also been shown to have selective adsorption of specific gases in a mixture.[62] For example, many studies have emphasized the potential for MOFs in effective low energy capture, storage, and utilization of anthropogenic CO_2.[46,63–65] Other examples of chemical separations include the work of Gascon *et al.* who report efficient separation of structurally similar propane/propene mixtures.[66] Although the gases separated in this instance only differ by one degree of saturation, their uses are very different, since propane is used as light hydrocarbon fuel, and propene is a useful monomeric precursor to many plastics.[67]

While MOFs have been shown to be great at storing, and separating gases, there is a drawback that is often overlooked. The opposite of adsorption is desorption, and to desorb a gas molecule that is strongly adsorbed to a MOF can be energetically intensive when we wish to remove guest gas molecules.[68] This challenge is often met with a balanced approach to adsorption. In this approach, the enthalpy of the adsorption process must be kept high enough to favour storage/separation, but not so high as to prevent desorption.[69] Recently, another approach has come into favour. Researchers have shown MOF materials with switchable porous behaviour. In these systems, the adsorptive properties change in response to a controlled stimulus.[70,71] The call for these materials is justified by need for milder desorptive processes. We find that CO_2 typically requires elevated temperature and/or high vacuum to desorb because of the strength of the MOF:CO_2 interactions. For this reason, promoting CO_2 desorption on an industrial scale would be very energy (and by extension, financially) intensive. In the interest of more efficient, on command desorption, researchers have studied flexible (switching) MOFs with dynamic adsorptivity.[72–74]

1.3.4 Stimuli-Responsive Adsorptive Switching in MOFs

The definition of switching (with respect to this thesis) is reversible changes in chemical and material properties in response to stimuli such as heat,[75] light,[76] pH,[77] or electrical current.[78] In an ideal situation, the changes in chemical properties persist over several duty cycles.[79] However, most materials show some degree of degradation over time. From an application point of view, if the number of duty cycles is financially reasonable, then replacing the material every n-cycles is acceptable.

There are many examples of switching adsorptivity in MOFs reported, and the

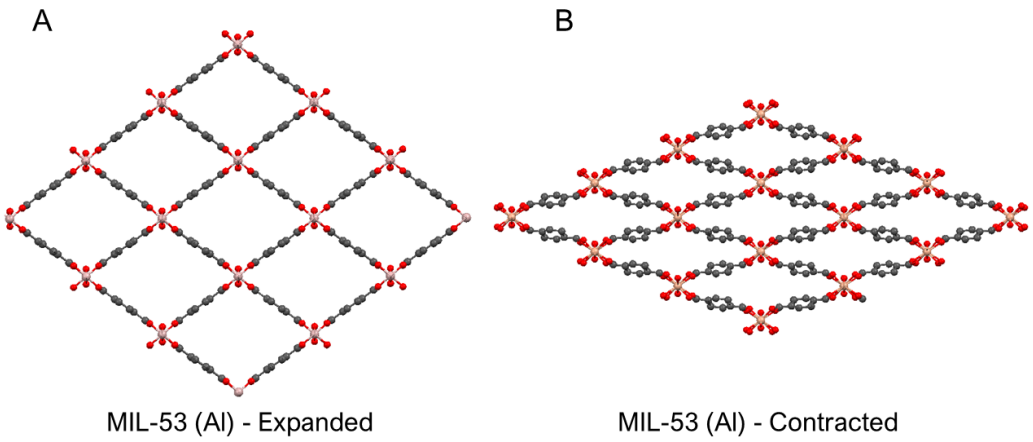

Figure 1.5: Expanded (A) and contracted (B) forms of structurally flexible MIL-53. MIL-53 undergoes structural deformation at low temperature to the contracted form and becomes expanded at higher temperature.

mechanism/motif which promotes these changes in porous behaviour also varies greatly.[80] For example, MOFs like MIL-53 (Cr, or Al based, Figure 1.5) display a structural flexibility, wherein the rhombic pores undergo reversible expansion (Figure 1.5A) and contraction (Figure 1.5B).[81] The structural flexibility of MIL-53 is observed in response to temperature, pressure, and hydration.

Researchers in the Ferey group determined that vacant MIL-53 exists in the contracted form in the temperature range of 125-150 K and expands in the temperature range of 325-375 K.[82] This mechanical deformation in MIL-53 has been used to selectively sieve CO_2 from CO_2/CH_4 mixtures.[83–86] Research suggests that the quadrupolar interactions (not displayed in CH_4) allow strong MOF:CO_2 interactions with the surface when the MOF undergoes expansion and is exposed to CO_2/CH_4 mixtures, with greater than 25% CO_2. While MIL-53 is arguably the most prototypical switching MOF, a variety of thermal and pressure gated switching are now known.[87–90]

1.3.5 Photoswitching Adsorptivity in MOFs

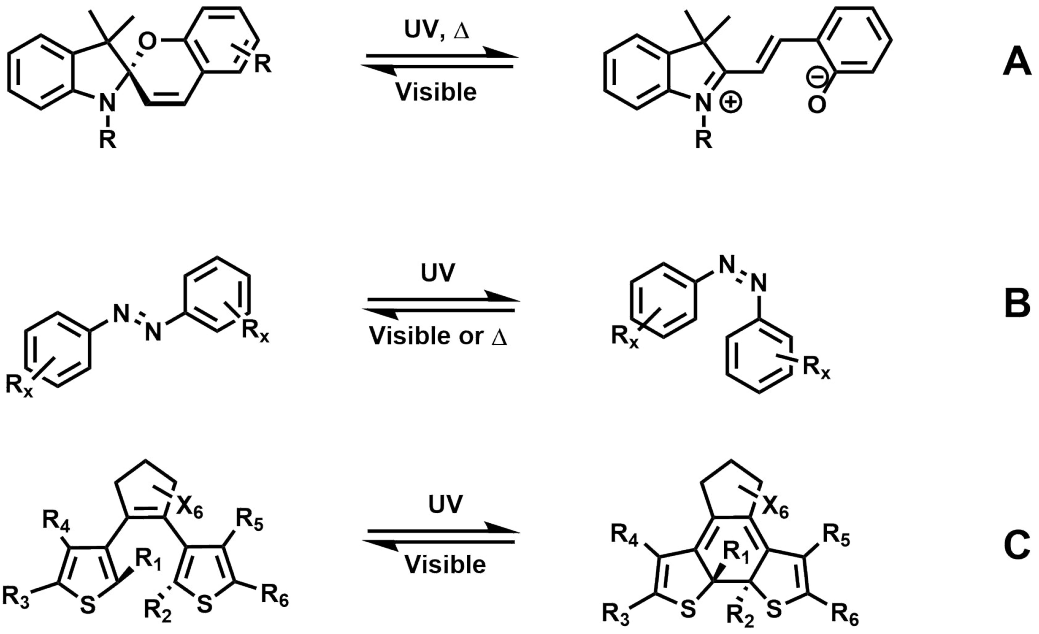

Figure 1.6: Spiropyran (SP, A), azobenzenes (B), and dithienylethenes (DTEs, C) which comprise most photoswitching MOFs in literature; photoisomerization produces isomers with distinct photochromic colour changes and new material properties which contrast the former isomer.

While we have only discussed thermal, and pressure gated MOF systems up to this point, there are also MOFs that display adsorptive changes in response to light. Photoswitching MOFs are created by the inclusion of light-reactive molecules.[91] When these molecules are exposed to the correct wavelengths of light, they undergo a reversible photochemical reaction that is often accompanied by a distinct change in the materials colour, which is more commonly known as a photochromic reaction.[92] Under UV light, these molecules absorb high energy photons and undergo a light triggered reaction to produce a ring-closed photoisomer. Concurrently, when irradiated with lower energy light, this photoisomer reverts to its former state. Thus, materials with these photoswitching groups can exist in two chemically unique states.[91–93] Incorporating these into a MOF would enable the MOF to potentially have different

adsorptive properties.[94–96]

Although there are many different types of photoswitches known in the literature, the most common ones observed in MOFs contain linkers that have spiropyrans (SP), azobenzenes, and dithienylethene (DTE) groups (Figure 1.6).

Spiropyran MOFs

Spiropyrans (SP, Figure 1.6A) undergo a light promoted ring opening isomerization to produce a charge separated isomer that is separated through long range conjugation.[97] This open (mercyanine) isomer strongly absorbs light in the visible spectrum of light, and typically produces a vivid photochromic shift in colour.[98] Photoswitching SP/MOF composites have been previously illustrated by Schwartz *et al.*, who report photoswitchable behaviour of MOFs with non-covalent guest SP switches. These researchers noted the distinct effect of the choice of MOF host on the visible colour change observed.[99] Concurrently, Healey *et al.* report MOF-808-SP, which displays photoswitchable adsorptivity towards CO_2.[100] Increased CO_2 adsorption can be attributed to the charge separated mercyanine isomer strongly interacting with quadrupolar CO_2. Alongside photoswitching gas sorption, Heinke and coworkers have reported MOF/SP materials that display photoswitching conductive behaviour.[101] Like photoswitching CO_2 adsorption reported by Healey *et al.*, collaborative research between the Simon and Wang groups saw SP/MOF hybrid materials with photoswitching ion retention for low energy desalination of water.[102] Advancement of these materials promises an energy-saving alternative to reverse osmosis, which is the traditional (and energy intensive) method by which salt water is desalinated.

Azobenzene MOFs

The second prevalent class of photoswitches are azobenzenes (Figure 1.6B), which change via light promoted cis/trans isomerization.[103] When irradiated with UV light, the trans-isomer of azobenzene undergoes a 180° bond rotation about the N=N (azo) motif to form cis-azobenzene, which subsequently changes molecular dipole and electronic behaviour.[104] Switching back to the trans-isomer is easily performed by applying thermal energy or longer wavelengths light. These isomers are measurably distinct with respect to their chemical, spectroscopic, and electrochemical behaviour in the bulk phase.[105]

MOFs with incorporated azobenzene photoswitches (much like SP/MOF composites) have also been shown to possess switching adsorptivity, as first illustrated by Zhou and co-workers.[106] Other examples of photoswitchable adsorption include azobenzene derivatives of an expanded Mg-MOF-74 reported by Browne *et al.*, wherein pendant side groups are embedded in hexagonal channels of the system.[107] These pendant motions via cis/trans isomerization modifies the pores behaviour, allowing retained dyes to exit the channels. This work highlighted potential for on command light-controlled adsorbate retention/release applications. More recent examples by Hecht and co-workers report post-synthetic modification (discussed in detail in Chapter 2) to build an outer shell azobenzene MOF, which controls guest retention of the unfunctionalized inner shell MOF.[108]

Types of Photoswitching MOFs

Before proceeding to discuss DTEs and DTE MOFs, it is important to discuss some nomenclature necessary to differentiate the different methods used to incorporate

these switches into MOFs. We defined this nomenclature to make it easier for researchers to clearly describe and classify photoswitching MOFs without the need for a cumbersome discussion in every manuscript regarding the advantage/disadvantage of each method of incorporation. The nomenclature is best illustrated with azobenzene-containing MOFs, but the advantages/disadvantages of each translate to all photoswitching MOFs (Figure 1.7).

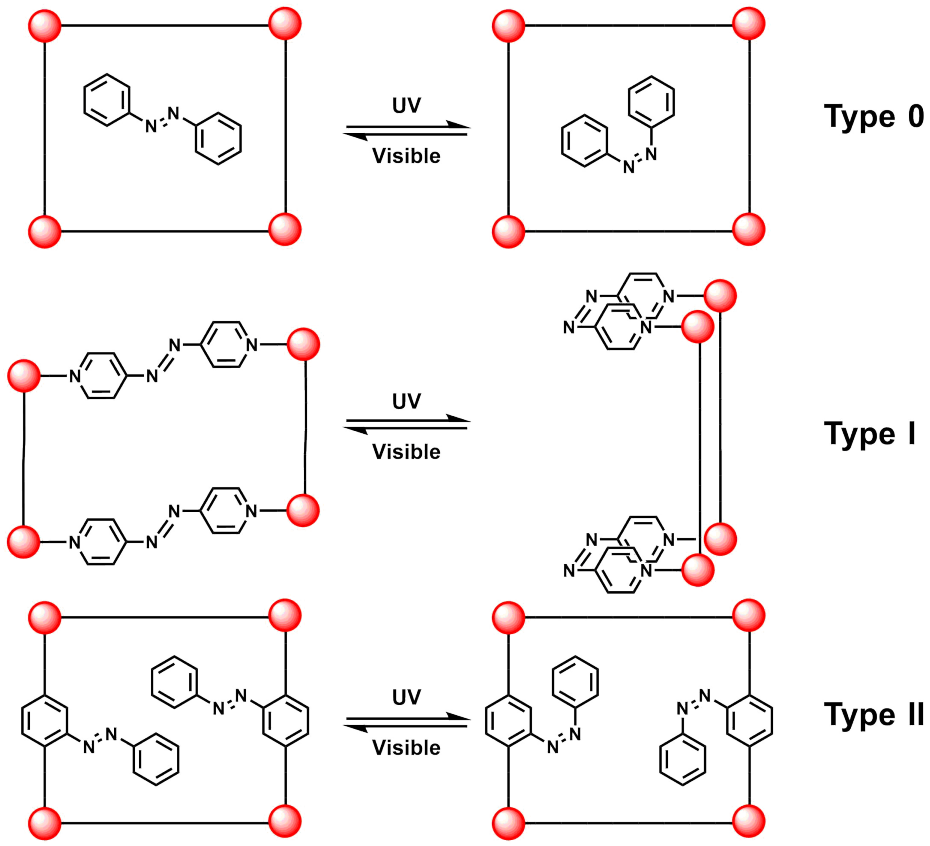

Figure 1.7: Simplified illustration of photoisomerization in Type 0, Type I and Type II azobenzene MOFs. Drastic mechanical deformation makes Type I photoswitching MOFs disfavoured compared to the pendulum group style exhibited by Type II MOFs.

In 2012, Kitagawa *et al.* disclosed azobenzene MOFs wherein, cis/trans isomerization of the guest azobenzene controls the MOFs adsorptive behaviour.[109] We refer to these systems as Type 0 MOFs. Type 0 MOFs highlight the interesting effects of

simple guest inclusion on its MOF host.

Many researchers have also used molecules such as 4,4'-azo(bis)pyridine, which tethers two metal nodes (Figure 1.7) across the photoswitching component. We refer to these systems as Type I (Figure 1.7). Type I photoswitching MOFs, with respect to Type 0 MOFs are considered more robust because the incorporated photoswitching material is less likely to exhibit pore leeching (desorb/leaving the MOF), since Type I photoswitches use linkers that covalently bond with nodes. Examples of Type I azobenzene MOFs include work by Kuchar *et al.* who report use of the previously mentioned 4,4'-azo(bis)pyridine linker in a Zn-based MOF.[110] However, because of the straining linker/framework assembly, no photochromic switching behaviour was observed. Other examples of Type I MOFs include Epley *et al.*, who use 4,4'-azobenzenedicarboxylate based MOFs for cargo release by intentional photodegradation of drug guest molecules.[111]

Stock and coworkers reported the synthesis of the first covalently incorporated azobenzene MOF with observable photoswitching inside the pore.[112] This was achieved by building the photoswitching azo-moiety off of the MOFs linker as a side arm that points into the pore (Figure 1.7). In these systems, the isomerization does not lead to stress/strain on the framework given that the bonds that change are free to do so in the pore. These systems are referred to as Type II systems.

Comparing Type 0 systems to Type II systems, no photomechanical strain occurs in either system, however, the latter has its photochromic moiety covalently bound inside the pore, so pore leeching (the switch desorbing, and leaving the MOF) is effectively eliminated. When we compare Type I systems to Type II systems, the photochromic motif is present as a pendant side group, which does not interfere with the structural integrity of the MOF during photoswitching. To clarify, MOFs are rigid

3D nanostructures; these light triggered bending and rotational mechanisms introduce disfavoured torsional strain in the MOF, which either results in accelerated material degradation by damaging the crystalline system (Figure 1.7), or photoisomerization does not occur at all or only occurs on the surface where the material is more flexible.

The three types of photoswitching MOFs are summarized below:

1. Type 0: Photoswitches occupy the pore as non-covalent guest.

2. Type I: Photoswitches covalently incorporate into the MOF. The azo-moiety is critical to the MOFs 3D structure, and linearly connect two nodes.

3. Type II: Photoswitches covalently incorporate into the MOF, and the photoactive moiety exists as a side arm, which is not structurally critical to the MOF.

Dithienylethene MOFs

Now that we have clarified the nomenclature describing the types of photoswitching MOFs, we may now move forward to discuss dithienylethenes (DTEs), which are the third prevalent photoswitch used in photoswitching MOFs (Figure 1.6C). These photoswitches undergo reversible 6π-electron electrocyclization under UV light (Figure 1.8A).[113] This reaction initiates under the appropriate wavelength (λ) of light when 3 vicinal double bonds undergo ring closure, which results in a new 6 membered ring, and one new carbon-carbon π-bond.[114]

This reaction proceeds through a conrotatory (same direction) rotation of the 1,6-site p-orbitals (Figure 1.8B) allowing constructive overlap of p-orbitals to form the new sigma bond.[113,114] The closed isomers diene motif lies in conjugation and forms an 8π-electron tetraene chain, which spans the molecule and allows long range electronic communication between substituents.[115] This increased π-conjugation produces

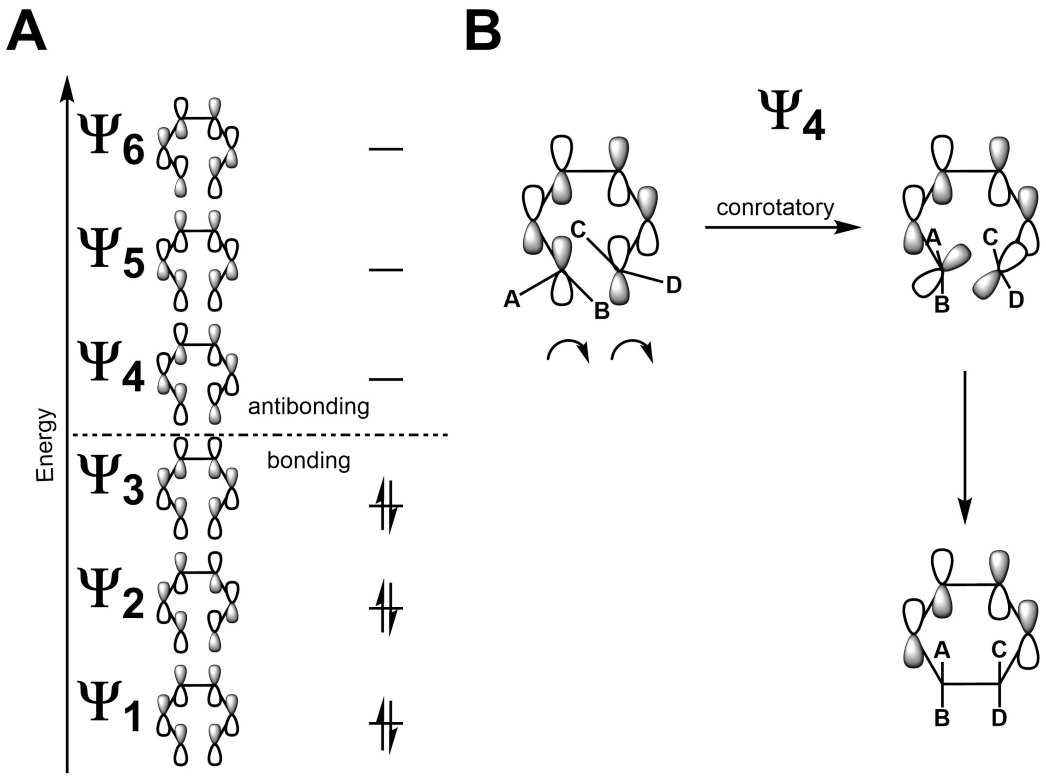

Figure 1.8: (A) Illustration of the molecular orbitals of a dithienylethene system as a simplified 1,3,5-hexatriene system (functionalities have been omitted for clarity). (B) Illustration of the conrotatory mechanism by which DTEs photocyclize via excitation of an electron into the LUMO.

a narrower HOMO-LUMO gap, which produces absorbance in the visible region.[113,114] The inverse reaction from closed to open form DTE readily occurs under visible wavelengths of light. Extensive research by Irie *et al.*,[116–118] and other researchers such as Herder *et al.* have illustrated the effects of DTE electronic structure and its effects on photoswitching duty cycles (changing back and forth, repeatedly).[119]

With respect to the open form isomer of DTEs, the closed form has vastly different material properties. The most prevalent difference between these isomers is optical properties. Reports from the Irie, Tian, and Ahn group, have established great literature precedent for use of DTEs in next-generation optical memory storage, and logic gate functions, using the measurable changes in spectroscopic response as 0/1 binary

outputs in memory writing and logic circuit applications.[120–122] Other groups such as the Browne group have studied the electrochemical behaviour behind these switches towards future photoswitchable conducting materials, as DTEs have been shown to be reversibly oxidized and reduced through a $2e^-$ redox process.[123,124]

However, the true power of DTEs is in their structural diversity (Figure 1.6). Using synthetic chemistry, we may alter essentially any site on these molecules, creating complex, conjugated heteroaromatic structures.[125,126] These structures replicate the core photoactive 1,3,5-hexatriene motif. Many DTEs and diarylethenes are reported in cross-disciplinary applications. Remarkable examples of these cross-disciplinary applications include light-controlled enzyme inhibition,[127] and light controlled reactivity of chemical reactivity,[128–131] as reported by Branda and coworkers.

One benefit DTEs have with respect to azobenzenes, and SP photoswitches that has not been mentioned yet is that DTEs may also become thermally stable through the correct balancing of the molecules electronic structure; for clarity, they become insensitive to thermal reversion pathways that accelerate involuntary ring opening pathways.[132] Thermally insensitive DTEs are reported in the extensive work of Irie and co-workers, whose research iconized the use of the 5-membered perfluorinated ring backbone (X = F, Figure 1.6C).[133] The synergistic balance of electronic structure in these perfluorinated systems afford thermal persistence, with lifetimes in select structures exceeding $\geq$10,000 cycles of thermally stable switching before the material becomes exhausted by the eventual convergence to a photoinactive state.[119]

With regards to DTE based MOFs, initial reports of DTE photoswitching MOFs by Benedict and coworkers disclose Type 0 photoswitching systems that use perfluorinated DTE guest molecules, which are like those studied by Irie and co-workers[134] This relatively simple inclusion of DTEs imparted photochromic change in single

crystal MOF samples. This initial example highlighted the simplicity in imparting photoswitching properties of the photochromic guest to its host.

The proceeding works of Zhou and coworkers report Type I DTE MOFs for light controlled generation of singlet oxygen.[135] Advancement of a similar Type I system by Guo and coworkers afforded DTE MOF systems for selective adsorptivity in C_2H_2/C_2H_4 gas mixtures, showing promising future application of these materials in petrochemical purification of light hydrocarbons.[136]

Type I DTEs are similar with respect to azobenzene systems; these linkers use coordinating side groups (R_3, R_6 = 4-pyridal, 4-carboxyphenyl, Figure 1.6C) that connect nodes and are structurally critical to the MOF. Guo and co-workers have illustrated a Type I DTE MOF (DMOF-1) with photoswitching pore behaviour.[137] This work was subsequently followed up by Barbour and co-workers who illustrated the importance of structural flexibility in the overall framework to accommodate the drastic changes in coordination geometry imparted by the change in planarity of the DTE photoswitch.[138] This was illustrated through crystallographic studies of DMOF-2 and DMOF-3. The results of this work established that continuous photomechanical motion in rigid frameworks negatively affects these materials, which justifies the need for Type II DTE MOFs for maximizing material lifetime/activity for prolonged use.[138]

Interestingly, very few examples of Type II DTE MOFs exist in the literature; Prior to 2017, the existing handful of Type II DTE MOF systems were reported by Benedict and co-workers These MOFs (UBMOF-1, UBMOF-2, and UBMOF-3) build aromatic sulfur heterocycles off linear phenanthrene linkers. The photophysical and structural properties of these systems are well studied through use of X-ray and UV-Vis spectroscopy while undergoing photoisomerization,[139] and desolvation.[140] Complementary work by Benedict and co-workers also modelled thienyl group orientation in the pore

to understand effects of (atrop)isomerism that exists in the pore on the overall photoswitchable behaviour of the bulk MOF material.[141]

1.4 Outlined Goals Of This Thesis

The scope of the proceeding thesis chapters will discuss methodology employed for rational design of new Type II DTE MOFs and our proof-of-concept experiments to illustrate their potential for future light controlled chemical separation materials.

Chapter 2 describes the foundational work that went into creating the prototype material, PSZ-1. The photoswitching capabilities of the prototype material are assessed through various forms of spectroscopy and gas sorption analysis. As well, the material is assessed for its solid-state filtration capabilities by pushing a solution of aromatic hydrocarbons through a solid bed of material.

The third chapter discusses our study on relations of ligand structure and photophysical properties to optimize the imparted switching stability of the MOF; we subsequently investigated an incorporation minimum. When achieved, photoswitching is below the limits of detection for UV-Visible spectroscopy in the bulk material. This MOFs light-controlled adsorptivities are compared to our previously reported MOF as reference material.

The fourth chapter discloses the synthesis and characterization of photoswitching porous materials which have fractional incorporation of photoswitching linkers; the spectroscopy, structural integrity, and analyte retention as a function of linker embedded are discussed; this chapter precedes proposed scopes of future work from the findings of this masters thesis.

Chapter 2

A New Type II DTE MOF Demonstrating Prospective Photoswitchable Adsorptivity

2.1 Introduction

2.1.1 Coauthorship Statement

The work discussed in Chapter 2 is reproduced with permission from Furlong, Brandon J, and Katz, Michael J, A Bistable Dithienylethene-Based Metal-Organic Framework Illustrating Optically Induced Changes in Chemical Separations. Journal of the American Chemical Society 2017, 139, 38, 13280-13283. Copyright 2017 American Chemistry Society. The original research topic was chosen by Dr. Michael J. Katz (MJK), Brandon J. Furlong (BJF) designed and performed the experimental work,

BJF collected the data, BJF performed the analysis, with the exception of the collection, and processing of single x-ray crystallography work performed by MJK. BJF prepared the first draft of the manuscript and figures, both BJF and MJK provided editing and feedback on the manuscript.

2.1.2 Chapter Introduction

This chapter discusses our initial efforts to illustrate that Type II DTE photoswitching MOFs can change their adsorptive properties in response to light. To develop this exploratory work, we followed 3 fundamental steps, as enumerated below:

1. Synthesize a photoswitching linker which has free thienyl groups
2. Synthesize a MOF that can accomodate this linker
3. Characterize the structure and photoswitching properties of this MOF

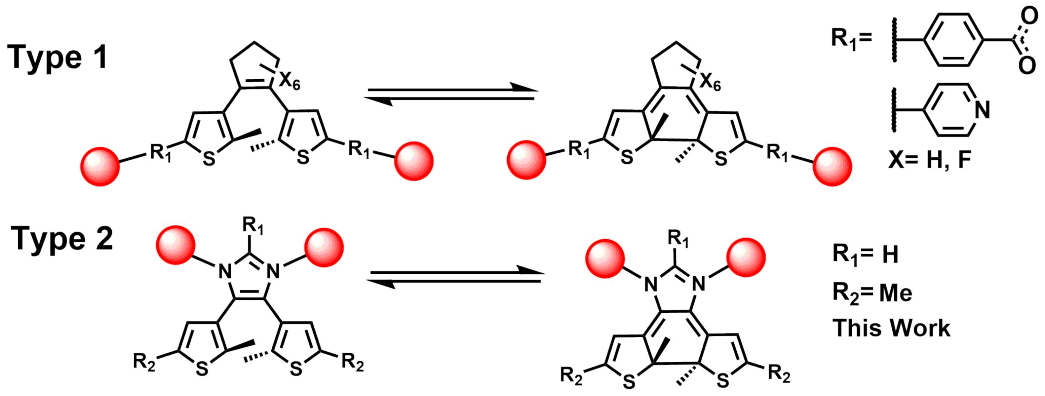

Figure 2.1: Dithienylethene-based linkers connecting metal nodes (spheres) either via the thienyl portions (Type I), or the ethene portion of the dithienylethene moiety (Type II). Reproduced with permission from Journal of the American Chemical Society 2017, 139, 38, 13280 - 13283. Copyright 2017 American Chemistry Society.

Prior to this work, the only known examples of Type II DTE MOFs are the UB-MOF materials reported by Benedict and co-workers[134,139–141] To synthesize a photoswitching linker with free thienyl groups, we used synthetic strategies of Wang and

co-workers to develop a DTE linker with a heterocyclic imidazole as the backbone.[142] The nitrogen lone pairs of the imidazolate anion allow ditopic linking between nodes (Figure 2.1). Using this imidazolate backbone, the need for bridging thienyl groups is eliminated. As a result, the thienyl groups of this linker are unhindered in the pore and may freely rotate and undergo switching without risk to the framework integrity.

While the majority of MOFs are commonly formed through metal-carboxylate bonds, 3-D MOFs with metal-imidazolate linkages known as Zeolitic Imidazolate Frameworks (ZIFs) are well known.[143] ZIFs are a subclass of MOFs that are formed from the assembly of tetrahedral metal cations such as Zn^{2+}, Cd^{2+} and Co^{2+} with imidazolate bridging anions.[144] The resulting structure of ZIFs mimic the complex cage structures of aluminosilicate-based zeolite materials. It was proposed that the imidazole DTE could be incorporated into the pore lining of a ZIF that is large enough to accomodate the thienyl groups in the pore channels. To integrate the imidazolate linker into the pore of a MOF, there are a few different synthetic approaches that are viable:

1. Pre-synthetic - single linker approach
2. Pre-synthetic - mixed linker approach
3. Post-synthetic modification (PSM)

Pre-synthetic approaches are the standard approach for MOF synthesis that use MOF linkers which are functionalized with the desired funcitonality.[143] There are many variables that influence pre-synthetic MOF synthesis such as temperature, time, pH, concentration, and stoichiometry. Using this approach, metal salts and linkers are reacted in solution and the reaction parameters are systematically analyzed for optimizing material quality. This may be performed using a single linker approach, or

mixed linker approach (i.e., more than one type of linker with the same topicity).[145]

Post-synthetic modification (PSM) is another strategy for MOF synthesis.[145] By reacting pre-synthesized MOF in a solution of another linker, then an exchange of parent linkers in pristine MOF with solution-phase linkers is facilitated over time.[146] By using PSM techniques, the overall topology of a MOF is often retained in many cases.[147] In effect, this allows us to design new materials that would not be obtainable if we approached MOF design with a pre-synthetic approach.[148]

PSM includes a practical choice in the MOF that is being modified, which allows control over pore shape and size; this technique provided the control needed to synthesize a MOF with the appropriate structural size and shape to sterically tolerate the thienyl rings occupying the 4,5-positions of the imidazole ring on the new linker.[149]

Another reason that PSM was chosen for this initial work is that the synthetic conditions for ZIFs are sensitive to linker concentrations and stoichiometry during the reaction of MOF formation.[150] This makes mixed linker MOF studies with *in-situ* strategies more difficult when working with ZIFs.

Further, in the interest of conserving synthetic work, effectively using precious synthetic intermediates, and effective use of research time, PSM was deemed the best approach for designing a Type II DTE MOF with PSM techniques on a pre-made ZIF.

With the strategy mapped out, this chapter details the synthesis of an imidazole derived DTE, and its incorporation into a MOF, followed by characterization of the new material and discussion of potential applications for photoswitching adsorptivity in this new system.

2.2 Experimental

2.2.1 Materials and Methods

Unless otherwise stated, all reagents were used as received from commercial suppliers without further purification. Dichloroethane and pyridine were purified by distillation and stored over activated 4Å molecular sieves. Column chromatography was performed using 230-400 mesh silica.

^{1}H NMR spectra were recorded on a Bruker Advance III 300 MHz NMR spectrometer using $CDCl_3$ or DMSO-d_6 + 3 drops sulfuric acid-d_2 (D_2SO_4) as the NMR solvent. All spectra for acidic mixtures were referenced to DMSO-d_6 during acquisition.

Solution-phase UV-Visible spectra were recorded on a Cary 100 Series UV-Visible Spectrometer, and solid samples were measured using an Ocean Optics USB4000 Spectrometer in reflectance mode. Solid state UV-Visible spectra were recorded in 1 % w/w KBr matrix. Photoisomerization experiments were carried out by use of a UV-lamp (Spectroline ENF-260C) suspended approximately 20 cm above the sample on shortwave setting ($\lambda \leq 254$ nm). For visible light ($\lambda \geq 515$ nm) irradiation cycles, an LED flashlight was shone through a low band-pass ($\lambda \leq 515$ nm) filter suspended approximately 20 cm above the sample.

Powder X-ray diffraction (PXRD) patterns were obtained using a Rigaku X-ray Ultima IV Diffractometer equipped with a copper X-ray source and a scintillation counter detector. Samples were measured from $3 - 20^\circ$ in 2θ using a scan speed of 1°/min.

Nitrogen gas adsorption isotherm data was collected at 77 K on a Micromeritics

3Flex surface area and porosity analyzer. All samples were activated on a Micromeritics Smart VacPrep instrument by initially heating the sample to 80 °C (5 °C/min) while slowly reducing the pressure (5 mmHg/s). The sample was maintained at this temperature and pressure for 1 h. After this time, the temperature was ramped to 90 °C (5 °C/min) for 2 h. Subsequently, the sample was heated to 110 °C (5 °C/min) and held at this temperature for 22 h. The sample was then cooled to room temperature after which the sample holder was back-filled with nitrogen gas.

For XRD analysis of ZIF-70, a yellow block-like crystal of ZIF-70 of dimension $0.15 \times 0.15 \times 0.2$ mm^3 was collected on a Rigaku diffractometer AFC-8 goniometer equipped with a Mo X-ray source provided by Proto Manufacturing. A ZIF-70 crystal was secured to a Mitgen micromount using Paratone oil and placed on an AFC-8 goniometer. The sample was cooled to 250 K using an Oxford 800 series cryo unit. A hemisphere of data was collected using the CrystalClear Expert 2.1 software suite in 0.5° width in ω using 5 second exposure times. For PSZ-1, A yellow block-like crystal of PSZ-1 with dimensions $0.17 \times 0.12 \times 0.12$ mm^3 was secured to a Mitgen micromount using Paratone oil and single crystal X-ray diffraction data was collected using a Rigaku Oxford Diffraction Synergy-S X-ray diffractometer equipped with an ROD HyPix-600HE hybrid photon counting (HPC) detector. Data was collected at 250 K using micro-focused Cu radiation. A data collection strategy to ensure maximum data redundancy was determined using CrysAlisPro. 250 K was chosen in order to minimize the effect of pore-bound solvent on the diffraction pattern for both structures. The structure was solved using direct methods called from within the Crystals software suite. The structure was subsequently refined in Crystals. For both ZIF-70 and PSZ-1, the final structural refinement included anisotropic temperature factors on all non-hydrogen atoms.

2.2.2 Synthesis of 1,2-Bis-(2,5-dimethyl-thiophen-3-yl)-ethanedione (2,5-DMTDK)

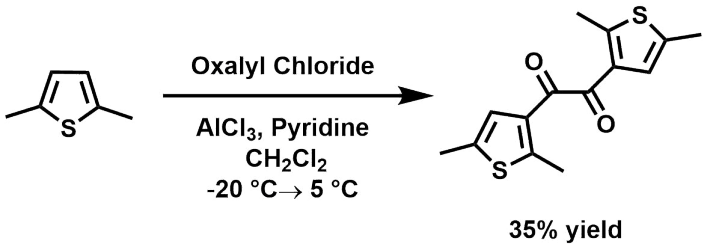

This molecule was synthesized following a previously reported procedure by Neilson *et al.*,[151] with some minor modifications. A dry 250 mL 3-neck round bottom flask was charged with anhydrous $AlCl_3$ (6.00 g, 45.4 mmol) and 25 mL of dry dichloromethane (DCM). The reaction was cooled to -20 °C after which 1.8 mL of distilled pyridine (1.76 g, 22.3 mmol) in 5 mL of DCM was added dropwise over 10 min. The solution was stirred for 5 min after which 2,5-dimethylthiophene (5.1 g, 45.4 mmol) in 5 mL of DCM was added dropwise over 10 min. Subsequently, 2.5 mL of oxalyl chloride (3.7 g, 28.9 mmol) in 20 mL of DCM was added dropwise over 30 min. The reaction was stirred until the temperature warmed to 5 °C. The reaction was subsequently quenched with cold water. Prior to extraction, filtering through celite was observed to reduce the formation of emulsions during extraction processes. The products were extracted with 3 × 100 mL of DCM, washed with an aqueous saturated Na_2CO_3 solution until a neutral pH was obtained, dried over $MgSO_4$, and concentrated under reduced pressure to obtain a dark reddish black oil. The oil was purified by column chromatography using 10 % EtOAc/Hexane to yield bright yellow powder. Yield: 2.35 g, 35 %. ^{1}H NMR (300 MHz, $CDCl_3$): δ (ppm) 2.38 (s, 6H),2.72 (s, 6H), 6.91 (s, 2H).

2.2.3 Synthesis of 4,5-bis(2,5-dimethyl-3-thienyl)-1H-imidazole (HL_1)

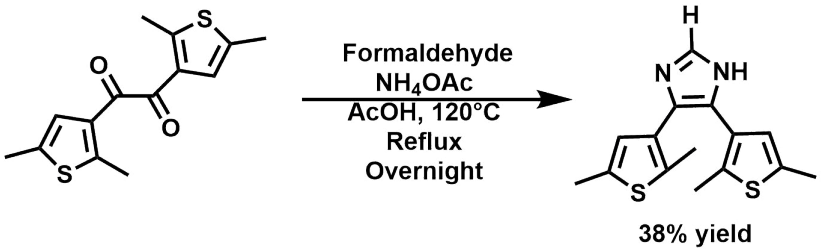

As per the procedure of Yam *et al.*,[142] 2,5-DMTDK (1.00 g, 3.59 mmol), NH_4OAc (8.31 g, 107 mmol), and formaldehyde (0.83 mL, 10.5 mmol), were dissolved in 20 mL of glacial acetic acid and refluxed overnight at 120 °C. The resulting mixture was concentrated under reduced pressure, diluted with water and neutralized with saturated Na_2CO_3. The organics were extracted using 3 × 50 mL of $CHCl_3$, dried with $MgSO_4$ and concentrated with reduced pressure to yield light beige solid. Yield: 450 mg, 38 %. ^{1}H NMR (300 MHz, $CDCl_3$): δ (ppm) 2.07 (s, 6H), 2.39 (s, 6H), 6.59 (br s, 2H), 7.68 (s, 1H)

2.2.4 Synthesis of ZIF-70

This procedure was adapted from Yaghi *et al.*,[152] $Zn(NO_3)_2 \cdot 6\,H_2O$ (200 mg, 0.68 mmol) was added to a 1 dram vial and dissolved in 1 mL of DMF with sonication to form a colorless solution. To this solution, a 1 mL solution of imidazole (46 mg, 0.68 mmol) and 2-nitroimidazole (76 mg, 0.68 mmol) in DMF was added. The resulting clear yellow solution was topped off with DMF to 3.4 mL, capped, and sonicated for 2-3 min. This mixture was then heated at 110 °C for 4 days. After 4 days, the hot DMF was decanted and the resulting yellow hexagonally shaped crystals were washed with 3 × 3 mL DMF followed by 3 × 3 mL of MeOH. The crystals were then decanted

into a clean vial and stored in fresh DMF until further use was required. ^{1}H NMR (300 MHz, DMSO-d_6 + 3 drops Sulfuric Acid-d_2): δ (ppm) 9.00 (s, 1H), 7.60 (d, 2H), 7.33 (s, 2H). Ratio of integration (Imidazole:Nitroimidazole): 1:0.71.

2.2.5 Synthesis of PSZ-1

Using procedure adapted from Farha *et al*,[153] HL_1 (57 mg, 0.20 mmol) was dissolved via sonication in 20 mL of *n*-BuOH. ZIF-70 (50 mg, 0.20 mmol) was added to solution and then the mixture was heated for 3 days at 110 °C. Once finished, the solution was cooled to room temperature, and the solution was decanted. The solid yellow crystals were washed with 3 × 20 mL of DMF and 3 × 20 mL of MeOH. The resulting solid was then decanted into a clean vial and stored in fresh DMF. ^{1}H NMR (300 MHz, DMSO-d_6 + 3 drops Sulfuric Acid-d_2): δ (ppm) 9.11 (s, 1H), 8.98 (s, 1H), 7.59 (s, 1H), 7.33 (s, 2H), 6.64 (s, 2H), 2.31 (s, 6H), 1.88 (s, 6H). Ratio of integration (Imidazole:Nitroimidazole:L_1): 1.00:0.70:0.27

2.2.6 Procedure for aromatic hydrocarbon filtration

A 75 mg dried sample of MOF (ZIF-70, PSZ-1-open, PSZ-1-closed, or PSZ-1-reopened) was packed into a 1 mL syringe. To this, 750 μL of 1:1:1, by mass, $CDCl_3$ solution of toluene, naphthalene, and pyrene was added over the top the sample. The solution was eluted through the syringe by the slow application of the plunger. The eluent was collected in an NMR tube. To this solution, 0.1 mL of 50 mg/mL solution of sulfolene in $CDCl_3$ was added as an external reference. The integration of the hydrocarbons were compared to the sulfolene protons (doublet, integration=4H, (CH_2). The ratio of the integrations (pre and post filtration) were multiplied by the initial concentration in order to obtain the concentration of the hydrocarbons in the filtrate.

2.3 Results and Discussion

2.3.1 Comments on Synthetic Chemistry Work

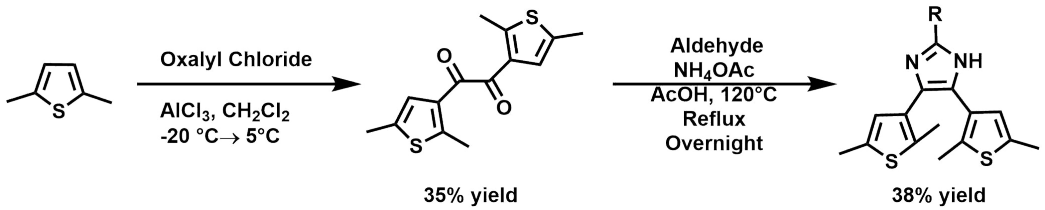

Figure 2.2: Outline of synthetic work performed to prepare a Type II imidazole based DTE. Through the coordinating nitrogens of the heterocyclic backbone, incorporation of DTEs is possible without utilizing 5-thienyl substituents

Figure 2.2 outlines the synthetic scheme we followed to prepare the Type II DTE photoswitch. Beginning from the readily available 2,5-dimethylthiophene, 2,5-DMTDK is a 1,2-dione synthesized through Friedel-Crafts acylation, using oxalyl chloride as the acylating reagent and $AlCl_3$ as the Lewis acid in a stoichiometric amount. This reaction produces a moderate yield (35 %) of 1,2-dione, which was determined to be pure enough via NMR to carry forward to the next step.

The second step is the cyclization of the synthesized 1,2-dione with the C_1 building block formaldehyde, with NH_4OAc as the source of nitrogen for imine formation. The NMR of the ligand is consistent with literature spectra.[151]

2.3.2 MOF and PSM Chemistry

With the ligand in hand, the PSM technique chosen for linker incorporation was solvent-assisted linker exchange (SALE).[154] SALE is the exchange of solution-phase linkers with an existing frameworks linkers over time.[143,145] Using SALE, an imidazole-based linker was incorporated into the structure of a ZIF (which is from here on referred to as HL_1).

To successfully exchange HL_1 via SALE, a ZIF with a large pore size would be necessary to accommodate HL_1, which has a steric profile of ∼6 Å across the 4,5-substituents. After reviewing the literature on known ZIF structures, ZIF-70 was chosen as the material that would be modified. A more in-depth discussion about ZIF-70 can be found in the in the single crystal X-ray diffraction (SCXRD) section of this chapter.

The exchange of HL_1 with ZIF-70 linkers was performed in *n*-butanol at 110 °C. Similar SALE experiments were performed in DMF as a side comparison, but the resulting material obtained from identical DMF reactions was of poor quality, as indicated by the clumped black heterogeneous solid that had no porosity. A possible explanation for this difference is the dimethylamine is a stronger base than the incoming L_1, meaning that the metal center becomes coordinatively saturated and does not want to exchange dimethylamine for the photoswitching linker.

The new material obtained from the butanol SALE conditions is aptly named **P**hoto-**S**witching **Z**IF-1 (PSZ-1). The following sections detail efforts to characterize, quantify and better understand the properties of this new material, highlighting applications as a photoswitching chemical filter.

2.3.3 ^{1}H NMR Analysis of PSZ-1

The extent of HL_1 incorporation into ZIF-70 during SALE processes was determined through solution-phase ^{1}H NMR spectroscopy by comparing the relative integrations of the three linkers present inside this MOF.

Figure 2.3 shows the relevant solution-phase ^{1}H NMR spectra of acid digested PSZ-1 (top), ZIF-70 (mid), and the free ligand HL_1(bottom) dissolved in the same solvent

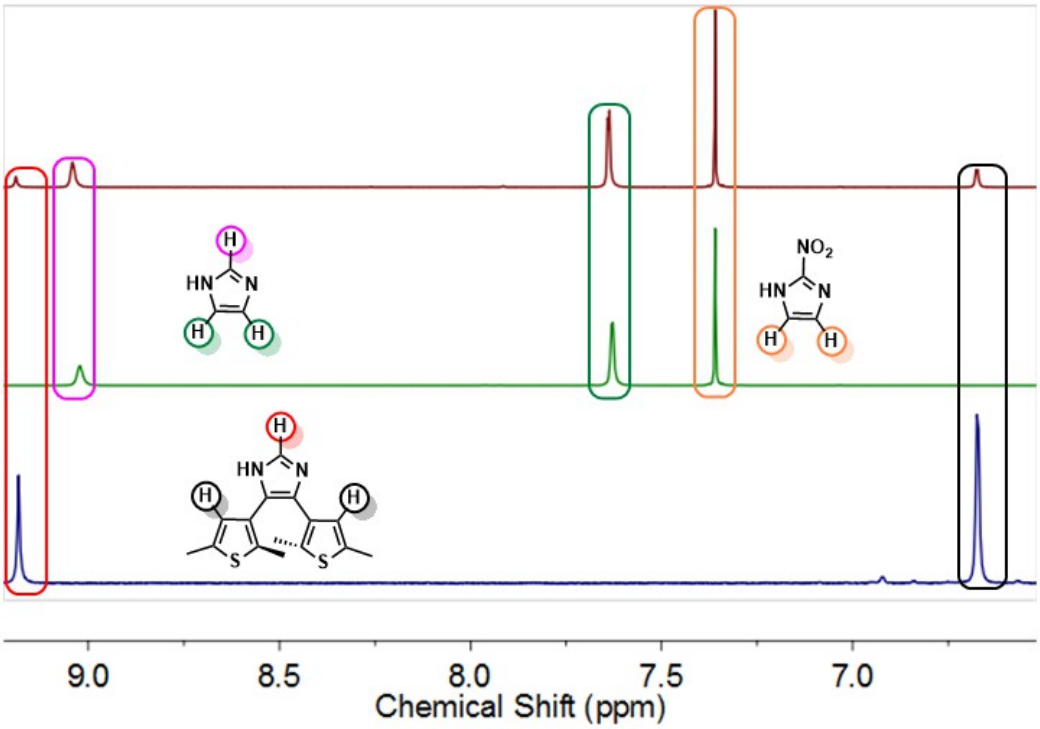

Figure 2.3: Solution-phase ^{1}H NMR of dissolved PSZ-1 (top), ZIF-70 (middle), and HL_1 (bottom) in a DMSO-d_6 and sulfuric acid-d_2 solution; the new peaks at 6.64 and 9.11 ppm illustrate that L_1 has been incorporated into ZIF-70 to form PSZ-1. Reproduced with permission from Journal of the American Chemical Society 2017, 139, 38, 13280 - 13283. Copyright 2017 American Chemistry Society.

system ($DMSO/D_2SO_4$). As shown, PSZ-1 has peaks that correspond to imidazole (pink and green), 2-nitroimidazole (orange) and signals that correspond to L_1 (red and black). These spectra indicate the presence of L_1 at a ratio of 0.27:1.00:0.70 L_1:Imidazolate:Nitro-imidazolate. This formula indicates that 12.5 % of the linkers in ZIF-70 are exchanged. If we assume that exclusively Linker 1 (Figure 2.5; the linker that decorates the large pore) exchanged with HL_1, then this would equate to ~50 % of the linkers that orient into the 1.59 Å pore are exchanged. To further assess the extent of the SALE reaction, a small sample of PSZ-1 was soaked in fresh solution of HL_1 for another day. This extra day had no effect on loading of L_1, as the integration of HL_1 in ^{1}H NMR remained the same even after subsequent SALE reactions. The

conclusion to draw from this is that no further substitution is possible and that the steric limits of the pore of PSZ-1 have been reached.

Since the majority of MOF applications are in the solid state, it is insufficient to characterize the MOF with strictly solution-phase methods. This led to the exploration of solid state characterizations of PSZ-1 and its structure in the next section.

2.3.4 Single Crystal XRD Analysis of PSZ-1

Table 2.1: Crystal data and structure refinement for ZIF-70/PSZ-1 CCDC numbers 1583508-1583510.

Compound	ZIF-70	PSZ-1	PSZ-1 (iso)
Formula	$C_{12}\,H_{11}\,N_9\,O_2\,Zn_2$	$C_{24}H_{23}N_{10}O_4S_2Zn_2$	$C_{24}H_{23}N_{10}O_4S_2Zn_2$
Formula Weight	440.96	710.39	710.39
Temperature (K)	250	250	250
Radiation	Mo(K_a)	Cu(K_a)	Cu(K_a)
Space Group	$P6_3/mmc$	$P6_3/mmc$	$P6_3/mmc$
a (Å)	27.0265	27.2188	27.2188
b (Å)	27.0265	27.2188	27.2188
c (Å)	17.8985	17.0357	17.0357
α, β, γ(°)	90, 90, 120	90, 90, 120	90, 90, 120
Volume (Å^3)	11322	10930	10930

Before studying PSZ-1 via SCXRD, we first opted to study crystals of ZIF-70. Although the structure of ZIF-70 is previously reported by Banerjee *et al.*,[152] the structure was re-examined to better understand the ligand distribution within the MOF. Re-examining ZIF-70 also provides a better predicitve model to help in understanding reactivity during the SALE process. To start, ZIF-70 is a mixed linker MOF composed of Zn^{2+}, imidazole, and nitroimidazole. The central Zn^{2+} metal center is coordinated to four structurally unique imidazolate linkers.

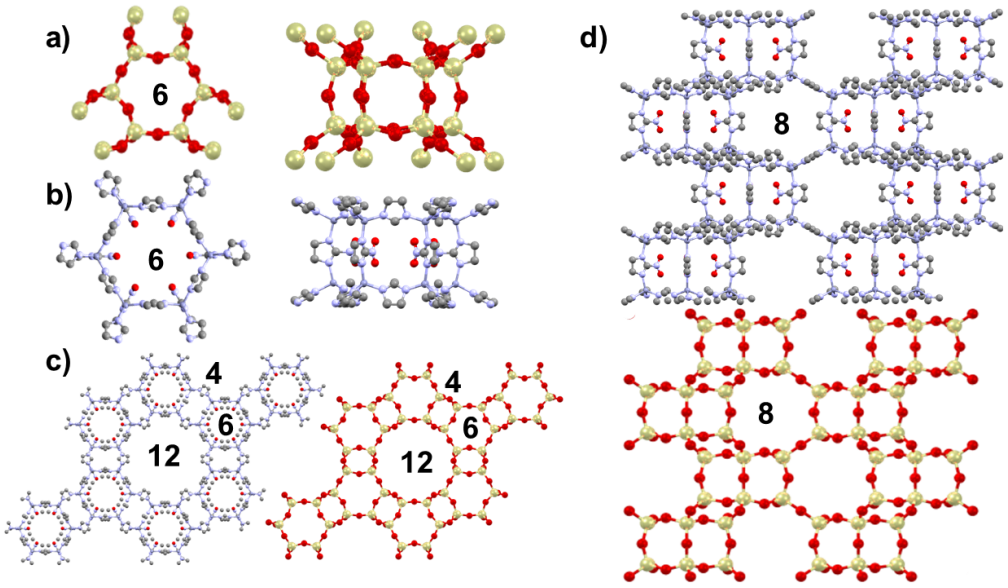

Figure 2.4: (a/b) the smallest 6-point hexagonal pore of ZIF-70 viewed down the c-axis, and a-axis respectively alongside the equivalent pore of gmelinite zeolite. 3 of the 4 unique imidazoles form this pore. The 4^{th} imidazole connects each small pore to three adjacent pores above and three adjacent pores below, and forms a 4-point connection. In this connectivity, a 12-point larger pore 1.59 nm pore (c) are formed. If the structure in (c) is viewed down the a-axis, we see the 8-point connectivity present in both gmelinite and ZIF-70. (Yellow Atoms: Si, Red Atoms: Oxygen, Blue Atoms: Nitrogen, Grey Atoms: Zn, Black Atoms: Carbon) Reproduced with permission from Journal of the American Chemical Society 2017, 139, 38, 13280 - 13283. Copyright 2017 American Chemistry Society.

Topological Breakdown of ZIF-70

As mentioned, ZIFs mimic the structures of complex zeolite structures, with primary difference being what composes them. Referring specifically to ZIF-70 vs. gmelinite, the Zn centers are filling the role of Si, and imidazoles are coordinated to the Zn centers with a metal-imidazole-metal bond angle of $\sim$144 $^\circ$ that mimics Si$-$O$-$Si bond angles. To that end, ZIF-70 has the gmelinite (gme) topology. Figure 2.4 illustrates the similarities between ZIF-70 and gmelinite. Figure 2.4a shows a hexagonal cage in gmelinite formed via Si$-$O bonds. Similarly, Figure 2.4b illustrtes the same cage, formed via Zn centres and imidazole linkers. This hexagonal cage tiles in a staggered

fashion via two bridging imidazolates that join these hexagonal cages together. The staggered pattern in both ZIF-70 and gmelinite can be seen in Figure 2.4d. In total, one hexagonal cage as seen in 2.4a/b is joined to six other hexagonal cages. When these bridging imidazoles join the 6-point cages, a 4-point cage forms (labelled 4 in (Figure 2.4c). The propogation of these 6-point and 4-point cages when viewed along the *c*-axis leads to formation of a larger pore that has 12 points and measures 1.59 nm wide (ZIF-70). When the structure is propogated along the *ab*-plane (Figure 2.4d) it can be seen that the void space created by the vertical staggering of the 6-point cages creates an 8 point cage. The final result of this topological assembly of 12, 8, 6, and 4 point cages resembles a honey-comb like structure, contrasting the previously discussed MOF-74, which has 1-D nanochannels that propogate down *c*-axis. Comparing the obtained crystal structure data (obtained at 250 K) with the gmelinite topology as shown confirms that ZIF-70 is isostructural with gmelinite. With the topology of this MOF mapped out, the ligand distribution within ZIF-70 was then analyzed.

Ligand Distribution in ZIF-70

A more clear depiction of ZIF-70 and the arrangement of the imidazolate linkers in three-dimensional space is provided in Figure 2.5. There are three imidazolates labelled Linker 1, 2, and 3 that are occupying the coordination environment of Zn^{2+}. Linkers 1 is oriented into the 15.9 Å pore and is the most important linker for this work, while Linker 2 is oriented into the 4-point cage that separates the hexagonal cages from each other. Linker 3 coordinates to other Zn centers 3-dimensionally to assemble the major structure of ZIF-70. Finally there is linker 4, which is a 2-nitroimidazolate linker. This linker acts as the vertical backbone of the 6-point cages. Judging from the information provided by the crystal structure of ZIF-70, we postulated that the linker

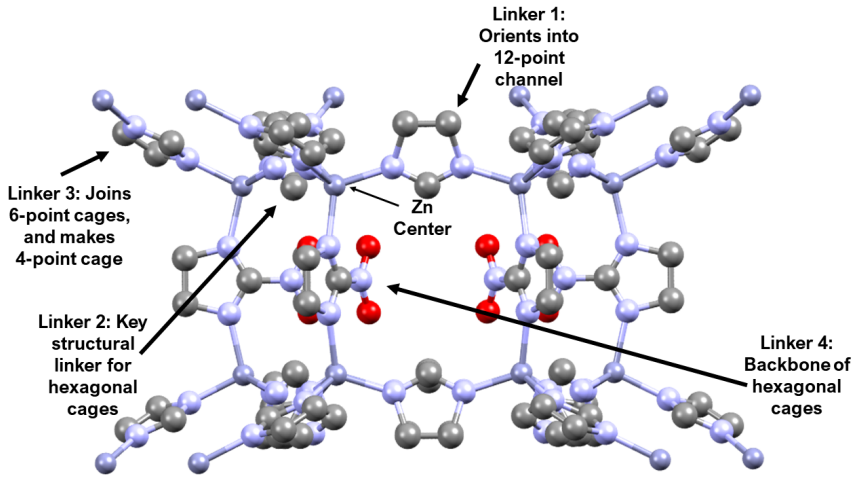

Figure 2.5: Side view of the pore of ZIF-70 illustrating the 4 unique linkers and their role in the overall structure of the MOF.

that is most likely to exchange with HL_1 would be Linker 1. The reasoning behind this initial prediction is that the 4,5-substituent sites of this linker orient themselves into the major 1.59 nm pore. Based on this observation that the 4,5-dithienyl substituted linker HL_1 would fit into this site as the sulfur heterocycles would occupy the free space in this large pore. This is the most likely substitution site as the steric environment required to fit L_1 into the other 3 positions is sterically impossible. This limits how many DTE linkers could be innstalled in the system. Given that 75% of the linkers are inaccessible to SALE with HL_1, only 25% of the total linkers can be substituted.

Crystal Structure of PSZ-1

With a better understanding of the structure of ZIF-70, the structure of PSZ-1 was explored (Figure 2.8). Initially, we were disheartened that the thiophene units of L_1 were not obviously observable in the difference map. Given that only 12.5 % of the ligands are substituted, it was anticipated that observing L_1 inside the pore of PSZ-1 would be challenging.

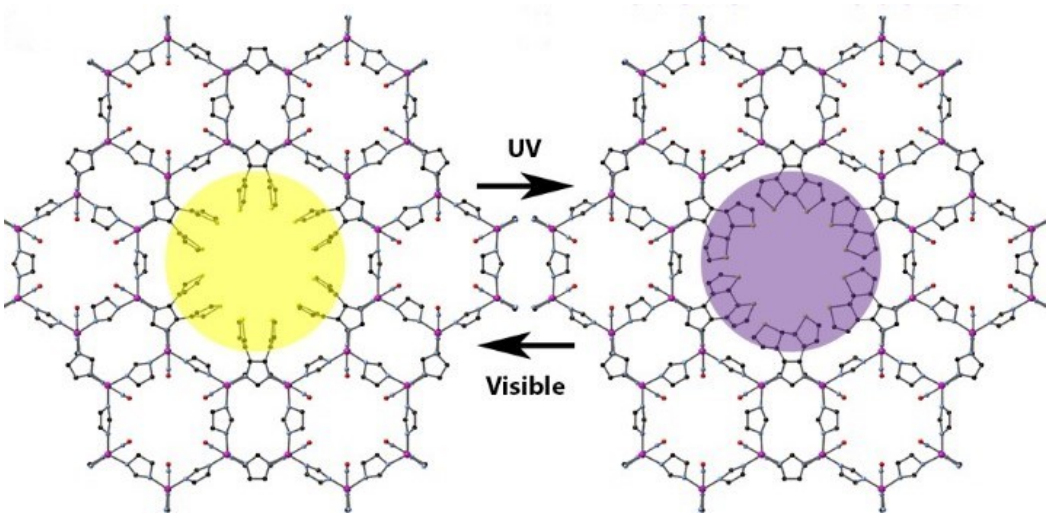

Figure 2.6: PSZ-1, formed via the solvent-assisted linker exchange (SALE) process with L_1 and ZIF-70 shown in both the open and closed conformation (modelled in crystal maker). Reproduced with permission from Journal of the American Chemical Society 2017, 139, 38, 13280 - 13283. Copyright 2017 American Chemistry Society.

Figure 2.7 illustrates the modelled disorder of the dimethylthiophene motif on L_1, which was another challenge encountered while solving the structure of PSZ-1. Assuming disorder of L_1 is 50/50 occupation in two places, each carbon atom in L_1 would diffract similarly to a hydrogen atom; any further disorder would further decrease the electron density (see 2.7. For this reason, very little diffraction data is present for this portion of the pore as seen in Figure 2.8.

To address the issue of L_1 and its disorder, each thiophene unit was geometrically placed at the appropriate bond length from the imidazole. The thiophene internal bonds (1-2, and 1-3 bond restraints) were fixed to their mean values with respect to one another (i.e., no bond length restraints were used to force a specific distance; similar bonds were forced to have an average difference of no more than 0.01 Å. The structure was allowed to refine so that the thiophene-imidazole bond was the only bond that could rotate. The occupancy was refined on the thiophene in order to determine the degree of incorporation. Using a shared isotropic temperature factor,

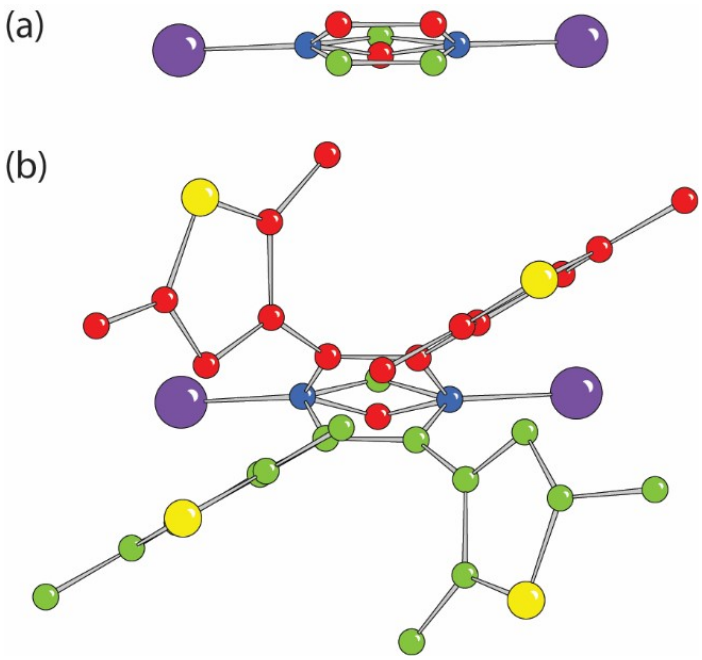

Figure 2.7: (a) side view of the disorder of the imidazole in ZIF-70. The angle between the two disordered units (the carbons in each disordered fragment are colour coded in green and red) is nearly 23 °. (b) side view of the disorder of the imidazole in PSZ-1. The angle between the two disordered units (the carbons in each disordered fragment are colour coded in green and red) is roughly 38 °. Reproduced with permission from Journal of the American Chemical Society 2017, 139, 38, 13280 - 13283. Copyright 2017 American Chemistry Society.

the thiophene moiety was able to refine its position until a minimum was observed.

The degree of linker incorporation determined through XRD studies showed good experimental agreement with the initial ^{1}H NMR studies (11.1 % vs. 12.5 % respectively). However, there is a considerable amount of unaccounted electron density in the region close to the linker. Once the structure was completed, it was observed that the angle between the two disordered imidazole rings was larger in PSZ-1 than ZIF-70 as illustrated in (Figure 2.7). This larger degree of disorder is attributed to the larger 4,5-dithienyl substituents, which are much more sterically encumbering than a proton.

These thiophene units were refined using thermal similarity restraints to that of the respective imidazolate. This was done in order to maintain reasonable anisotropic displacement parameters. Due to the forced thermal similarity restraints, the occupancy of these thiophene units are unreasonably lower because of disorder. However, due to the disorder in the structure and the concomitant low electron density of the thiophene portion of the linker, no further modeling was deemed reasonable.

Did A Double SALE Occur?

While not initially noticed at a first glance, the comparison of the ligand distribution in the hexagonal cages between PSZ-1 and ZIF-70 suggests that this reaction was more complex than initially perceived. More than one ligand displacement has occurred in the structure of PSZ-1. Figure 2.4 shows that there are 2-nitroimidazolates occupying coordination sites that are normally occupied by linker 3 (Figure 2.5) in the structure of ZIF-70.

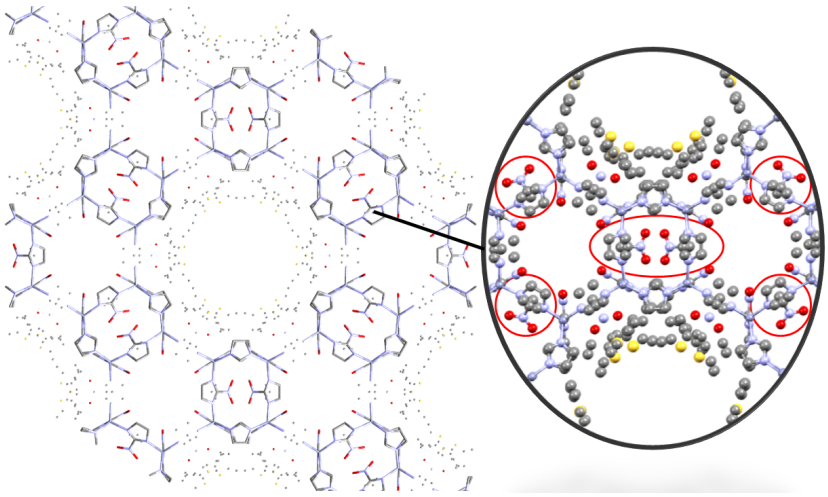

Figure 2.8: Close up of the *c*-axis of PSZ-1 illustrating the difference in linker distribution. The 2-nitroimidazolate linkers circled in red did not occupy these sites prior to the SALE reaction.

What is speculated to have happened is that the 2-nitroimidazolate linkers which

compose the backbone of the smaller pore of ZIF-70 shifted to this new position in order to maintain structural integrity of the MOF during the SALE (refer back to Figure 2.6). As the imidazoles that line the larger channel of ZIF-70 exit the pore, they leave behind vacant charge sites on the metal. As nitro groups are strong electron-withdrawing groups, a reasonable mechanistic proposal would be that these 2-nitroimidazolates shifted their position to help maintain structural integrity of the MOF using the dipolar nitro group, and facilitate the exchange between the imidazolate and L_1.

2.3.5 PXRD Analysis of PSZ-1

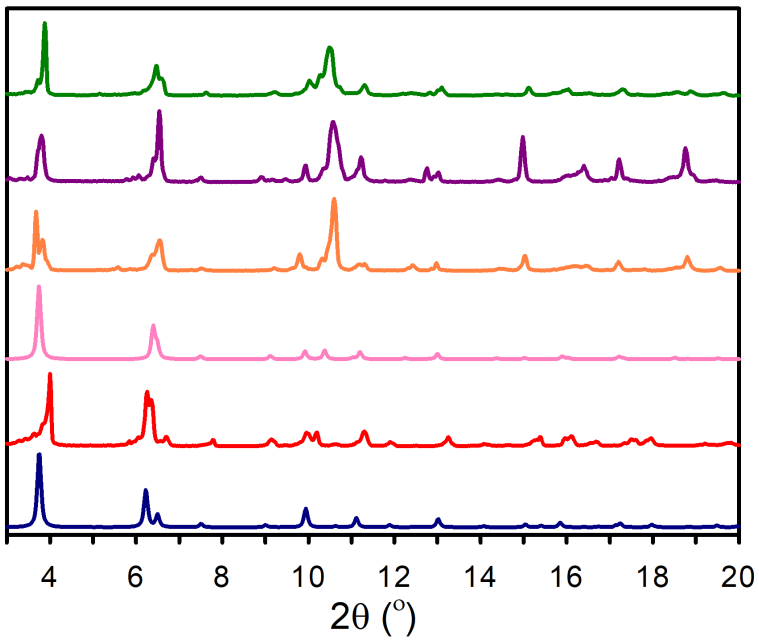

Figure 2.9: PXRD of ZIF-70 (Red), PSZ-1 Open (Orange) and PSZ-1 Closed (Purple), PSZ-1 5 Cycles (Green) plotted against the predicted PXRD of ZIF-70 (Blue) and PSZ-1 (Pink). Reproduced with permission from Journal of the American Chemical Society 2017, 139, 38, 13280 - 13283. Copyright 2017 American Chemistry Society.

Single Crystal X-ray Diffraction (SCXRD) is an excellent solid state characterization technique for structural determination. The previous section illustrated our efforts

to determine the linker loading and its positioning inside of the prepared porous material. With the linker quantified via ^{1}H NMR and structurally characterized using SCXRD, I next measured the solid state switching stability and its effect on the solid-state structure as a whole. PSZ-1 is visibly photo-active and changes from a yellowish orange to violet upon exposure to UV light. To test the materials solid-state structural stability over repeated cycles of irradiation with UV-Visible light, we performed Powder X-ray Diffraction (PXRD).

As indicated by the PXRD data in Figure 2.9, the synthesized materials are in good agreement with the simulated diffractograms. The diffraction pattern of ZIF-70 (red trace) is in good agreement with the simulated structure of PSZ-1 (pink trace). Since PSZ-1 incorporates the DTE photoswitching component in a Type II fashion, negligible structural rearrangement is expected on the overall framework of the MOF.

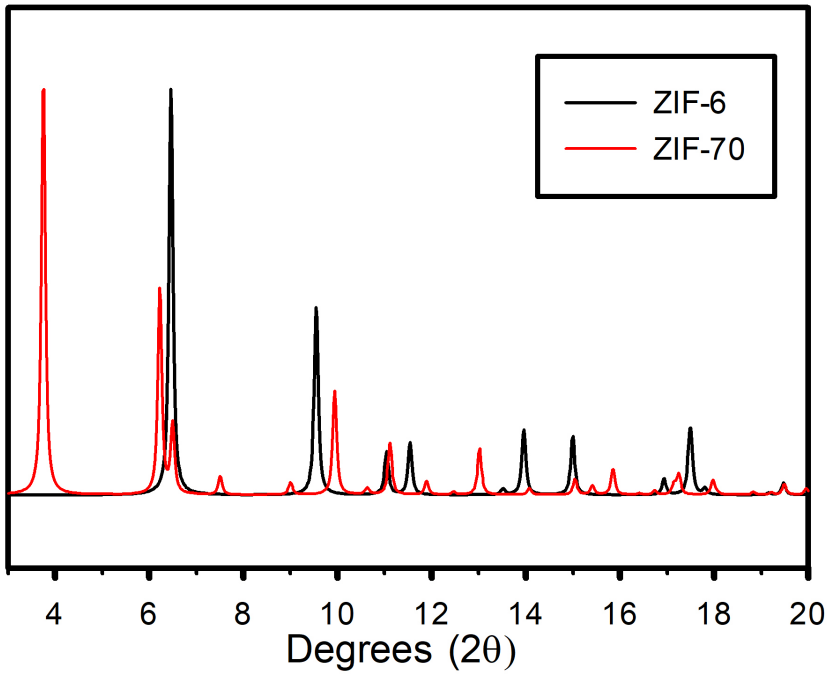

Figure 2.10: Overlapping PXRD of ZIF-70 (Orange), and ZIF-6 (Blue) illustrating the overlapping of major diffraction indices.

For this reason, we initially expected that the diffractograms of these compounds would be identical. However, it was observed that the peak at approximately 10.5° in 2θ is much greater in intensity than expected. This is suspected to be an impurity of ZIF-6, which formed during the SALE reaction of ZIF-70 with HL_1 to form PSZ-1. Since ZIF-6 is only made up of Zn and imidazoles, this could also help to explain why the 2-nitroimidazolates moved in the structure of PSZ-1. As this is an exchange reaction, it is likely that surface Zn ions and exchanged Linker 1 reassembled in solution and formed ZIF-6. This was further evidenced by the discovery of single crystals of ZIF-6 in a sample of PSZ-1.

The low angle diffractions of ZIF-6 at $\sim$ 6.5 and 9.5° in 2θ, which are the (011) and (020) plane respectively. These diffraction peaks are closely overlapping with the peak corresponding to the (101) and (002) plane of ZIF-70 (at 6.5 and 9.5 degrees (2θ) with the low angle diffraction peaks that correspond to ZIF-70/PSZ-1 (Figure 2.10). This suggests that HL_1 was able to incorporate and form PSZ-1 because of vacant spaces in the parent MOF created by exchanged linkers and leeched metal ions, which formed a new MOF as a side product.

The PXRD data of PSZ-1 suggests that even after 5 cycles of UV and Visible light triggered photoswitching, the crystallinity of the material appears unaffected, thus suggesting that the photoswitching process is not damaging the material.

2.3.6 BET Surface Area Analysis of PSZ-1

The intended goal of this research is to prepare a photo-switching MOF for more efficient gas separations. Naturally, gas adsorption experiments were performed to assess the porous properties of PSZ-1 using N_2 (77 K) gas-adsorption to assess the adsorptivity.

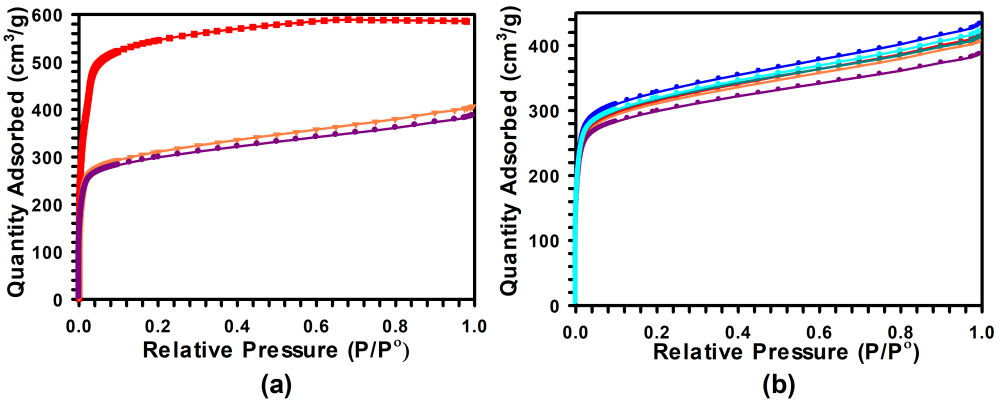

Figure 2.11: (a) Nitrogen gas adsorption isotherm at 77 K of ZIF-70 (red trace: BET surface area = 2000 m^2/g), PSZ-1-open (orange trace) and PSZ-1-closed (purple trace); BET surface area = 1250 m^2/g for both. (b) The effect of photo-cycling PSZ-1 as monitored by N_2 gas adsorption analysis at 77 K. Samples of PSZ-1 were exposed to UV-light to form PSZ-1-closed prior to measurements. After measurements, the sample was once again converted from PSZ-1-open to PSZ-1-closed and the gas uptake re-collected. The gas adsorption data illustrates very little change in surface area after multiple open/close cycles. Reproduced with permission from Journal of the American Chemical Society 2017, 139, 38, 13280 - 13283. Copyright 2017 American Chemistry Society.

As shown in Figure 2.11A, ZIF-70 has a Brunauer-Emmett-Teller (BET) surface area of 1750 m^2/g. This is the literature value as previously measured by Yaghi and co-workers PSZ-1 (orange trace) was measured to have a BET surface area of 1250 m^2/g. As PSZ-1-O was solvent exchanged multiple times in butanol, DMF and MeOH and then activated at elevated temperatures under high vacuum, the possibility of L_1 occupying the pore of PSZ-1 as a non-covalent guest (Type 0) was ruled out.

Next, the same sample of PSZ-1-O was exposed to UV light to promote photoisomerization to PSZ-1-C and then analyzed under identical experimental conditions. It was observed post-experiment that the sample of PSZ-1 had changed back to its yellow crystals while undergoing analysis. This means that PSZ-1-C reverted to PSZ-1-O independently and that the purple trace in Figure 2.11 represents the surface area

of PSZ-1-O after cycloreversion. Under identical conditions used in PXRD experiments, PSZ-1 was irradiated with UV light to undergo 5 cycles of photoisomerization and reversion, with the surface area of PSZ-1 being measured between each cycle (Figure 2.11B).

The BET surface area of PSZ-1 remains around 1250 m^2/g with an average variance of $\pm$ 50 m^2/g between cycles, which was considered an acceptable level of variation between samples.

We concluded that the light induced photoisomerization process of L_1 has no detrimental effects on the porous 3-D structure of PSZ-1. Despite the rate of cyclo-reversion being too fast to measure a surface area of PSZ-1-C, we have shown that the structure of PSZ-1 is stable even after 5 cycles of UV irradiation and thermal cycloreversion. Efforts to circumvent thermal cyclo-reversion is a matter that will be discussed in more detail in Chapter 3.

2.3.7 UV-Vis Spectroscopic Analysis of PSZ-1

In the previous sections, solid state properties of the MOF were determined including the linker loading of L_1, crystal structure, and porosity. It is also very important to examine and understand the spectroscopic properties of both the photoswitch and the MOF. Prior to studying the MOF, HL_1 was studied in solution to understand how the linker behaves spectroscopically and allow us to better predict the spectroscopic properties of PSZ-1.

As shown in Figure 2.12, in methanol solution, HL_1 photocyclizes when exposed to $\lambda \geq 254$ nm light. Over time with exposure to 254 nm light, absorptions at $\sim$ 300, 350 and 550 nm form, with a simultaneous decrease in the largest absorption peak centered

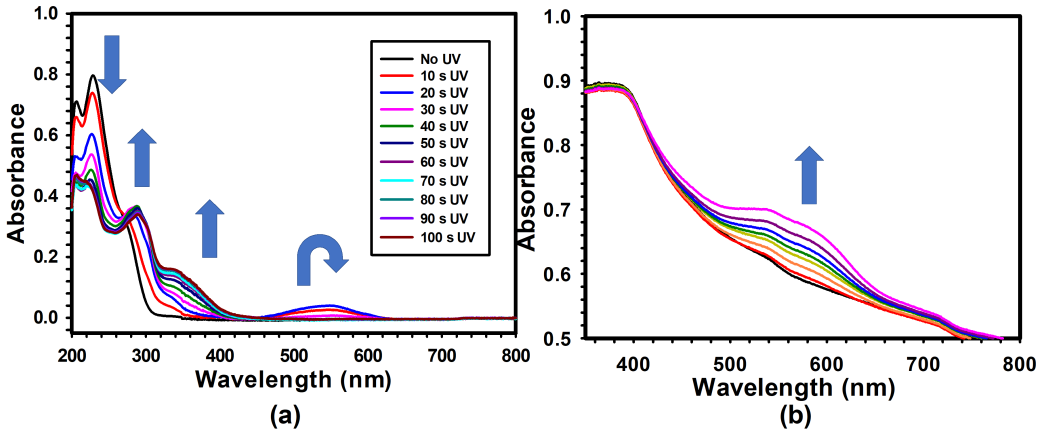

Figure 2.12: (**a**) 10^{-4} M solution of HL_1 in degassed MeOH. The solution was exposed to 10 second intervals of UV exposure up to 100 seconds. The closed form of HL_1 can be observed at 550 nm in the initial exposures (10–30 seconds) followed by a complete loss of intensity in following exposures. The product undergoes decay as illustrated by the loss of the coloured forms absorbance at 550 nm as well as decrease in the relative maxima at 230 nm, with a subsequent increase at 290 and 350 nm. (**b**) Solid State UV-Visible spectra of 1 % w/w PSZ-1 in KBr as a function of UV-light exposure time (1 min exposures up to 5 min, then a 5 min exposure to 10 min followed by a 10 min exposure, totaling to 20 min total exposure time). Reproduced with permission from Journal of the American Chemical Society 2017, 139, 38, 13280 - 13283. Copyright 2017 American Chemistry Society.

at 228 nm. The peak centered at 550 nm is attributed to visible light absorption by the photoisomer of HL_1. The peak centered at 550 nm reaches its maximum at $\sim$ 20 seconds of UV exposure, but quickly disappears back into the baseline over the span of a few minutes, eventually resulting in a total loss of absorption at 550 nm.

Meanwhile, the peaks centered at around 300 and 350 nm only continue to grow with additional UV exposure, with an irreversible loss of the absorption at 228 nm. This suggests that in solution, HL_1 is irreversibly undergoing photoisomerization to an undetermined by-product. While the structure of the degraded photoswitch was not isolated or determined, it is speculated that HL_1 formed a photoinactive isomer (Figure 2.13). To investigate this further, a sample of HL_1 was irradiated with excess

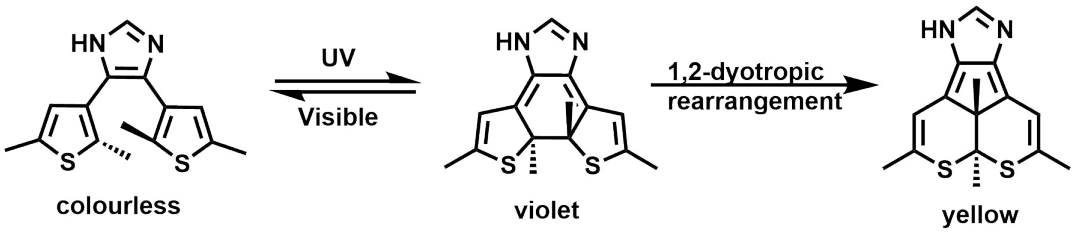

Figure 2.13: Proposed side reaction for irreversible loss of HL_1 in the closed form by 1,2-dyotropic rearrangement

UV light for several hours and then analyzed by APPI-MS, which indicated that the major [M+H] peak was 289 m/z, which corresponds to the molar mass of protonated HL_1. However, as this solution has been irradiated with excess UV light, it is impossible for this solution to contain open HL_1, which means that this compound has to be a photoinactive isomer. Photoinactive byproducts such as the structure illustrated in Figure 2.13 have been previously isolated by Irie *et al.*.[155] Interestingly, no evidence for formation of this byproduct was observed in the solid state (Figure 2.12), indicating that L_1 inside PSZ-1 is more stable to photodegradation than its solution-phase counterpart. As a control, ZIF-70 was also analyzed under the same conditions as PSZ-1 and showed no absorbance in the 550 nm region. With the spectroscopic behaviour of the ligand characterized, we turned our attention towards obtaining a better understanding of the spectroscopic properties of the MOF.

PSZ-1 was next studied in the solid state to assess its spectroscopic response over multiple cycles of UV and Visible light irradiation. Yellow crystals of PSZ-1-O convert to violet crystals of PSZ-1-C upon exposure to UV-light ($\lambda \leq 254$ nm). Similar to HL_1 in solution, a drastic colour change was observed for PSZ-1, which was accompanied by a new absorption band at 550 nm (Figure 2.12). If PSZ-1-C is subsequently exposed to visible light ($\lambda \geq 515$ nm), then PSZ-1-O is regenerated.

To illustrate the reversibility of the photo-isomerization process of PSZ-1, the MOF

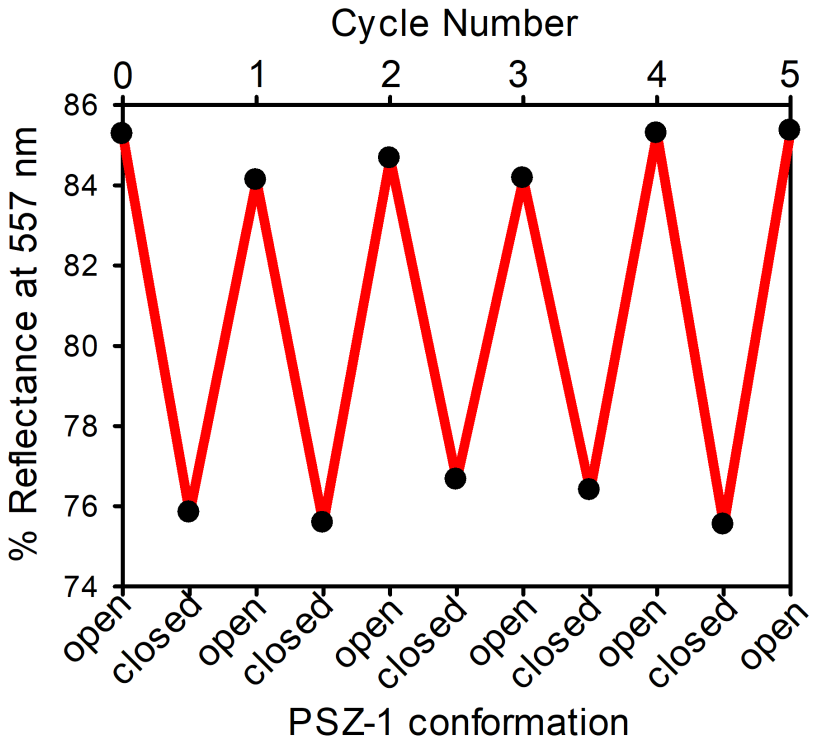

Figure 2.14: Solid state UV-Visible Spectroscopy of PSZ-1. The % reflectance at 557 nm was monitored under different irradiation wavelengths (254 nm for UV, and $\lambda \geq 515$ nm for visible light). The drop in % reflectance is attributed to increased absorbance at 557 nm, which is a result of formation of the closed form isomer of the incorporated imidazolate linker. PSZ-1 was shown to be cyclable up to a minimum of 5 times with no degradation. Reproduced with permission from Journal of the American Chemical Society 2017, 139, 38, 13280 - 13283. Copyright 2017 American Chemistry Society.

was exposed to five UV-Visible exposure cycles allowing PSZ-1 to change between conformations, and then revert back to the open conformation over time. PSZ-1's spectroscopic response was monitored in % Reflectance as illustrated in Figure 2.14. The consistent drop in % reflectance is attributed to the photo-isomerization of HL_1 to its closed form isomer, and the following increase to the near orginal % reflectance is observed to be the cycloreversion of HL_1 to its open form conformation. Another

important observation from these spectroscopic properties is that unlike HL_1 in solution, based on the reflectance spectra and NMR analysis of dissolved MOF post radiation, there is no evidence of any decay of PSZ-1 to a photo-inactive state.

2.3.8 Photoswitchable Uptake Studies

This section details investigations into the photoswitching properties of PSZ-1 for photoswitching adsorptivity. Type II photoswitching MOFs have potential to alter the environment of the pore/pore aperture without significantly altering the framework of the MOF. This allows for changes in adsorptivity to occur via light-controlled excitation, which has literature precedent as illustrated in the work of Guo and co-workers as well as Yaghi and co-workers who illustrate that photo-active MOFs have switchable retention of guest molecules inside the pore for cargo uptake/release applications. As mentioned in the gas sorption section, the thermal-reversion of L_1 was too fast to study gas phase differences between PSZ-1-O and PSZ-1-C, thus alternative methods of analysis were devised.

To demonstrate potential separation properties of PSZ-1, a solution-phase filter experiment that resembles the work of Moon *et al.* was devised.[156] For context, the work of Moon *et al.* To demonstrate that PSZ-1 possesses different adsorptivity between the open and closed conformers, the elution and separation of a 1:1:1 weight % solution (5 mg/mL) of toluene, naphthalene and pyrene through the MOF pore was analyzed. Further, 100 μL of 50 mg/mL sulfolene was used as an external reference to monitor the concentration of the analytes post-filtration. Internal standards are not suitable for this experiment because the concentration of sulfolene that exits the MOF pore cannot be determined post-filtration, and would render the obtained concentrations of analyte meaningless. For this reason, the eluent is spiked with external standard

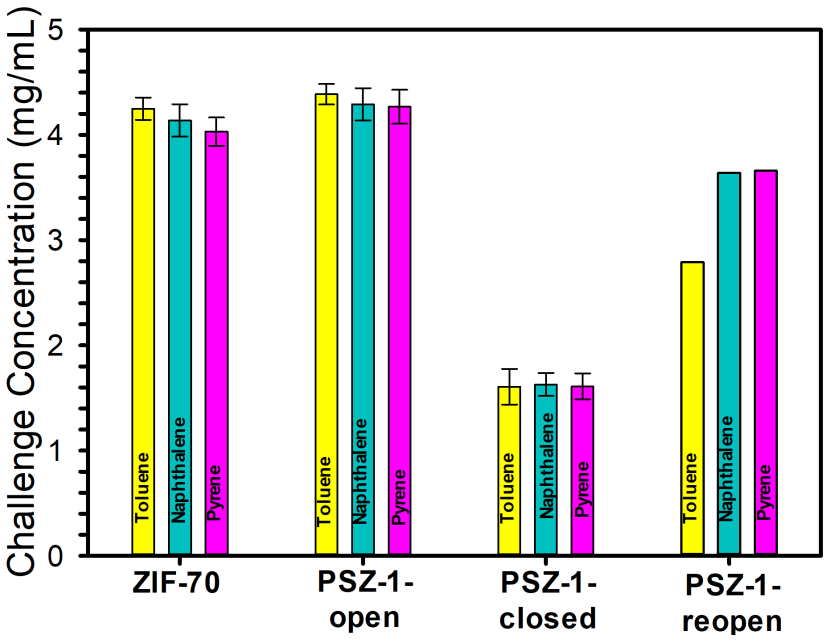

Figure 2.15: Concentration of aromatic hydrocarbon filtrate through the MOF filters; toluene (Yellow), naphthalene (Turquoise), and pyrene (Purple). Reproduced with permission from Journal of the American Chemical Society 2017, 139, 38, 13280 - 13283. Copyright 2017 American Chemistry Society.

of a known concentration instead of using an internal reference. Sulfolene was used specifically because its ^{1}H NMR signals do not overlap with any of the eluent peaks.

The original intent of this experiment was to investigate the possibility of a size-exclusion effect (i.e., could we selectively adsorb the relatively small analyte toluene, as the larger analytes diffuse through or around the crystalline nanochannels). However, the results obtained in Figure 2.15 seem to indicate that this is not the trend that is being observed. As shown in Figure 2.15, when the control sample ZIF-70 is used as a filter, there is little retention of analytes. When PSZ-1-O is used as a filter, there is a slight increase in analyte retention when compared to ZIF-70. When PSZ-1-C is used as a filter, a large retention of analytes is observed indicating that the exposure to UV light has changed the pore characteristics.

There are generally 2 accepted ways to interpret this change in adsorptivity:

1. The photoswitching linker that lines the pore has introduced a change in pore size.

2. The change in electronic structure from photoisomerization has altered the polarizability inside pore.

The lack of any differences in concentration between analytes would strongly suggest that the observed changes in the MOF is likely electronic and not steric in origin, which is supported by previously reported findings by Huang *et al.* who performed similar diffusion studies on Type II Azobenzene MOFs with dye guests that are sensitive to changes in polarization.[157] As another test, a sample of PSZ-1-C was allowed to relax back to PSZ-1-O and was then reused as a filter. The obtained concentrations show that the solution-phase adsorptivity resemble PSZ-1-O, which indicates reversible behaviour.

2.4 Conclusions

In summary, a Type II photoswitching MOF derived from a dithienylethene photoswitching linker was synthesized and characterized. PSZ-1 shows a reversible photoisomerization between the UV absorbing open conformation (PSZ-1-open) and the visible-light absorbing closed conformation (PSZ-1-closed). We demonstrated that light can be used to change the host-guest interactions to make it easier to alter the elution rate allowing separations based on host-guest interactions such as those shown with toluene, naphthalene, and pyrene. With PSZ-1 and the tailorability of DTE photoswitches, new properties can be introduced into the pore without the need to necessarily consider the synthetic challenges of introducing carboxylate or pyridyl

groups onto the thienyl moieties.

Chapter 3

Quantitative Determination of Linker Content For Observing Photo-inactivity in a Photoswitching Metal-Organic Framework

3.1 Introduction

In Chapter 2, light controlled adsorptive behaviour from a novel Type II photoswitching DTE MOF (PSZ-1) used as a fixed adsorbing bed is reported. PSZ-1 showed different adsorption properties, which corresponded with the molecular state of the photochromic DTE linker that lined the inside of the pore. There were no observable signs of material degradation, as determined through various spectroscopic, X-ray,

and porosity studies.[158]

Moving forward from the work described in Chapter 2, one of the material properties that needed to be addressed to make studying PSZ-1 and future related materials practical was improving the lifetimes of the photocyclized isomer.

As previously observed (qualitatively), the lifetime of PSZ-1 in the closed form (PSZ-1-C) was short-lived (i.e., a few minutes). This observed chemical behaviour is due to thermal cyclo-reversion (TCR).[159] TCR is a side process in DTE/DAE chemistry by which the closed isomer reverts to the respective open isomer independently of UV-Visible light via thermal processes. The rapid rate of TCR observed in PSZ-1 limited our ability to perform gas-phase photoswitching adsorption studies of PSZ-1-C. this is because PSZ-1-C reverts to PSZ-1-O by the time the instrument begins collecting gas adsorption data.

Studies by Kitagawa *et al.* show that the rate of TCR in DTE molecules vary with the electronic structure and sterics of substituents vicinal to the reactive carbon sites.[160,161] For example, its been well established that structural motifs with extended π-conjugation such as fused aromatics, and heterocyclic moieties contribute greater aromatic stablization energy to the photoisomer and negate this involuntary process.

Other useful building blocks include the perfluorocyclopentene motif that holds the the thienyl groups anti-parallel to one another. In specific cases, the perfluorinated ring structure renders the molecule thermally stable, and more resilient to oxidative degradation pathways.[162–165] Irie has also illustrated that electron-rich methoxy groups ($-OCH_3$) improve the stability of the DTE isomer via electron donation onto the reactive carbon sites, which stabilizes the σ-bond that forms under UV-irradiation.

To study the PSZ MOF system and improve the photoswitching stability systematically, the photochromic linker HL_1 was retained as the core skeleton to serve as a point of reference for this study. The 2-imidazoyl site of the HL_1 core structure was considered an interesting and good starting point to move forward, as substitents at this position are typically inaccessible in perfluorocycloalkene derivatives.

In the PSZ system, the 2-imidazoyl substituent points out of the main 1.6 nm channel when integrated into the structure of PSZ-1, which was determined through previously obtained crystal data. Knowing this, non-hydrogen substituents can change the photophysical properties of the linker, since the 2-imidazoyl position is in-plane with the 8-π electron conjugated system when excited to the closed isomer. Altering the photo properties of the linker also changes the electronic structure of the photoswitching linker, which can also directly alter the gas adsorption of the MOF for a more efficient uptake in analyte.

The introduction of these new substituents is also an easy task. By using essentially any substituted aldehydes with the previously synthesized 1,2-dione precursor, a small library of new HL_x type linkers and photoswitching MOFs can be synthesized and characterized using previously established protocol from Chapter 2.

3.2 Experimental

3.2.1 Materials and Methods

Unless otherwise specified, all reagents were used as received from commercial suppliers without further purification. Dichloromethane (DCM) and pyridine were distilled and stored over activated 4 Å molecular sieves. All column chromatography was performed with 230-400 mesh silica. For non-MOF samples, all ^{1}H NMR were recorded

on a Bruker AVANCE 500 MHz NMR spectrometer using $CDCl_3$ or DMSO-d_6. For MOF samples, and filtration experiments, a Bruker AVANCE III 300 MHz NMR spectrometer was used. For MOF samples, DMSO-d_6 + 3 drops of deuterated sulfuric acid (D_2SO_4) was used as the NMR solvent (the spectra for the MOFs was referenced to DMSO-d_6). For filtration experiments, $CDCl_3$ was used as the solvent. Solid state UV-Visible measurements were recorded on an Ocean Optics USB4000 Spectrometer using the reflectance probe accessory (Integration time: 200 ms; Scans averaged: 10; Boxcar width: 10). Solution-phase UV-Visible measurements were performed on a Cary 100 Series UV-Visible Spectrometer in the range of 200-650 nm. Kinetic experiments were measured on the Cary 100 Series UV-Visible Spectrometer using the included kinetic profile monitoring with 60 second intervals between measurements. Powder X-ray diffraction (PXRD) patterns were obtained using a Rigaku X-ray Ultima IV Diffractometer equipped with a copper X-ray source and a scintillation counter detector. Samples were measured from 3-20° in 2θ using a scan speed of 1 °/min. Nitrogen gas adsorption isotherm data were collected at 77 K on a Micromeritics Tristar 3020 surface area and porosity analyzer. All samples were activated on a Micromeritics Smart VacPrep instrument by heating the sample to 120 °C (5 °C/min) while slowly reducing the pressure (5 mmHg/s) within the sample holder. The sample was maintained at this temperature and low pressure for 10 h. The sample was then cooled to room temperature after which the sample holder was backfilled with nitrogen gas.

3.2.2 Protocol for Photoswitching Linkers

Using protocol from Chapter 2, 1,2-bis-(2,5-dimethyl-thiophen-3-yl)-ethanedione (1.00 g, 3.5 mmol), NH_4OAc (8.31 g, 105 mmol), and 10.5 mmol of the corresponding aldehyde (HL_1: formaldehyde; HL_2: acetaldehyde; HL_3: benzaldehyde) were dissolved

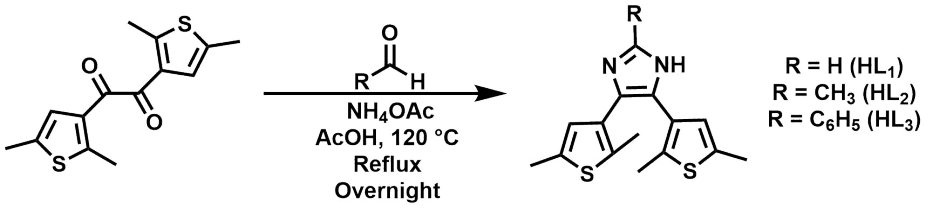

in 20 mL of glacial acetic acid in sealed pressure vessel and refluxed overnight at 120 °C with stirring. The resulting mixture was concentrated under reduced pressure, and the residue was diluted with with water and neutralized with slow addition of saturated Na_2CO_3 solution until pH paper turned green indicating pH in the range of 7-8. The resulting precipitate was extracted using 3 × 50 mL portions of $CHCl_3$, dried with $MgSO_4$, and concentrated under reduced pressure to yield a light beige solid.

4,5-bis(2,5-dimethyl-3-thienyl)-2-methyl-1H-imidazole (HL_2)

Yield: 410 mg, 38 %. ^{1}H NMR (500 MHz, $CDCl_3$): δ (ppm) 6.58 (s, 2H), 2.40 (s, 3H), 2.34 (s, 3H), 1.98 (s, 3H). Two sets of broadly overlapped isomers indicating an isomeric mixture are observed in non-acidified DMSO-d_6.

4,5-bis(2,5-dimethyl-3-thienyl)-2-phenyl-1H-imidazole (HL_3)

Yield: 600 mg, 46 %. ^{1}H NMR (500 MHz, DMSO-d_6): δ (ppm) 12.48 (s, 1H) 8.02 (d, J = 7.2 Hz 2H), 7.43 (t, J = 7.2 Hz, 2H), 7.33 (t, J = 7.2 Hz 1H), 6.73 (s, 1H), 6.56 (s, 1H) 2.40 (s, 3H), 2.32 (s, 3H), 2.14 (s, 3H) 1.97 (s, 3H).

3.2.3 Synthetic Protocol for PSZ MOF

This procedure is reported in our previous work and is based on the Solvent-Assisted Linker Exchange (SALE) protocol. To a 25 mL vial, HL_x (0.20 mmol) was added and dissolved via sonication in 20 mL of *n*-BuOH. To this solution, ZIF-70 (50 mg, 0.20 mmol) was added and the mixture was heated for 3 days at 110 °C.

Afterwards, the solution was cooled to room temperature, and the solvent decanted. The solid yellow crystals were washed with 3 × 20 mL portions of DMF and 3 × 20 mL portions of MeOH. The resulting solid was then decanted into a clean vial and stored in fresh DMF until needed for further use. Prior to use, the crystals were solvent exchanged with methanol and then thermally activated through the use of a vacuum oven at 100 °C. PSZ-2 was synthesized using HL_2 (60 mg, 0.20 mmol). The imidazole:nitroimidazole:L_2 was 1.00:0.70:0.05.

The synthesis of PSZ-3 using HL_3 (75 mg, 0.20 mmol) was attempted using the outlined preparation above. The MOF was dissolved and analyzed in DMSO-d_6 + 3 drops D_2SO_4. No indication of HL_3 was observed in the ^{1}H NMR spectrum.

3.3 Results and Discussion

3.3.1 Characterization of Free Linkers

HL_1-HL_3 were prepared via the reaction of 1,2-bis(2,5-dimethyl-thien-3-yl)ethanedione, excess ammonium acetate and the corresponding aldehyde (formaldehyde, acetaldehyde and benzaldehyde respectively for HL_1, HL_2, and HL_3). The structures were confirmed by ^{1}H NMR, and their respective yields were determined to be 58 %, 38 %, and 46 %.

The ^{1}H NMR of HL_1 is shown in Figure 3.1. The spectrum was recorded in both DMSO-d_6 (Figure 3.1; bottom spectrum), and DMSO-d_6 acidified with 1 drop of D_2SO_4 (Figure 3.1; top spectrum).

In the acid-free ^{1}H NMR, we noted that there are two atropisomers. These atropisomers of HL_1 are produced by restricted single bond rotation of the thienyl rings

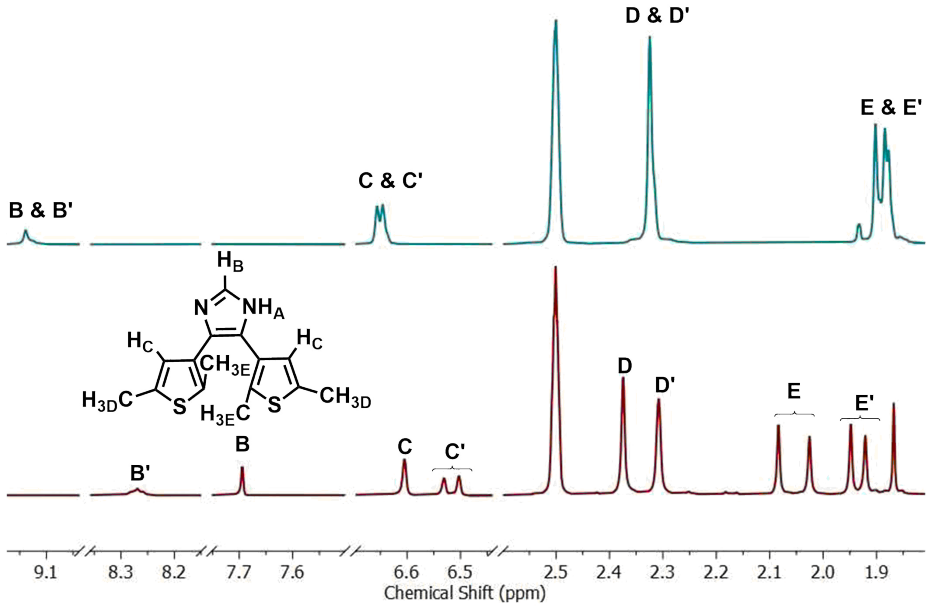

Figure 3.1: ^{1}H NMR of HL_1 in neutral DMSO-d_6 (bottom spectrum), and DMSO-d_6 acidified with 1 drop of D_2SO_4 (top spectrum).

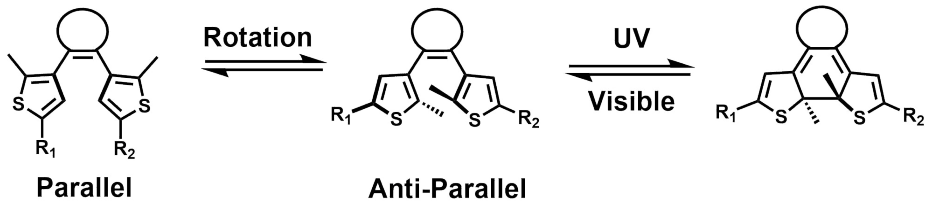

Figure 3.2: Illustration of the parallel and anti-parallel atropisomers of DTEs. The parallel atropisomer is photoinactive, while the anti-parallel atropisomer can photoisomerize.

that results in two distinct conformations for the thienyl rings (Figure 3.2). HL_1 appears to be an almost 1:1 ratio of atropisomers in non-acidic DMSO-d_6 solution. When the solution is acidified, we only observe 1 set of peaks for the molecule, but at a different chemical shift than either of the previously mentioned atropisomers in the acid-free NMR. The acidified NMR solvent appears to allow free interconversion between atropisomers of protonated HL_1, which creates a spectrum with one set of shifted ^{1}H NMR peaks.

This trend was also observed with HL_2, which shows a mixture of isomers in neutral DMSO-d_6 solution. The corresponding peaks for HL_2 in DMSO-d_6 solution are broadly overlapping and show two sets of peaks. When analyzed in acidic DMSOd_6 solution, only one set of peaks are observable. With HL_3, we once again see two sets of peaks consistent with the presence of atropisomers, as the two sets of peaks in HL_3 exist in a 1:1 ratio.

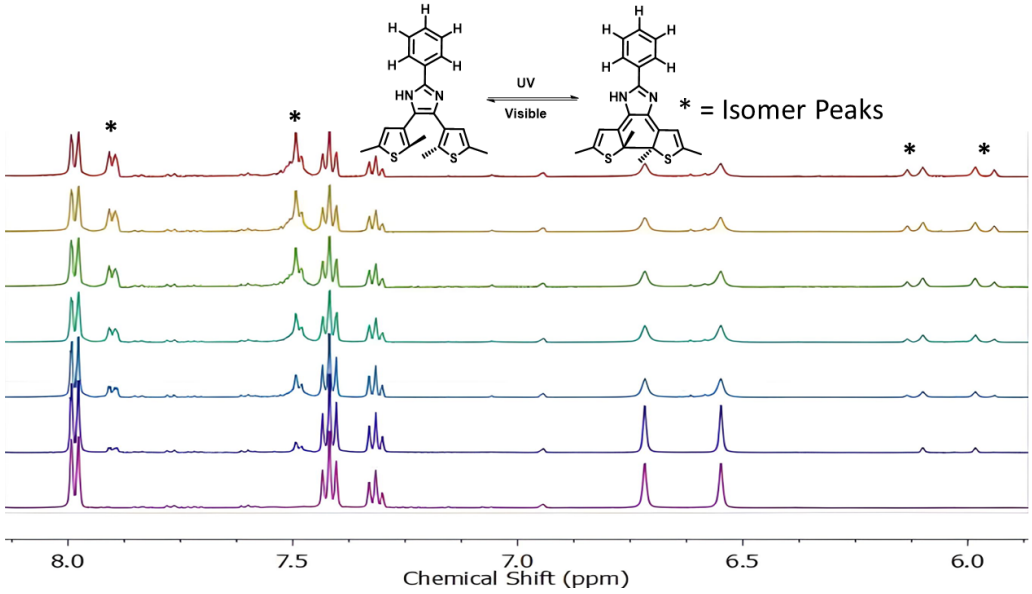

Figure 3.3: ^{1}H NMR stack of HL_3 in degassed DMSO-d_6. The same pristine sample (purple trace, bottom) was irradiated in 10 minute intervals to ensure homogeneous irradiation of the sample in the tube until peak growth stopped at 60 minutes (red trace, top). Small peaks (asterisked) of HL_3-closed begin to appear in the spectrum as a function of UV light exposure over time.

In working with HL_1-HL_3 in solution for the NMR data, I took the opportunity to shine UV-light on the NMR tubes to see if a colour change is visible and persists for the three linkers. Indeed, all three linkers show a distinct colour change (see below for quantitative analysis). Perhaps most interestingly is that the colour change of HL_3 (i.e., a change from colourless to violet) persisted longer than HL_1 and HL_2. The characteristic violet colour of HL_3 in a degassed J Young NMR Tube persisted for 3 days

and was successfully observed in the ^{1}H NMR spectrum of HL_3 (Figure 3.3). Interestingly, solution-phase NMR shows that the material is susceptible to degradation if exposed to excessive UV. This was determined by monitoring the NMR spectrum over time and observing the irreversible growth of new broadened peaks (7.89, 7.42, 6.10, and 5.95 ppm) in the spectrum, with subsequent loss of open isomer peaks. No such degradation is observed in the solid state of HL_3. This data suggested that HL_3 may have the necessary lifetime in the closed form of the linker to allow us to explore gas-phase adsorption in the closed form.

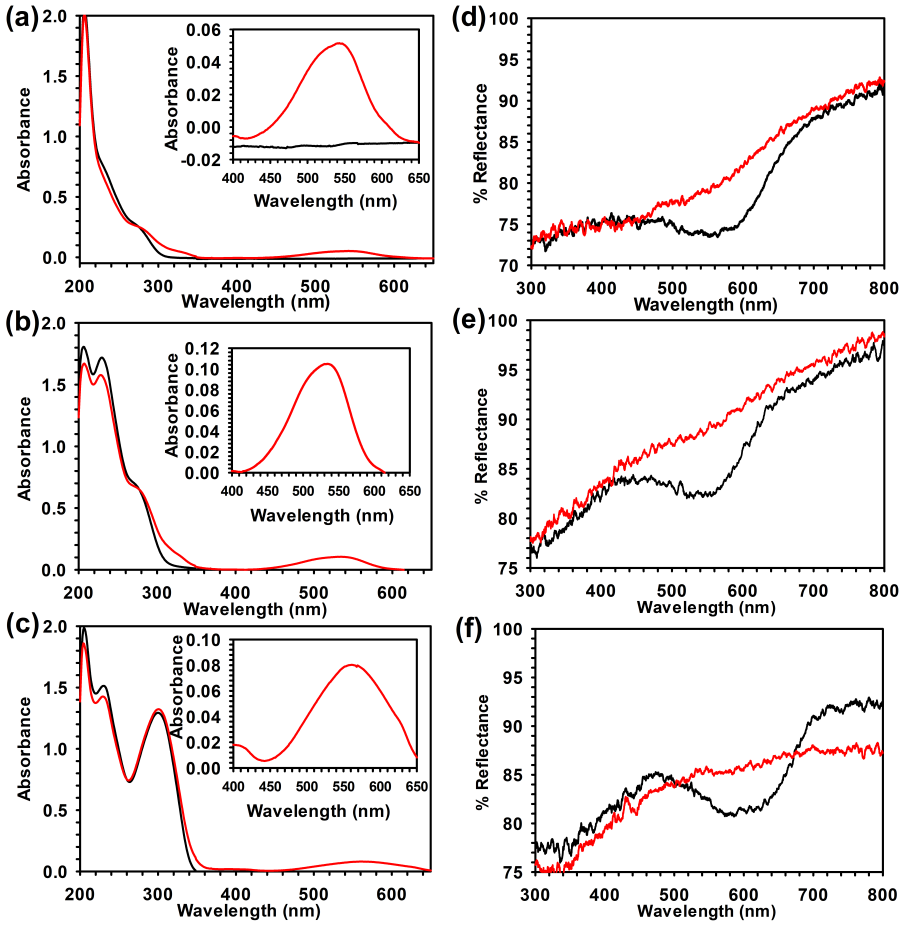

Figure 3.4: (a) Solution-phase UV-Vis of 2.0×10^{-4} M HL_1 solution in MeOH (b) Solution-phase UV-Vis of 2.0×10^{-4} M HL_2 solution in MeOH (c) Solution-phase UV-Vis of 2.0×10^{-4} M HL_3 solution in MeOH (d) Solid-phase UV-Vis of HL_2 (e) Solid-phase UV-Vis of HL_2 (f) Solid-phase UV-Vis of HL_3.

To further explore the photoisomerization of these linkers, we examined the spectroscopic behaviour via UV-Vis spectroscopy. By only varying the 2-imidazoyl position, it is simpler to attribute the change in electronic structure and photo-physical behaviour to the new substituent (Figure 3.4). For HL_1-HL_3, the as-synthesized linkers showed no absorption at wavelengths greater than 350 nm (i.e., lower energy). The absorptions below 350 nm are attributed to the thienyl groups and the phenyl group (HL_3).

Upon photo irradiation with UV-light under degassed conditions, a new absorption band showed up at 538, 534, and 550 nm (Figure 3.4, a-c). This band is consistent with what we would expect for the closed isomer. Given the similar concentration of these solutions, HL_2 either has a higher extinction coefficient in the closed state, or the photostationary equilibrium between the open/closed state favours greater concentration of the closed form.

We also explored the photoisomerization of these linkers in the solid state. As shown in Figure 3.4 (d-f), a similar change in the behaviour of the linkers around 550-600 nm range is observed. Specifically, the three linkers reflect less light, which is attributed to greater absorption at 550, 560, and 600 nm for HL_1, HL_2, and HL_3 respectively.

Following up on these observations, we examined the thermal cycloreversion rates as a function of time at room temperature using solution-phase UV-Vis spectroscopy (Figure 3.5). Solutions of HL_x were irradiated with the short wavelength setting of the UV lamp for formation of the closed isomer until the change in the visible light absorbance plateaued. These solutions were then allowed to stand at room temperature; the loss of absorption of the closed isomer was subsequently monitored until it receded into the baseline. The thermal cycloreversion of HL_x follows a first-order rate law indicating that thermal cycloreversion are uni-molecular in rate. The

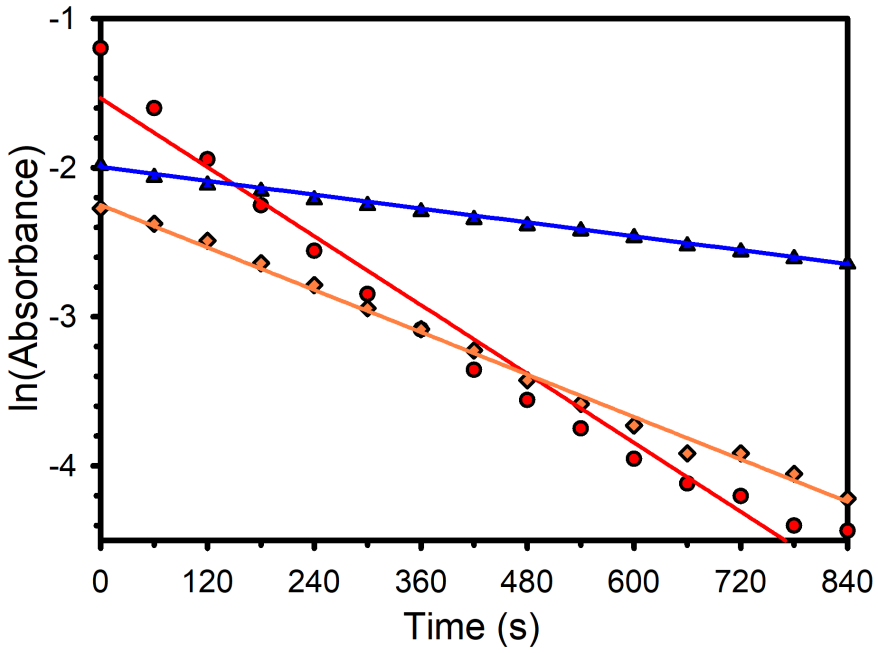

Figure 3.5: Thermal cycloreversion of closed isomers to open isomers of HL_1 (red dots), HL_2 (blue triangles), and HL_3 (orange squares) in 10^{-4} M acetonitrile solutions. Absorbance loss in the visible region was monitored as a function of time. First order rate constants were determined from the slope of the line.

rate constants obtained for thermal cycloreversion are reported in the following table:

Table 3.1: Experimentally Calculated Kinetic Parameters for HL_x

Linker (Sample Name)	Rate Constant (s^{-1})	Half-Life (s)
HL_1	0.0039	174
HL_2	0.0008	864
HL_3	0.0024	264

This obtained data suggests that electron-donating substituents are beneficial for the overall stability of the closed form isomer of our linkers. To further probe this trend we fit the obtained rate constants to a Hammett Plot as seen in Figure 3.6. Similar work has been performed by Kitagawa *et al.*, while performing structural

analysis of DTEs modified at their reactive center. Hammett Plots (Equation 3.6) depict the relationship between kinetic rates and substituent constant σ.

$$log\frac{k_H}{k} = \sigma^+\rho \tag{3.1}$$

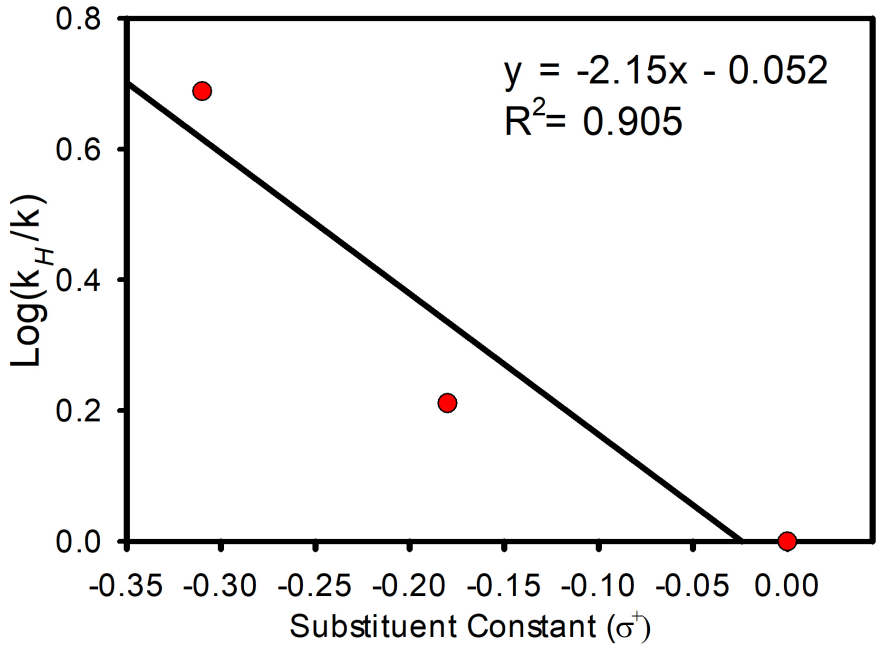

Figure 3.6: Hammett Plot analysis of the effect of 2-imidazoyl substituents on the lifetime of the closed form isomer of imidazole based DTE photoswitches. Where k is the rate of thermal cycloreversion (s^{-1}), k_H is the reference rate of a proton substituent (s^{-1}). The Hammett parameters were obtained from Chem. Rev. 1991, 91, 165-195.

In Equation 3.1, k is the rate constant of the measured substrate, k_H is the rate of the proton substituted molecule (HL_1 in this study), and ρ is the reaction constant. In the logarithmic form of the equation, a plot of the log of the ratio of rate constants as a function of substitution constant results in a slope of the line equal to the reaction constant (ρ). The obtained value of ρ is an informative measurement that provides information about the mechanism by which the measured species proceeds to react. A

positive value indicates negative charge is built during the reaction; a negative value indicates that the reaction builds positive charge, at the reactive site (the reactive thienyl carbons, i.e., the inner methyl groups).

The obtained Hammett parameter (ρ = -2.15) from the trendline experimentally agrees with a build-up of positive charge and indicates that electron donating groups are beneficial for the overall lifetime and thermal stability of the HL_x series of linkers at the 2-imidazoyl position. Through this substituent analysis, we obtained a better understanding about improving the electronic effects in a previously uncharacterized molecular site. With these new linkers characterized, we moved forward and attempted to build them into a MOF.

3.3.2 Synthesis and Linker Loading of PSZ MOFs

With our linkers spectroscopically characterized, we moved forward and used these linkers in SALE protocol similar to the procedure used to synthesize PSZ-1.

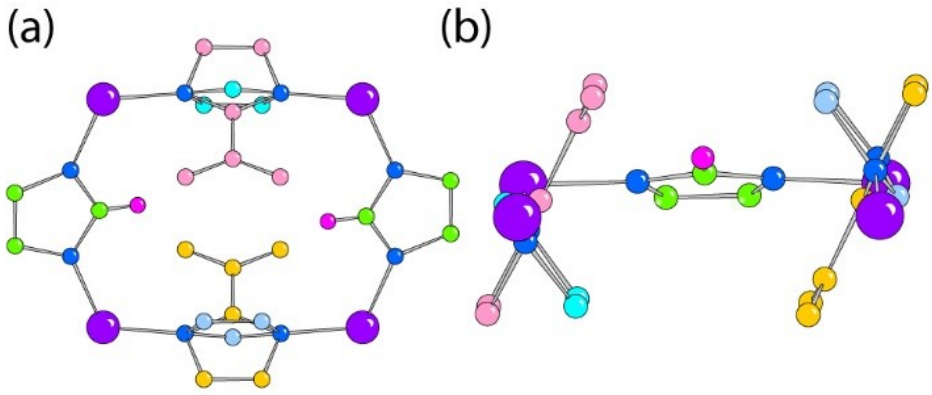

Figure 3.7: The structure of PSZ-1 showing the steric profile around the atom (magenta) bonded to the C_2 position of the DTE-containing imidazole; the bond distance represents a C-H bond in the figure. The structure shows the disordered imidazolates and nitroimidazolates (light blue/pale blue, and pink/orange respectively) that limit the sterics above and below the linker. The structure also shows the limited space caused by the DTE from the neighbouring 1.6 nm pore. (a) top view down the c-axis. (b) side view showing only one of the two DTE-containing linkers.

The SALE between HL_1 and ZIF-70 was discussed in Chapter 2. As a reminder, dissolving the post-SALE MOF and analyzing the ^{1}H NMR, we were only able to incorporate 12.5 % linker, corresponding to 50 % of Linker 1 in the large pore. Similar analysis was performed for the other two linkers.

The SALE between HL_2 and ZIF-70 (PSZ-2) showed that only 2.9 % L_2 was incorporated; this represents 11.4 % of the imidazoles decorating the large pore. Given that L_2 is expected to have a higher pK_a than imidazole and nitroimidazole,[166] the low linker incorporation is likely attributed to steric limitations associated with the methyl group in the 2-imidazoyl position of L_2 rather than any limit caused by competitive substitution. Figure 3.7 shows the local structure of PSZ-1 surrounding the L_1 linker, where green atoms represent the carbons and blue atoms represent the nitrogen atoms; the magenta atom is the proton on HL_1. This can be viewed as the position of the methyl and phenyl group of HL_2 and HL_3 respectively. On either side of the 2-imidazoyl postion of L_x there is a roughly 1:1 mixture of imidazole (carbon atoms represented in light blue and pale blue) and nitroimidazole (carbon atoms represented in pink and mustard). The extra spatial requirements of the additional methyl group in L_2 are sterically more hindering, when compared to L_1.

To determine if the exchange is occurring uniquely on defect-laden surface of PSZ-2, crystals of ZIF-70 were gently crushed with mortar and pestle and then lightly ground into a powder prior to SALE. NMR analysis of the crystals indicate that no additional incorporation of HL_1-HL_3 occurs in PSZ MOFs whether the sample of parent ZIF-70 is pristine, or ground up crystals. With this information, we now know that the 2.9 % inclusion of L_2 in PSZ-2 does not represent surface-only functionalization, but is the steric limits of the linkers ability to incorporate into the structure of ZIF-70 because of disfavoured steric interactions from the methyl group of L_2 within the MOF.

Examining the SALE between ZIF-70 and HL_3, we see that no HL_3 is incorporated into ZIF-70. This is not surprising given that steric interactions illustrated in Figure 3.7 combined with the size of the phenyl group on HL_3. This clearly indicates that the SALE process did not occur, and that the MOF retrieved from the reaction is simply the parent MOF: ZIF-70. The chemistry of HL_3 with ZIF-70 was not further explored.

3.3.3 PXRD Analysis of PSZ-2

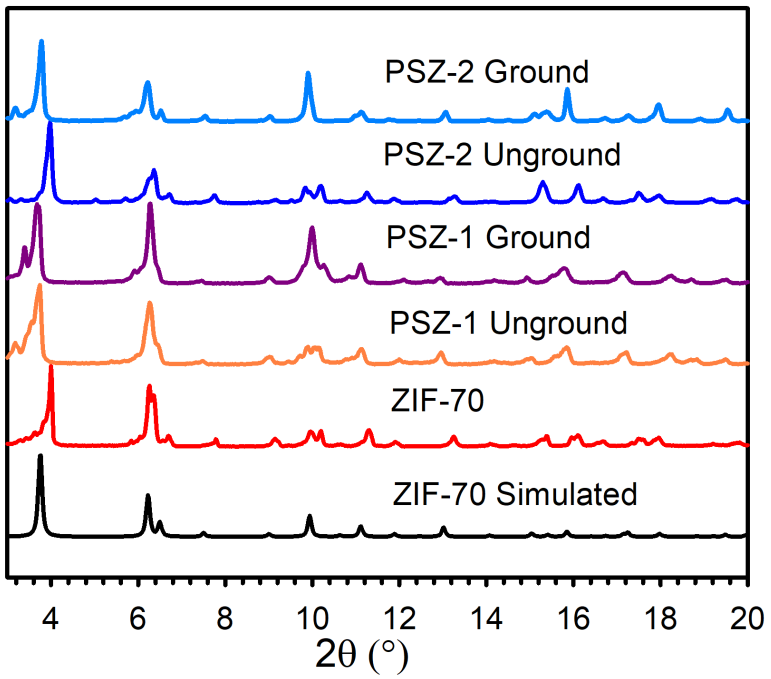

Figure 3.8: Simulated PXRD of ZIF-70 (black). PXRDs of ZIF-70 (red). PSZ-1 made from crystals of ZIF-70 (orange) and ground up crystals of PSZ-1 (purple). PSZ-2 made from crystals of ZIF-70 (dark blue) and ground up crystals of ZIF-70 (light blue).

To ensure the crystallinity of the MOFs were not damaged during the exchange and grinding processes, we performed PXRD analysis (Figure 3.8). The PXRD of ZIF-70, PSZ-1, and PSZ-2 are shown, illustrating that the effects of grinding on the

MOFs crystallinity is negligible. PSZ-2 is isostructural with PSZ-1, and ZIF-70 as its diffraction pattern is consistent with the previously characterized MOFs.

The slight shift in peak positions, as seen by the change in the (1 0 0) at 3.8 ° (2θ) is due to changes in the unit cell volume caused by the occupation of molecules in the pore and the associated change in the thermal expansion coefficient of the materials.

Peaks at 6 ° and 10 ° in 2θ that previously indicated the presence of ZIF-6 (refer back to 2.10) are not present. We concluded that PSZ-2 remains crystalline and is isostructural to ZIF-70. For this reason we chose to move on and perform other solid state techniques.

3.3.4 Gas Adsorption Analysis of PSZ-2

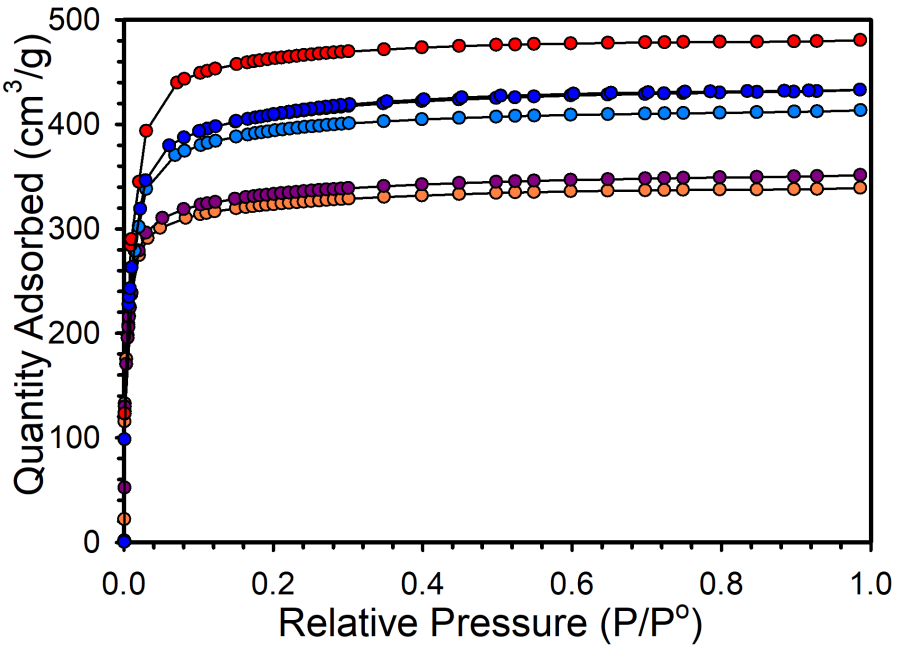

Figure 3.9: N_2 gas adsorption isotherms of ZIF-70 (Red, 1900 m^2/g), PSZ-2 (Dark Blue, 1750 m^2/g), PSZ-2 (Ground) (Light Blue, 1700 m^2/g), PSZ-1 (Orange, 1250 m^2/g), and PSZ-1 (Ground) (Purple, 1300 m^2/g).

Complementing the obtained PXRD data in the previous subsection, we also used gas adsorption to study the porosity of PSZ-2. This would help us to determine if the porosity of these MOFs are affected by the grinding process used for investigating surface defects (Figure 3.8). PSZ-2 has a BET surface area of 1750 m^2/g, which is a small decrease in porosity with respect to parent MOF ZIF-70. This is unsurprising given that a sparse 2.9 % of L_2 was incorporated into the structure.

Furthermore, we determined that grinding ZIF-70 prior to the SALE process slightly ($\sim$50 m^2/g) impacts the surface area of PSZ-1 and PSZ-2 but is within a tolerable range of difference with the expected porosity. We concluded that grinding ZIF-70 for use in PSM creates minimal defects in the structural integrity of these MOFs, with respect to adsorptivity.

3.3.5 Solid State UV-Vis Spectroscopy of PSZ-2

To analyze the photoswitching properties of PSZ-2, we opted to study PSZ-2 with solid-state UV-Vis Spectroscopy and determine how PSZ-2 behaves in comparison to PSZ-1. PSZ-2 contains roughly 20 % of the linker content of PSZ-1. Despite lower % incorporation, we were still interested in testing this material and determining how it behaves with PSZ-1 as a reference. Figure 3.10 shows the monitored change in % reflectance in the 550 nm region of light where the absorbance of closed form HL_1 and HL_2 appear.

Over 5 duty cycles, PSZ-1 shows a reproducible 10 % variation in reflectance which corresponds to increased absorption at 550 nm; PSZ-2 shows no notable change in the 500-600 nm range over the course of 5 cycles. Given that PSZ-1 demonstrates a 10 % change in reflectance with 12.5 % linker incorporation, PSZ-2 would proportionally illustrate a 2 % change in reflectance with a 2.9 % incorporation. Such a subtle

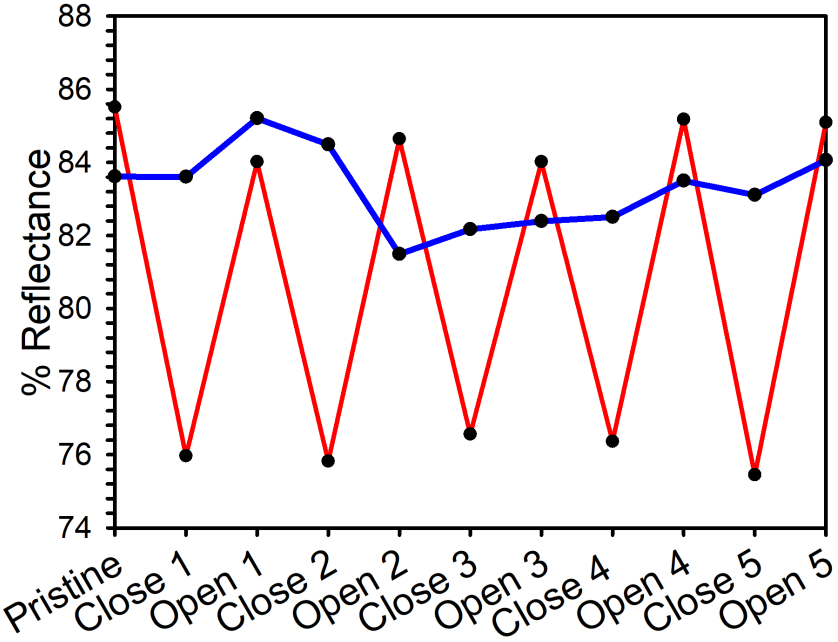

Figure 3.10: % reflectance of PSZ-1 and PSZ-2 at $\sim$ 550 nm after irradiation (UV exposure) and reopening (thermal reopening for 10 min at room temperature). PSZ-1 (red) has a noticeable 10% drop in % reflectance for up to 5 cycles while PSZ-2 (blue) shows no sign of photoswitching activity.

change is not observable with our instrumentation, as a change this small is indistinguishable from background noise. One interpretation of this data is that PSZ-2 is not photoswitching at all; however, we propose that this conclusion is unlikely based on the observation that HL_2 photoswitches in the solid and solution-phase, alternatively we propose that the observed lack of photoswitching is because there is simply not enough of HL_2 to trigger a spectroscopically discernable signal.

While PSZ-2 does not show any obvious signs of photoisomerization, we propose that we can learn more about PSZ-1 from these results. One of the challenges of working with MOFs is that there is always an issue between what is occurring at the surface vs. what is occurring inside the material. For photoisomerization, there is the possibility of the isomerization to occur exclusively on the surface or through a

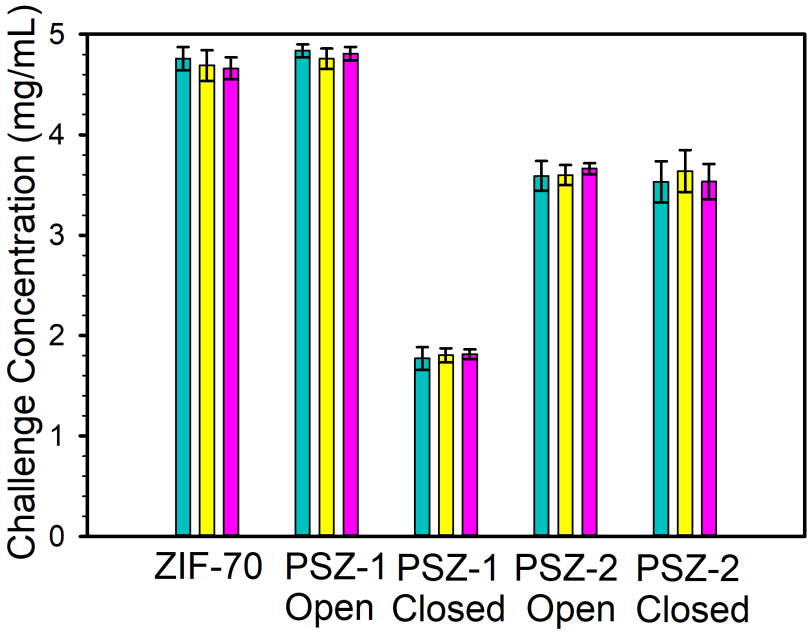

Figure 3.11: Comparison of the performance of PSZ-2 as a photoactive filter against predecessor PSZ-1

fractional quantity of incorporated molecules. In the case of PSZ-1 (Chapter 2), this could suggest that a fraction of HL_1 molecules are isomerizing and are responsible for the light-induced change in the filtration properties. Given that PSZ-1 decreases in % reflectance with 12.5 % total linker incorporation and PSZ-2 is unresponsive, we propose that more than 2.9 % of the maximum 12.5 % incorporated L_1 linkers in PSZ-1 are undergoing photoswitching to produce the observed structure function relationship observed in Chapter 2.

3.3.6 Photoactive Filter Tests of PSZ-2

The final and most important test we used to characterize PSZ-2 is using PSZ-2 as photoactive filter and determining how it performs with respect to PSZ-1. In Chapter 2, PSZ-1 displayed switchable pore dynamics as a function of light irradiation;

this was illustrated through the light controlled retention in a relatively simple mixture of toluene, naphthalene, and pyrene eluents. At 12.5 % incorporation of HL_1, PSZ-1 showed significant retention of analytes. With 2.9 % incorporation of HL_2 in PSZ-2, which is approximately 20 % of the loading in PSZ-1, we predicted that the photoactive filtration would be worse than PSZ-1 as the number of linkers available to photoswitch and promote switching adsorptivity are not as abundant. As illustrated in Figure 3.11, PSZ-2 does not show any difference in adsorptivity between PSZ-2-O and PSZ-2-C. The filtration data suggests that the photoactive properties of PSZ-1, and other photoswitching MOFs are due to the majority of the linkers switching in the pores and not just a small fraction of ($\leq$ 2.9 %) surface-only linkers.

3.4 Conclusions

The determination of photochromic switching ratios in porous materials is a difficult metric to determine as scattering and light penetration in bulk solids create great difficulties for accurate measurements. While researchers have previously characterized switching ratios of MOF digests, and thin films, this is one of the first studies quantifying switching ratios in a bulk solid. In this work, we examined the structure and photoswitching properties of two photoactive MOFs, PSZ-1 and PSZ-2. Given the lower (21 %) linker incorporation associated with PSZ-2 relative to PSZ-1 we were able to set a lower-limit on the number of photoactive linkers in the MOF needed for a change in the separation properties of PSZ MOFs to occur. This work suggests that the change in properties of Type II photoswitching MOFs is due to a large degree of photoswitching and not a superficial number of linkers. Given these results, it should be possible to tune the amount of linker incorporation in order to optimize chemical separation in solution and in the gas phase. With the information obtained from the

work performed in the current and former chapter, we determined a new logical direction to take this work, in order to study the effect of photoswitching MOFs across a wide range of linker incorporations.

Chapter 4

A UiO Mixed Linker Approach Towards Optimizing Light Switchable Adsorptivity

4.1 Introduction

In the previous chapter, we explored how linker incorporation in PSZ MOFs affected photoswitching separation. PSZ-1 has 12.5 % HL_1 incorporated into its pore; which equals 50 % of the exchangeable linkers in the large pore and is the steric limit of HL_1 in the pore of ZIF-70. At 12.5 % linker loading, we observe photochromism, as well as a shift in the materials adsorptivity towards solution-phase separations. Meanwhile, PSZ-2 has 2.9 % HL_2 incorporated ($\sim$10 % of the exchangeable linkers in the large pore are exchanged). This material (PSZ-2) shows no photochromism or switching adsorptvity. This lack of switchable adsorptivity indicates that there is insufficient linker incorporation to show notable change in the materials filtration capabilities.

We inferred that between the two measured degrees of incorporation (in PSZ-1 and PSZ-2), there is a 40% difference in linker content (in the large pore) wherein we expect a threshold for switching adsorptivity in PSZ MOFs. These results presented us with an interesting question regarding the PSZ family of MOFs. Simply put, could we control the degree of linker exchange in our MOF, and determine the % linker content that induces photoswitching adsorptive behaviour? The challenge here is that making PSZ-1, or other PSZs, with precision tuned degrees of linker incorporation is non-trivial. To illustrate this, it is worth discussing the two main approaches by which we introduce linkers in MOFs and how neither of these methods are likely to lead to desired outcome in PSZ MOFs. These two methods are *de novo* synthesis and PSM methods.[167] *De novo* methods can also be described as a "from scratch" approach. These methods involve the synthesis of MOFs by the reaction of linkers and metal salts (that generate complex nodes *in-situ*) at defined stoichiometries. The reaction solvent is often *N,N*-dimethylformamide (DMF), and runs at elevated temperatures, often in the range of 80-120 °C.[167] When discussing *de novo* syntheses, it is worth noting how ZIF-based MOFs differ with respect to MOFs that are formed from linkers that use multitopic carboxylates as node attachment groups. Synthesizing carboxylate-based MOFs with mixed ligands often produces structures that have the same topology (see Chapter 1). For example, UiO (Universitetet i Oslo) MOFs and MOF-5 are easily prepared with a mixture of linkers.[168] These linkers have the same overall length but can have different functional groups that point into the pore (e.g., DTEs). Generally, these functionalized linkers produce MOFs with the same topology if the linker connects the metal nodes in the same fashion as the unfunctionalized linker.[167] For example, UiO-66 is formed with benzenedicarboxylate (BDC), but biphenyl and terphenyl dicarboxylates (BPDC and TPDC respectively) make MOFs with expanded pores that are isoreticular (i.e., same net shape/topology)

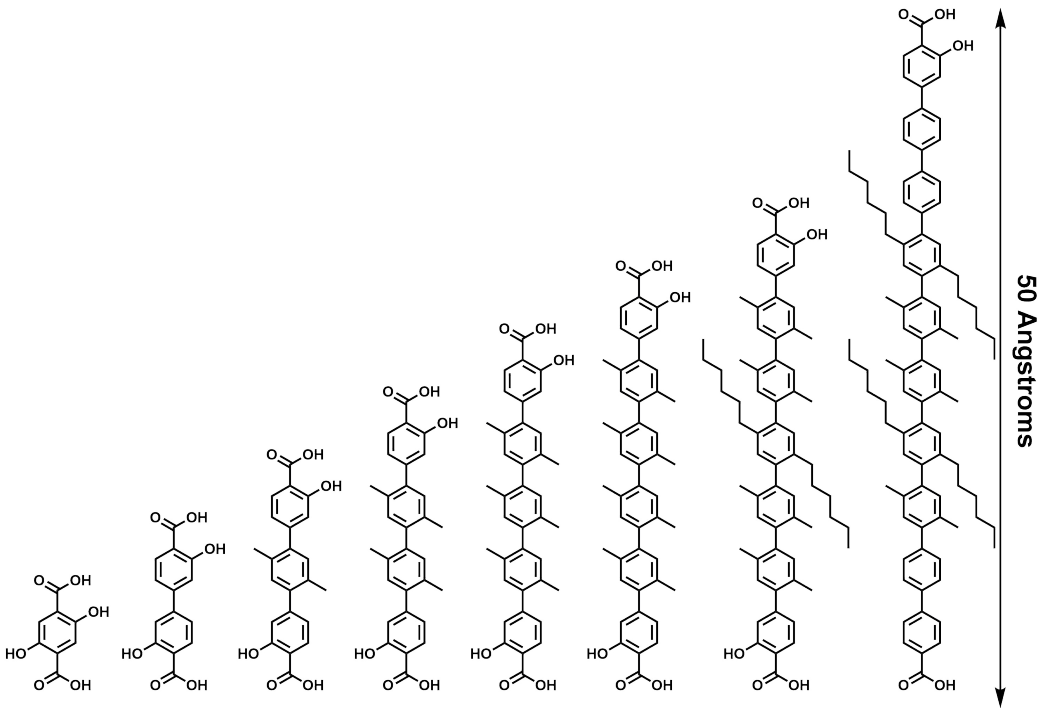

Figure 4.1: Elongated 2,5-dihydroxydicarboxylic acid linkers used by Yaghi and coworkers for the synthesis of large pore MOF-74 derivatives.

with UiO-66 (UiO-67/BPDC, UiO-68/TPDC respectively).[169] Expanded MOFs that are isoreticular with hexagonal MOF-74 are also known. These channels range from 14–98 Å and are prepared by using expanded linkers with similar binding motifs to 2,5-dihydroxy-1,4-benzenedicarboxylate; the linkers used in this mentioned work range from 1-11 aromatic rings in length.[170] The important part is that the terminal aromatic rings are functionalized with a carboxylate and hydroxy group to emulate the binding motif of 2,5-dihydroxy-1,4-benzenedicarboxylate (Figure 4.1). However, *de novo* approaches when making a ZIF can create completely different framework topologies.[143] In fact, depending on the linker(s) used in the synthesis, the reaction can generate many different ZIF topologies. For example, Figure 4.2 illustrates an example encountered in this work. The honeycomb network of ZIF-70 assembles from Zn^{2+} ions and a 1:1 mixture of imidazole/2-nitroimidazole. Increasing the concentration of

the linker mixture (imidazole in this case) can lead to formation of ZIF-6.[1]

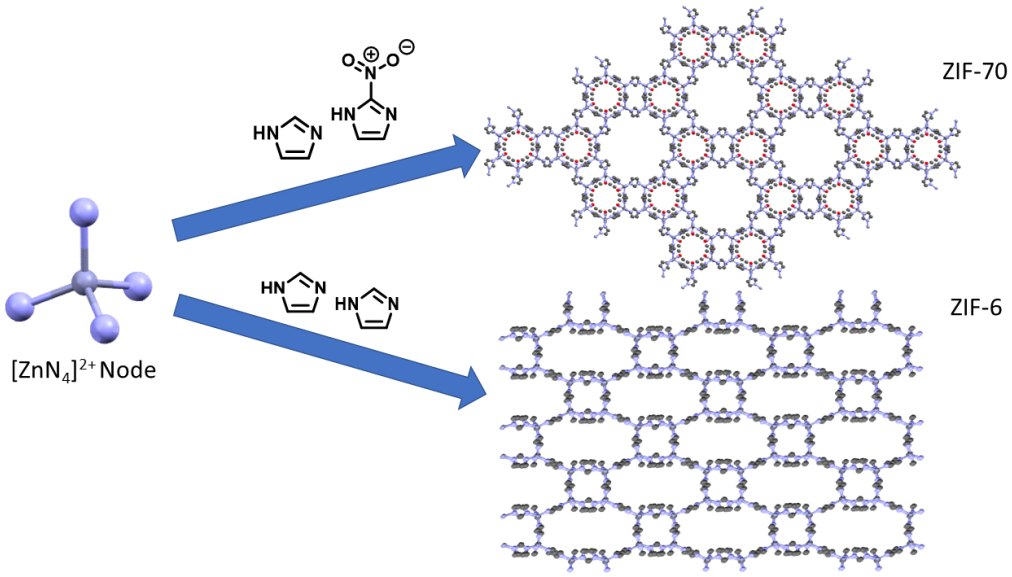

Figure 4.2: Illustration of vastly different ZIF topologies which result from stoichiometric changes in *de novo* MOF syntheses. An equimolar mixture of imidazole/ 2-nitroimidazole reacts with Zn nodes to produce ZIF-70, yet identical reaction conditions which use 2 eq. of imidazole results in the formation of ZIF-6.

The net shape and structure of the pore in ZIF-6 is completely different from ZIF-70, even though chemically they only differ by a linker. Previous reports by Yaghi and coworkers also illustrate broad structural diversity in ZIFs by reporting 25 structurally unique ZIFs via modification of linker size, functional groups, and linker ratios.[171] The take home message here is that reticular synthesis works well for metal/carboxylate-based MOFs, but not as well for ZIFs. The implication here is that even though we made PSZ-1 and have identified that the linker fits into the pore, attempts to make the same material via an equivalent *de novo* reaction with different amounts of HL_1 in PSZ-1 is certain to fail. This is the reason why we initially chose a PSM approach in Chapter 2 and 3. For PSM, the approach is to introduce the desired linker into the MOF by solvothermal exchange/incorporation linkers with pre-synthesized MOF.

[1]Authors, Unpublished Work: Crystals of ZIF-6 have been isolated from reactions that intended to form ZIF-70

This often retains the parent topology and enables us to incorporate the linker in a predictable fashion.[148,153] The challenge with controlling PSM techniques is best illustrated by the synthetic approach used to make PSZ-1. As previously reported in Chapter 2 and 3, SALE is an efficient PSM technique in MOF chemistry. SALE allowed us to selectively incorporate HL_x into pre-synthesized ZIF-70. The challenge with SALE is that it may not be possible to incorporate less photoswitch and simultaneously ensure that the linker is homogeneous throughout the MOF. Exchange between ZIF-70 and HL_x is performed at a 1:4 ratio (1 eq. of linker in the large pore versus 4 eq. of HL_1 respectively). This ensured that competition between linkers leaving and entering did not result in incomplete substitution inside the MOF during the exchange. During SALE, more nucleophilic linkers should drive the exchange forward, but when the nucleophilicities are similar in magnitude, the use of excess linker is important for driving the desired reaction forward. The conclusion here is that SALE is not the ideal approach for the formation of PSZ-1 with various levels of L_1 incorporation. Given that both *de novo* and SALE are not likely to yield variable degrees of L_1, or related linkers, in the PSZ family of MOFs, we chose to explore the role of % photoswitch incorporation using a different MOF system. To address the question in this chapter, we need a MOF that could easily tune the amount of photoswitch and test the role of % linker on the separation properties. Perhaps one of the best systems to explore is the UiO family of MOFs.[172–175] UiO-based MOFs contain zirconium clusters as nodes ($[Zr_6O_4(OH)_4]^{12+}$: Zr_6 node) that connect via linear ditopic organic linkers. UiO-66, -67, and -68, have been prepared with mixed linker de novo approaches to include simple functional groups (e.g., $-NH_2$, $-OH$, para $(-OH)_2$ units) as well as complex side groups for tailored applications.[169,175] For example, the Kaskel group reports UiO-68 type linkers with side group L-proline motifs for asymmetric aldol condensations.[176] Hupp group has also reported squaramide functionalized UiO

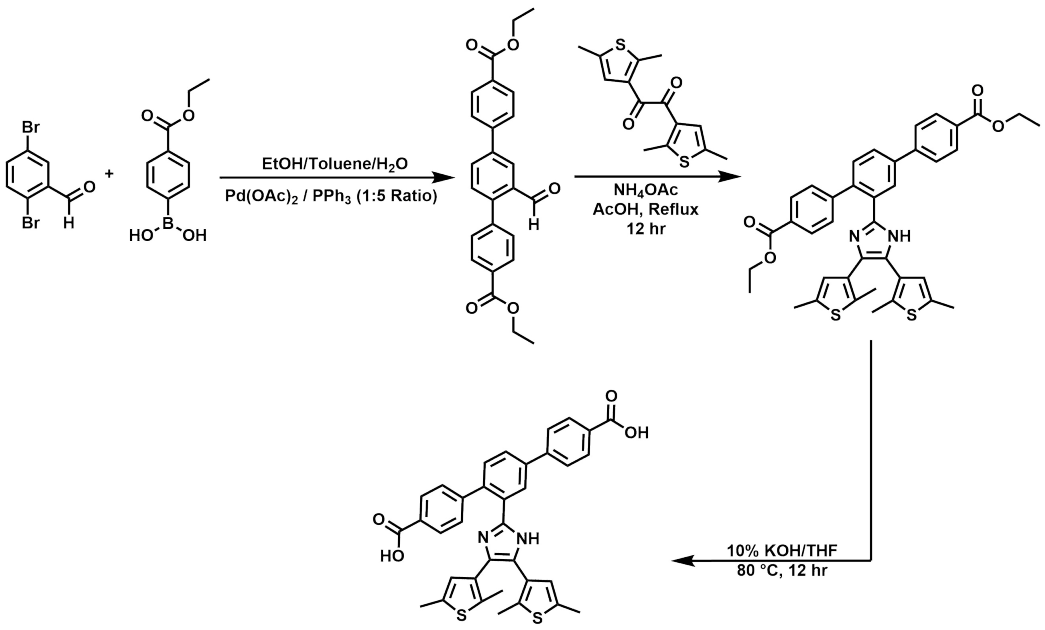

Figure 4.3: Synthetic scheme developed for the synthesis of a DTE functionalized terphenyldicarboxylate linker.

MOFs for efficient Friedel-Crafts catalysis.[177] Photoswitching UiO MOF derivatives are reported by the Heinke and Hecht groups using Type II SP,[178] and azobenzene linkers respectively.[179] Given these precedent findings, we pursued the synthesis of a UiO material as the host MOF for our embedded Type II DTE photoswitch. To address these goals, the imidazole DTE linker system was redesigned by reacting our previously synthesized 1,2-dione precursor with an aldehyde tagged terphenyldicarboxylate (TPDC-CHO).[180] By doing this we can prepare a pendant group DTE that builds the photoswitching moiety off the TPDC linker (Figure 4.3) functionality, similar to the work of Hecht, and Heinke. This proceeding chapter presents the study of new family of UiO topology MOF (Figure 4.4) with stoichiometric control over incorporation of a Type II DTE to investigate the effect of photoswitching linker content on the chemical separation.

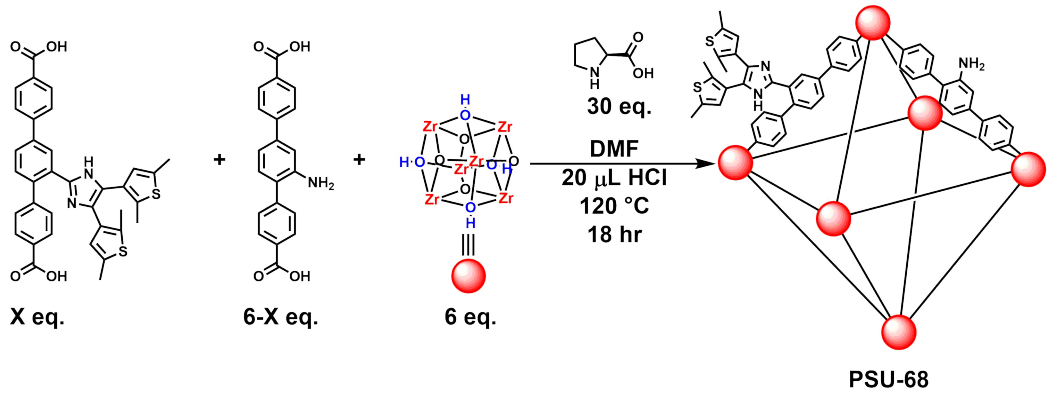

Figure 4.4: Synthetic conditions used for the synthesis of DTE-grafted terphenyldicarboxylate linkers in a UiO-topology MOF. The new system is named Photoswitching UiO-68 (PSU-68).

4.2 Experimental

4.2.1 Materials and Methods

Unless otherwise specified, all reagents were used as received from commercial suppliers without further purification. Dichloromethane and pyridine were distilled and stored over activated 4 Å molecular sieves. All column chromatography was performed with 230-400 mesh silica. All ^{1}H NMR were recorded on a Bruker Advance III 300 MHz NMR spectrometer using DMSO-d_6 for starting materials and DMSO-d_6 + 3 drops of deuterated sulfuric acid (D_2SO_4) for the Et_2TPDC–DTE and H_2TPDC–DTE. For MOF samples, and filtration experiments, a Bruker Avannce III 300 MHz NMR spectrometer was used, with DMSO-d_6 + 3 drops of D_2SO_4 as the NMR solvent for MOF analysis (the spectra for the MOFs was referenced to DMSO-d_6), and $CDCl_3$ as the solvent for filtration studies. Samples were measured from 3-20 ° in 2θ using a scan speed of 1 °/min. Nitrogen gas adsorption isotherm data were collected at 77 K on a Micromeritics Tristar 3020 surface area and porosity analyzer. All samples were activated on a Micromeritics Smart VacPrep instrument by heating the sample to 150 °C (5 °C/min) while slowly reducing the pressure (5 mmHg/s) within the sample

holder. The sample was maintained at this temperature and low pressure for 10 h. The sample was then cooled to room temperature after which the sample holder was backfilled with nitrogen gas.

4.2.2 Synthesis of $Et_2TPDC-NH_2$

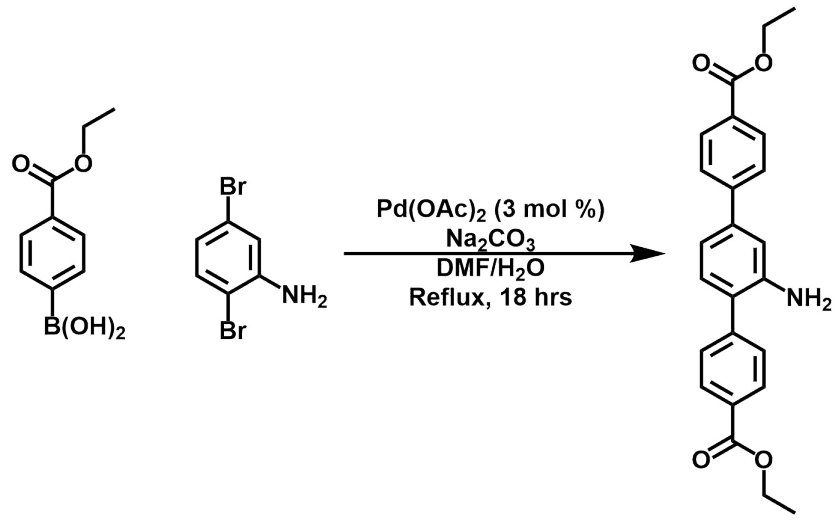

5.79 g of ethyl-4-carboxyphenylboronic acid (5 eq., 29.8 mmol), 1.5 g of 2,5-dibromoaniline (1 eq., 5.97 mmol), and 2.28 g of Na_2CO_3 (3.6 eq., 21.5 mmol) were dissolved in 100 mL of DMF/H_2O (1:1) mixture while sparging with N_2 gas. After 20 minutes of sparging with N_2 gas, $Pd(OAc)_2$ (40 mg, 3 mol %) was added to the mixture, and the reaction was heated at 110 °C for 18 hours. TLC analysis in 30 % EtOAc/Hexane showed the consumption of aniline starting material and a single bright blue spot (R_f=0.3). The mixture was then diluted with 100 mL of H_2O and the organics were extracted with 3 × 100 mL of EtOAc, subsequently dried over $MgSO_4$ and concentrated under rotary evaporation to produce a pale-yellow solid. The solid was purified by column chromatography using 30 % ethyl acetate/hexane. The resulting compound was a bright yellow solid (1.61 g, 69 % yield). ^{1}H NMR (300 MHz, DMSO-d_6): δ (ppm) 8.04 (d, J = 8.5 Hz, 2H), 8.03 (d, J = 8.5 Hz, 2H),

7.77 (d, J = 8.5 Hz, 2H), 7.64 (d, J = 8.5 Hz, 2H), 7.17 (d, J = 7.9 Hz, 1H), 7.10 (d, J = 1.8 Hz 1H), 7.02 (dd, J = 7.9 Hz, 1.8 Hz 1H), 4.33 (q, J = 7.2 Hz, 2H), 4.32 (q, J = 7.2 Hz, 2H), 1.35 (t, J = 7.2 Hz, 3H), 1.34 (t, J = 7.2 Hz, 3H).[181]

4.2.3 Synthesis of $H_2TPDC-NH_2$

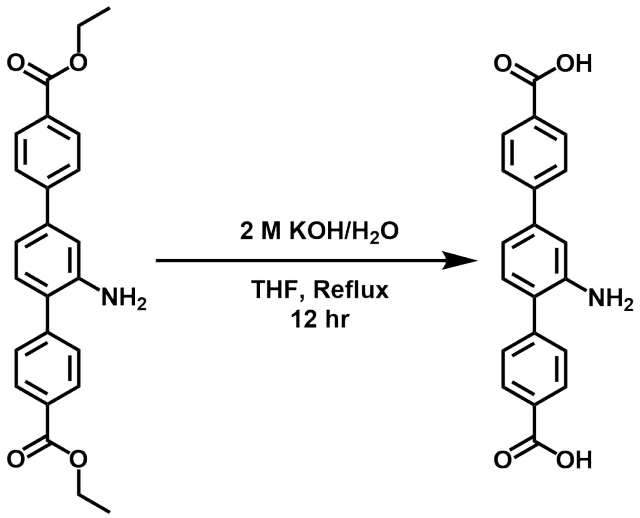

1.2 g of $Et_2TPDC\text{-}NH_2$ (3.1 mmol) was dissolved in 100 mL of THF in a single neck round bottom flask, to this solution aqueous 2 M KOH (100 mL) was added and refluxed for 12 hours. The mixture was cooled to room temperature, and the organic layer was removed using rotary evaporation. The aqueous layer was diluted with another 100 mL of H_2O and then placed in an ice bath, and subsequently acidified with 4M HCl until litmus paper turned red. A bright yellow precipitate resulted after acidification. The precipitate was isolated by suction filtration and washed with 3×50 mL of H_2O to wash away any remaining acid. The solid was dried overnight in a vacuum oven. (935 mg, 91 % yield), ^{1}H NMR (300 MHz, DMSO-d_6) δ (ppm) 8.02 (d, J = 8.2 Hz, 4H), 7.74 (d, J = 8.2 Hz, 2H), 7.61 (d, J = 8.2 Hz, 2H), 7.17 (d, J = 7.9 Hz, 1H), 7.16 (d, J = 1.8 Hz, 1H), 7.02 (dd, J = 7.9, 1.8 Hz, 1H), 5.25 (br s, 2H).[181]

4.2.4 Synthesis of $Et_2TPDC-CHO$

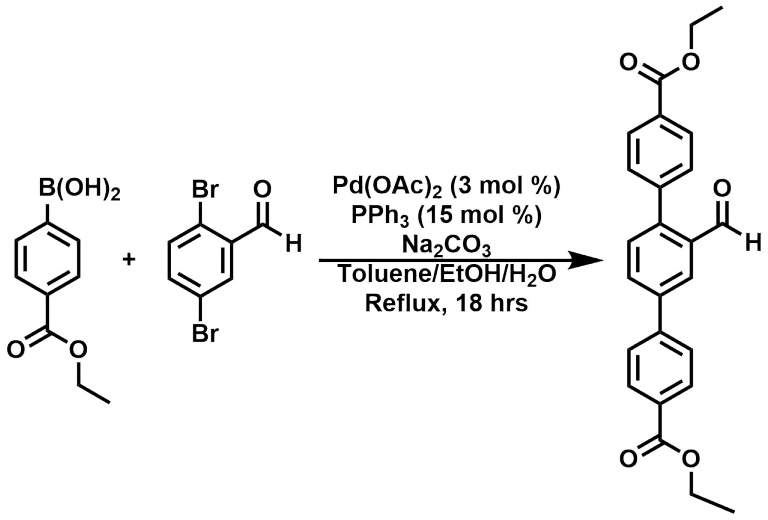

3.67 g of ethyl 4-carboxyphenylboronic acid (5 eq., 18.9 mmol), 1.00 g of 2,5-dibromobenzaldehyde (1 eq., 3.8 mmol), 1.44 g of Na_2CO_3 (3.6 eq., 13.6 mmol), and 148 mg of PPh_3 (15 mol %) was dissolved in a 1:1:1 mixture of Toluene/EtOH/H_2O with stirring; the solution was sparged with N_2 for 20 minutes. $Pd(OAc)_2$ (25 mg, 3 mol %) was added to the reaction mixture and refluxed under N_2 atmosphere for 18 hours. TLC analysis in 30 % EtOAc/Hexane confirmed consumption of the aldehyde starting materials. The mixture was cooled to room temperature. The mixture was then diluted with 100 mL of H_2O and the organics were extracted with 3×50 mL of EtOAc, dried over $MgSO_4$ and concentrated under rotary evaporation. A yellow precipitate of crude Et_2TPDC-CHO was obtained. The product was purified by recrystallization from hot acetone to yield a white solid (1.25 g, 82 % yield) ^{1}H NMR (300 MHz, DMSO-d_6) δ (ppm) 9.97 (s, 1H), 8.27 (d, J = 1.8 Hz, 1H), 8.16 (dd, J = 8.1 Hz, 1.8 Hz, 1H), 8.09 (d, J = 8.4 Hz, 2H), 8.08 (d, J = 8.4 Hz, 2H), 7.96 (d, J = 8.4 Hz, 2H), 7.70 (d, J = 8.1 Hz, 1H), 7.66 (d, J = 8.4 Hz, 2H), 4.37 (q, J = 7.2 Hz, 2H), 4.35 (q, J = 7.2 Hz, 2H), 1.35 (t, J = 7.2 Hz, 3H), 1.34 (t, J = 7.2 Hz, 3H).[180]

4.2.5 Synthesis of Et_2TPDC−DTE

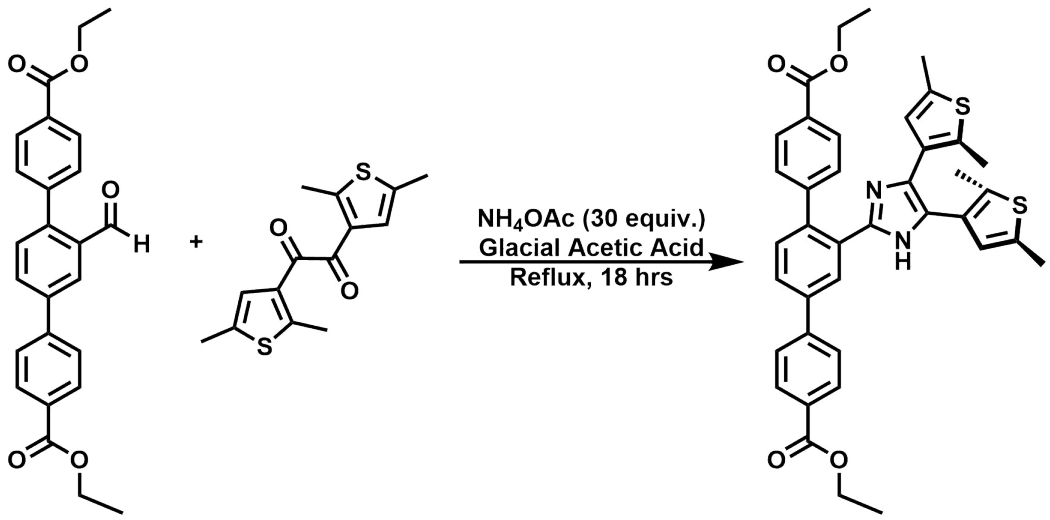

722 mg of Et_2TPDC−CHO (1 eq., 1.80 mmol) and 500 mg of 1,2-Bis-(2,5-dimethyl-thiophen-3-yl)-ethanedione (1 eq., 1.80 mmol), and 4.15 g of NH_4OAc (30 eq., 54 mmol) were dissolved in 30 mL of glacial acetic acid with stirring and refluxed overnight. The mixture was cooled to room temperature, concentrated under rotary evaporation, and diluted with 100 mL of H_2O. The suspension was neutralized with dropwise addition of 2M Na_2CO_3 and the organics were separated with 3 × 50 mL of $CHCl_3$. The organics were dried over $MgSO_4$, filtered and concentrated under rotary evaporation, and redissolved once more in minimal hot acetone to crystallize Et_2TPDC−DTE out of solution as an ivory colored solid. (800 mg, 67% yield) ^{1}H NMR (300 MHz, DMSO-d_6 + 3 drops D_2SO_4) δ (ppm) 1.29 (t, J = 7.2 Hz, 3H), 1.32 (t, J = 7.2 Hz, 3H), 1.84 (s, 6H), 2.33 (s, 6H), 4.33 (q, J = 7.1 Hz, 2H), 4.31 (q, J = 7.1 Hz, 2H), 6.59 (s, 1H), 6.58 (s, 1H), 7.41 (d, J = 8.6 Hz, 2H), 7.82 (d, J = 8.1 Hz, 1H), 7.98 (d, J = 8.6 Hz, 2H), 8.02 (d, J = 8.6 Hz, 2H), 8.09 (d, J = 8.6 Hz, 2H), 8.19 (dd, J = 8.1, 1.8 Hz, 1H), 8.36 (d, J = 1.8 Hz, 1H).

4.2.6 Synthesis of H_2TPDC−DTE

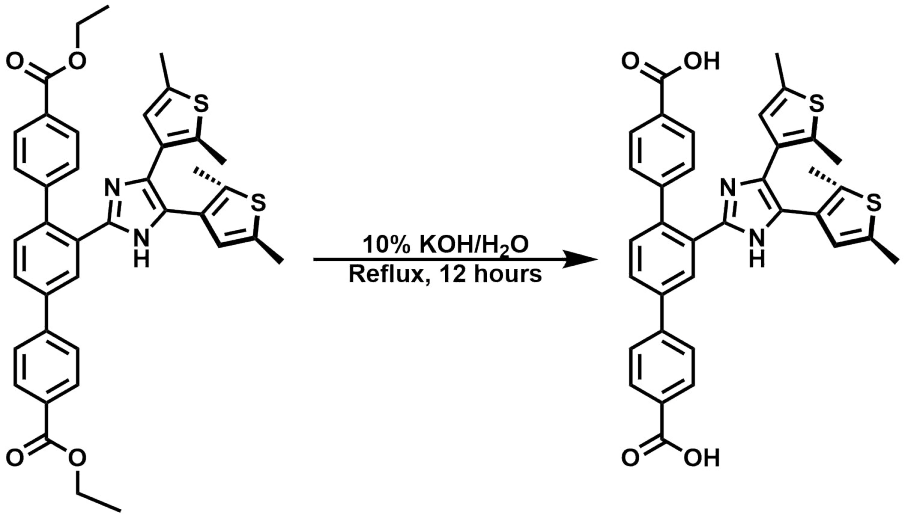

400 mg of Et_2TPDC−DTE (0.61 mmol) was dissolved in 50 mL of THF. To this solution, aqueous 2M KOH (100 mL) was added and refluxed overnight. The mixture was cooled to room temperature, and the organic layer was removed using rotary evaporation. The aqueous layer was diluted with another 100 mL of H_2O and then acidified with 4M HCl until litmus paper turned red. A tan brown precipitate resulted from acidification which was isolated with suction filtration and washed with 3×50 mL of H_2O to remove trace acid. (300 mg, 82% yield) ^{1}H NMR (300 MHz, DMSO-d_6 + 3 drops of D_2SO_4) δ (ppm) 1.83 (s, 6H), 2.33 (s, 6H), 6.58 (s, 2H), 7.38 (d, J = 8.6 Hz, 2H), 7.81 (d, J = 8.30 Hz, 1H), 7.97 (d, J = 8.6 Hz, 2H), 7.99 (d, J = 8.6 Hz, 2H), 8.07 (d, J = 8.6 Hz, 2H), 8.18 (dd, J = 8.3, 1.3 Hz, 1H), 8.35 (d, J = 1.3 Hz, 1H).

4.2.7 $[Zr_6O_4(OH)_4](TPDC-NH_2)_6$ (UiO-68-NH_2)

This protocol is modified from the reported work of Blight and co-workers.[182] In a 50 mL screw top vial, 54 mg $ZrCl_4$ (1 eq., 0.23 mmol), 74 mg of H_2TPDC−NH_2 (1 eq., 0.22 mmol), and 130 mg L-proline (5 eq., 1.13 mmol) was dissolved in 10 mL

of DMF under sonication (10 minutes). After adding 20 μL of conc. HCl to solution, the mixture was sonicated for another 10 minutes. The mixture was then heated at 120 °C for 12 hours. The resulting beige solid was washed with 3 × 20 mL of DMF, and 3 × 20 mL of acetone with centrifugation between washings. The solid was dried with heat and reduced pressure for 2 hours and was then activated via Smart VacPrep for gas adsorption analysis.

4.2.8 $[Zr_6O_4(OH)_4](TPDC-NH_2)_{6-x}(TPDC-DTE)_x$

Table 4.1: Reaction Stoichiometry For Synthesis of PSU-68 MOFs

MOF (Sample Name)	$ZrCl_4$ (mg)	H_2TPDC-NH_2 (mg)	H_2TPDC−DTE (mg)
PSU-68 1 eq	54	62	23
PSU-68 2 eq	54	49	47
PSU-68 3 eq	54	37	70
PSU-68 4 eq	54	24	93
PSU-68 5 eq	54	12	117
PSU-68 6 eq	54	0	140

This outlined preparation uses PSU-68 (1 eq. as the example procedure). These MOFs were synthesized using the modified prep of Blight and co-workers.[182] In a 50 mL screw top jar, 54 mg of $ZrCl_4$ (1 eq., 0.232 mmol), 62 mg of H_2TPDC−NH_2 (0.186 mmol), 23 mg of H_2TPDC−DTE (0.038 mmol), and 130 mg of L-proline (5 eq., 1.13 mmol), were dissolved in 10 mL of DMF and sonicated for 10 minutes After adding 20 μL of conc. HCl to solution, the mixture was sonicated for another 10 minutes. The mixture was then heated at 120 °C for 12 hr. The resulting beige solid was washed with 3 × 20 mL of DMF, and 3 × 20 mL of acetone with centrifugation between washings. The solid was dried with heat and reduced pressure for 2 hours and was then activated via Smart VacPrep for gas adsorption analysis.

4.3 Results and Discussion

4.3.1 Synthesis of UiO-68 Derivatives

This chapter explores effects of tuning the number of photoactive linkers on the separation properties of UiO-68-based MOFs. With UiO-based MOFs, such as UiO-66 and UiO-67, synthesis and functionalization are easy and very reproducible. However, with respect to UiO-68 MOFs, there is an abundance of reports in the literature that are difficult to reproduce. This suggests that there is likely some unknown synthetic features that have not been ascertained in these systems. A consistent synthesis of UiO-68-NH_2 with literature surface area was achieved using reported methodology of Blight and co-workers.[182] This procedure uses L-proline modifier and conc. HCl as additives in the reaction. While it is not clear why this method worked best, this procedure produced the most consistent quality of materials over the course of the project.

By modifying linker stoichiometry of this procedure, we synthesized a family of six MOFs with UiO topology bearing a DTE moiety grafted off the central aromatic ring of the TPDC organic strut. This family of materials was named PSU-68 (Photo Switching UiO-68). For clarity, this series of MOFs were denoted as PSU-68 X eq. where X denotes the equivalence of DTE used for preparation of the MOF (i.e., PSU-68 3 eq. is PSU-68 which was made using 3 equivalences of H_2TPDC−DTE).

4.3.2 ^{1}H NMR Analysis of PSU-68

Six MOFs were synthesized by adjusting the ratio of H_2TPDC−NH_2:H_2TPDC−DTE from 6:0 all the way to 0:6 linker equivalence in incremental steps of 1 eq. of linker. In each case, after reacting the reagents in a vial overnight at 120 °C, an ivory powder

was produced. To initially determine if the DTE-containing linker was incorporated, MOF digests in DMSO-d_6 were analyzed via ^{1}H NMR.

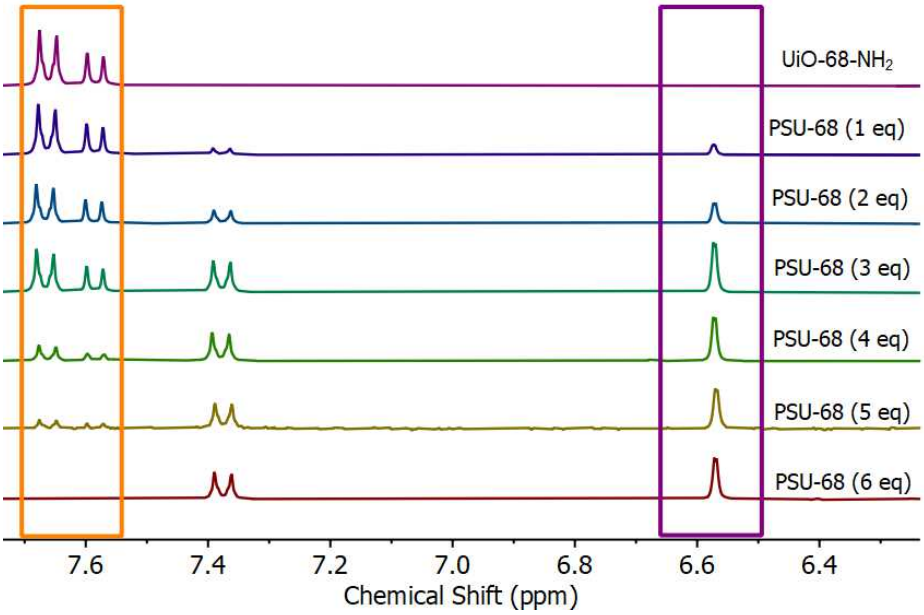

Figure 4.5: ^{1}H NMR stack of UiO-68-NH_2 and PSU-68 MOFs (1-6 equivalence) in DMSO-d_6. Peaks corresponding to the NH_2 linker are highlighted in orange and peaks corresponding to the DTE-derived linker are highlighted in purple. As expected, the intensity of the NH_2 linker peaks fade as the degree of the DTE-derived linker incorporation increases.

Figure 4.5 shows the 6.3-7.7 ppm region of the NMR spectrum. In this region, there are peaks associated with both the TPDC$-NH_2$ and the TPDC-DTE linkers. It is however worth noting that we should be cautious about these results reflecting the overall chemical formula of the MOF since defects formation due to linker vacancies are well known in UiO-based MOFs. Returning to the NMR (Figure 4.5), following the purple frame (H_2TPDC-DTE) in comparison with the orange frame (H_2TPDC$-NH_2$), we see a qualitative increase in the amount of TPDC-DTE and a decrease in the amount of TPDC$-NH_2$. If we follow the signals highlighted in purple, we see intensifying peaks appearing in the δ6.6 region corresponding to the 3-thienyl peaks of the H_2TPDC linker.

$$\%Incorporation \;=\; \frac{Int(\delta 7.4)}{Int(\delta 7.6) + Int(\delta 7.4)} \times 100\ \% \tag{4.1}$$

Quantitatively, we can determine the ratio of TPDC-DTE:TPDC$-NH_2$ in the PSU-68 sample with Equation 4.1. Using the relative integrations of the peaks at δ7.4 and dividing by the sum of the integrations at δ7.6 and δ7.4, then multiplying by 100 to obtain a percentage. The logic behind this equation is that these ^{1}H NMR signals are distinct, separate, and integrate to 2 protons for their respective molecules, which makes determining the % linker incorporation a quick task.

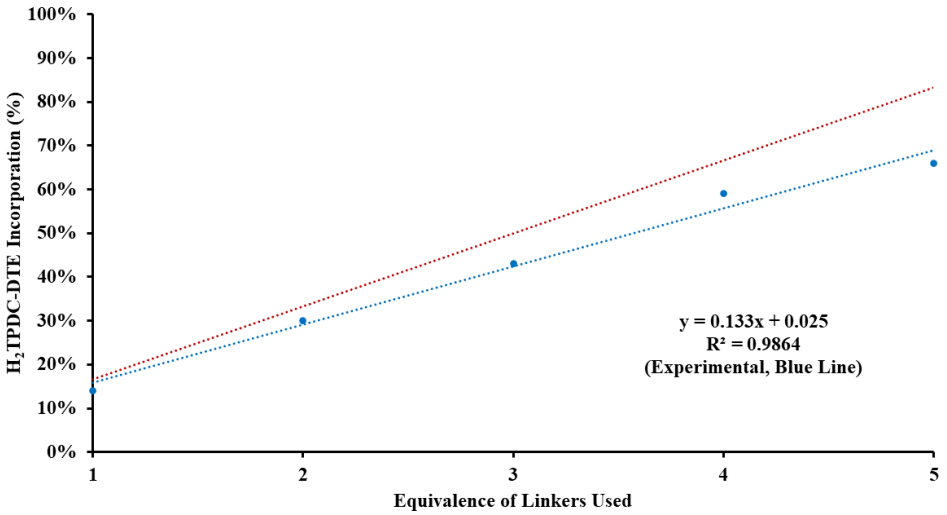

Figure 4.6: Plot of % H_2TPDC$-$DTE loading against the stoichiometric equivalence of photoswitching linker used for the synthesis of the respective PSU-68 sample. The % incorporation (blue) deviates from the theoretical incorporation (which assumes 100 % of the linker used is incorporated).

This data is summarized in Figure 4.6, which illustrates the % incorporation is consistently less than the theoretical maximum for linker incorporation. Overall, the more DTE-containing linker is incorporated, the larger the deviation, with the 5 eq. of linker illustrating the largest discrepancy between linker percentages.

Table 4.2: Summarizing Table of % Incorporation in PSU-68 MOFs (Average of 3 Simultaneous Trials

MOF (Sample Name)	Incorporation (%)	Theoretical (%)
PSU-68 1 eq.	14	17
PSU-68 2 eq.	30	33
PSU-68 3 eq.	43	50
PSU-68 4 eq.	59	67
PSU-68 5 eq.	66	83

Within the context of this data, there are two possible interpretations. If we assume that both linkers incorporated into the MOF according to the ratio initially provided, a 17 % deviation would be equivalent to approximately one missing linker; this is according to the chemical formula of these UiO MOFs, $[Zr_6O_4(OH)_4(TPDC-NH_2)_{6-x}(TPDC-DTE)_x]$. Alternatively, it is possible that the framework is not able to accommodate as many DTE-based linkers due to steric crowding in the pore, so the larger linker incorporations would contain more DTE-free linker. Had the COVID pandemic not halted research at this critical juncture, the six PSU-68 MOFs would have been analyzed using quantitative NMR to determine the number of node defects present.

4.3.3 PXRD Analysis of PSU-68 Derivatives

We next used PXRD to determine if these samples are isostructural with its UiO-68 parent material. As illustrated in Figure 4.7, experimentally prepared UiO–68-NH_2 (red trace) shows excellent agreement with the simulated PXRD of unfunctionalized UiO-68 (black trace). PSU-68 (1-6 eq.) all show the same diffraction pattern as parent UiO-68-NH_2 and simulated UiO-68. Another piece of information that can be extracted from this plot is that any defects present in the microcrystalline samples do not appear to drastically affect diffraction in these materials. We concluded that

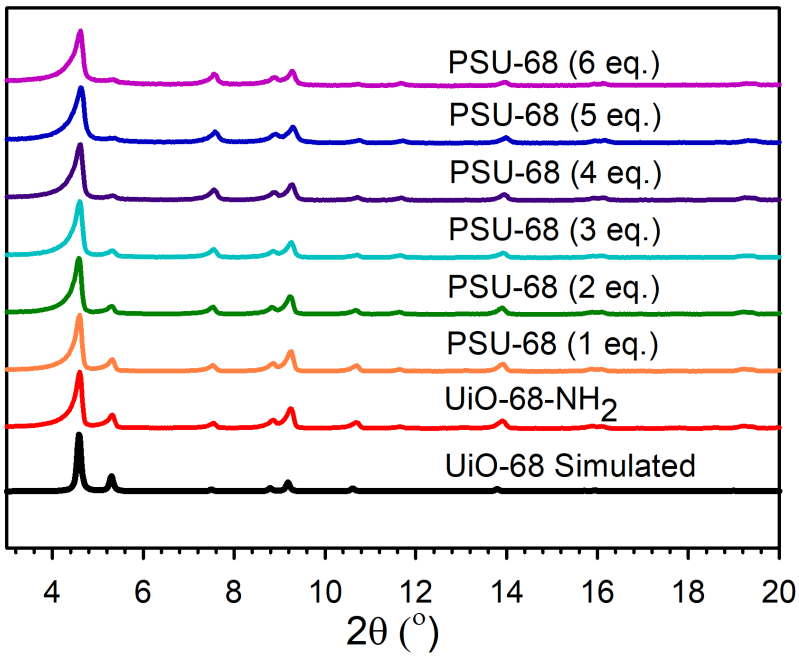

Figure 4.7: PXRD Stack of UiO-68-NH_2 and PSU-68 series of MOFs with varying degree of linker incorporation. As illustrated, the materials retain their crystallinity and resemble the parent material, UiO-68 as shown by the strong agreeance between their PXRDs.

the structure of these materials are a UiO topology, and that the crystallinity of these structures are not susceptible to the amount of linker loaded into the material. No single crystal X-ray studies could be performed on these MOFs as these materials form micro-crystalline powders.

4.3.4 Gas Sorption Studies on PSU-68 MOFs

To further characterize these MOFs, we measured their nitrogen gas adsorption isotherms at 77 K. Starting with the parent UiO-68-NH_2, we observe a BET surface area of 3800-4100 m^2/g. This is in the same range as the literature value for the surface area of UiO-68, which is reported to be around 3500-3800 m^2/g.[181] The novel PSU-68 series has varying surface area, which is related to the amount of TPDC-DTE

present in the pore. Adding the DTE component to the framework can have opposing effects, which makes it challenging to predict if the surface area should increase or decrease. For example, the DTE side group adds more surface for a gas to interact with. Thus, we could predict that the surface area will increase. However, the addition of the DTE component also adds molecular weight, so the SSA (surface area per gram of material) should decrease. If we also try factor in changes in defect density (in the material), then this discussion becomes even more convoluted; it has been suggested that the dominant factor of these opposing effects changes as a function of linker length.[183]

As we increase the amount of DTE linker, the SSA of the MOFs decrease (Figure 4.8a). This suggests that molecular weight has more of an effect on the system than the added surface of the DTE side group. To probe this deeper and differentiate the interplay of potential defects and molar mass of the framework, quantitative NMR would be needed to determine the molecular formula of the MOF.

The surface area of the UiO MOFs was also plotted against the TPDC-DTE linker stoichiometry of each sample to obtain a trendline (Figure 4.8d). It was noticed that there is a negative linear correlation between the SSA of PSU-68 samples and the TPDC-DTE linker loading; it was also noticed that the surface areas of PSU-68 5 eq. and 6 eq. are very similar to one another from this plot. We believe that this similarity in adsorptivity is a result of 5 and 6 eq. having the same (or similar) levels of linker content in the pore. This results from the pores of the 6 eq. sample being sterically crowded to the point that no more TPDC-DTE linker fits into the framework (i.e., the interplay of defects and linker content in PSU-68 6 eq. coincidentally adsorbs N_2 similarly to PSU-68 5 eq.).

To further assess this observation, we accounted for the molecular weight of the

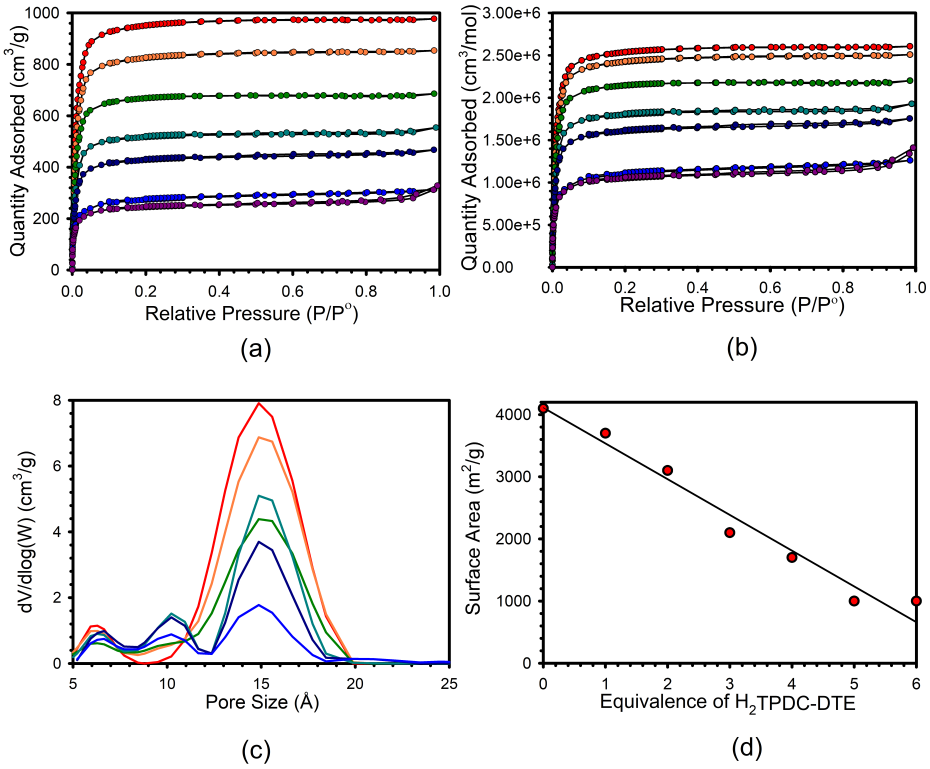

Figure 4.8: (a) N_2 gas adsorption isotherms of UiO-68 and PSU-68 series of MOFs illustrating an expected decrease in overall gas sorption and surface area of the material (b) Overall gas sorption of the porous materials from (a) expressed in cm^3/mol in order to normalize the y-axis to ensure that the gas sorption of the synthesized materials is not simply a result of different molecular weights (c) pore size distribution of UiO-68 and PSU-68 series of materials. A gradual decrease in the major 15 Å pore with a shift to smaller sized pores can be observed with greater loading of H_2TPDC−DTE (d) Linear relationship materials surface area in relation to the loading of H_2TPDC−DTE.

PSU-68 samples, which vary drastically depending on the amount of DTE-linker present. These materials have different molecular weights, so one material may be more porous when analyzing the data with a per pore basis but appear less porous when reporting gravimetric surface area (m^2/g). With isostructural MOFs like the PSU-68 series, a per mole comparison is reflective of singular pore analysis and is meaningful; this assumes the number of defects are constant. When gas uptake is analyzed using a per pore basis (Figure 4.8b), we see that the change in gas uptake

between 0 and 1 eq. is minimal, followed by more drastic decreases in uptake between 2-5 eq. and then another minimal change in uptake between the 5 and 6 eq. samples. This plot suggests that increasing the molar mass (via increasing TPDC-DTE content) is playing a role in decreasing the overall quantity of gas uptake. It is speculated from this plot that the similar uptake of 5 and 6 eq. samples shows further evidence that we have reached a steric limit in the pores of PSU-68, since the difference in uptake should theoretically show similar decreases in porosity, as observed between the 4 eq. and 5 eq. samples.

To follow up on this per pore analysis, we also performed pore size distribution analysis to determine the effect of the linker on the pore distribution present in the UiO MOF materials (Figure 4.8). We see two pores measured at 6 and 15 Å in the parent material UiO-68-NH_2 that agrees with previous reports that use the same preparation for UiO-68 MOFs.[181] With the addition of TPDC−DTE, we begin seeing a decrease in the number of 15 Å pores, with a subsequent increase in pores measuring 10 Å wide. While the number of 6 Å pores decreases, it is not as affected by the introduction of more DTE linkers. This data indicates that greater inclusion of H_2TPDC−DTE narrows the pore width of the major 15 Å pore to 10 Å.

4.3.5 Spectroscopic Analysis of PSU-68 MOFs

Unfortunately, due to the COVID-19 pandemic, no data on the spectroscopy and photoswitchable cycling of these MOFs or linkers was obtainable.

4.3.6 Photoactive Filtrations using PSU-68 MOFs

With the materials characterized to confirm their structural integrity and linker incorporation, we investigated the performance of these MOFs as photoactive filters using

methodology developed in Chapter 2, to frame the performance of the PSU-68 materials with PSZ-1 as a reference material. Through a 1 mL syringe with 50 mg of each MOF acting as a solid-phase plug, a solution of 1:1:1 (by mass) toluene, naphthalene, and pyrene in $CDCl_3$ was eluted through this filter plug and the analyte concentrations were monitored pre-filtration and post-filtration by ^{1}H NMR spectroscopy. To deconvolute Figure 4.9, we plotted the performance of PSU-68 by the ratio of enhanced retention (uptake); this is the analyte quantity retained in the closed form divided by the analyte quantity in the respective open form of the MOF. From Figure 4.9, we observe mild enhancement in uptake with 2 eq. of TPDC-DTE, followed by a dip in activity between 3 and 5 eq. where there is diminished uptake, and finally a spike in uptake again at 6 eq.

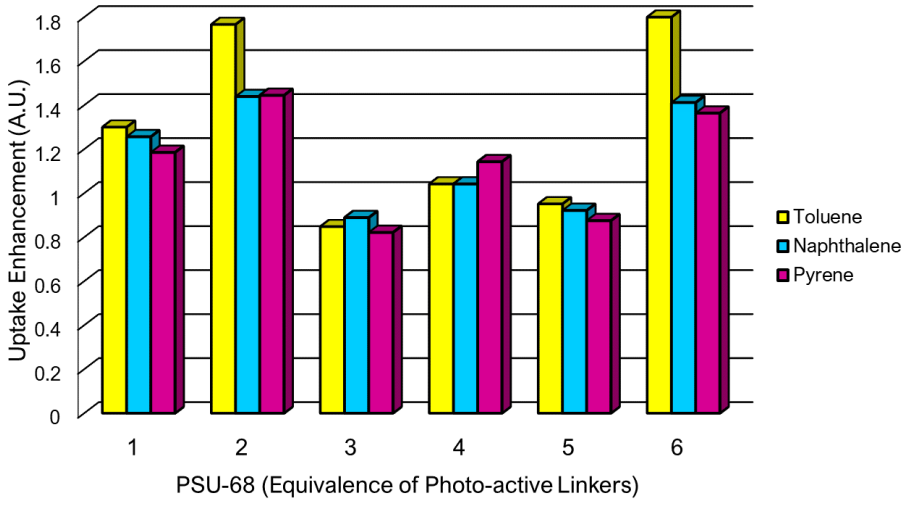

Figure 4.9: A bar graph depicting and comparing the relative uptakes of UiO-68-NH_2 and PSU-68 with varying equivalence of TPDC-DTE linker loading to monitor chemical separation as response to linker loading content.

Referring to PSZ-1 for a moment, the calculated uptake enhancement was determined to be 14× greater than PSZ-1-O. From this obtained data, the maximum uptake enhancement of PSU-68 is 1.8×. Considering that all PSU-68 variants have more linker than PSZ-1, it was surprising that PSU-68 did not perform as well, or

better than PSZ-1 when subjected to the same procedures. It was also unexpected to see a "valley" between 2 and 6 eq. where there was diminished activity.

An explanation for this observation is that the TPDC-DTE linker (and by extension PSU-68) was qualitatively observed to photoisomerize under UV light slowly (on the time span of a few minutes); this contrasts HL_1-HL_3 from Chapter 3, which photoisomerizes in a few seconds under UV light. Despite efforts to maximize photoisomerization through longer UV light durations, PSU-68 did not show improved adsorptivity in response to longer exposure time.

There are a few ways to interpret this data: one interpretation is that TPDC-DTE does not efficiently photoisomerize under UV light. This is not uncommon, as there are known examples of dithienylethene/diarylethene molecules that do not exhibit photochromism because of structural and electronic effects that inhibit the process. This interpretation is supported by the qualitative observation that TPDC-DTE (and PSU-68) emits bright yellow light when irradiated with 365 nm light (to promote photoisomerization). This emission is speculated to be an absorption of light by the TPDC moiety, which efficiently absorbs around the 350 nm region of the UV-Visible spectrum. This absorbance band most likely inadvertently overlaps with the absorbance band that promotes photoisomerization in the DTE moiety of the linker. Overlapping absorbance bands can lead to diminished photoswitching if the extinction coefficient for the competing processes have large differences in magnitude; if the incoming photons are preferentially absorbed by the TPDC absorbance band, then this would lead to slower and impeded photoswitching response in TPDC-DTE, and PSU-68 by extension. With less photoisomerized linker, we would most likely observe diminished adsorption/retention of diffusing analyte in the pore. This rationale explains the subpar separation behaviour of the PSU-68 materials, despite greater linker

content when compared to PSZ-1, and would have been further probed with UV-Vis experiments with more time to work on this project.

To discuss another observation, it is believed that the reason why 6 eq. shows increased retention and 5 eq. does not relates back to the steric environment of the pore as analyte elutes through. With PSU-68 (6 eq. we may be observing a difference in retention that results from sufficient crowding inside the pore; this forces analyte diffusing through the pore to exit the pores slower, since they interact with the linkers that are packed into the pore. However, as this is speculation, it is necessary to further test this speculation with quantitative NMR and UV-Visible analysis to further understand the linkers photophysical properties and confirm the true amount of linker difference between these samples.

4.4 Conclusions

In summary, we have reported the synthesis and characterization of novel Type II photoswitching UiO MOFs with pendant group dithienylethenes (PSU-68). PSU-68 was synthesized with varying quantities of photoswitching linker, ranging from 1-6 equivalence of linker as determined via ^{1}H NMR. These materials are of the well-defined UiO-topology as determined by PXRD, and were determined to be porous via N_2 isotherms. While the material did not display photoswitching adsorptivity, results obtained from photoactive filtration studies suggest the need for further study into the coordinated effects of ligand loading, pore environment and electronic structure to obtain the desired photoswitching response inside the MOF. We must also ensure that the pores are not so sterically crowded, that the photoswitching process and thus the analyte retention is hindered.

The results obtained in this chapter are very interesting when you think about how these results relate back to PSZ-1. Why would PSZ-1 show greater retention with 12.5 % linker incorporation, but PSU-68 effectively shows little, or no adsorptivity increase, despite greater quantities of photoswitching linker incorporation?

The work in this chapter suggests that incorporating photoswitch linkers into a MOF superficially (like with PSU-68) does not simply promise photoswitchable adsorptivity. The difference in the orientation and linker occupation of PSZ-1 and PSU-68 could helped us to rationalize why PSU-68 shows very different solution-phase adsorptivity, despite having more incorporated photoswitch than PSZ-1; the photoswitch lines the pore of PSZ-1 (instead of being suspended inside the pore like PSU-68) may explain this difference in behaviour.

Chapter 5

Conclusions and Future Work: What Would Be Done With 5 More Years?

5.1 Conclusions

Before proceeding to discuss future work, it is important to summarize the findings in this masters thesis work. This work presented PSZ-1 as one of the first examples of a Type II DTE photoswitching MOF being used for novel photoswitching adsorption. With further study into ligand functionalization of the core imidazole DTE skeleton, we learned that these photoswitches respond positively to electron donation, and extended aromaticity at the 2-imidazoyl site. In the 4^{th} chapter, we investigated the effect of linker loading on solution-phase adsorption in a UiO-based MOF system and developed the PSU-68 series of MOFs. While these MOFs contain TPDC-DTE photoswitch, unexpected electronic effects produced a diminished photoswitching response.

The results of this thesis work have highlighted that although PSZ-1 is limited by fast thermal cycloreversion processes, Type II photoswitching MOFs may have potential as efficient smart-adsorbents if a better photoswitch can be built off of a MOF linker. Some excellent points to consider when moving forward and builiding upon this work include a more extensive study into the photophysical properties of these switches. Some of the relevant properties that would be beneficial to study with these molecules include quantum yields of cyclization/cycloreversion, measuring and maximizing the amount of closed isomer obtainable (i.e., photostationary equilibrium) and a more thorough study into effects on the material from prolonged usage (i.e., does the switch decay or irreversibly isomerize over time?). These metrics would allow future researchers in this discipline to design better photoswitches, and in-turn better MOFs.

There are many fruitful directions to take within this field of research because relative to other disciplines, this field is very new. With respect to the work presented in this thesis, I will now discuss some ideas that I believe are effective and constructive ways to build off of this immediate work.

5.2 PSU-67 MOFs

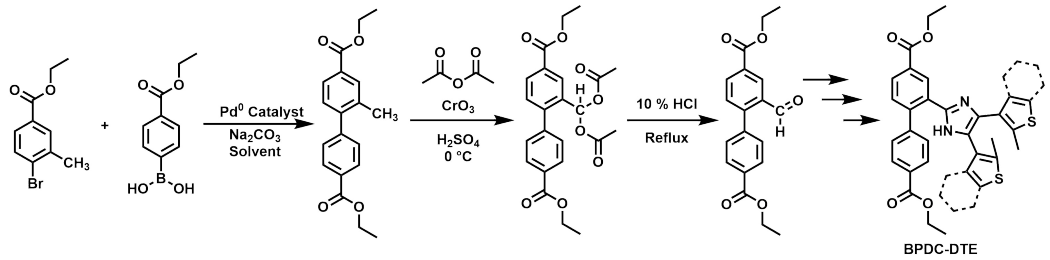

Figure 5.1: Proposed synthetic route for the design of BPDC photoswitching linkers which would allow direction comparison and contrast with previously synthesized PSU-68 materials.

In Chapter 4, we synthesized the novel DTE linker H_2TPDC−DTE and built this photoswitching linker into the pore of a UiO MOF, which was aptly named PSU-68. Concurrent with this reported work, I have previously obtained spectroscopic data of biphenyl functionalized linkers which displays fast and efficient photochromism in the solid state. A BPDC (biphenyldicarboxylate) DTE photoswitch (and by extension the resulting MOFs) would serve as a great side-by-side comparison with the reported TPDC-DTE photoswitch. With more time to perform research, I would pursue the synthesis of BPDC functionalized linkers for the synthesis of photoswitching UiO-67 MOF analogs which contain aldehyde side groups.[184,185] These linkers would produce new photoswitching MOFs which would serve as a great direct comparison with the previously reported PSU-68 materials. Figure 5.1 shows the synthetic protocol that would be used to obtain an aldehyde tagged BPDC linker as a synthetic precursor to a functionalized DTE photoswitch.

Additionally, I am greatly interested in expanding the possible functionalities we can decorate the thienyl rings with.[130,186] This would allow us to more thoroughly explore, and understand the photophysical properties which govern these linkers; previous efforts have been made to synthesize more complex functionalized linkers, but the intermediates are incredibly sensitive to light, heat and moisture and require more time and experience to work with. By optimizing the photophysical properties we may be able to obtain more thermally stable closed-isomers, or tune photoswitching adsorptivity for target analytes. For example, previous work by Irie and co-workers has shown that methoxy substituents have aided stabilization of the closed form isomer. To introduce new functionality to the thienyl groups, I would start with more complex thiophene starting materials, and through a series of synthetic steps (Figure 5.2) create a new series of 1,2-dione synthetic precursors. The inclusion of extended aromaticity in the form of fused benzo/phenyl side groups should introduce greater photowitching

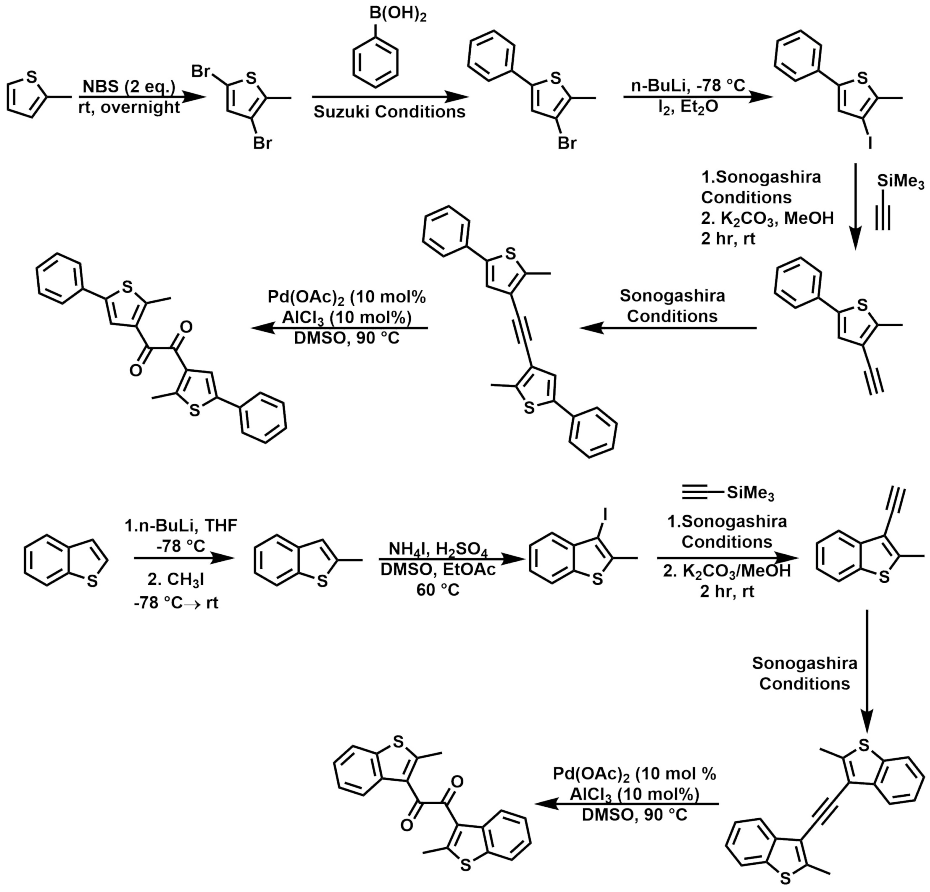

Figure 5.2: Proposed synthetic route for the design of more complex substituted 1,2-thienyl diketone precursors.

stability, and shifts in absorption maxima to lower energy wavelengths of light.

5.3 Photoswitching Conductivity

Another proposal for future work is investigating photoswitching DTE MOFs for switching conductivity; Shustova and co-workers have illustrated photoswitching conductivity in DTE MOFs for light responsive circuits.[187] The change in conjugation between the DTE-O and DTE-C isomers using UV light creates a bridge of extended conjugation, allowing charge delocalization throughout the molecule (Figure 5.3).

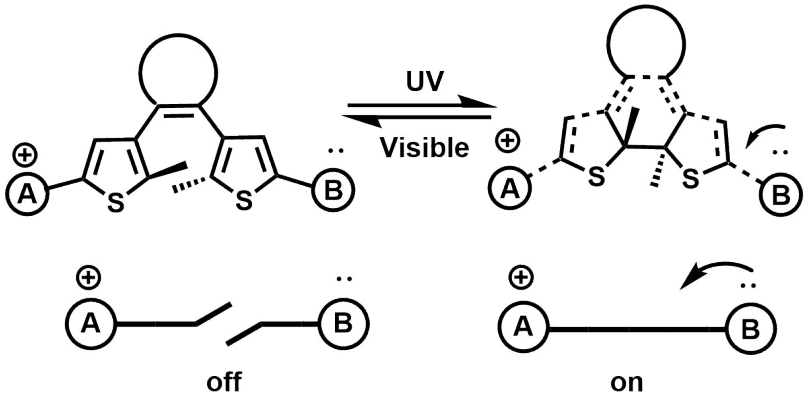

Figure 5.3: DTEs with charge separated A (positive charge) and B (negative charge) interacting through extended π conjugation of DTE-C which is illustrated as dotted lines denoting the path through which charge delocalizes.

While there are many fruitful directions that this project may advance in, the proposed future work is believed to be sensible, and viable pathways towards photoswitching DTE MOFs with improved photoswitching adsorptivity to build upon the initial findings of this masters thesis.

Appendices

No.	Shift1 (ppm	H's	Type	J (Hz)	Multiplet1	(ppm)
1	6.91	2	q	1.10	M01	[6.87 .. 6.94]
2	2.72	6	s	-	M02	[2.67 .. 2.77]
3	2.38	6	dd	1.10, 0.57	M03	[2.37 .. 2.39]

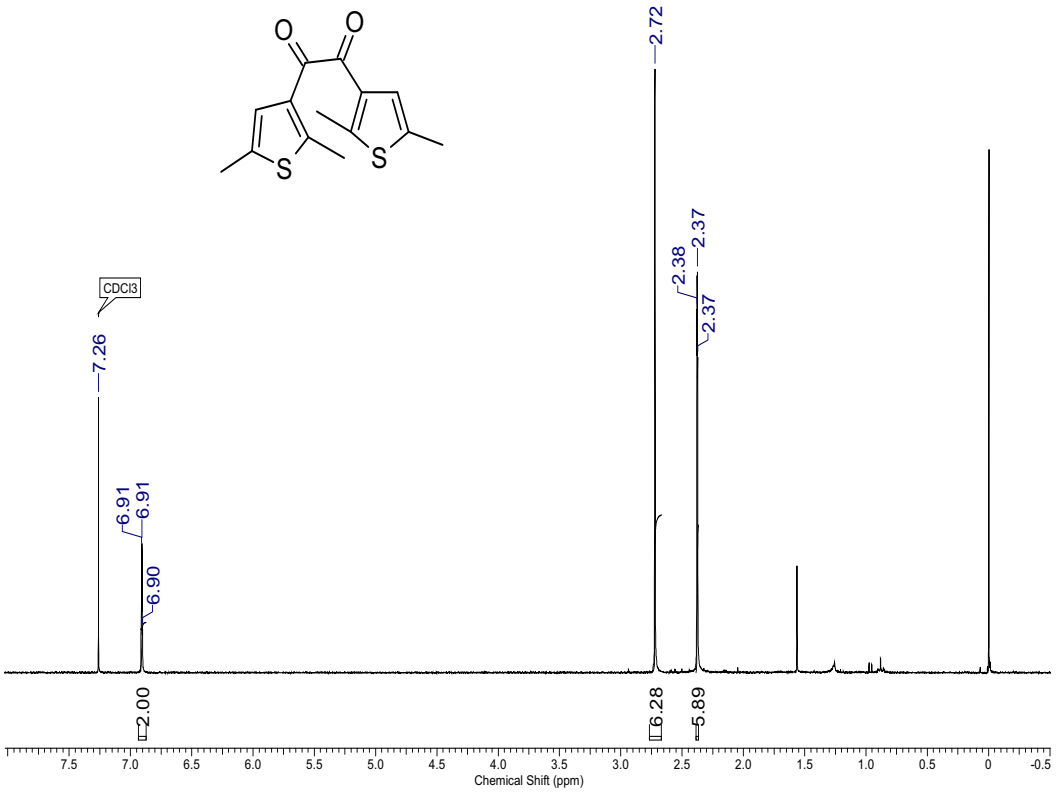

Figure 5.4: ^{1}H NMR of 1,2-bis(2,5-dimethyl-3-thiophenyl)ethanedione at 300 MHz

No.	Shift1 (ppm	H's	Type	Multiplet1	(ppm)
1	9.18	1	s	M01	[9.17 .. 9.19]
2	6.67	1	s	M02	[6.66 .. 6.69]
3	6.67	2	s	M05	[6.66 .. 6.69]
4	2.34	6	s	M03	[2.32 .. 2.36]
5	1.91	6	s	M04	[1.89 .. 1.93]

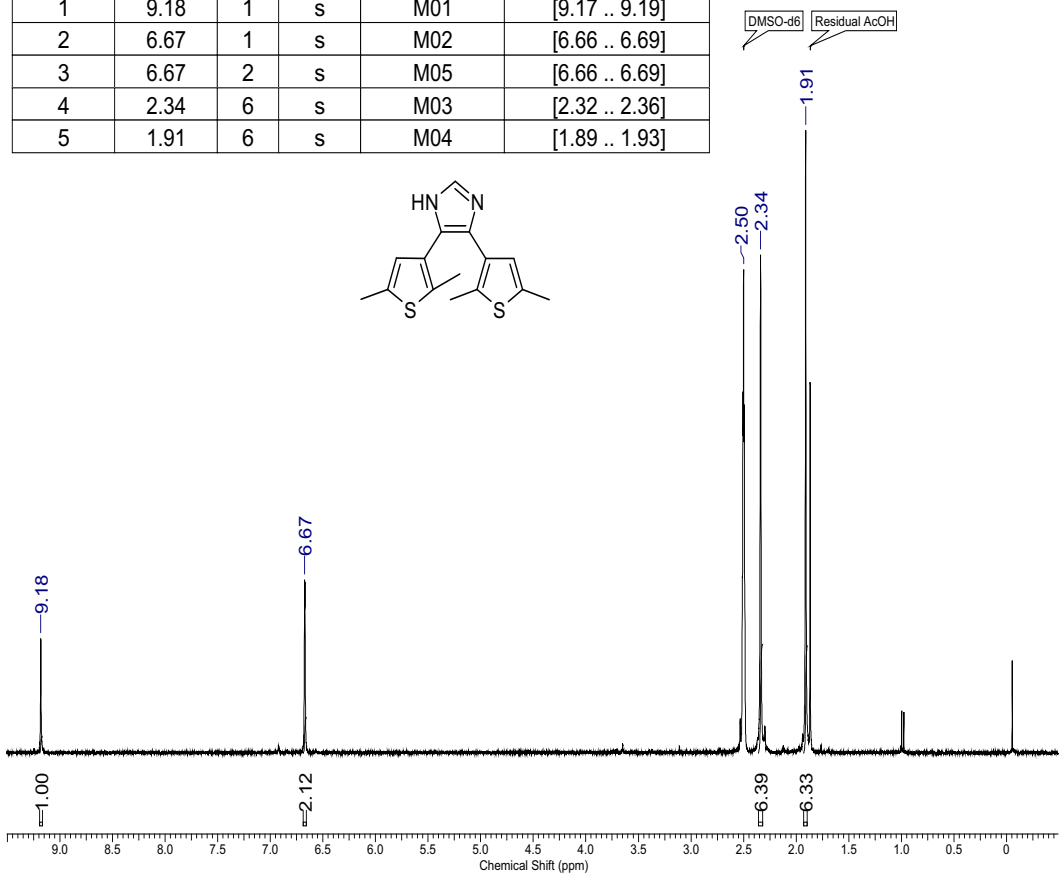

Figure 5.5: ^{1}H NMR of 4,5-bis(2,5-dimethyl-3-thiophenyl)-1H-imidazole (HL_1) in DMSO-d_6 at 300 MHz

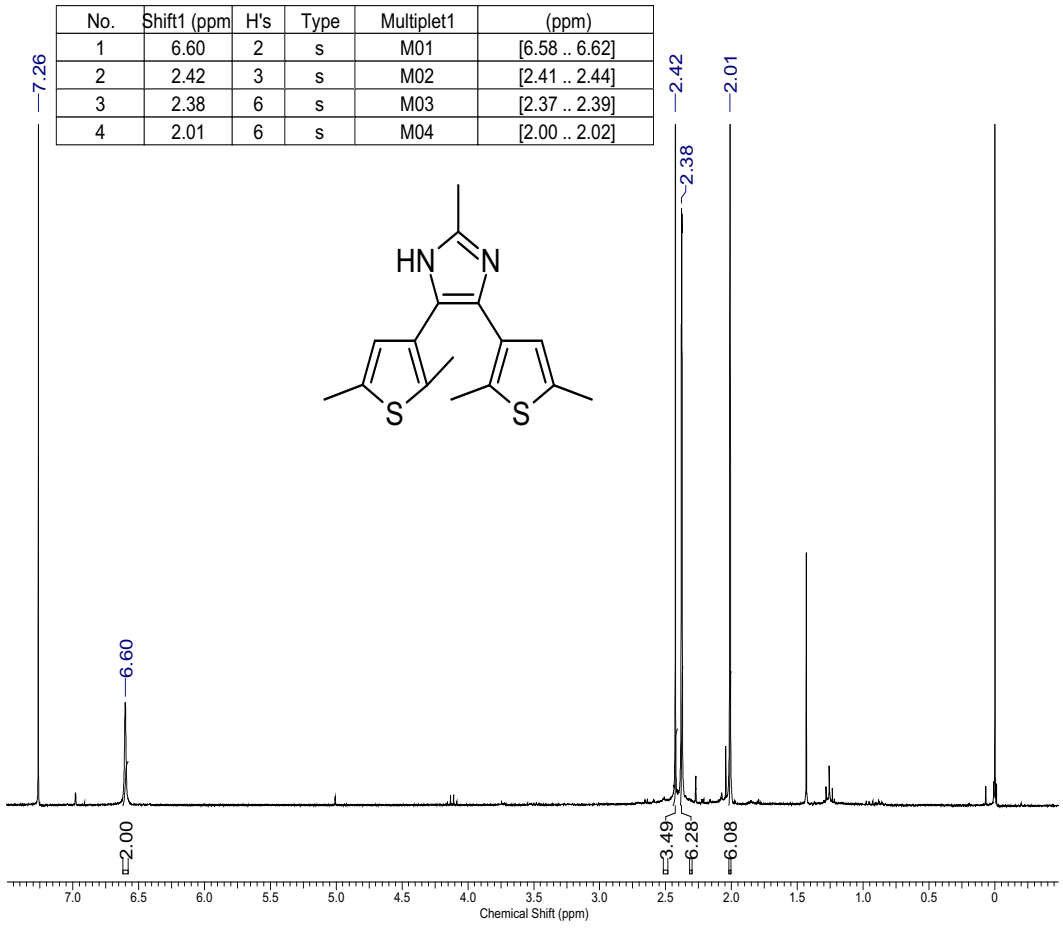

Figure 5.6: ^{1}H NMR of 4,5-bis(2,5-dimethyl-3-thiophenyl)-2-methyl-1H-imidazole (HL_2) in $CDCl_3$ at 300 MHz

No.	Shift1 (ppm	H's	Type	J (Hz)	Multiplet1	(ppm)
1	12.55	1	br. s	-	M01	[12.40 .. 12.66]
2	8.07	2	t	7.20	M02	[7.97 .. 8.15]
3	7.49	2	t	7.20	M03	[7.44 .. 7.57]
4	7.38	1	t	7.20	M04	[7.35 .. 7.42]
5	6.79	1	s	-	M05	[6.77 .. 6.81]
6	6.63	1	s	-	M06	[6.60 .. 6.65]
7	2.46	3	s	-	M07	[2.43 .. 2.48]
8	2.37	3	s	-	M08	[2.34 .. 2.40]
9	2.20	3	s	-	M09	[2.17 .. 2.22]
10	2.03	3	s	-	M10	[2.00 .. 2.05]

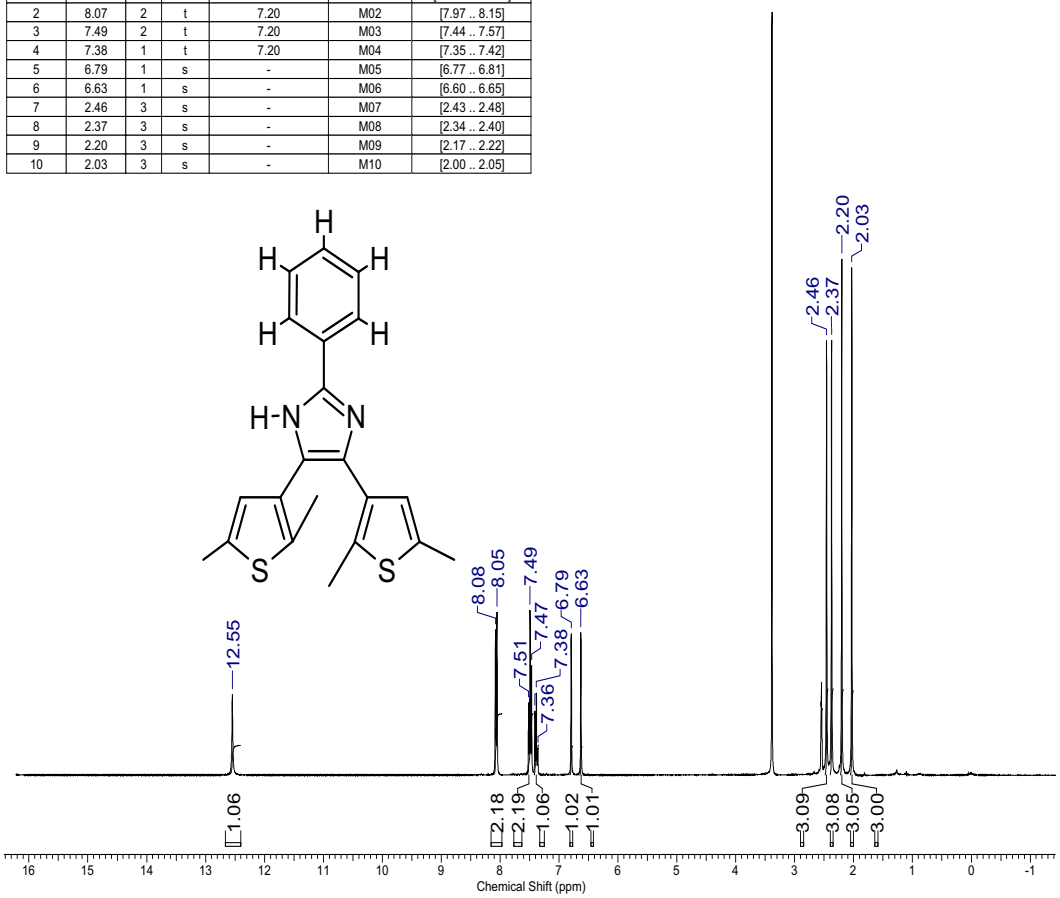

Figure 5.7: ^{1}H NMR of 4,5-bis(2,5-dimethyl-3-thiophenyl)-2-phenyl-1H-imidazole (HL_3) in DMSO-d_6 at 300 MHz

No.	Shift1 (ppm)	H's	Type	J (Hz)	Multiplet1	(ppm)
1	7.83	1	d	7.70	M02	[7.80 .. 7.85]
2	7.72	1	d	7.70	M03	[7.69 .. 7.74]
3	7.33	1	m	7.70	M04	[7.31 .. 7.37]
4	7.28	1	m	7.70	M05	[7.26 .. 7.31]
5	7.09	1	br. s.	-	M01	[7.06 .. 7.12]
6	2.60	3	br. s.	-	M06	[2.57 .. 2.62]

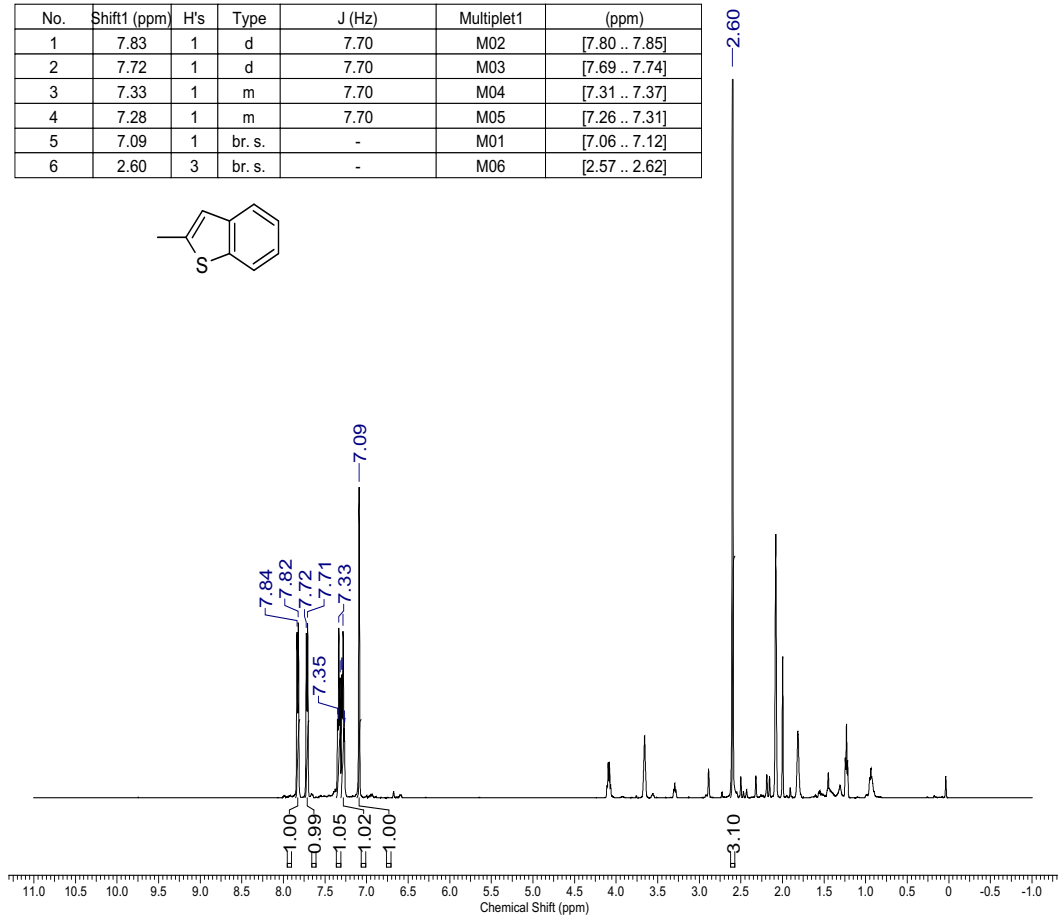

Figure 5.8: ^{1}H NMR of 2-methylbenzothiophene in acetone-d_6 at 300 MHz

No.	Shift1 (ppm)	H's	Type	J (Hz)	Multiplet1	(ppm)
1	7.89	1	d	8.07	M01	[7.87 .. 7.91]
2	7.71	1	d	8.07	M02	[7.68 .. 7.74]
3	7.49	1	td	7.61, 0.92	M03	[7.46 .. 7.52]
4	7.42	1	td	7.60, 0.90	M04	[7.39 .. 7.45]
5	2.57	3	br. s	-	M05	[2.56 .. 2.59]

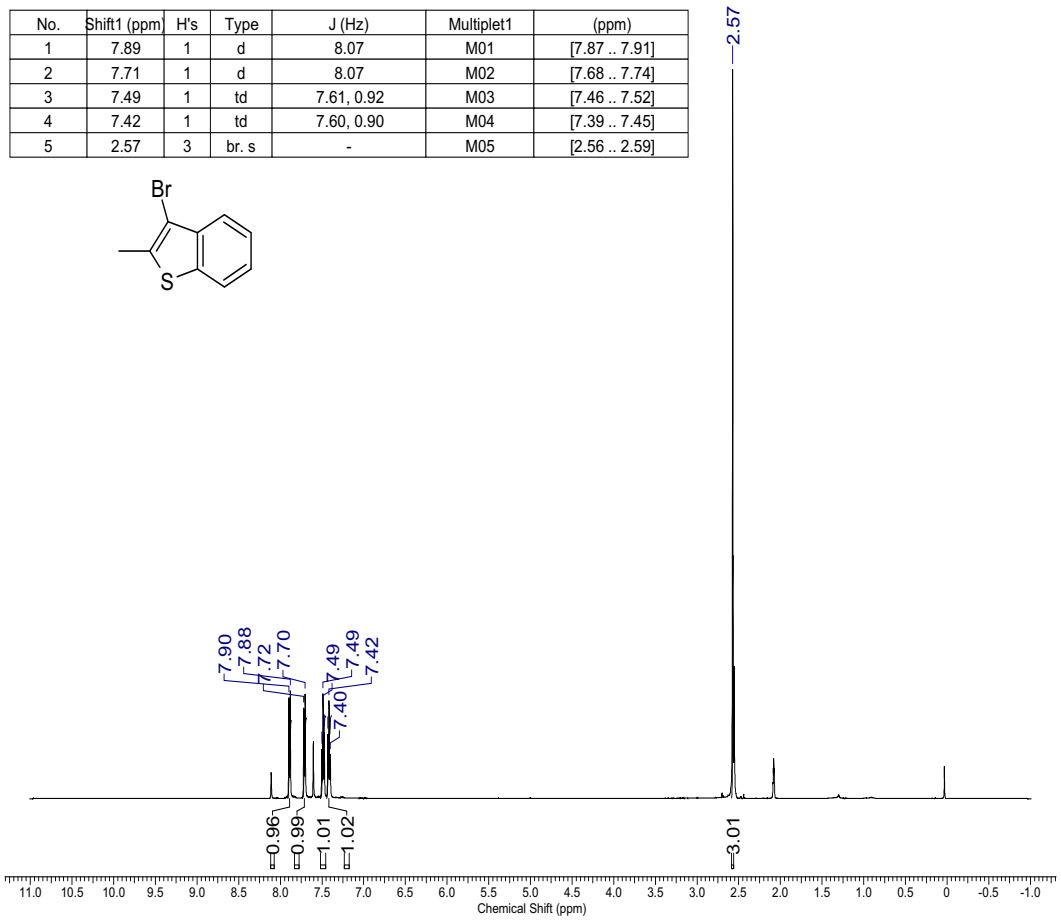

Figure 5.9: ^{1}H NMR of 3-bromo-2-methylbenzothiophene in acetone-d_6 at 300 MHz

No.	Shift1 (ppm	H's	Type	J (Hz)	Multiplet1	(ppm)
1	8.04	4	dq	8.40, 1.80	M05	[8.00 .. 8.07]
2	7.76	2	dt	8.40, 1.80	M04	[7.72 .. 7.79]
3	7.63	2	dt	8.40, 1.80	M03	[7.60 .. 7.66]
4	7.15	2	d	7.70	M02	[7.13 .. 7.17]
5	7.01	1	dd	7.70, 1.80	M01	[6.98 .. 7.03]
6	5.12	1	br. s.	-	M10	[5.09 .. 5.16]
7	4.34	2	q	7.20	M06	[4.29 .. 4.39]
8	4.34	2	q	7.10	M07	[4.29 .. 4.39]
9	1.34	3	t	7.20	M09	[1.31 .. 1.37]
10	1.34	3	t	7.10	M08	[1.31 .. 1.37]

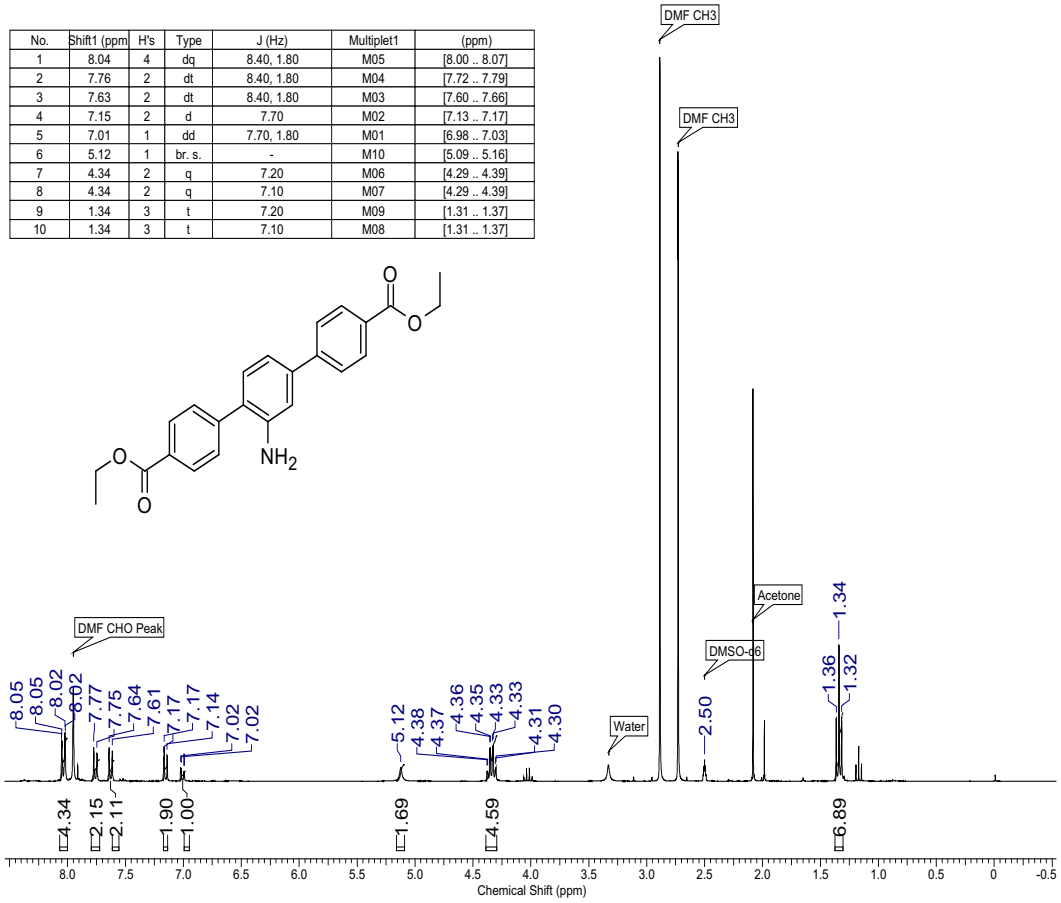

Figure 5.10: ^{1}H NMR of 1,4-bis(4-ethoxycarbonylphenyl)-3-aniline (Et_2TPDC-NH_2)

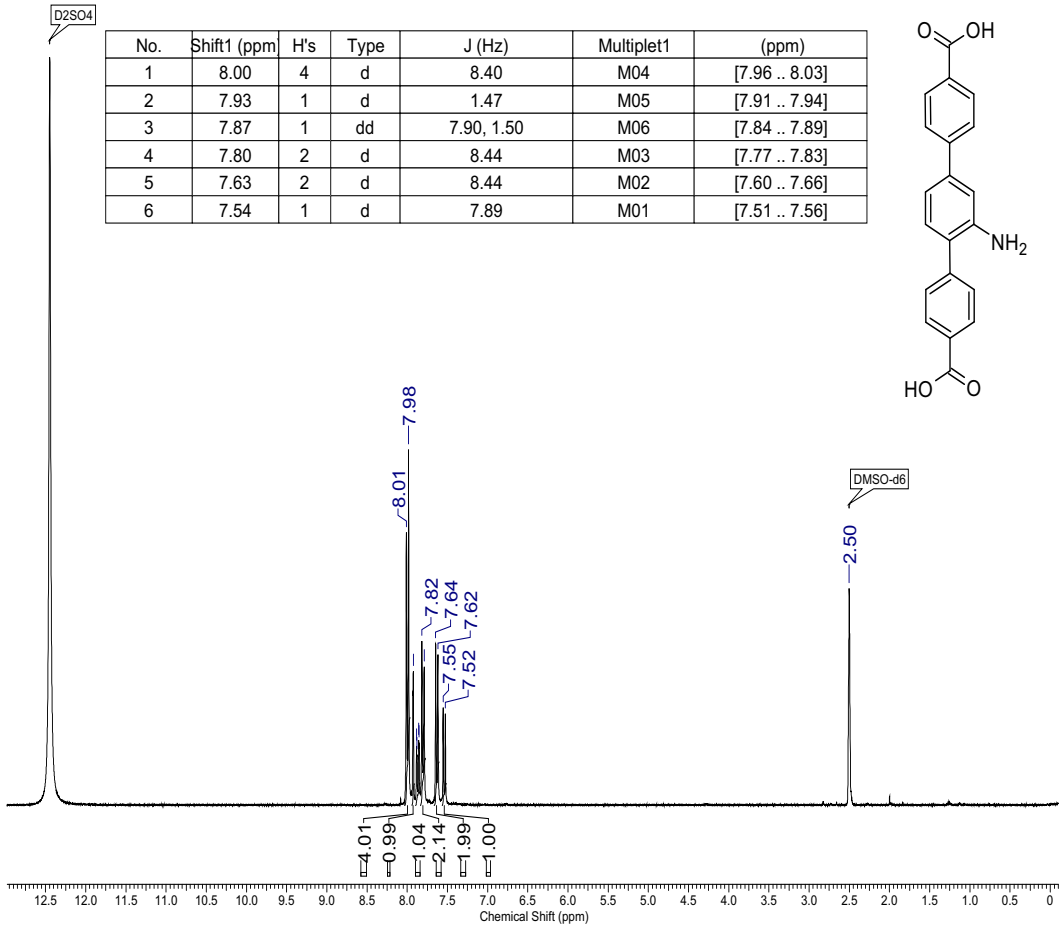

Figure 5.11: ^{1}H NMR of 1,4-bis(4-carboxyphenyl)-3-aniline (H_2TPDC-NH_2) in DMSO-d_6

No.	Shift1 (ppm	H's	Type	J (Hz)	Multiplet1	(ppm)
1	9.95	1	s	-	M05	[9.95 .. 9.96]
2	8.26	1	d	1.80	M06	[8.24 .. 8.27]
3	8.15	1	dd	8.07, 1.83	M07	[8.13 .. 8.17]
4	8.09	3	dd	8.44, 1.80	M08	[8.07 .. 8.11]
5	7.94	1	dt	8.44, 1.83	M09	[7.93 .. 7.97]
6	7.67	1	d	8.07	M11	[7.63 .. 7.69]
7	7.65	2	dt	8.44, 1.83	M10	[7.63 .. 7.69]
8	4.36	2	q	6.90	M04	[4.32 .. 4.40]
9	4.36	2	q	6.90	M03	[4.32 .. 4.40]
10	1.35	3	t	7.15	M02	[1.33 .. 1.38]
11	1.35	3	t	7.15	M01	[1.33 .. 1.38]

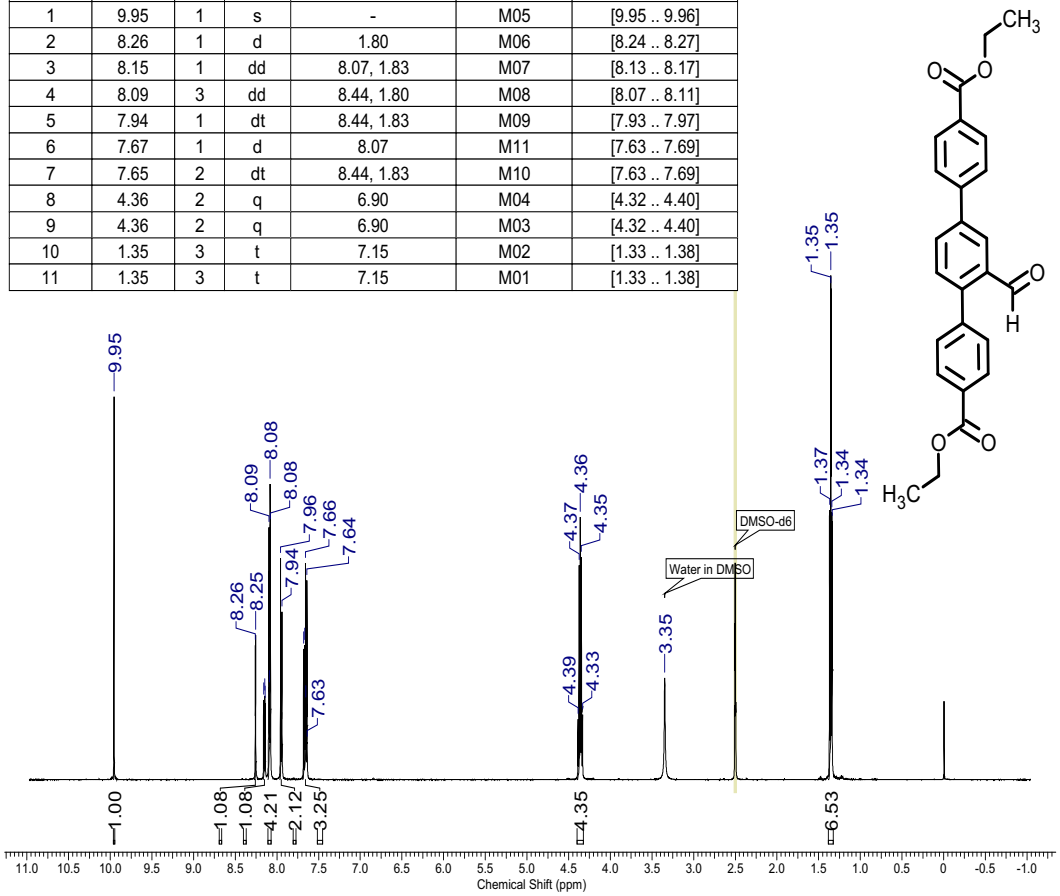

Figure 5.12: ^{1}H NMR of 1,4-bis(4-ethoxycarbonylphenyl)-3-benzaldehyde (Et_2TPDC-CHO)in DMSO-d_6

No.	Shift1 (ppm	H's	Type	J (Hz)	Multiplet1	(ppm)
1	8.36	1	d	2.00	M04	[8.35 .. 8.37]
2	8.19	1	dd	8.10, 2.00	M05	[8.17 .. 8.21]
3	8.09	2	m	8.60, 1.80	M07	[8.07 .. 8.12]
4	8.02	2	dt	8.60, 1.80	M08	[8.00 .. 8.04]
5	7.98	2	m	8.62, 1.80	M06	[7.96 .. 8.00]
6	7.82	1	d	8.10	M03	[7.80 .. 7.84]
7	7.41	3	dt	8.60, 1.80	M02	[7.39 .. 7.44]
8	6.59	1	s	-	M01	[6.56 .. 6.61]
9	6.58	1	s	-	M15	[6.55 .. 6.61]
10	4.33	2	q	7.00	M09	[4.27 .. 4.38]
11	4.31	2	q	7.10	M10	[4.27 .. 4.38]
12	2.33	6	s	-	M14	[2.31 .. 2.35]
13	1.84	6	s	-	M13	[1.82 .. 1.86]
14	1.32	4	t	7.06	M11	[1.26 .. 1.35]
15	1.29	3	t	7.15	M12	[1.26 .. 1.36]

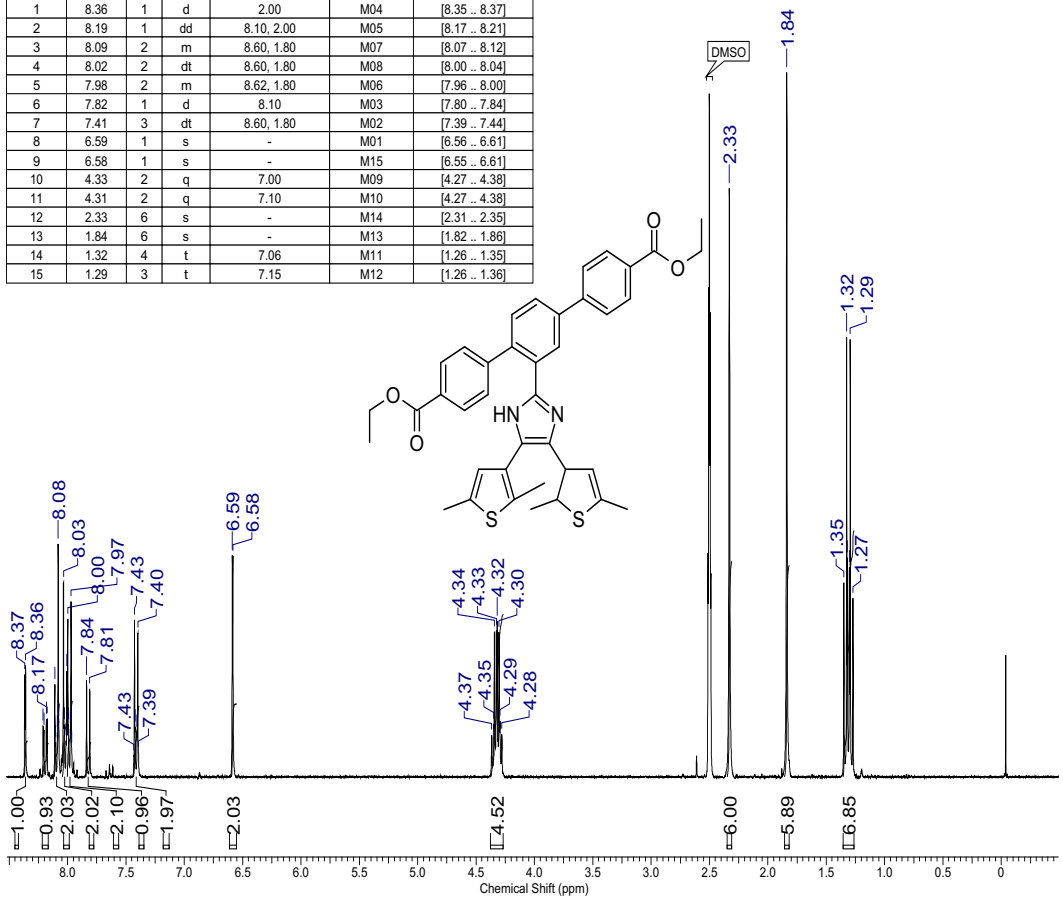

Figure 5.13: ^{1}H NMR of the complex molecule named (Et_2TPDC-DTE)in DMSO-d_6

No.	Shift1 (ppm)	H's	Type	J (Hz)	Multiplet1	(ppm)
1	8.35	1	d	1.30	M03	[8.34 .. 8.37]
2	8.18	1	d	8.10	M07	[8.15 .. 8.21]
3	8.07	2	d	8.10	M08	[8.04 .. 8.10]
4	8.00	2	d	8.30	M10	[7.97 .. 8.02]
5	7.97	2	d	8.10	M09	[7.93 .. 7.99]
6	7.81	1	d	8.30	M06	[7.78 .. 7.85]
7	7.38	2	d	8.30	M05	[7.35 .. 7.42]
8	6.58	2	s	-	M04	[6.54 .. 6.61]
9	2.33	6	s	-	M02	[2.29 .. 2.36]
10	1.83	6	s	-	M01	[1.80 .. 1.86]

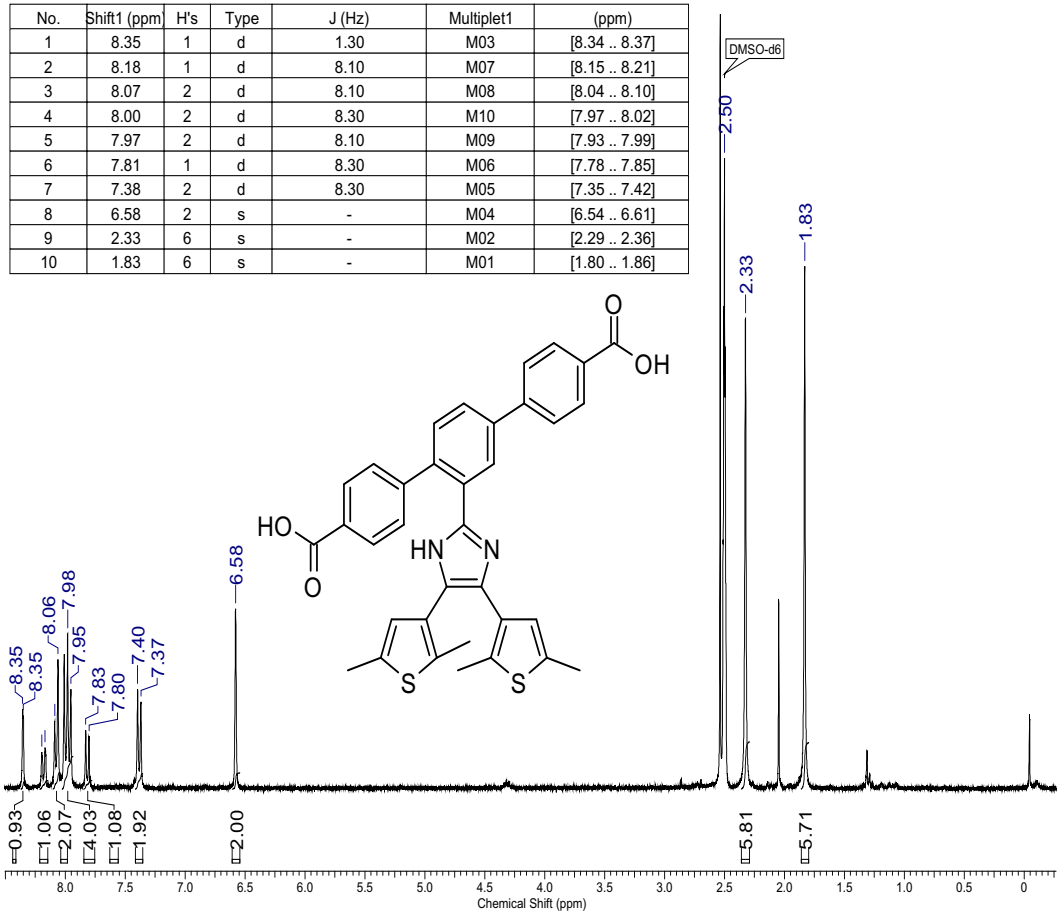

Figure 5.14: ^{1}H NMR of the complex molecule named (H_2TPDC-DTE)in DMSO-d_6

Single Crystal X-ray Crystallography Data

```
data_global
_audit_creation_date        "2017-07-20"
_audit_creation_method CRYSTALS_ver_14.61_build_6236


# start of 'script/refcif.dat'
_publ_contact_author_name         'Structure solved by - Michael Katz'
_publ_contact_author_address
;
 Department of Chemistry,
 Memorial University of Newfoundland,
 St. John's NL,
 Canada, A1B 3X5.
;

_publ_contact_author_phone        '+1-709-864-8745'
_publ_contact_author_fax          '+1-709-864-4042'
_publ_contact_author_email        'mkatz@mun.ca'
_publ_requested_journal           'J. Am. Chem. Soc.'

_publ_section_title
# Title of paper - generally just the systematic or trivial name
;
Bistable Dithienylethene-Based Metal-Organic Framework
Illustrating Optically Induced Changes in Chemical Separations
;
```

```
# The loop structure below should contain the names and addresses of all
# authors, in the required order of publication. Repeat as necessary.


loop_
 _publ_author_name
 _publ_author_address
'Brandon J. Furlong'
;
 Department of Chemistry,
 Memorial University of Newfoundland,
 St. John's NL,
 Canada, A1B 3X7.
;
 'Michael J. Katz'
;
 Department of Chemistry,
 Memorial University of Newfoundland,
 St. John's NL,
 Canada, A1B 3X7.
;

_publ_section_exptl_refinement
;
```

```
The H atoms were were positioned geometrically.
The H atoms were initially refined with soft restraints on the
bond lengths and angles to regularise their geometry
(C---H in the range 0.93--0.98,
N---H in the range 0.86--0.89
N---H to 0.86
O---H = 0.82
\%A)
and
U~iso~(H) (in the range 1.2-1.5 times U~eq~ of the parent atom),
after which the positions were refined with riding constraints
(Cooper et al, 2010).

Cooper, R. I., Thompson, A. L. & Watkin, D. J. (2010). J. Appl. Cryst.
43, 1100-1107.

;
data_ZIF-70_250K

_exptl_special_details
;
 The crystal was
placed in the cold stream of an Oxford
Cryosystems 800 series open-flow nitrogen cryostat (Cosier &
Glazer, 1986) with a nominal stability of 0.1K.
```

```
Cosier, J. & Glazer, A.M., 1986. J. Appl. Cryst. 105-107.
;
# End of 'script/refcif.dat'
#end of refcif
_cell_length_a                    27.0265(8)
_cell_length_b                    27.0265(8)
_cell_length_c                    17.8985(9)
_cell_angle_alpha                 90
_cell_angle_beta                  90
_cell_angle_gamma                 120
_cell_volume                      11322.1(8)
_cell_oxdiff_length_a                  27.0320(10)
_cell_oxdiff_length_b                  27.0328(12)
_cell_oxdiff_length_c                  17.8873(9)
_cell_oxdiff_angle_alpha               90.066(4)
_cell_oxdiff_angle_beta                89.940(4)
_cell_oxdiff_angle_gamma               119.981(4)
_cell_oxdiff_volume                    11322.1(8)
_cell_oxdiff_measurement_reflns_used   13191

_symmetry_space_group_name_H-M_alt 'P 63/m 2/m 2/c'
_symmetry_space_group_name_H-M 'P 63/m m c'
_symmetry_space_group_name_Hall   ?
loop_
 _symmetry_equiv_pos_as_xyz
 'x,y,z'
```

```
 '-x,-y,-z'
 'x-y,x,z+1/2'
 '-x+y,-x,-z+1/2'
 '-y,x-y,z'
 'y,-x+y,-z'
 '-x,-y,z+1/2'
 'x,y,-z+1/2'
 '-x+y,-x,z'
 'x-y,x,-z'
 'y,-x+y,z+1/2'
 '-y,x-y,-z+1/2'
 '-x+y,y,z'
 'x-y,-y,-z'
 'y,x,z+1/2'
 '-y,-x,-z+1/2'
 'x,x-y,z'
 '-x,-x+y,-z'
 'x-y,-y,z+1/2'
 '-x+y,y,-z+1/2'
 '-y,-x,z'
 'y,x,-z'
 '-x,-x+y,z+1/2'
 'x,x-y,-z+1/2'

loop_
_atom_type_symbol
```

```
_atom_type_scat_dispersion_real
_atom_type_scat_dispersion_imag
_atom_type_scat_Cromer_Mann_a1
_atom_type_scat_Cromer_Mann_b1
_atom_type_scat_Cromer_Mann_a2
_atom_type_scat_Cromer_Mann_b2
_atom_type_scat_Cromer_Mann_a3
_atom_type_scat_Cromer_Mann_b3
_atom_type_scat_Cromer_Mann_a4
_atom_type_scat_Cromer_Mann_b4
_atom_type_scat_Cromer_Mann_c
_atom_type_scat_source
 C       0.0033   0.0016   2.3100  20.8439   1.0200  10.2075   1.5886   0.5687
   0.8650  51.6512   0.2156 'International Tables Vol C 4.2.6.8 and 6.1.1.4'
 H       0.0000   0.0000   0.4930  10.5109   0.3229  26.1257   0.1402   3.1424
   0.0408  57.7998   0.0030 'International Tables Vol C 4.2.6.8 and 6.1.1.4'
 N       0.0061   0.0033  12.2126   0.0057   3.1322   9.8933   2.0125  28.9975
   1.1663   0.5826 -11.5290 'International Tables Vol C 4.2.6.8 and 6.1.1.4'
 O       0.0106   0.0060   3.0485  13.2771   2.2868   5.7011   1.5463   0.3239
   0.8670  32.9089   0.2508 'International Tables Vol C 4.2.6.8 and 6.1.1.4'
 Zn      0.2839   1.4301  14.0743   3.2655   7.0318   0.2333   5.1652  10.3163
   2.4100  58.7097   1.3041 'International Tables Vol C 4.2.6.8 and 6.1.1.4'


_cell_formula_units_Z                  12
```

```
# Given Formula = C6 H4.50 N5.50 O3 Zn1.00
# Dc =      1.61 Fooo =   5453.00 Mu =     22.22 M =    267.02
# Found Formula = C3.51 H3.22 N2.63 O0.59 Zn0.59
# Dc =      0.78 FOOO =   2664.00 Mu =     12.83 M =    129.96

_chemical_formula_sum             'C12 H11 N9 O2 Zn2'
_chemical_formula_moiety          'C12 H11 N9 O2 Zn2'
_chemical_compound_source               ?
_chemical_formula_weight            444.08



_cell_measurement_reflns_used   13189
_cell_measurement_theta_min     2.0820
_cell_measurement_theta_max     24.1360
_cell_measurement_temperature          250

_exptl_crystal_description        'hexagonal prism'
_exptl_crystal_colour             'yellow'
_exptl_crystal_size_max           0.2
_exptl_crystal_size_mid           0.15
_exptl_crystal_size_min           0.15

_exptl_crystal_density_diffrn     0.781
_exptl_crystal_density_method     'not measured'
# dispersive F(000):
_exptl_crystal_F_000              2664.001
```

```
_exptl_absorpt_coefficient_mu     1.283

# Sheldrick geometric approximatio 1.00 1.00
_exptl_absorpt_correction_T_min                  0.84704
_exptl_absorpt_correction_T_max                  1.00000
_exptl_absorpt_correction_type            multi-scan
_exptl_absorpt_process_details
;
CrysAlisPro 1.171.38.41o (Rigaku Oxford Diffraction, 2015)
Empirical absorption correction using spherical harmonics,
 implemented in SCALE3 ABSPACK scaling algorithm.
;
_oxdiff_exptl_absorpt_empirical_full_min          0.894
_oxdiff_exptl_absorpt_empirical_full_max          1.225
_oxdiff_exptl_absorpt_empirical_details
;
Empirical correction (ABSPACK) includes:
- Absorption correction using spherical harmonics
- Frame scaling
- Detector area scaling
;

_diffrn_source 'fine-focus sealed X-ray tube'
_diffrn_source_type 'Enhance (Mo) X-ray Source'
_diffrn_radiation_probe x-ray
_diffrn_radiation_type 'Mo K\a'
```

```
_diffrn_radiation_wavelength 0.71073
_diffrn_radiation_monochromator graphite
_diffrn_measurement_device 'Rigaku Saturn 70 AFC8'
_diffrn_measurement_device_type
;
dtrek-CrysAlisPro-abstract goniometer
imported rigaku-d*trek images
;
_diffrn_ambient_temperature        250
_diffrn_detector 'CCD plate'
_diffrn_reflns_number 173404
_diffrn_reflns_av_R_equivalents 0.1291
_diffrn_reflns_av_sigmaI/netI 0.1346
_diffrn_reflns_limit_h_min -36
_diffrn_reflns_limit_h_max 37
_diffrn_reflns_limit_k_min -36
_diffrn_reflns_limit_k_max 37
_diffrn_reflns_limit_l_min -24
_diffrn_reflns_limit_l_max 24
_diffrn_reflns_theta_min 1.7401
_diffrn_reflns_theta_max 29.5382
_diffrn_measured_fraction_theta_max 0.9840
_diffrn_reflns_theta_full 29.4729
_diffrn_measured_fraction_theta_full 0.9840
_diffrn_orient_matrix_type 'CrysAlisPro convention (1999,Acta A55,543-557)'
_diffrn_orient_matrix_UB_11       0.0295731000
```

```
_diffrn_orient_matrix_UB_12       0.0160799000
_diffrn_orient_matrix_UB_13       0.0083489000
_diffrn_orient_matrix_UB_21      -0.0065647000
_diffrn_orient_matrix_UB_22       0.0025510000
_diffrn_orient_matrix_UB_23       0.0377099000
_diffrn_orient_matrix_UB_31       0.0000093000
_diffrn_orient_matrix_UB_32      -0.0255443000
_diffrn_orient_matrix_UB_33       0.0089842000
_diffrn_measurement_details
;
List of Runs (angles in degrees, time in seconds):

  # Type    Start    End  Width  t~exp~   \w     \q     \k     \f   Frames
------------------------------------------------------------------------------
  1  \w    -70.00 110.00   0.50    5.00    --   20.00  54.00   0.00  360
  2  \w    -70.00 110.00   0.50    5.00    --   20.00  54.00  90.00  360
  3  \w    -70.00 110.00   0.50    5.00    --   20.00  54.00 180.00  360
  4  \w    -70.00 110.00   0.50    5.00    --   20.00  54.00 270.00  360
;
_diffrn_measurement_method '\w scans'
_symmetry_cell_setting hexagonal
_space_group_IT_number 194
_space_group_crystal_system hexagonal
_space_group_name_H-M_alt 'P 63/m m c'
_reflns_odcompleteness_completeness 98.40
_reflns_odcompleteness_theta 29.47
```

```
_reflns_odcompleteness_iscentric 1
_chemical_oxdiff_formula Zn(N2C3H3)0.5(N2C3NO2H2)1.5


# If a reference occurs more than once, delete the author
# and date from subsequent references.
_computing_data_collection        'Rigaku Crystal Clear Expert 2.1 SM'
_computing_cell_refinement        'CrystAlis Pro'
_computing_data_reduction         'CrystAlis Pro'
_computing_structure_solution     'SHELXS 86 (Sheldrick, 1986)'
_computing_structure_refinement   'CRYSTALS (Betteridge et al., 2003)'
_computing_publication_material   'CRYSTALS (Betteridge et al., 2003)'

# Number of reflections without Friedels Law is 0
# Number of reflections with Friedels Law is 5676
# Theoretical number of reflections is about 9929


_reflns_number_total              5676
_reflns_limit_h_min               -12
_reflns_limit_h_max               12
_reflns_limit_k_min               0
_reflns_limit_k_max               6
_reflns_limit_l_min               0
_reflns_limit_l_max               44
```

```
_atom_sites_solution_primary      direct #heavy,direct,difmap,geom,iterative
_atom_sites_solution_hydrogens    geom

_refine_diff_density_min          -7.95
_refine_diff_density_max          8.48


# The current dictionary definitions do not cover the
# situation where the reflections used for refinement were
# selected by a user-defined sigma threshold


# The values actually used during refinement
_oxford_reflns_threshold_expression_ref     I>3.0\s(I)
_refine_ls_number_reflns          2498
_refine_ls_number_restraints      128
_refine_ls_number_parameters      152
_oxford_refine_ls_R_factor_ref    0.1364
_refine_ls_wR_factor_ref          0.3030
_refine_ls_goodness_of_fit_ref    0.8295
_refine_ls_shift/su_max           0.0147975
_refine_ls_shift/su_mean          0.0015604
```

```
# The values computed with all filters except I/sigma
_oxford_reflns_number_all         5652
_refine_ls_R_factor_all           0.2066
_refine_ls_wR_factor_all          0.3549

# The values computed with a 2 sigma cutoff - a la SHELX
_reflns_threshold_expression      I>2.0\s(I)
_reflns_number_gt                 2933
_refine_ls_R_factor_gt            0.1464
_refine_ls_wR_factor_gt           0.3125

# choose from: rm (reference molecule of known chirality),
# ad (anomolous dispersion - Flack), rmad (rm and ad),
# syn (from synthesis), unk (unknown) or . (not applicable).
_chemical_absolute_configuration  '.'


_refine_ls_structure_factor_coef  Fsqd
_refine_ls_matrix_type            full
_refine_ls_hydrogen_treatment     constr         # undef, noref, refall,
   # refxyz, refU, constr or mixed
_refine_ls_extinction_method
    'None'
_oxford_refine_ls_scale 1.048(13)
_refine_ls_weighting_scheme       calc
_refine_ls_weighting_details
```

```
;
 Method, part 1, Chebychev polynomial, (Watkin, 1994, Prince, 1982)
 [weight] = 1.0/[A~0~*T~0~(x)+A~1~*T~1~(x) ... +A~n-1~]*T~n-1~(x)]
 where A~i~ are the Chebychev coefficients listed below and x= Fcalc/Fmax
 Method = Robust Weighting (Prince, 1982)
 W = [weight] * [1-(deltaF/6*sigmaF)^2^]^2^
 A~i~ are:
 0.385E+04 0.645E+04 0.409E+04 0.183E+04 482.
;
# Insert your own references if required - in alphabetical order
_publ_section_references
;

Betteridge, P.W., Carruthers, J.R., Cooper, R.I.,
Prout, K. & Watkin, D.J. (2003). J. Appl. Cryst. 36, 1487.

Prince, E.
Mathematical Techniques in Crystallography
and Materials Science
Springer-Verlag, New York, 1982.

Sheldrick, G. M. (2008). Acta Cryst A64, 112-122.

Watkin D.J. (1994).
Acta Cryst, A50, 411-437.
;
```

```
# Uequiv = arithmetic mean of Ui i.e. Ueqiv = (U1+U2+U3)/3

# Replace last . with number of unfound hydrogen atoms attached to an atom.

# ..._refinement_flags_...
# . no refinement constraints          S special position constraint on site
# G rigid group refinement of site     R riding atom
# D distance or angle restraint on site T thermal displacement constraints
# U Uiso or Uij restraint (rigid bond)  P partial occupancy constraint


loop_
_atom_site_label
_atom_site_type_symbol
_atom_site_fract_x
_atom_site_fract_y
_atom_site_fract_z
_atom_site_U_iso_or_equiv
_atom_site_occupancy
_atom_site_adp_type
_atom_site_refinement_flags_posn
_atom_site_refinement_flags_adp
_atom_site_refinement_flags_occupancy
_atom_site_disorder_assembly
_atom_site_disorder_group
```

```
_atom_site_attached_hydrogens
Zn1 Zn 0.55641(5) 0.66721(5) 0.57877(8) 0.0660 1.0000 Uani . . . . . .
N1 N 0.6182(4) 0.6605(4) 0.5295(7) 0.0865 1.0000 Uani . U . . . .
N2 N 0.5724(6) 0.6663(7) 0.6897(11) 0.1328 1.0000 Uani . U . . . .
N3 N 0.5557(3) 0.7358(3) 0.5460(3) 0.0978 1.0000 Uani D U . . . .
N4 N 0.4835(3) 0.6001(3) 0.5463(4) 0.0829 1.0000 Uani D U . . . .
N22 N 0.4978(9) 0.6674(10) 0.7500 0.1174 1.0000 Uani S TU . . . .
O22 O 0.4768(6) 0.6675(7) 0.6908(8) 0.1418 1.0000 Uani . . . . . .
C11 C 0.6751(6) 0.7001(7) 0.5191(10) 0.1069 1.0000 Uani . U . . . .
C12 C 0.6144(6) 0.6144(6) 0.500000(7) 0.0865 1.0000 Uani S TU . . . .
C21 C 0.6259(9) 0.6680(9) 0.7087(12) 0.1471 1.0000 Uani . U . . . .
C22 C 0.5483(11) 0.6672(11) 0.7500 0.1175 1.0000 Uani S TU . . . .
C31 C 0.5818(6) 0.7652(3) 0.4675(15) 0.1037 0.618(19) Uani D U P . 5 .
C32 C 0.5461(5) 0.7730(3) 0.5784(11) 0.0947 0.618(19) Uani DS TU P . 5 .
C33 C 0.4912(17) 0.7199(8) 0.5075(11) 0.0969 0.382(19) Uani D U P . 6 .
C34 C 0.5797(8) 0.7899(4) 0.5612(7) 0.0961 0.382(19) Uani DS TU P . 6 .
C41 C 0.4408(6) 0.6106(6) 0.5019(10) 0.0902 0.457(16) Uani D U P . 7 .
C42 C 0.4530(3) 0.5470(3) 0.5660(7) 0.0657 0.457(16) Uani DS TU P . 7 .
C43 C 0.4707(2) 0.5806(2) 0.4689(16) 0.0814 0.543(16) Uani D U P . 8 .
C44 C 0.44062(18) 0.55938(18) 0.5818(10) 0.0656 0.543(16) Uani DS TU P . 8 .
H111 H 0.6915 0.7389 0.5282 0.16(4) 1.0000 Uiso R . . . . .
H121 H 0.5800 0.5800 0.5000 0.16(4) 1.0000 Uiso RS . . . . .
H211 H 0.6537 0.6679 0.6764 0.16(4) 1.0000 Uiso R . . . . .
H311 H 0.5972 0.7521 0.4294 0.16(4) 0.618(19) Uiso R . P . 5 .
H321 H 0.5312 0.7656 0.6269 0.16(4) 0.618(19) Uiso RS . P . . .
H331 H 0.4621 0.6840 0.4894 0.16(4) 0.382(19) Uiso R . P . 6 .
```

```
H341 H 0.6160 0.8080 0.5852 0.16(4) 0.382(19) Uiso RS . P . 6 .
H411 H 0.4476 0.6451 0.4809 0.16(4) 0.457(16) Uiso R . P . 7 .
H421 H 0.4690 0.5310 0.5988 0.16(4) 0.457(16) Uiso RS . P . 7 .
H431 H 0.4945 0.5978 0.4274 0.16(4) 0.543(16) Uiso R . P . 8 .
H441 H 0.4383 0.5617 0.6345 0.16(4) 0.543(16) Uiso RS . P . 8 .

loop_
_atom_site_aniso_label
_atom_site_aniso_U_11
_atom_site_aniso_U_22
_atom_site_aniso_U_33
_atom_site_aniso_U_23
_atom_site_aniso_U_13
_atom_site_aniso_U_12
Zn1 0.0653(8) 0.0464(6) 0.0953(9) -0.0118(7) 0.0096(7) 0.0347(6)
N1 0.067(5) 0.071(5) 0.125(7) -0.021(5) 0.022(5) 0.037(4)
N2 0.100(8) 0.126(8) 0.192(12) 0.001(7) -0.010(6) 0.072(7)
N3 0.130(9) 0.065(5) 0.115(8) 0.001(5) -0.001(7) 0.060(6)
N4 0.063(4) 0.056(4) 0.123(5) 0.000(4) 0.002(4) 0.025(3)
N22 0.095(9) 0.106(8) 0.188(13) 0.0000 0.0000 0.077(7)
O22 0.114(10) 0.189(14) 0.152(10) 0.012(11) 0.009(8) 0.099(10)
C11 0.082(7) 0.081(7) 0.140(9) -0.027(7) 0.022(7) 0.028(6)
C12 0.068(5) 0.068(5) 0.122(10) -0.017(4) 0.017(4) 0.033(6)
C21 0.106(9) 0.148(10) 0.196(13) -0.002(9) -0.003(8) 0.070(9)
C22 0.096(9) 0.106(8) 0.188(13) 0.0000 0.0000 0.078(7)
C31 0.135(12) 0.074(8) 0.123(11) 0.002(8) -0.001(10) 0.067(8)
```

```
C32 0.125(11) 0.067(6) 0.112(10) -0.001(5) -0.001(9) 0.063(6)
C33 0.131(12) 0.060(9) 0.116(12) 0.004(9) -0.006(11) 0.060(9)
C34 0.127(11) 0.068(7) 0.113(10) -0.001(5) -0.001(9) 0.064(6)
C41 0.068(9) 0.058(8) 0.128(10) 0.012(9) 0.001(9) 0.019(7)
C42 0.046750(3) 0.046750(3) 0.128100(3) -0.004880(3) 0.004880(3) 0.041860(3)
C43 0.069(8) 0.054(8) 0.116(10) 0.005(8) 0.006(8) 0.027(7)
C44 0.046748(3) 0.046748(3) 0.128095(3) -0.004882(3) 0.004882(3) 0.041863(3)

loop_
 _geom_bond_atom_site_label_1
 _geom_bond_site_symmetry_1
 _geom_bond_atom_site_label_2
 _geom_bond_site_symmetry_2
 _geom_bond_distance
 _geom_bond_publ_flag
Zn1 . N1 . 1.975(9)    yes
Zn1 . N2 . 2.034(19)    yes
Zn1 . N3 . 1.954(9)    yes
Zn1 . N4 . 1.984(8)    yes
N1 . C11 . 1.377(16)    yes
N1 . C12 . 1.309(12)    yes
N2 . C21 . 1.46(2)    yes
N2 . C22 . 1.268(19)    yes
N3 . C31 . 1.59(3)    yes
N3 . C32 . 1.296(7)    yes
N4 . C41 . 1.54(3)    yes
```

```
N4 . C42 . 1.295(6)    yes
N22 . O22 8_556 1.202(14)    yes
N22 . O22 . 1.202(14)    yes
N22 . C22 . 1.37(3)    yes
C11 . C11 22_556 1.36(3)    yes
C11 . H111 . 0.924    no
C12 . H121 . 0.931    no
C21 . C21 8_556 1.48(4)    yes
C21 . H211 . 0.950    no
C31 . C31 17_565 1.386(10)    yes
C31 . H311 . 0.955    no
C32 . H321 . 0.935    no
C33 . C33 17_565 1.389(10)    yes
C33 . H331 . 0.950    no
C34 . H341 . 0.950    no
C41 . C41 21_665 1.388(10)    yes
C41 . H411 . 0.934    no
C42 . H421 . 0.950    no
C43 . C43 21_665 1.387(10)    yes
C43 . H431 . 0.939    no
C44 . H441 . 0.950    no
loop_
 _geom_angle_atom_site_label_1
 _geom_angle_site_symmetry_1
 _geom_angle_atom_site_label_2
 _geom_angle_site_symmetry_2
```

```
 _geom_angle_atom_site_label_3
 _geom_angle_site_symmetry_3
 _geom_angle
 _geom_angle_publ_flag
N1 . Zn1 . N2 . 103.9(6)    yes
N1 . Zn1 . N3 . 111.3(4)    yes
N2 . Zn1 . N3 . 114.1(5)    yes
N1 . Zn1 . N4 . 106.5(3)    yes
N2 . Zn1 . N4 . 113.2(5)    yes
N3 . Zn1 . N4 . 107.7(3)    yes
Zn1 . N1 . C11 . 130.9(8)    yes
Zn1 . N1 . C12 . 126.9(9)    yes
C11 . N1 . C12 . 102.2(11)    yes
Zn1 . N2 . C21 . 116.1(14)    yes
Zn1 . N2 . C22 . 135.8(13)    yes
C21 . N2 . C22 . 108.1(19)    yes
Zn1 . N3 . C31 . 121.8(5)    yes
Zn1 . N3 . C32 . 134.7(9)    yes
C31 . N3 . C32 . 102.5(12)    yes
Zn1 . N4 . C41 . 118.4(5)    yes
Zn1 . N4 . C42 . 136.4(8)    yes
C41 . N4 . C42 . 102.9(11)    yes
O22 8_556 N22 . O22 . 123.5(19)    yes
O22 8_556 N22 . C22 . 118.2(10)    yes
O22 . N22 . C22 . 118.2(10)    yes
N1 . C11 . C11 22_556 108.7(7)    yes
```

```
N1 . C11 . H111 . 125.0    no
C11 22_556 C11 . H111 . 125.2    no
N1 22_556 C12 . N1 . 118.0(15)    yes
N1 22_556 C12 . H121 . 121.0    no
N1 . C12 . H121 . 121.0    no
C21 8_556 C21 . N2 . 103.5(12)    yes
C21 8_556 C21 . H211 . 127.5    no
N2 . C21 . H211 . 129.1    no
N22 . C22 . N2 . 121.6(11)    yes
N22 . C22 . N2 8_556 121.6(11)    yes
N2 . C22 . N2 8_556 117(2)    yes
N3 . C31 . C31 17_565 106.1(5)    yes
N3 . C31 . H311 . 127.6    no
C31 17_565 C31 . H311 . 126.1    no
N3 17_565 C32 . N3 . 122.6(18)    yes
N3 17_565 C32 . H321 . 118.7    no
N3 . C32 . H321 . 118.7    no
C33 17_565 C33 . N3 . 104.9(5)    yes
C33 17_565 C33 . H331 . 127.3    no
N3 . C33 . H331 . 127.7    no
N3 17_565 C34 . N3 . 122.4(19)    yes
N3 17_565 C34 . H341 . 118.8    no
N3 . C34 . H341 . 118.8    no
N4 . C41 . C41 21_665 106.4(5)    yes
N4 . C41 . H411 . 126.9    no
C41 21_665 C41 . H411 . 126.6    no
```

```
N4 21_665 C42 . N4 . 121.3(15)    yes
N4 21_665 C42 . H421 . 119.2    no
N4 . C42 . H421 . 119.2    no
N4 . C43 . C43 21_665 107.4(5)    yes
N4 . C43 . H431 . 126.3    no
C43 21_665 C43 . H431 . 126.1    no
N4 . C44 . N4 21_665 121.2(16)    yes
N4 . C44 . H441 . 119.4    no
N4 21_665 C44 . H441 . 119.4    no


_iucr_refine_instructions_details
;
#
# Punched on 20/07/17 at 19:33:26
#
#LIST     12
BLOCK SCALE X'S
CONT ZN(1,U'S)
CONT N(1,U'S) UNTIL C(44)
EQUIV C(42,U'S) C(44,U'S)
EQUIV C(41,OCC) C(42,OCC) C(43,OCC) C(44,OCC)
CONT H(431,OCC) H(411,OCC) H(421,OCC) H(441,OCC)
WEIGHT -1 C(43,OCC) C(44,OCC) H(431,OCC) H(441,OCC)
EQUIV C(31,OCC) C(32,OCC) C(33,OCC) C(34,OCC),
CONT H(311,OCC) H(321,OCC) H(331,OCC) H(341,OCC)
```

```
WEIGHT -1 C(33,OCC) C(34,OCC) H(331,OCC) H(341,OCC)
RIDE C ( 11,X'S) H( 111,X'S)
RIDE C ( 12,X'S) H( 121,X'S)
RIDE C ( 21,X'S) H( 211,X'S)
RIDE C ( 31,X'S) H( 311,X'S)
RIDE C ( 32,X'S) H( 321,X'S)
RIDE C ( 33,X'S) H( 331,X'S)
RIDE C ( 34,X'S) H( 341,X'S)
RIDE C ( 41,X'S) H( 411,X'S)
RIDE C ( 42,X'S) H( 421,X'S)
RIDE C ( 43,X'S) H( 431,X'S)
RIDE C ( 44,X'S) H( 441,X'S)
EQUIV H(111,U[ISO]) UNTIL H(441)
END
#
# Punched on 20/07/17 at 19:33:26
#
#LIST     16
NO
PLANAR N(3) C(32) C(31) C(31,9,1,0,1) N(3,9,1,0,1)
PLANAR N(3) C(33) C(33,9,1,0,1) N(3,9,1,0,1) C(34)
PLANAR N(4), C(43) C(43,11,1,1,1) N(4,11,1,1,1) C(44)
PLANAR N(4), C(41) C(41,11,1,1,1) N(4,11,1,1,1) C(42)
DIST 0,0.01 = MEAN N(4) TO C(42), N(4) TO C(44),
CONT N(4,11,1,1,1) TO C(42), N(4,11,1,1,1) TO C(44),
CONT N(3) TO C(32), N(3) TO C(34), N(3,9,1,0,1) TO C(32),
```

```
CONT N(3,9,1,0,1) TO C(34)
DIST 0,0.01 = MEAN N(4) TO C(43), N(4) TO C(41).
CONT N(3) TO C(33), N(3) TO C(31)
DIST 0,0.01 = MEAN C(41) TO C(41,11,1,1,1),
CONT C(43) TO C(43,11,1,1,1),
CONT C(31) TO C(31,9,1,0,1),
CONT C(33) TO C(33,9,1,0,1)
U(IJ)'S  0.0, 0.010000 = N(4) TO C(41)
U(IJ)'S  0.0, 0.010000 = N(4) TO C(42)
U(IJ)'S  0.0, 0.010000 = N(4) TO C(43)
U(IJ)'S  0.0, 0.010000 = N(4) TO C(44)
U(IJ)'S  0.0, 0.010000 = N(3) TO C(31)
U(IJ)'S  0.0, 0.010000 = N(3) TO C(32)
U(IJ)'S  0.0, 0.010000 = N(3) TO C(33)
U(IJ)'S  0.0, 0.010000 = N(3) TO C(34)
U(IJ)'S  0.0, 0.010000 = N(2) TO C(21)
U(IJ)'S  0.0, 0.010000 = N(2) TO C(22)
U(IJ)'S  0.0, 0.010000 = N(1) TO C(11)
U(IJ)'S  0.0, 0.010000 = N(1) TO C(12)
U(IJ)'S  0.0, 0.010000 = C(32) TO C(34)
U(IJ)'S  0.0, 0.005000 = N(22) TO C(22)
END
;

data_PSZ-1_isotropic
```

```
_exptl_special_details
;
 The crystal was
placed in the cold stream of an Oxford
Cryosystems 800 series open-flow nitrogen cryostat (Cosier &
Glazer, 1986) with a nominal stability of 0.1K.

Cosier, J. & Glazer, A.M., 1986. J. Appl. Cryst. 105-107.
;
# End of 'script/refcif.dat'
#end of refcif
_cell_length_a                    27.2188(5)
_cell_length_b                    27.2188(5)
_cell_length_c                    17.0357(8)
_cell_angle_alpha                 90
_cell_angle_beta                  90
_cell_angle_gamma                 120
_cell_volume                      10930.2(6)
_cell_oxdiff_length_a                  27.2168(6)
_cell_oxdiff_length_b                  27.1942(7)
_cell_oxdiff_length_c                  17.0499(4)
_cell_oxdiff_angle_alpha               90.062(2)
_cell_oxdiff_angle_beta                89.973(2)
_cell_oxdiff_angle_gamma               119.985(2)
_cell_oxdiff_volume                    10930.2(4)
_cell_oxdiff_measurement_reflns_used   13383
```

```
_symmetry_space_group_name_H-M_alt 'P 63/m 2/m 2/c'
_symmetry_space_group_name_H-M 'P 63/m m c'
_symmetry_space_group_name_Hall   ?
loop_
 _symmetry_equiv_pos_as_xyz
 'x,y,z'
 '-x,-y,-z'
 'x-y,x,z+1/2'
 '-x+y,-x,-z+1/2'
 '-y,x-y,z'
 'y,-x+y,-z'
 '-x,-y,z+1/2'
 'x,y,-z+1/2'
 '-x+y,-x,z'
 'x-y,x,-z'
 'y,-x+y,z+1/2'
 '-y,x-y,-z+1/2'
 '-x+y,y,z'
 'x-y,-y,-z'
 'y,x,z+1/2'
 '-y,-x,-z+1/2'
 'x,x-y,z'
 '-x,-x+y,-z'
 'x-y,-y,z+1/2'
 '-x+y,y,-z+1/2'
```

```
 '-y,-x,z'
 'y,x,-z'
 '-x,-x+y,z+1/2'
 'x,x-y,-z+1/2'

loop_
_atom_type_symbol
_atom_type_scat_dispersion_real
_atom_type_scat_dispersion_imag
_atom_type_scat_Cromer_Mann_a1
_atom_type_scat_Cromer_Mann_b1
_atom_type_scat_Cromer_Mann_a2
_atom_type_scat_Cromer_Mann_b2
_atom_type_scat_Cromer_Mann_a3
_atom_type_scat_Cromer_Mann_b3
_atom_type_scat_Cromer_Mann_a4
_atom_type_scat_Cromer_Mann_b4
_atom_type_scat_Cromer_Mann_c
_atom_type_scat_source
 C       0.0181   0.0091   2.3100  20.8439   1.0200  10.2075   1.5886   0.5687
   0.8650  51.6512   0.2156 'International Tables Vol C 4.2.6.8 and 6.1.1.4'
 H       0.0000   0.0000   0.4930  10.5109   0.3229  26.1257   0.1402   3.1424
   0.0408  57.7998   0.0030 'International Tables Vol C 4.2.6.8 and 6.1.1.4'
 N       0.0311   0.0180  12.2126   0.0057   3.1322   9.8933   2.0125  28.9975
   1.1663   0.5826 -11.5290 'International Tables Vol C 4.2.6.8 and 6.1.1.4'
 O       0.0492   0.0322   3.0485  13.2771   2.2868   5.7011   1.5463   0.3239
```

```
   0.8670  32.9089   0.2508 'International Tables Vol C 4.2.6.8 and 6.1.1.4'
 S       0.3331   0.5567   6.9053   1.4679   5.2034  22.2151   1.4379   0.2536
   1.5863  56.1720   0.8669 'International Tables Vol C 4.2.6.8 and 6.1.1.4'
 Zn     -1.5491   0.6778  14.0743   3.2655   7.0318   0.2333   5.1652  10.3163
   2.4100  58.7097   1.3041 'International Tables Vol C 4.2.6.8 and 6.1.1.4'

_cell_formula_units_Z                    16

# Given Formula = C24 H24 N9 O2.00 S2.00 Zn1
# Dc =      1.46 Fooo =   4944.00 Mu =     30.11 M =    600.03
# Found Formula = C12.67 H8.60 N7.42 O2.84 S0.50 Zn1.50
# Dc =      1.03 FOOO =   3395.17 Mu =     22.26 M =    424.16

_chemical_formula_sum             'C12.67 H8.60 N7.42 O2.84 S0.50 Zn1.50'
_chemical_formula_moiety          'C12.67 H8.60 N7.42 O2.84 S0.50 Zn1.50'
_chemical_compound_source                ?
_chemical_formula_weight           424.16


_cell_measurement_temperature   250.00(10)
_cell_measurement_reflns_used   13383
_cell_measurement_theta_min     3.7120
_cell_measurement_theta_max     74.9520

_exptl_crystal_description        'hexagonal prism'
_exptl_crystal_colour             'yellow'
```

```
_exptl_crystal_size_max           0.17
_exptl_crystal_size_mid           0.12
_exptl_crystal_size_min           0.12

_exptl_crystal_density_diffrn     1.031
_exptl_crystal_density_method     'not measured'
# dispersive F(000):
_exptl_crystal_F_000              3395.166
_exptl_absorpt_coefficient_mu     2.226

_exptl_absorpt_correction_T_min                  0.44920
_exptl_absorpt_correction_T_max                  1.00000
_exptl_absorpt_correction_type            multi-scan
_exptl_absorpt_process_details
;
CrysAlisPro 1.171.39.27b (Rigaku Oxford Diffraction, 2015)
Empirical absorption correction using spherical harmonics,
 implemented in SCALE3 ABSPACK scaling algorithm.
;
_oxdiff_exptl_absorpt_empirical_full_min          0.748
_oxdiff_exptl_absorpt_empirical_full_max          1.700
_oxdiff_exptl_absorpt_empirical_details
;
Empirical correction (ABSPACK) includes:
- Absorption correction using spherical harmonics
- Frame scaling
```

;

_diffrn_ambient_temperature 250.00(10)

_diffrn_ambient_environment N~2~

_diffrn_source 'micro-focus sealed X-ray tube'

_diffrn_source_type 'PhotonJet (Cu) X-ray Source'

_diffrn_radiation_probe x-ray

_diffrn_radiation_type 'Cu K\a'

_diffrn_radiation_wavelength 1.54184

_diffrn_radiation_monochromator mirror

_diffrn_measurement_device 'four-circle diffractometer'

_diffrn_measurement_device_type 'XtaLAB Synergy, Dualflex, HyPix'

_diffrn_detector 'CCD plate'

_diffrn_detector_type HyPix

_diffrn_reflns_number 57181

_diffrn_reflns_av_R_equivalents 0.0459

_diffrn_reflns_av_sigmaI/netI 0.0553

_diffrn_reflns_limit_h_min -19

_diffrn_reflns_limit_h_max 34

_diffrn_reflns_limit_k_min -30

_diffrn_reflns_limit_k_max 31

_diffrn_reflns_limit_l_min -21

_diffrn_reflns_limit_l_max 21

_diffrn_reflns_theta_min 3.7509

_diffrn_reflns_theta_max 77.7792

_diffrn_measured_fraction_theta_max 0.9906

```
_diffrn_reflns_theta_full 66.4915
_diffrn_measured_fraction_theta_full 0.9989
_diffrn_orient_matrix_type 'CrysAlisPro convention (1999,Acta A55,543-557)'
_diffrn_orient_matrix_UB_11      -0.0510601000
_diffrn_orient_matrix_UB_12      -0.0487766000
_diffrn_orient_matrix_UB_13       0.0424589000
_diffrn_orient_matrix_UB_21      -0.0122294000
_diffrn_orient_matrix_UB_22      -0.0381285000
_diffrn_orient_matrix_UB_23      -0.0726612000
_diffrn_orient_matrix_UB_31       0.0389101000
_diffrn_orient_matrix_UB_32      -0.0210910000
_diffrn_orient_matrix_UB_33       0.0328915000
_diffrn_measurement_details
;
List of Runs (angles in degrees, time in seconds):

  # Type    Start    End  Width  t~exp~   \w     \q     \k     \f   Frames
------------------------------------------------------------------------
  1  \w    -60.00  26.00   0.50   17.50    --  -47.45  37.00   0.00  172
  2  \w    -99.00 -13.00   0.50   63.00    --  -86.25  37.00 -60.00  172
  3  \w   -120.00 -87.00   0.50   17.50    --  -47.45 -77.00   0.00   66
  4  \w   -120.00 -70.00   0.50   17.50    --  -47.45-125.00 -60.00  100
  5  \w   -120.00 -70.00   0.50   17.50    --  -47.45-125.00 -30.00  100
  6  \w     36.00 110.00   0.50   63.00    --  107.75 -99.00 150.00  148
  7  \w     95.00 178.00   0.50   63.00    --  107.75  19.00  90.00  166
  8  \w     92.00 178.00   0.50   63.00    --  107.75 125.00-120.00  172
```

```
  9  \w     36.00 110.00   0.50   63.00    --  107.75 -99.00-180.00  148
 10  \w     35.00 121.00   0.50   63.00    --  107.75-125.00 -30.00  172
;
_diffrn_measurement_method '\w scans'
_diffrn_oxdiff_ac3_digest_frames
;
010a05eeebc61c3b61b2e16166c56a50c701416da94
;
_diffrn_oxdiff_ac3_digest_hkl
;
0133d96d2333189eb5eddd101e5ae39350442e
;
_symmetry_cell_setting hexagonal
_space_group_IT_number 194
_space_group_crystal_system hexagonal
_space_group_name_H-M_alt 'P 63/m m c'
_reflns_odcompleteness_completeness 99.89
_reflns_odcompleteness_theta 66.49
_reflns_odcompleteness_iscentric 1
_chemical_oxdiff_formula ZnN9C24H24O2S2


# If a reference occurs more than once, delete the author
# and date from subsequent references.
_computing_data_collection        'Rigaku Crystal Clear Expert 2.1 SM'
_computing_cell_refinement        'CrystAlis Pro'
```

```
_computing_data_reduction          'CrystAlis Pro'
_computing_structure_solution      'SHELXS 86 (Sheldrick, 1986)'
_computing_structure_refinement    'CRYSTALS (Betteridge et al., 2003)'
_computing_publication_material    'CRYSTALS (Betteridge et al., 2003)'

# Number of reflections without Friedels Law is 0
# Number of reflections with Friedels Law is 4211
# Theoretical number of reflections is about 7743

_reflns_limit_h_min                -17
_reflns_limit_h_max                0
_reflns_limit_k_min                0
_reflns_limit_k_max                34
_reflns_limit_l_min                0
_reflns_limit_l_max                21

_atom_sites_solution_primary       direct #heavy,direct,difmap,geom,iterative
_atom_sites_solution_hydrogens     geom

_refine_diff_density_min           -0.53
_refine_diff_density_max           1.54


# The current dictionary definitions do not cover the
# situation where the reflections used for refinement were
# selected by a user-defined sigma threshold
```

```
# The values actually used during refinement
_oxford_reflns_threshold_expression_ref     I>3.0\s(I)
_refine_ls_number_reflns          2275
_refine_ls_number_restraints      652
_refine_ls_number_parameters      239
_oxford_refine_ls_R_factor_ref    0.1190
_refine_ls_wR_factor_ref          0.3664
_refine_ls_goodness_of_fit_ref    3.3025
_refine_ls_shift/su_max           0.0884982
_refine_ls_shift/su_mean          0.0037717


# The values computed with all filters except I/sigma
_oxford_reflns_number_all         4211
_refine_ls_R_factor_all           0.1476
_refine_ls_wR_factor_all          0.4100

# The values computed with a 2 sigma cutoff - a la SHELX
_reflns_threshold_expression      I>2.0\s(I)
_reflns_number_gt                 2518
_refine_ls_R_factor_gt            0.1230
_refine_ls_wR_factor_gt           0.3719

# choose from: rm (reference molecule of known chirality),
```

```
# ad (anomolous dispersion - Flack), rmad (rm and ad),
# syn (from synthesis), unk (unknown) or . (not applicable).
_chemical_absolute_configuration  '.'


_refine_ls_structure_factor_coef  Fsqd
_refine_ls_matrix_type            full
_refine_ls_hydrogen_treatment     constr         # undef, noref, refall,
   # refxyz, refU, constr or mixed
_refine_ls_extinction_method
    'None'
_oxford_refine_ls_scale 0.375(2)
_refine_ls_weighting_scheme       calc
_refine_ls_weighting_details
;
 Method= Modified Sheldrick
 w=1/[\s^2^(F^2^) + ( 0.10P)^2^ + 0.00P]
 ,where P=(max(Fo^2^,0) + 2Fc^2^)/3
;
# Insert your own references if required - in alphabetical order
_publ_section_references
;

Betteridge, P.W., Carruthers, J.R., Cooper, R.I.,
Prout, K. & Watkin, D.J. (2003). J. Appl. Cryst. 36, 1487.
```

Prince, E.

Mathematical Techniques in Crystallography

and Materials Science

Springer-Verlag, New York, 1982.

Sheldrick, G. M. (2008). Acta Cryst A64, 112-122.

Watkin D.J. (1994).

Acta Cryst, A50, 411-437.

;

Uequiv = arithmetic mean of Ui i.e. Ueqiv = (U1+U2+U3)/3

Replace last . with number of unfound hydrogen atoms attached to an atom.

..._refinement_flags_...

. no refinement constraints S special position constraint on site

G rigid group refinement of site R riding atom

D distance or angle restraint on site T thermal displacement constraints

U Uiso or Uij restraint (rigid bond) P partial occupancy constraint

loop_

_atom_site_label

_atom_site_type_symbol

_atom_site_fract_x

```
_atom_site_fract_y
_atom_site_fract_z
_atom_site_U_iso_or_equiv
_atom_site_occupancy
_atom_site_adp_type
_atom_site_refinement_flags_posn
_atom_site_refinement_flags_adp
_atom_site_refinement_flags_occupancy
_atom_site_disorder_assembly
_atom_site_disorder_group
_atom_site_attached_hydrogens
Zn1 Zn 0.55463(4) 0.66780(3) 0.42927(8) 0.1026 1.0000 Uani . . . . . .
N31 N 0.5752(3) 0.6712(3) 0.3125(5) 0.1566 1.0000 Uani D . . . . .
N32 N 0.4953(4) 0.6687(5) 0.2500 0.1448 1.0000 Uani DS T . . . .
O32 O 0.4749(3) 0.6677(3) 0.3135(4) 0.1599 1.0000 Uani D . . . . .
C31 C 0.5497(4) 0.6716(4) 0.2500 0.1579 1.0000 Uani DS T . . . .
C32 C 0.6249(4) 0.6720(4) 0.2897(3) 0.2021 1.0000 Uani D . . . . .
N41 N 0.4816(2) 0.6008(2) 0.4619(3) 0.1162 1.0000 Uani D U . . . .
N42 N 0.4730(2) 0.5270(2) 0.3832(6) 0.1069 0.515(3) Uani DS TU P . 1 .
O42 O 0.5226(3) 0.5586(4) 0.3634(5) 0.1306 0.515(3) Uani D . P . 1 .
C41 C 0.4497(2) 0.5503(2) 0.4366(6) 0.0977 0.515(3) Uani DS TU P . 1 .
C42 C 0.4425(2) 0.6071(3) 0.5111(5) 0.1249 0.515(3) Uani D U P . 1 .
C43 C 0.4712(2) 0.5785(2) 0.5393(6) 0.1179 0.485(3) Uani D U P . 2 .
C44 C 0.43850(19) 0.56150(19) 0.4265(10) 0.1150 0.485(3) Uani DS TU P . 2 .
N11 N 0.5520(2) 0.7340(2) 0.4662(3) 0.1258 1.0000 Uani D U . . . .
N12 N 0.6222(6) 0.8111(3) 0.4093(7) 0.1106 0.375(3) Uani DS TU P . 3 .
```

```
O12 O 0.6404(5) 0.7794(5) 0.3957(6) 0.1256 0.375(3) Uani D . P . 3 .
C11 C 0.5698(6) 0.7849(3) 0.4503(7) 0.1144 0.375(3) Uani DS TU P . 3 .
C12 C 0.5019(4) 0.7260(3) 0.5042(4) 0.1353 0.375(3) Uani D U P . 3 .
C13 C 0.5708(3) 0.7605(2) 0.5413(6) 0.1418 0.625(3) Uani D U P . 4 .
C14 C 0.5464(4) 0.7732(2) 0.4344(9) 0.1163 0.625(3) Uani DS TU P . 4 .
N21 N 0.6177(2) 0.66043(18) 0.4746(3) 0.1220 1.0000 Uani D U . . . .
C21 C 0.6129(3) 0.6159(3) 0.5093(5) 0.1127 0.5000 Uani D U . . . .
C22 C 0.6769(3) 0.6970(3) 0.4639(4) 0.1311 0.5000 Uani D U . . . .
C23 C 0.7029(2) 0.6706(2) 0.4949(5) 0.1249 0.5000 Uani D U . . . .
C24 C 0.7022(4) 0.7533(3) 0.4226(4) 8.2041(12) 0.2222(16) Uiso D . P . 5 .
C25 C 0.6793(5) 0.7650(6) 0.3465(5) 8.2219(12) 0.2222(16) Uiso D . P . 5 .
C26 C 0.7558(4) 0.8081(4) 0.4467(5) 8.2336(12) 0.2222(16) Uiso D . P . 5 .
S27 S 0.7615(5) 0.8487(4) 0.3860(6) 8.2598(12) 0.2222(16) Uiso D . P . 5 .
C28 C 0.7184(6) 0.8274(6) 0.3242(5) 8.2360(12) 0.2222(16) Uiso D . P . 5 .
C29 C 0.7794(6) 0.7977(8) 0.5208(6) 8.2334(12) 0.2222(16) Uiso D . P . 5 .
C30 C 0.6966(9) 0.8400(9) 0.250000(9) 8.2337(12) 0.2222(16) Uiso DS . P . 5 .
C241 C 0.7654(2) 0.6908(3) 0.4997(5) 8.1609(12) 0.2222(16) Uiso D . P . 6 .
C251 C 0.8003(3) 0.7044(4) 0.5756(7) 8.1699(12) 0.2222(16) Uiso D . P . 6 .
C261 C 0.8053(4) 0.7019(4) 0.4301(7) 8.1705(12) 0.2222(16) Uiso D . P . 6 .
S271 S 0.8604(2) 0.7208(4) 0.4672(11) 8.1681(12) 0.2222(16) Uiso DS . P . 6 .
C281 C 0.86187(19) 0.7237(4) 0.5530(10) 8.1718(12) 0.2222(16) Uiso DS . P . 6 .
C291 C 0.7720(8) 0.6890(4) 0.3548(7) 8.1811(12) 0.2222(16) Uiso D . P . 6 .
C301 C 0.8970(7) 0.7372(4) 0.6266(14) 8.1787(12) 0.2222(16) Uiso D . P . 6 .
H321 H 0.6525 0.6725 0.3244 0.2446 1.0000 Uiso R . . . . .
H421 H 0.4504 0.6406 0.5386 0.1452 0.515(3) Uiso R . P . 1 .
H431 H 0.4958 0.5953 0.5829 0.1420 0.485(3) Uiso R . P . 2 .
```

```
H441 H 0.4354 0.5646 0.3714 0.1404 0.485(3) Uiso RS . P . 2 .
H121 H 0.4734 0.6911 0.5259 0.1729 0.375(3) Uiso R . P . 3 .
H131 H 0.5827 0.7459 0.5833 0.1737 0.625(3) Uiso R . P . 4 .
H141 H 0.5342 0.7671 0.3812 0.1491 0.625(3) Uiso RS . P . 4 .
H211 H 0.5775 0.5857 0.5268 0.1367 0.5000 Uiso R . . . . .
H251 H 0.6427 0.7417 0.3248 8.2798(12) 0.0801(16) Uiso R . P . 5 .
H2511 H 0.7924 0.7061 0.6295 8.2146(12) 0.0801(16) Uiso R . P . 6 .
H2911 H 0.7969 0.6943 0.3125 8.2373(12) 0.0801(16) Uiso R . P . 6 .
H2912 H 0.7548 0.7115 0.3465 8.2373(12) 0.0801(16) Uiso R . P . 6 .
H2913 H 0.7435 0.6501 0.3578 8.2373(12) 0.0801(16) Uiso R . P . 6 .
H3011 H 0.9299 0.7461 0.5965 8.2265(12) 0.0801(16) Uiso R . P . 6 .
H3012 H 0.9023 0.7703 0.6527 8.2265(12) 0.0801(16) Uiso R . P . 6 .
H3013 H 0.8909 0.7090 0.6643 8.2265(12) 0.0801(16) Uiso R . P . 6 .
H301 H 0.7283 0.8761 0.2383 8.3218(12) 0.0801(16) Uiso R . P . 5 .
H302 H 0.6647 0.8441 0.2617 8.3218(12) 0.0801(16) Uiso R . P . 5 .
H303 H 0.6883 0.8156 0.2061 8.3218(12) 0.0801(16) Uiso R . P . 5 .
H291 H 0.8158 0.8309 0.5210 8.3159(12) 0.0801(16) Uiso R . P . 5 .
H292 H 0.7608 0.7949 0.5692 8.3159(12) 0.0801(16) Uiso R . P . 5 .
H293 H 0.7835 0.7653 0.5141 8.3159(12) 0.0801(16) Uiso R . P . 5 .
H221 H 0.6943 0.7325 0.4377 0.1582 0.2778(16) Uiso R . P . . .
H231 H 0.7424 0.6832 0.4928 0.1492 0.2778(16) Uiso R . P . . .


loop_
_atom_site_aniso_label
_atom_site_aniso_U_11
_atom_site_aniso_U_22
```

```
_atom_site_aniso_U_33
_atom_site_aniso_U_23
_atom_site_aniso_U_13
_atom_site_aniso_U_12
Zn1 0.0771(7) 0.0642(6) 0.1721(14) 0.0032(5) -0.0146(5) 0.0396(5)
N31 0.098(4) 0.130(5) 0.263(7) 0.000(5) 0.016(5) 0.073(4)
N32 0.089(4) 0.115(6) 0.249(8) 0.0000 0.0000 0.065(4)
O32 0.114(4) 0.179(5) 0.208(6) 0.016(5) 0.009(4) 0.089(4)
C31 0.057(4) 0.064(5) 0.351(9) 0.0000 0.0000 0.029(4)
C32 0.121(5) 0.197(7) 0.298(8) -0.004(6) 0.014(6) 0.087(5)
N41 0.087(3) 0.077(3) 0.169(4) -0.003(3) 0.000(3) 0.030(2)
N42 0.081(3) 0.081(3) 0.155(6) 0.005(3) -0.005(3) 0.037(5)
O42 0.076(4) 0.097(5) 0.210(7) -0.015(5) 0.020(5) 0.036(4)
C41 0.072(3) 0.072(3) 0.158(6) 0.003(3) -0.003(3) 0.042(4)
C42 0.102(5) 0.085(5) 0.175(6) -0.009(5) 0.009(5) 0.037(5)
C43 0.086(4) 0.081(5) 0.165(6) -0.002(5) -0.018(5) 0.027(5)
C44 0.080(4) 0.080(4) 0.167(6) 0.013(4) -0.013(4) 0.027(5)
N11 0.155(3) 0.087(3) 0.158(4) 0.001(3) 0.003(3) 0.078(3)
N12 0.119(5) 0.076(5) 0.151(7) 0.003(3) 0.006(6) 0.059(2)
O12 0.089(5) 0.080(5) 0.235(8) 0.019(6) 0.019(6) 0.063(4)
C11 0.133(4) 0.076(5) 0.153(6) 0.003(3) 0.006(5) 0.066(2)
C12 0.164(5) 0.088(5) 0.163(6) 0.002(6) 0.004(6) 0.069(5)
C13 0.162(5) 0.106(5) 0.184(6) 0.009(5) -0.008(6) 0.086(4)
C14 0.147(5) 0.075(4) 0.151(6) -0.002(3) -0.005(5) 0.073(2)
N21 0.079(3) 0.073(3) 0.214(5) 0.024(3) -0.014(3) 0.039(2)
C21 0.075(4) 0.077(5) 0.198(6) 0.022(5) -0.004(5) 0.046(3)
```

```
C22 0.084(5) 0.076(5) 0.220(6) 0.020(6) -0.012(6) 0.031(5)
C23 0.077(4) 0.081(5) 0.209(6) 0.031(5) -0.014(6) 0.034(4)


loop_
 _geom_bond_atom_site_label_1
 _geom_bond_site_symmetry_1
 _geom_bond_atom_site_label_2
 _geom_bond_site_symmetry_2
 _geom_bond_distance
 _geom_bond_publ_flag
Zn1 . N31 . 2.056(9)    yes
Zn1 . N41 . 1.991(6)    yes
Zn1 . N11 . 1.943(5)    yes
Zn1 . N21 . 1.982(5)    yes
N31 . C31 . 1.275(7)    yes
N31 . C32 . 1.397(7)    yes
N32 . O32 8_555 1.210(6)    yes
N32 . O32 . 1.210(6)    yes
N32 . C31 . 1.440(8)    yes
C32 . C32 8_555 1.353(9)    yes
C32 . H321 . 0.950    no
N41 . C41 . 1.278(6)    yes
N41 . C42 . 1.431(8)    yes
N42 . O42 21_665 1.231(7)    yes
N42 . O42 . 1.231(7)    yes
```

```
N42 . C41 . 1.425(8)    yes
C42 . C42 21_665 1.352(9)    yes
C42 . H421 . 0.950    no
C43 . C43 21_665 1.352(9)    yes
C43 . H431 . 0.950    no
C44 . H441 . 0.950    no
N11 . C11 . 1.248(7)    yes
N11 . C12 . 1.425(8)    yes
N12 . O12 17_565 1.212(7)    yes
N12 . O12 . 1.212(7)    yes
N12 . C11 . 1.420(9)    yes
C12 . C12 17_565 1.360(9)    yes
C12 . H121 . 0.950    no
C13 . C13 17_565 1.356(8)    yes
C13 . H131 . 0.950    no
C14 . H141 . 0.950    no
N21 . C23 22_556 1.421(6)    yes
N21 . C21 22_556 1.298(7)    yes
N21 . C21 . 1.296(7)    yes
N21 . C22 . 1.419(6)    yes
C21 . H211 22_556 1.117    no
C21 . H211 . 0.950    no
C22 . C23 . 1.343(6)    yes
C22 . C24 . 1.505(6)    yes
C22 . H221 . 0.950    no
C23 . C23 22_556 1.534(13)    yes
```

C23 . C241 . 1.505(6) yes

C23 . H231 . 0.950 no

C24 . C25 . 1.539(7) yes

C24 . C26 . 1.531(7) yes

C24 . H221 . 0.557 no

C25 . C28 . 1.534(8) yes

C25 . H251 . 0.950 no

C26 . H293 22_556 1.066 no

C26 . C29 22_556 1.764(18) yes

C26 . S27 . 1.464(7) yes

C26 . C29 . 1.507(7) yes

S27 . C28 17_565 2.270(14) yes

S27 . C28 . 1.462(7) yes

C28 . H301 24_565 1.216 no

C28 . H303 8_555 0.883 no

C28 . C30 17_565 1.747(17) yes

C28 . C30 . 1.508(7) yes

C29 . H293 22_556 0.709 no

C29 . C29 22_556 1.117(19) yes

C29 . H291 . 0.950 no

C29 . H292 . 0.950 no

C29 . H293 . 0.950 no

C30 . H302 8_555 0.950 no

C30 . H301 8_555 0.950 no

C30 . H303 8_555 0.950 no

C30 . H303 24_565 1.265 no

```
C30 . H303 17_565 1.265    no
C30 . H302 24_565 0.784    no
C30 . H302 17_565 0.784    no
C30 . H301 17_565 0.780    no
C30 . H301 . 0.950    no
C30 . H302 . 0.950    no
C30 . H303 . 0.950    no
C241 . C251 . 1.536(7)    yes
C241 . C261 . 1.533(7)    yes
C241 . H231 . 0.566    no
C251 . H3011 13_655 1.054    no
C251 . C281 . 1.534(7)    yes
C251 . H2511 . 0.950    no
C261 . S271 . 1.463(6)    yes
C261 . C291 . 1.507(7)    yes
S271 . C281 . 1.463(7)    yes
C281 . C301 13_655 1.507(7)    yes
C281 . C301 . 1.507(7)    yes
C291 . H2911 . 0.950    no
C291 . H2912 . 0.950    no
C291 . H2913 . 0.950    no
C301 . C301 13_655 1.55(3)    yes
C301 . H2511 13_655 1.143    no
C301 . H3011 . 0.950    no
C301 . H3012 . 0.950    no
C301 . H3013 . 0.950    no
```

```
H301 . H301 17_565 0.653    no
H301 . H301 24_565 0.766    no
H301 . H301 8_555 0.399    no
H302 . H302 17_565 0.641    no
H302 . H302 24_565 0.754    no
H302 . H302 8_555 0.397    no

loop_
 _geom_angle_atom_site_label_1
 _geom_angle_site_symmetry_1
 _geom_angle_atom_site_label_2
 _geom_angle_site_symmetry_2
 _geom_angle_atom_site_label_3
 _geom_angle_site_symmetry_3
 _geom_angle
 _geom_angle_publ_flag
N31 . Zn1 . N41 . 115.8(3)    yes
N31 . Zn1 . N11 . 114.1(2)    yes
N41 . Zn1 . N11 . 106.1(2)    yes
N31 . Zn1 . N21 . 98.7(3)    yes
N41 . Zn1 . N21 . 108.49(18)    yes
N11 . Zn1 . N21 . 113.7(2)    yes
Zn1 . N31 . C31 . 132.1(6)    yes
Zn1 . N31 . C32 . 120.6(5)    yes
C31 . N31 . C32 . 107.3(9)    yes
O32 8_555 N32 . O32 . 126.7(11)    yes
```

```
O32 8_555 N32 . C31 . 116.7(6)    yes
O32 . N32 . C31 . 116.7(6)    yes
N32 . C31 . N31 . 123.3(5)    yes
N32 . C31 . N31 8_555 123.3(5)    yes
N31 . C31 . N31 8_555 113.2(11)    yes
N31 . C32 . C32 8_555 106.1(4)    yes
N31 . C32 . H321 . 125.4    no
C32 8_555 C32 . H321 . 128.5    no
Zn1 . N41 . C41 . 136.2(6)    yes
Zn1 . N41 . C42 . 120.9(3)    yes
C41 . N41 . C42 . 100.5(7)    yes
O42 21_665 N42 . O42 . 127.8(15)    yes
O42 21_665 N42 . C41 . 116.1(7)    yes
O42 . N42 . C41 . 116.1(7)    yes
N42 . C41 . N41 . 118.6(6)    yes
N42 . C41 . N41 21_665 118.6(6)    yes
N41 . C41 . N41 21_665 122.5(11)    yes
N41 . C42 . C42 21_665 108.1(3)    yes
N41 . C42 . H421 . 125.5    no
C42 21_665 C42 . H421 . 126.4    no
N41 . C43 . C43 21_665 108.2(3)    yes
N41 . C43 . H431 . 125.4    no
C43 21_665 C43 . H431 . 126.4    no
N41 . C44 . N41 21_665 123.0(15)    yes
N41 . C44 . H441 . 118.5    no
N41 21_665 C44 . H441 . 118.5    no
```

```
Zn1 . N11 . C11 . 141.8(7)    yes

Zn1 . N11 . C12 . 118.8(4)    yes

C11 . N11 . C12 . 94.5(9)    yes

O12 17_565 N12 . O12 . 132.6(19)    yes

O12 17_565 N12 . C11 . 113.7(10)    yes

O12 . N12 . C11 . 113.7(10)    yes

N12 . C11 . N11 . 113.5(7)    yes

N12 . C11 . N11 17_565 113.5(7)    yes

N11 . C11 . N11 17_565 132.9(15)    yes

N11 . C12 . C12 17_565 109.0(3)    yes

N11 . C12 . H121 . 124.7    no

C12 17_565 C12 . H121 . 126.3    no

N11 . C13 . C13 17_565 109.0(3)    yes

N11 . C13 . H131 . 124.9    no

C13 17_565 C13 . H131 . 126.1    no

N11 . C14 . N11 17_565 127.9(14)    yes

N11 . C14 . H141 . 116.0    no

N11 17_565 C14 . H141 . 116.0    no

C23 22_556 N21 . C21 22_556 104.6(5)    yes

C23 22_556 N21 . Zn1 . 129.6(4)    yes

C21 22_556 N21 . Zn1 . 125.5(4)    yes

C23 22_556 N21 . C21 . 100.4(5)    yes

C21 22_556 N21 . C21 . 15.4(8)    yes

Zn1 . N21 . C21 . 125.9(4)    yes

C23 22_556 N21 . C22 . 31.0(4)    yes

C21 22_556 N21 . C22 . 100.9(5)    yes
```

```
Zn1 . N21 . C22 . 128.0(4)    yes

C21 . N21 . C22 . 105.1(5)    yes

H211 22_556 C21 . N21 22_556 109.6    no

H211 22_556 C21 . N21 . 109.4    no

N21 22_556 C21 . N21 . 115.5(6)    yes

H211 22_556 C21 . H211 . 56.7    no

N21 22_556 C21 . H211 . 121.8    no

N21 . C21 . H211 . 122.5    no

N21 . C22 . C23 . 107.1(5)    yes

N21 . C22 . C24 . 123.8(5)    yes

C23 . C22 . C24 . 129.2(5)    yes

N21 . C22 . H221 . 126.0    no

C23 . C22 . H221 . 126.8    no

C24 . C22 . H221 . 2.4    no

C23 22_556 C23 . N21 22_556 97.5(4)    yes

C23 22_556 C23 . C22 . 29.6(5)    yes

N21 22_556 C23 . C22 . 107.8(5)    yes

C23 22_556 C23 . C241 . 130.6(4)    yes

N21 22_556 C23 . C241 . 123.3(5)    yes

C22 . C23 . C241 . 128.9(5)    yes

C23 22_556 C23 . H231 . 131.8    no

N21 22_556 C23 . H231 . 125.4    no

C22 . C23 . H231 . 126.6    no

C241 . C23 . H231 . 5.2    no

C22 . C24 . C25 . 125.3(6)    yes

C22 . C24 . C26 . 126.6(6)    yes
```

```
C25 . C24 . C26 . 108.0(4)    yes
C22 . C24 . H221 . 4.0    no
C25 . C24 . H221 . 127.4    no
C26 . C24 . H221 . 124.2    no
C24 . C25 . C28 . 108.0(4)    yes
C24 . C25 . H251 . 126.0    no
C28 . C25 . H251 . 124.0    no
C24 . C26 . H293 22_556 88.1    no
C24 . C26 . C29 22_556 99.4(6)    yes
H293 22_556 C26 . C29 22_556 27.2    no
C24 . C26 . S27 . 103.7(4)    yes
H293 22_556 C26 . S27 . 161.9    no
C29 22_556 C26 . S27 . 135.1(8)    yes
C24 . C26 . C29 . 109.2(7)    yes
H293 22_556 C26 . C29 . 25.3    no
C29 22_556 C26 . C29 . 39.0(7)    yes
S27 . C26 . C29 . 147.1(8)    yes
C28 17_565 S27 . C26 . 145.4(6)    yes
C28 17_565 S27 . C28 . 49.7(6)    yes
C26 . S27 . C28 . 116.5(5)    yes
C25 . C28 . H301 24_565 132.0    no
C25 . C28 . H303 8_555 74.9    no
H301 24_565 C28 . H303 8_555 66.2    no
C25 . C28 . C30 17_565 118.5(7)    yes
H301 24_565 C28 . C30 17_565 31.3    no
H303 8_555 C28 . C30 17_565 43.6    no
```

C25 . C28 . S27 17_565 137.3(5) yes

H301 24_565 C28 . S27 17_565 89.0 no

H303 8_555 C28 . S27 17_565 123.6 no

C30 17_565 C28 . S27 17_565 89.4(8) yes

C25 . C28 . S27 . 103.6(4) yes

H301 24_565 C28 . S27 . 119.9 no

H303 8_555 C28 . S27 . 168.5 no

C30 17_565 C28 . S27 . 136.7(8) yes

S27 17_565 C28 . S27 . 50.1(5) yes

C25 . C28 . C30 . 109.0(7) yes

H301 24_565 C28 . C30 . 31.0 no

H303 8_555 C28 . C30 . 36.1 no

C30 17_565 C28 . C30 . 13.5(9) yes

S27 17_565 C28 . C30 . 102.5(6) yes

S27 . C28 . C30 . 147.3(8) yes

C26 . C29 . C26 22_556 138.9(8) yes

C26 . C29 . H293 22_556 40.0 no

C26 22_556 C29 . H293 22_556 101.8 no

C26 . C29 . C29 22_556 83.1(11) yes

C26 22_556 C29 . C29 22_556 58.0(9) yes

H293 22_556 C29 . C29 22_556 57.6 no

C26 . C29 . H291 . 99.5 no

C26 22_556 C29 . H291 . 91.4 no

H293 22_556 C29 . H291 . 123.1 no

C29 22_556 C29 . H291 . 86.6 no

C26 . C29 . H292 . 118.9 no

C26 22_556 C29 . H292 . 93.7 no

H293 22_556 C29 . H292 . 124.3 no

C29 22_556 C29 . H292 . 148.5 no

H291 . C29 . H292 . 109.5 no

C26 . C29 . H293 . 109.4 no

C26 22_556 C29 . H293 . 30.8 no

H293 22_556 C29 . H293 . 71.0 no

C29 22_556 C29 . H293 . 39.1 no

H291 . C29 . H293 . 109.5 no

H292 . C29 . H293 . 109.5 no

C28 8_555 C30 . C28 . 114.0(9) yes

C28 8_555 C30 . H302 8_555 109.8 no

C28 . C30 . H302 8_555 133.6 no

C28 8_555 C30 . H301 8_555 98.9 no

C28 . C30 . H301 8_555 78.6 no

H302 8_555 C30 . H301 8_555 109.5 no

C28 8_555 C30 . H303 8_555 119.0 no

C28 . C30 . H303 8_555 33.2 no

H302 8_555 C30 . H303 8_555 109.5 no

H301 8_555 C30 . H303 8_555 109.5 no

C28 8_555 C30 . H303 24_565 152.3 no

C28 . C30 . H303 24_565 83.8 no

H302 8_555 C30 . H303 24_565 63.0 no

H301 8_555 C30 . H303 24_565 62.5 no

H303 8_555 C30 . H303 24_565 87.7 no

C28 8_555 C30 . H303 17_565 83.8 no

C28 . C30 . H303 17_565 152.3 no

H302 8_555 C30 . H303 17_565 45.5 no

H301 8_555 C30 . H303 17_565 77.7 no

H303 8_555 C30 . H303 17_565 153.2 no

C28 8_555 C30 . C28 17_565 140.5(12) yes

C28 . C30 . C28 17_565 63.7(8) yes

H302 8_555 C30 . C28 17_565 91.5 no

H301 8_555 C30 . C28 17_565 41.8 no

H303 8_555 C30 . C28 17_565 81.5 no

C28 8_555 C30 . C28 24_565 63.7(8) yes

C28 . C30 . C28 24_565 140.5(12) yes

H302 8_555 C30 . C28 24_565 73.9 no

H301 8_555 C30 . C28 24_565 63.8 no

H303 8_555 C30 . C28 24_565 173.3 no

C28 8_555 C30 . H302 24_565 93.6 no

C28 . C30 . H302 24_565 119.2 no

H302 8_555 C30 . H302 24_565 42.1 no

H301 8_555 C30 . H302 24_565 151.5 no

H303 8_555 C30 . H302 24_565 86.0 no

C28 8_555 C30 . H302 17_565 119.2 no

C28 . C30 . H302 17_565 93.6 no

H302 8_555 C30 . H302 17_565 50.5 no

H301 8_555 C30 . H302 17_565 140.6 no

H303 8_555 C30 . H302 17_565 62.0 no

C28 8_555 C30 . H301 17_565 53.4 no

C28 . C30 . H301 17_565 80.3 no

```
H302 8_555 C30 . H301 17_565 141.2    no
H301 8_555 C30 . H301 17_565 51.4    no
H303 8_555 C30 . H301 17_565 108.9    no
C28 8_555 C30 . H301 . 78.6    no
C28 . C30 . H301 . 98.9    no
H302 8_555 C30 . H301 . 104.2    no
H301 8_555 C30 . H301 . 24.2    no
H303 8_555 C30 . H301 . 131.7    no
C28 8_555 C30 . H302 . 133.6    no
C28 . C30 . H302 . 109.8    no
H302 8_555 C30 . H302 . 24.1    no
H301 8_555 C30 . H302 . 104.2    no
H303 8_555 C30 . H302 . 90.2    no
C28 8_555 C30 . H303 . 33.2    no
C28 . C30 . H303 . 119.0    no
H302 8_555 C30 . H303 . 90.2    no
H301 8_555 C30 . H303 . 131.7    no
H303 8_555 C30 . H303 . 104.0    no
H303 24_565 C30 . H303 17_565 72.6    no
H303 24_565 C30 . C28 17_565 28.8    no
H303 17_565 C30 . C28 17_565 88.9    no
H303 24_565 C30 . C28 24_565 88.9    no
H303 17_565 C30 . C28 24_565 28.8    no
C28 17_565 C30 . C28 24_565 92.7(13)    yes
H303 24_565 C30 . H302 24_565 95.6    no
H303 17_565 C30 . H302 24_565 78.3    no
```

```
C28 17_565 C30 . H302 24_565 122.8    no
C28 24_565 C30 . H302 24_565 100.1    no
H303 24_565 C30 . H302 17_565 78.3    no
H303 17_565 C30 . H302 17_565 95.6    no
C28 17_565 C30 . H302 17_565 100.1    no
C28 24_565 C30 . H302 17_565 122.8    no
H302 24_565 C30 . H302 17_565 29.4    no
H303 24_565 C30 . H301 17_565 113.8    no
H303 17_565 C30 . H301 17_565 95.8    no
C28 17_565 C30 . H301 17_565 89.1    no
C28 24_565 C30 . H301 17_565 67.3    no
H302 24_565 C30 . H301 17_565 147.0    no
H303 24_565 C30 . H301 . 77.7    no
H303 17_565 C30 . H301 . 62.5    no
C28 17_565 C30 . H301 . 63.8    no
C28 24_565 C30 . H301 . 41.8    no
H302 24_565 C30 . H301 . 140.6    no
H303 24_565 C30 . H302 . 45.5    no
H303 17_565 C30 . H302 . 63.0    no
C28 17_565 C30 . H302 . 73.9    no
C28 24_565 C30 . H302 . 91.5    no
H302 24_565 C30 . H302 . 50.5    no
H303 24_565 C30 . H303 . 153.2    no
H303 17_565 C30 . H303 . 87.7    no
C28 17_565 C30 . H303 . 173.3    no
C28 24_565 C30 . H303 . 81.5    no
```

```
H302 24_565 C30 . H303 . 62.0    no
H302 17_565 C30 . H301 17_565 165.5    no
H302 17_565 C30 . H301 . 151.5    no
H301 17_565 C30 . H301 . 43.0    no
H302 17_565 C30 . H302 . 42.1    no
H301 17_565 C30 . H302 . 152.5    no
H301 . C30 . H302 . 109.5    no
H302 17_565 C30 . H303 . 86.0    no
H301 17_565 C30 . H303 . 85.5    no
H301 . C30 . H303 . 109.5    no
H302 . C30 . H303 . 109.5    no
C23 . C241 . C251 . 125.7(5)    yes
C23 . C241 . C261 . 126.2(5)    yes
C251 . C241 . C261 . 108.2(4)    yes
C23 . C241 . H231 . 8.8    no
C251 . C241 . H231 . 134.5    no
C261 . C241 . H231 . 117.4    no
C241 . C251 . H3011 13_655 114.6    no
C241 . C251 . C281 . 108.0(4)    yes
H3011 13_655 C251 . C281 . 85.7    no
C241 . C251 . H2511 . 134.3    no
H3011 13_655 C251 . H2511 . 66.5    no
C281 . C251 . H2511 . 117.4    no
C241 . C261 . S271 . 103.6(4)    yes
C241 . C261 . C291 . 109.1(7)    yes
S271 . C261 . C291 . 147.3(7)    yes
```

```
C261 . S271 . C261 13_655 116.1(10)    yes
C261 . S271 . C281 . 116.5(4)    yes
C261 13_655 S271 . C281 . 116.5(4)    yes
C251 . C281 . C251 13_655 134.2(10)    yes
C251 . C281 . C301 13_655 51.7(8)    yes
C251 13_655 C281 . C301 13_655 109.1(7)    yes
C251 . C281 . S271 . 103.7(4)    yes
C251 13_655 C281 . S271 . 103.7(4)    yes
C301 13_655 C281 . S271 . 147.2(7)    yes
C251 . C281 . C301 . 109.1(7)    yes
C251 13_655 C281 . C301 . 51.7(8)    yes
C301 13_655 C281 . C301 . 61.8(14)    yes
S271 . C281 . C301 . 147.2(7)    yes
C261 . C291 . H2911 . 108.1    no
C261 . C291 . H2912 . 114.2    no
H2911 . C291 . H2912 . 109.5    no
C261 . C291 . H2913 . 106.0    no
H2911 . C291 . H2913 . 109.5    no
H2912 . C291 . H2913 . 109.5    no
C301 13_655 C301 . C281 . 59.1(7)    yes
C301 13_655 C301 . H2511 13_655 140.1    no
C281 . C301 . H2511 13_655 107.2    no
C301 13_655 C301 . H3011 . 144.4    no
C281 . C301 . H3011 . 90.9    no
H2511 13_655 C301 . H3011 . 62.7    no
C301 13_655 C301 . H3012 . 71.1    no
```

```
C281 . C301 . H3012 . 113.3    no
H2511 13_655 C301 . H3012 . 138.9    no
H3011 . C301 . H3012 . 109.5    no
C301 13_655 C301 . H3013 . 103.2    no
C281 . C301 . H3013 . 122.2    no
H2511 13_655 C301 . H3013 . 49.2    no
H3011 . C301 . H3013 . 109.5    no
H3012 . C301 . H3013 . 109.5    no
C21 22_556 H211 . C21 . 17.0    no
C301 13_655 H2511 . C251 . 78.0    no
C251 13_655 H3011 . C301 . 82.7    no
H301 17_565 H301 . H301 24_565 31.4    no
H301 17_565 H301 . C28 24_565 116.3    no
H301 24_565 H301 . C28 24_565 146.6    no
H301 17_565 H301 . C30 . 54.5    no
H301 24_565 H301 . C30 . 52.8    no
C28 24_565 H301 . C30 . 106.9    no
H301 17_565 H301 . H301 8_555 90.0    no
H301 24_565 H301 . H301 8_555 58.6    no
C28 24_565 H301 . H301 8_555 151.1    no
C30 . H301 . H301 8_555 77.9    no
H301 17_565 H301 . C30 17_565 82.5    no
H301 24_565 H301 . C30 17_565 75.8    no
C28 24_565 H301 . C30 17_565 95.7    no
C30 . H301 . C30 17_565 28.0    no
H301 8_555 H301 . C30 17_565 75.2    no
```

```
H302 17_565 H302 . H302 24_565 31.8    no
H302 17_565 H302 . C30 . 55.0    no
H302 24_565 H302 . C30 . 53.3    no
H302 17_565 H302 . H302 8_555 90.0    no
H302 24_565 H302 . H302 8_555 58.2    no
C30 . H302 . H302 8_555 77.9    no
H302 17_565 H302 . C30 24_565 83.0    no
H302 24_565 H302 . C30 24_565 76.3    no
C30 . H302 . C30 24_565 28.0    no
H302 8_555 H302 . C30 24_565 75.3    no
C30 . H303 . C30 24_565 16.8    no
C30 . H303 . C28 8_555 110.7    no
C30 24_565 H303 . C28 8_555 107.5    no
C26 22_556 H293 . C29 . 122.0    no
C26 22_556 H293 . C29 22_556 114.6    no
C29 . H293 . C29 22_556 83.3    no
C22 . H221 . C24 . 173.6    no
C23 . H231 . C241 . 166.0    no


_iucr_refine_instructions_details
;
#
# Punched on 20/07/17 at 19:36:21
#
#LIST     12
```

```
BLOC SCALE X'S
CONT ZN(1,U'S) UNTIL C(32)
CONT N(41,U'S) UNTIL C(44)
CONT N(11,U'S) UNTIL C(14)
CONT N(21,U'S) UNTIL C(23)
CONT C(24,U[ISO]) UNTIL C(301)
EQUIV PART(1,OCC) PART(2,OCC)
WEIGHT -1 PART(2,OCC)
EQUIV PART(3,OCC) PART(4,OCC)
WEIGHT -1 PART(4,OCC)
EQUIV PART(5,U[ISO]) PART(6,U[ISO])
EQUIV PART(5,OCC) PART(6,OCC) H(221,OCC) H(231,OCC)
WEIGHT -1 H(221,OCC) H(231,OCC)
RIDE C ( 32,X'S) H( 321,X'S)
RIDE C ( 42,X'S) H( 421,X'S)
RIDE C ( 43,X'S) H( 431,X'S)
RIDE C ( 44,X'S) H( 441,X'S)
RIDE C ( 12,X'S) H( 121,X'S)
RIDE C ( 13,X'S) H( 131,X'S)
RIDE C ( 14,X'S) H( 141,X'S)
RIDE C ( 21,X'S) H( 211,X'S)
RIDE C ( 25,X'S) H( 251,X'S)
RIDE C ( 29,X'S) H( 291,X'S) H( 292,X'S) H( 293,X'S)
RIDE C ( 30,X'S) H( 301,X'S) H( 302,X'S) H( 303,X'S)
RIDE C ( 251,X'S) H(2511,X'S)
RIDE C ( 291,X'S) H(2911,X'S) H(2912,X'S) H(2913,X'S)
```

```
RIDE C ( 301,X'S) H( 3011,X'S) H( 3012,X'S) H( 3013,X'S)
RIDE C ( 22,X'S) H( 221,X'S)
RIDE C ( 23,X'S) H( 231,X'S)
END
#
# Punched on 20/07/17 at 19:36:21
#
#LIST     16
NO
PLANAR N(11) C(12) C(11) N(12) O(12) N(11,9,1,0,1) C(12,9,1,0,1)
PLANAR N(11) C(13) C(14) C(13,9,1,0,1) N(11,9,1,0,1)
PLANAR N(41) C(41) N(42) O(42) N(42) N(41,11,1,1,1) C(42,11,1,1,1)
PLANAR N(41) C(43) C(44) C(43,11,1,1,1) N(41,11,1,1,1)
PLANAR C(21) N(21) C(22) C(23) N(21,-11,1,0,0,1) C(24) C(241)
REM NITRO RESTRAINTS
DIST 0,0.01=MEAN C(11) TO N(12),
CONT C(31) TO N(32),
CONT C(41) TO N(42)
DIST 0,0.01=MEAN N(12) TO O(12),
CONT N(32) TO O(32),
CONT N(42) TO O(42)
REM IMIDAZOLE RESTRAINTS
REM N TO C1 CARBON
DIST 0,0.01=MEAN N(11) TO C(11), N(11) TO C(14),
CONT N(21) TO C(21), N(21,-11,1,0,0,1) TO C(21)
CONT N(31) TO C(31),
```

```
CONT N(41) TO C(41), N(41) TO C(44)
REM N TO C2/C3
DIST 0,0.01=MEAN N(11) TO C(12), N(11) TO C(13),
CONT N(21) TO C(22), N(21,-11,1,0,0,1) TO C(23),
CONT N(31) TO C(32),
CONT N(41) TO C(42), N(41) TO C(43)
REM C2 TO C3 MAY NEED TO BE REMOVED
DIST 0,0.01 =MEAN C(12) TO C(12,9,1,0,1), C(13) TO C(13,9,1,0,1),
CONT  C(23) TO C(22),
CONT C(32) TO C(32,-4)
CONT C(43) TO C(43,11,1,1,1), C(42) TO C(42,11,1,1,1)
REM 1,3 RESTRAINTS FOR CARBON'S IN THIOPHENE
DIST 0,0.01 = MEAN C(21) TO C(22), C(21) TO C(23)
REM THIOPHENE RESTRAINTS
REM MAKE THE TWO RINGS PLANAR
PLANAR C(22) C(24) C(25) C(26) S(27) C(28) C(29) C(30)
PLANAR C(23) C(241) C(251) C(261) S(271) C(281) C(291) C(301)
REM MAKE THE THIOPHENE-IMIDAZOLE BONDS IDENTICAL
REM ALSO INCLUDES THE METHYL BONDS SINCE THEY ARE OF SIMLIAR LENGTH
DIST 0,0.01=MEAN C(22) TO C(24), C(23) TO C(241),
CONT C(26) TO C(29), C(28) TO C(30),
CONT C(261) TO C(291), C(281) TO C(301)
REM MAKE ALL THE C-C BONDS IN THE THIOPHENE EQUAL
DIST 0,0.01=MEAN  C(24) TO C(25), C(25) TO C(28), C(26) TO C(24),
CONT C(241) TO C(251), C(251) TO C(281), C(261) TO C(241)
REM MAKE ALL THE C-S BONDS IN THE THIOPHENE EQUAL
```

```
DIST 0,0.01=MEAN C(26) TO S(27), C(28) TO S(27),
CONT C(261) TO S(271), C(281) TO S(271)
REM 1,3 SIMILARITY RESTRAINTS FROM IMIDAZOLE TO THIOPHENE
DIST 0,0.01=MEAN C(22) TO C(25), C(22) TO C(26),
CONT C(23) TO C(251), C(23) TO C(261)
REM 1,3 SIMILARITY RESTRAINTS FOR THE METHYL GROUPS
DIST 0,0.01=MEAN C(30) TO C(25), C(29) TO C(24),
CONT C(301) TO C(251), C(291) TO C(241)
DIST 0,0.01=MEAN C(30) TO S(27), C(29) TO S(27),
CONT C(301) TO S(271), C(291) TO S(271)
REM 1,3 SIMILARITY THAT ARE LIKELY UNNECESSARY
REM DIST 0,0.01=MEAN N(21) TO C(24), C(23) TO C(24),
REM CONT N(21,-11,1,0,0,1) TO C(241), C(22) TO C(241)
REM 1,3 BOND DISTANCE RESTRAINTS IN THIOPHENE
DIST 0,0.01=MEAN C(24) TO C(28), C(26) TO C(28), C(26) TO C(25),
CONT C(241) TO C(281), C(261) TO C(281), C(261) TO C(251)
DIST 0,0.01=MEAN C(24) TO S(27), C(25) TO S(27),
CONT C(241) TO S(271), C(251) TO S(271)
REM KEEP THE THIOPHENE GEOMETRY RELATIVE TO THE IMIDAZOLE CORRECT
DIST 0,0.01 = MEAN C(24) TO C(23), C(241) TO C(22),
CONT C(24) TO N(21), C(241) TO N(21,-11,1,0,0,1)
REM THERMAL SIMILARITY RESTRAINTS FOR ONE ZN-N BOND.
REM U(IJ)'S  0.0, 0.010000 = ZN(1) TO N(31)
REM THERMAL SIMILARITY RESTRAINTS FOR IMIDAZOLE DISORDER
U(IJ)'S  0.0, 0.010000 = N(41) TO C(41)
U(IJ)'S  0.0, 0.010000 = N(42) TO C(41)
```

```
U(IJ)'S  0.0, 0.010000 = N(41) TO C(44)
U(IJ)'S  0.0, 0.010000 = N(41) TO C(43)
U(IJ)'S  0.0, 0.010000 = N(41) TO C(42)
U(IJ)'S  0.0, 0.010000 = N(11) TO C(11)
U(IJ)'S  0.0, 0.010000 = N(11) TO C(14)
U(IJ)'S  0.0, 0.010000 = N(12) TO C(11)
U(IJ)'S  0.0, 0.010000 = N(11) TO C(13)
U(IJ)'S  0.0, 0.010000 = N(11) TO C(12)
U(IJ)'S  0.0, 0.010000 = N(21) TO C(21)
U(IJ)'S  0.0, 0.010000 = N(21) TO C(22)
U(IJ)'S  0.0, 0.010000 = N(21) TO C(23)
REM   SHIFTLIMIT   START (DO NOT REMOVE THIS LINE)
LIMIT      0.01000000 U[ISO]
LIMIT      0.01000000 X
LIMIT      0.01000000 Y
LIMIT      0.01000000 Z
LIMIT      0.01000000 U[11]
LIMIT      0.01000000 U[22]
LIMIT      0.01000000 U[33]
LIMIT      0.01000000 U[12]
LIMIT      0.01000000 U[13]
LIMIT      0.01000000 U[23]
LIMIT      0.01000000 OCC
REM   SHIFTLIMIT   END (DO NOT REMOVE THIS LINE)
END
;
```

```
data_PSZ-1_anisotropic

_exptl_special_details
;
 The crystal was
placed in the cold stream of an Oxford
Cryosystems 800 series open-flow nitrogen cryostat (Cosier &
Glazer, 1986) with a nominal stability of 0.1K.

Cosier, J. & Glazer, A.M., 1986. J. Appl. Cryst. 105-107.
;
# End of 'script/refcif.dat'
#end of refcif
_cell_length_a                    27.2188(5)
_cell_length_b                    27.2188(5)
_cell_length_c                    17.0357(8)
_cell_angle_alpha                 90
_cell_angle_beta                  90
_cell_angle_gamma                 120
_cell_volume                      10930.2(6)
_cell_oxdiff_length_a                  27.2168(6)
_cell_oxdiff_length_b                  27.1942(7)
_cell_oxdiff_length_c                  17.0499(4)
_cell_oxdiff_angle_alpha               90.062(2)
```

```
_cell_oxdiff_angle_beta                89.973(2)
_cell_oxdiff_angle_gamma               119.985(2)
_cell_oxdiff_volume                    10930.2(4)
_cell_oxdiff_measurement_reflns_used   13383

_symmetry_space_group_name_H-M_alt 'P 63/m 2/m 2/c'
_symmetry_space_group_name_H-M 'P 63/m m c'
_symmetry_space_group_name_Hall   ?
loop_
 _symmetry_equiv_pos_as_xyz
 'x,y,z'
 '-x,-y,-z'
 'x-y,x,z+1/2'
 '-x+y,-x,-z+1/2'
 '-y,x-y,z'
 'y,-x+y,-z'
 '-x,-y,z+1/2'
 'x,y,-z+1/2'
 '-x+y,-x,z'
 'x-y,x,-z'
 'y,-x+y,z+1/2'
 '-y,x-y,-z+1/2'
 '-x+y,y,z'
 'x-y,-y,-z'
 'y,x,z+1/2'
 '-y,-x,-z+1/2'
```

```
 'x,x-y,z'
 '-x,-x+y,-z'
 'x-y,-y,z+1/2'
 '-x+y,y,-z+1/2'
 '-y,-x,z'
 'y,x,-z'
 '-x,-x+y,z+1/2'
 'x,x-y,-z+1/2'

loop_
_atom_type_symbol
_atom_type_scat_dispersion_real
_atom_type_scat_dispersion_imag
_atom_type_scat_Cromer_Mann_a1
_atom_type_scat_Cromer_Mann_b1
_atom_type_scat_Cromer_Mann_a2
_atom_type_scat_Cromer_Mann_b2
_atom_type_scat_Cromer_Mann_a3
_atom_type_scat_Cromer_Mann_b3
_atom_type_scat_Cromer_Mann_a4
_atom_type_scat_Cromer_Mann_b4
_atom_type_scat_Cromer_Mann_c
_atom_type_scat_source
 C       0.0181   0.0091   2.3100  20.8439   1.0200  10.2075   1.5886   0.5687
   0.8650  51.6512   0.2156 'International Tables Vol C 4.2.6.8 and 6.1.1.4'
 H       0.0000   0.0000   0.4930  10.5109   0.3229  26.1257   0.1402   3.1424
```

```
   0.0408  57.7998   0.0030 'International Tables Vol C 4.2.6.8 and 6.1.1.4'
 N       0.0311   0.0180  12.2126   0.0057   3.1322   9.8933   2.0125  28.9975
   1.1663   0.5826 -11.5290 'International Tables Vol C 4.2.6.8 and 6.1.1.4'
 O       0.0492   0.0322   3.0485  13.2771   2.2868   5.7011   1.5463   0.3239
   0.8670  32.9089   0.2508 'International Tables Vol C 4.2.6.8 and 6.1.1.4'
 S       0.3331   0.5567   6.9053   1.4679   5.2034  22.2151   1.4379   0.2536
   1.5863  56.1720   0.8669 'International Tables Vol C 4.2.6.8 and 6.1.1.4'
 Zn     -1.5491   0.6778  14.0743   3.2655   7.0318   0.2333   5.1652  10.3163
   2.4100  58.7097   1.3041 'International Tables Vol C 4.2.6.8 and 6.1.1.4'


_cell_formula_units_Z                    16

# Given Formula = C24 H24 N9 O2.00 S2.00 Zn1
# Dc =      1.46 Fooo =   4944.00 Mu =     30.11 M =    600.03
# Found Formula = C9.69 H8.32 N7.43 O2.86 S0.09 Zn1.50
# Dc =      0.91 FOOO =   3005.68 Mu =     18.93 M =    375.69

_chemical_formula_sum             'C9.69 H8.32 N7.43 O2.86 S0.09 Zn1.50'
_chemical_formula_moiety          'C9.69 H8.32 N7.43 O2.86 S0.09 Zn1.50'
_chemical_compound_source               ?
_chemical_formula_weight            375.69


_cell_measurement_temperature   250.00(10)
_cell_measurement_reflns_used   13383
```

```
_cell_measurement_theta_min     3.7120
_cell_measurement_theta_max     74.9520

_exptl_crystal_description        'hexagonal prism'
_exptl_crystal_colour             'yellow'
_exptl_crystal_size_max           0.17
_exptl_crystal_size_mid           0.12
_exptl_crystal_size_min           0.12

_exptl_crystal_density_diffrn     0.913
_exptl_crystal_density_method     'not measured'
# dispersive F(000):
_exptl_crystal_F_000              3005.685
_exptl_absorpt_coefficient_mu     1.893

# Sheldrick geometric approximatio 1.00 1.00
_exptl_absorpt_correction_T_min                  0.44920
_exptl_absorpt_correction_T_max                  1.00000
_exptl_absorpt_correction_type            multi-scan
_exptl_absorpt_process_details
;
CrysAlisPro 1.171.39.27b (Rigaku Oxford Diffraction, 2015)
Empirical absorption correction using spherical harmonics,
 implemented in SCALE3 ABSPACK scaling algorithm.
;
_oxdiff_exptl_absorpt_empirical_full_min          0.748
```

```
_oxdiff_exptl_absorpt_empirical_full_max          1.700
_oxdiff_exptl_absorpt_empirical_details
;
Empirical correction (ABSPACK) includes:
- Absorption correction using spherical harmonics
- Frame scaling
;

_diffrn_ambient_temperature 250.00(10)
_diffrn_ambient_environment N~2~
_diffrn_source 'micro-focus sealed X-ray tube'
_diffrn_source_type 'PhotonJet (Cu) X-ray Source'
_diffrn_radiation_probe x-ray
_diffrn_radiation_type 'Cu K\a'
_diffrn_radiation_wavelength 1.54184
_diffrn_radiation_monochromator mirror
_diffrn_measurement_device 'four-circle diffractometer'
_diffrn_measurement_device_type 'XtaLAB Synergy, Dualflex, HyPix'
_diffrn_detector 'CCD plate'
_diffrn_detector_type HyPix
_diffrn_reflns_number 57181
_diffrn_reflns_av_R_equivalents 0.0459
_diffrn_reflns_av_sigmaI/netI 0.0553
_diffrn_reflns_limit_h_min -19
_diffrn_reflns_limit_h_max 34
_diffrn_reflns_limit_k_min -30
```

```
_diffrn_reflns_limit_k_max 31
_diffrn_reflns_limit_l_min -21
_diffrn_reflns_limit_l_max 21
_diffrn_reflns_theta_min 3.7509
_diffrn_reflns_theta_max 77.7792
_diffrn_measured_fraction_theta_max 0.9906
_diffrn_reflns_theta_full 66.4915
_diffrn_measured_fraction_theta_full 0.9989
_diffrn_orient_matrix_type 'CrysAlisPro convention (1999,Acta A55,543-557)'
_diffrn_orient_matrix_UB_11      -0.0510601000
_diffrn_orient_matrix_UB_12      -0.0487766000
_diffrn_orient_matrix_UB_13       0.0424589000
_diffrn_orient_matrix_UB_21      -0.0122294000
_diffrn_orient_matrix_UB_22      -0.0381285000
_diffrn_orient_matrix_UB_23      -0.0726612000
_diffrn_orient_matrix_UB_31       0.0389101000
_diffrn_orient_matrix_UB_32      -0.0210910000
_diffrn_orient_matrix_UB_33       0.0328915000
_diffrn_measurement_details
;
List of Runs (angles in degrees, time in seconds):

  # Type    Start    End  Width  t~exp~   \w     \q     \k     \f   Frames
------------------------------------------------------------------------------
  1  \w    -60.00  26.00   0.50   17.50    --  -47.45  37.00   0.00  172
  2  \w    -99.00 -13.00   0.50   63.00    --  -86.25  37.00 -60.00  172
```

```
  3  \w   -120.00 -87.00   0.50   17.50    --  -47.45 -77.00   0.00   66
  4  \w   -120.00 -70.00   0.50   17.50    --  -47.45-125.00 -60.00  100
  5  \w   -120.00 -70.00   0.50   17.50    --  -47.45-125.00 -30.00  100
  6  \w     36.00 110.00   0.50   63.00    --  107.75 -99.00 150.00  148
  7  \w     95.00 178.00   0.50   63.00    --  107.75  19.00  90.00  166
  8  \w     92.00 178.00   0.50   63.00    --  107.75 125.00-120.00  172
  9  \w     36.00 110.00   0.50   63.00    --  107.75 -99.00-180.00  148
 10  \w     35.00 121.00   0.50   63.00    --  107.75-125.00 -30.00  172
;
_diffrn_measurement_method '\w scans'
_diffrn_oxdiff_ac3_digest_frames
;
010a05eeebc61c3b61b2e16166c56a50c701416da94
;
_diffrn_oxdiff_ac3_digest_hkl
;
0133d96d2333189eb5eddd101e5ae39350442e
;
_symmetry_cell_setting hexagonal
_space_group_IT_number 194
_space_group_crystal_system hexagonal
_space_group_name_H-M_alt 'P 63/m m c'
_reflns_odcompleteness_completeness 99.89
_reflns_odcompleteness_theta 66.49
_reflns_odcompleteness_iscentric 1
_chemical_oxdiff_formula ZnN9C24H24O2S2
```

```
# If a reference occurs more than once, delete the author
# and date from subsequent references.
_computing_data_collection        'Rigaku Crystal Clear Expert 2.1 SM'
_computing_cell_refinement        'CrystAlis Pro'
_computing_data_reduction         'CrystAlis Pro'
_computing_structure_solution     'SHELXS 86 (Sheldrick, 1986)'
_computing_structure_refinement   'CRYSTALS (Betteridge et al., 2003)'
_computing_publication_material   'CRYSTALS (Betteridge et al., 2003)'

# Number of reflections without Friedels Law is 0
# Number of reflections with Friedels Law is 4211
# Theoretical number of reflections is about 7720

_reflns_limit_h_min               -17
_reflns_limit_h_max               0
_reflns_limit_k_min               0
_reflns_limit_k_max               34
_reflns_limit_l_min               0
_reflns_limit_l_max               21

_atom_sites_solution_primary      direct #heavy,direct,difmap,geom,iterative
_atom_sites_solution_hydrogens    geom

_refine_diff_density_min          -0.59
```

```
_refine_diff_density_max          1.49


# The current dictionary definitions do not cover the
# situation where the reflections used for refinement were
# selected by a user-defined sigma threshold

# The values actually used during refinement
_oxford_reflns_threshold_expression_ref     I>0.5\s(I)
_refine_ls_number_reflns          3394
_refine_ls_number_restraints      347
_refine_ls_number_parameters      316
_oxford_refine_ls_R_factor_ref    0.1274
_refine_ls_wR_factor_ref          0.1581
_refine_ls_goodness_of_fit_ref    1.0152
_refine_ls_shift/su_max           0.6778872
_refine_ls_shift/su_mean          0.0381631


# The values computed with all filters except I/sigma
_oxford_reflns_number_all         4211
_refine_ls_R_factor_all           0.1379
_refine_ls_wR_factor_all          0.1974

# The values computed with a 2 sigma cutoff - a la SHELX
_reflns_threshold_expression      I>2.0\s(I)
```

```
_reflns_number_gt                 2518
_refine_ls_R_factor_gt            0.1143
_refine_ls_wR_factor_gt           0.1393

# choose from: rm (reference molecule of known chirality),
# ad (anomolous dispersion - Flack), rmad (rm and ad),
# syn (from synthesis), unk (unknown) or . (not applicable).
_chemical_absolute_configuration  '.'



_refine_ls_structure_factor_coef  Fsqd
_refine_ls_matrix_type            full
_refine_ls_hydrogen_treatment     constr         # undef, noref, refall,
   # refxyz, refU, constr or mixed
_refine_ls_extinction_method
    'None'
_oxford_refine_ls_scale 0.387(2)
_refine_ls_weighting_scheme       calc
_refine_ls_weighting_details
;
 Method, part 1, Chebychev polynomial, (Watkin, 1994, Prince, 1982)
 [weight] = 1.0/[A~0~*T~0~(x)+A~1~*T~1~(x) ... +A~n-1~]*T~n-1~(x)]
 where A~i~ are the Chebychev coefficients listed below and x= Fcalc/Fmax
 Method = Robust Weighting (Prince, 1982)
 W = [weight] * [1-(deltaF/6*sigmaF)^2^]^2^
 A~i~ are:
```

```
 12.2 19.7 12.0 5.21 1.41
;
# Insert your own references if required - in alphabetical order
_publ_section_references
;

Betteridge, P.W., Carruthers, J.R., Cooper, R.I.,
Prout, K. & Watkin, D.J. (2003). J. Appl. Cryst. 36, 1487.

Prince, E.
Mathematical Techniques in Crystallography
and Materials Science
Springer-Verlag, New York, 1982.

Sheldrick, G. M. (2008). Acta Cryst A64, 112-122.

Watkin D.J. (1994).
Acta Cryst, A50, 411-437.
;

# Uequiv = arithmetic mean of Ui i.e. Ueqiv = (U1+U2+U3)/3

# Replace last . with number of unfound hydrogen atoms attached to an atom.

# ..._refinement_flags_...
# . no refinement constraints          S special position constraint on site
```

```
# G rigid group refinement of site      R riding atom
# D distance or angle restraint on site T thermal displacement constraints
# U Uiso or Uij restraint (rigid bond)  P partial occupancy constraint


loop_
_atom_site_label
_atom_site_type_symbol
_atom_site_fract_x
_atom_site_fract_y
_atom_site_fract_z
_atom_site_U_iso_or_equiv
_atom_site_occupancy
_atom_site_adp_type
_atom_site_refinement_flags_posn
_atom_site_refinement_flags_adp
_atom_site_refinement_flags_occupancy
_atom_site_disorder_assembly
_atom_site_disorder_group
_atom_site_attached_hydrogens
Zn1 Zn 0.55456(3) 0.66778(2) 0.42901(5) 0.1036 1.0000 Uani . . . . . .
N31 N 0.5755(3) 0.6707(2) 0.3128(5) 0.1569 1.0000 Uani D . . . . .
N32 N 0.4956(3) 0.6680(3) 0.2500 0.1269 1.0000 Uani DS T . . . .
O32 O 0.4756(2) 0.6673(2) 0.3111(3) 0.1492 1.0000 Uani D . . . . .
C31 C 0.5509(3) 0.6708(3) 0.2500 0.1225 1.0000 Uani DS T . . . .
C32 C 0.6258(3) 0.6725(3) 0.2902(3) 0.1786 1.0000 Uani D . . . . .
```

```
N41 N 0.48212(17) 0.60041(16) 0.4622(3) 0.1159 1.0000 Uani D U . . . .
N42 N 0.47405(18) 0.52595(18) 0.3841(5) 0.1091 0.480(7) Uani DS TU P . 1 .
O42 O 0.5227(3) 0.5563(3) 0.3651(5) 0.1250 0.480(7) Uani D . P . 1 .
C41 C 0.4499(2) 0.5501(2) 0.4371(6) 0.0957 0.480(7) Uani DS TU P . 1 .
C42 C 0.4427(2) 0.6077(2) 0.5096(5) 0.1233 0.480(7) Uani D U P . 1 .
C43 C 0.4724(2) 0.5782(2) 0.5403(5) 0.1214 0.520(7) Uani D U P . 2 .
C44 C 0.43968(19) 0.56032(19) 0.4279(9) 0.1111 0.520(7) Uani DS TU P . 2 .
N11 N 0.55094(19) 0.73430(17) 0.4666(3) 0.1316 1.0000 Uani D U . . . .
N12 N 0.6211(5) 0.8106(2) 0.4088(6) 0.1117 0.427(8) Uani DS TU P . 3 .
O12 O 0.6419(3) 0.7826(3) 0.3941(5) 0.1276 0.427(8) Uani D . P . 3 .
C11 C 0.5675(5) 0.7838(3) 0.4496(6) 0.1130 0.427(8) Uani DS TU P . 3 .
C12 C 0.4991(4) 0.7241(3) 0.5043(4) 0.1434 0.427(8) Uani D U P . 3 .
C13 C 0.5728(3) 0.7611(2) 0.5412(5) 0.1425 0.573(8) Uani D U P . 4 .
C14 C 0.5445(4) 0.7722(2) 0.4336(8) 0.1242 0.573(8) Uani DS TU P . 4 .
N21 N 0.61706(16) 0.66045(14) 0.4755(3) 0.1239 1.0000 Uani D U . . . .
C21 C 0.6139(3) 0.6169(3) 0.5097(5) 0.1072 0.5000 Uani D U . . . .
C22 C 0.6755(3) 0.6965(3) 0.4620(5) 0.1375 0.5000 Uani D U . . . .
C23 C 0.7025(2) 0.6692(2) 0.4924(5) 0.1305 0.5000 Uani D U . . . .
C24 C 0.7019(4) 0.7516(3) 0.4193(4) 0.1593 0.042(4) Uani D . P . 5 .
C25 C 0.6776(6) 0.7641(6) 0.3466(6) 0.1604 0.042(4) Uani D . P . 5 .
C26 C 0.7583(4) 0.8036(4) 0.4376(6) 0.1904 0.042(4) Uani D . P . 5 .
S27 S 0.7693(6) 0.8498(4) 0.3773(8) 0.2367 0.042(4) Uani D . P . 5 .
C28 C 0.7186(8) 0.8243(7) 0.3211(6) 0.1695 0.042(4) Uani D . P . 5 .
C29 C 0.7852(7) 0.7945(9) 0.5080(7) 0.2033 0.042(4) Uani D . P . 5 .
C30 C 0.6974(12) 0.8401(11) 0.250000(10) 0.1637 0.042(4) Uani DS T P . 5 .
C241 C 0.7646(2) 0.6904(3) 0.4912(6) 0.1494 0.042(4) Uani D . P . 6 .
```

```
C251 C 0.8035(4) 0.7062(4) 0.5614(8) 0.1566 0.042(4) Uani D . P . 6 .
C261 C 0.8001(4) 0.7012(4) 0.4176(8) 0.1673 0.042(4) Uani D . P . 6 .
S271 S 0.8618(2) 0.7236(4) 0.4418(11) 0.1512 0.042(4) Uani DS T P . 6 .
C281 C 0.8632(2) 0.7263(4) 0.5317(11) 0.1618 0.042(4) Uani DS T P . 6 .
C291 C 0.7644(8) 0.6868(5) 0.3457(8) 0.2109 0.042(4) Uani D . P . 6 .
C301 C 0.9041(7) 0.7423(4) 0.5979(16) 0.1602 0.042(4) Uani D . P . 6 .
H321 H 0.6534 0.6730 0.3249 0.2446 1.0000 Uiso R . . . . .
H421 H 0.4506 0.6412 0.5372 0.1452 0.480(7) Uiso R . P . 1 .
H431 H 0.4970 0.5951 0.5839 0.1420 0.520(7) Uiso R . P . 2 .
H441 H 0.4366 0.5634 0.3728 0.1404 0.520(7) Uiso RS . P . 2 .
H121 H 0.4706 0.6892 0.5260 0.1729 0.427(8) Uiso R . P . 3 .
H131 H 0.5848 0.7465 0.5831 0.1737 0.573(8) Uiso R . P . 4 .
H141 H 0.5323 0.7662 0.3804 0.1491 0.573(8) Uiso RS . P . 4 .
H211 H 0.5784 0.5867 0.5272 0.1367 0.5000 Uiso R . . . . .
H251 H 0.6410 0.7407 0.3249 0.2204 0.042(4) Uiso R . P . 5 .
H2511 H 0.7957 0.7079 0.6154 0.1553 0.042(4) Uiso R . P . 6 .
H2911 H 0.7892 0.6921 0.3034 0.1780 0.042(4) Uiso R . P . 6 .
H2912 H 0.7471 0.7093 0.3374 0.1780 0.042(4) Uiso R . P . 6 .
H2913 H 0.7358 0.6479 0.3487 0.1780 0.042(4) Uiso R . P . 6 .
H3011 H 0.9369 0.7512 0.5679 0.1671 0.042(4) Uiso R . P . 6 .
H3012 H 0.9094 0.7754 0.6240 0.1671 0.042(4) Uiso R . P . 6 .
H3013 H 0.8980 0.7140 0.6356 0.1671 0.042(4) Uiso R . P . 6 .
H301 H 0.7291 0.8762 0.2383 0.2625 0.042(4) Uiso R . P . 5 .
H302 H 0.6655 0.8442 0.2617 0.2625 0.042(4) Uiso R . P . 5 .
H303 H 0.6891 0.8157 0.2061 0.2625 0.042(4) Uiso R . P . 5 .
H291 H 0.8216 0.8277 0.5083 0.2566 0.042(4) Uiso R . P . 5 .
```

```
H292 H 0.7666 0.7916 0.5564 0.2566 0.042(4) Uiso R . P . 5 .
H293 H 0.7893 0.7620 0.5013 0.2566 0.042(4) Uiso R . P . 5 .
H221 H 0.6929 0.7321 0.4358 0.1582 0.458(4) Uiso R . P . . .
H231 H 0.7420 0.6818 0.4904 0.1492 0.458(4) Uiso R . P . . .

loop_
_atom_site_aniso_label
_atom_site_aniso_U_11
_atom_site_aniso_U_22
_atom_site_aniso_U_33
_atom_site_aniso_U_23
_atom_site_aniso_U_13
_atom_site_aniso_U_12
Zn1 0.0785(5) 0.0654(5) 0.1730(10) 0.0037(3) -0.0141(3) 0.0406(3)
N31 0.114(4) 0.119(5) 0.257(8) 0.005(4) 0.000(5) 0.072(3)
N32 0.087(4) 0.101(5) 0.205(9) 0.0000 0.0000 0.056(4)
O32 0.110(3) 0.171(5) 0.186(5) 0.005(3) 0.008(3) 0.085(3)
C31 0.088(5) 0.073(4) 0.212(11) 0.0000 0.0000 0.044(4)
C32 0.108(4) 0.180(8) 0.265(12) -0.003(6) 0.007(5) 0.086(5)
N41 0.085(2) 0.078(2) 0.171(4) 0.000(2) 0.000(2) 0.0305(19)
N42 0.081(4) 0.081(4) 0.164(9) 0.002(3) -0.002(3) 0.040(5)
O42 0.070(4) 0.093(5) 0.198(9) 0.000(5) 0.013(5) 0.030(3)
C41 0.069(4) 0.069(4) 0.162(7) 0.003(3) -0.003(3) 0.044(4)
C42 0.101(6) 0.086(5) 0.178(8) -0.015(5) 0.007(6) 0.044(5)
C43 0.088(5) 0.079(5) 0.171(7) 0.000(5) -0.018(5) 0.022(4)
C44 0.079(4) 0.079(4) 0.161(8) 0.015(4) -0.015(4) 0.029(6)
```

N11 0.158(4) 0.090(3) 0.172(4) 0.001(3) 0.008(3) 0.081(3)

N12 0.112(8) 0.071(4) 0.166(10) 0.002(4) 0.005(7) 0.056(4)

O12 0.100(6) 0.080(5) 0.213(10) 0.022(6) 0.029(7) 0.053(5)

C11 0.125(7) 0.067(5) 0.166(8) 0.004(3) 0.009(7) 0.063(4)

C12 0.164(9) 0.094(6) 0.184(9) 0.003(6) 0.023(7) 0.074(6)

C13 0.173(8) 0.100(6) 0.179(7) -0.003(6) -0.017(7) 0.086(6)

C14 0.154(8) 0.081(5) 0.161(8) -0.001(3) -0.002(7) 0.077(4)

N21 0.078(2) 0.073(2) 0.221(5) 0.025(3) -0.010(3) 0.0374(17)

C21 0.068(5) 0.081(6) 0.180(7) 0.031(6) 0.012(6) 0.043(3)

C22 0.084(5) 0.090(6) 0.232(9) 0.032(7) -0.005(7) 0.038(5)

C23 0.078(5) 0.090(6) 0.213(9) 0.041(6) -0.011(6) 0.034(5)

C24 0.14(4) 0.10(3) 0.26(5) 0.03(3) 0.04(3) 0.07(3)

C25 0.17(5) 0.09(3) 0.25(6) 0.02(4) 0.04(4) 0.09(4)

C26 0.16(4) 0.13(3) 0.30(6) -0.03(3) 0.04(3) 0.08(3)

S27 0.21(5) 0.18(4) 0.29(6) -0.01(3) 0.01(3) 0.07(3)

C28 0.20(5) 0.08(3) 0.27(6) 0.02(2) 0.01(2) 0.10(3)

C29 0.13(5) 0.15(4) 0.30(7) 0.01(4) 0.01(4) 0.05(4)

C30 0.21(6) 0.06(4) 0.27(7) 0.0000 0.0000 0.11(4)

C241 0.094(19) 0.09(3) 0.28(5) 0.07(4) 0.00(3) 0.06(3)

C251 0.09(4) 0.09(4) 0.29(5) 0.05(5) 0.00(3) 0.05(4)

C261 0.10(3) 0.12(4) 0.29(5) 0.12(4) 0.02(3) 0.06(3)

S271 0.080(15) 0.11(2) 0.28(5) 0.14(3) 0.068(15) 0.053(12)

C281 0.11(4) 0.10(4) 0.28(5) 0.06(4) 0.03(2) 0.048(19)

C291 0.13(6) 0.14(6) 0.31(7) 0.08(7) -0.01(5) 0.03(6)

C301 0.12(5) 0.06(4) 0.27(6) 0.05(5) 0.02(3) 0.03(3)

```
loop_
 _geom_bond_atom_site_label_1
 _geom_bond_site_symmetry_1
 _geom_bond_atom_site_label_2
 _geom_bond_site_symmetry_2
 _geom_bond_distance
 _geom_bond_publ_flag
Zn1 . N31 . 2.051(8)    yes
Zn1 . N41 . 1.988(4)    yes
Zn1 . N11 . 1.969(4)    yes
Zn1 . N21 . 1.975(4)    yes
N31 . C31 . 1.263(7)    yes
N31 . C32 . 1.398(7)    yes
N32 . O32 8_555 1.171(5)    yes
N32 . O32 . 1.171(5)    yes
N32 . C31 . 1.469(8)    yes
C32 . C32 8_555 1.369(9)    yes
C32 . H321 . 0.950    no
N41 . C41 . 1.276(6)    yes
N41 . C42 . 1.434(8)    yes
N42 . O42 21_665 1.204(6)    yes
N42 . O42 . 1.204(6)    yes
N42 . C41 . 1.452(9)    yes
C42 . C42 21_665 1.371(9)    yes
C42 . H421 . 0.950    no
C43 . C43 21_665 1.379(9)    yes
```

```
C43 . H431 . 0.950    no
C44 . H441 . 0.950    no
N11 . C11 . 1.222(6)    yes
N11 . C12 . 1.445(9)    yes
N12 . O12 17_565 1.178(7)    yes
N12 . O12 . 1.178(7)    yes
N12 . C11 . 1.441(9)    yes
C12 . C12 17_565 1.387(9)    yes
C12 . H121 . 0.950    no
C13 . C13 17_565 1.380(9)    yes
C13 . H131 . 0.950    no
C14 . H141 . 0.950    no
N21 . C23 22_556 1.414(6)    yes
N21 . C21 22_556 1.291(8)    yes
N21 . C21 . 1.283(8)    yes
N21 . C22 . 1.408(6)    yes
C21 . H211 22_556 1.124    no
C21 . H211 . 0.950    no
C22 . C23 22_556 0.828(11)    yes
C22 . C23 . 1.383(6)    yes
C22 . C24 . 1.487(6)    yes
C22 . H221 . 0.950    no
C23 . C23 22_556 1.592(13)    yes
C23 . C241 . 1.488(6)    yes
C23 . H231 . 0.950    no
C24 . C25 . 1.520(7)    yes
```

```
C24 . C26 . 1.512(8)    yes
C25 . C28 . 1.515(8)    yes
C25 . H251 . 0.950    no
C26 . H293 22_556 1.134    no
C26 . C29 22_556 1.60(2)    yes
C26 . S27 . 1.532(8)    yes
C26 . C29 . 1.491(7)    yes
S27 . C28 . 1.532(8)    yes
C28 . H301 24_565 1.220    no
C28 . C30 17_565 1.767(19)    yes
C28 . H303 8_555 0.852    no
C28 . C30 . 1.493(7)    yes
C29 . H291 22_556 1.051    no
C29 . H293 22_556 0.595    no
C29 . H291 . 0.950    no
C29 . H292 . 0.950    no
C29 . H293 . 0.950    no
C30 . H302 8_555 0.950    no
C30 . H301 8_555 0.950    no
C30 . H303 8_555 0.950    no
C30 . H303 24_565 1.281    no
C30 . H303 17_565 1.281    no
C30 . H302 24_565 0.782    no
C30 . H302 17_565 0.782    no
C30 . H301 17_565 0.778    no
C30 . H301 . 0.950    no
```

```
C30 . H302 . 0.950    no
C30 . H303 . 0.950    no
C241 . C251 . 1.511(7)    yes
C241 . C261 . 1.520(7)    yes
C251 . H3011 13_655 1.114    no
C251 . H3013 13_655 1.299    no
C251 . C281 . 1.516(8)    yes
C251 . H2511 . 0.950    no
C261 . S271 . 1.529(7)    yes
C261 . C291 . 1.490(7)    yes
S271 . C281 . 1.533(8)    yes
C281 . C301 13_655 1.489(7)    yes
C281 . C301 . 1.489(7)    yes
C291 . H2911 . 0.950    no
C291 . H2912 . 0.950    no
C291 . H2913 . 0.950    no
C301 . H2511 13_655 1.104    no
C301 . C301 13_655 1.79(3)    yes
C301 . H3011 . 0.950    no
C301 . H3012 . 0.950    no
C301 . H3013 . 0.950    no
H2511 . H3013 13_655 0.602    no
H301 . H301 17_565 0.633    no
H301 . H301 24_565 0.749    no
H301 . H301 8_555 0.399    no
H302 . H302 17_565 0.621    no
```

```
H302 . H302 24_565 0.737    no
H302 . H302 8_555 0.397    no
H291 . H291 22_556 0.402    no

loop_
 _geom_angle_atom_site_label_1
 _geom_angle_site_symmetry_1
 _geom_angle_atom_site_label_2
 _geom_angle_site_symmetry_2
 _geom_angle_atom_site_label_3
 _geom_angle_site_symmetry_3
 _geom_angle
 _geom_angle_publ_flag
N31 . Zn1 . N41 . 116.0(2)    yes
N31 . Zn1 . N11 . 114.8(2)    yes
N41 . Zn1 . N11 . 105.84(18)    yes
N31 . Zn1 . N21 . 98.8(2)    yes
N41 . Zn1 . N21 . 107.46(15)    yes
N11 . Zn1 . N21 . 113.84(18)    yes
Zn1 . N31 . C31 . 132.8(5)    yes
Zn1 . N31 . C32 . 121.1(5)    yes
C31 . N31 . C32 . 106.1(7)    yes
O32 8_555 N32 . O32 . 125.5(8)    yes
O32 8_555 N32 . C31 . 117.2(4)    yes
O32 . N32 . C31 . 117.2(4)    yes
N32 . C31 . N31 . 122.1(4)    yes
```

```
N32 . C31 . N31 8_555 122.1(4)    yes
N31 . C31 . N31 8_555 115.8(9)    yes
N31 . C32 . C32 8_555 106.0(4)    yes
N31 . C32 . H321 . 125.5    no
C32 8_555 C32 . H321 . 128.5    no
Zn1 . N41 . C41 . 136.6(5)    yes
Zn1 . N41 . C42 . 119.9(3)    yes
C41 . N41 . C42 . 100.2(6)    yes
O42 21_665 N42 . O42 . 126.6(12)    yes
O42 21_665 N42 . C41 . 116.7(6)    yes
O42 . N42 . C41 . 116.7(6)    yes
N42 . C41 . N41 21_665 118.1(5)    yes
N42 . C41 . N41 . 118.1(5)    yes
N41 21_665 C41 . N41 . 123.4(9)    yes
N41 . C42 . C42 21_665 107.8(3)    yes
N41 . C42 . H421 . 125.8    no
C42 21_665 C42 . H421 . 126.4    no
N41 . C43 . C43 21_665 107.7(3)    yes
N41 . C43 . H431 . 126.0    no
C43 21_665 C43 . H431 . 126.4    no
N41 . C44 . N41 21_665 124.9(13)    yes
N41 . C44 . H441 . 117.5    no
N41 21_665 C44 . H441 . 117.5    no
Zn1 . N11 . C11 . 140.8(6)    yes
Zn1 . N11 . C12 . 117.4(3)    yes
C11 . N11 . C12 . 96.1(7)    yes
```

```
O12 17_565 N12 . O12 . 124.4(13)    yes
O12 17_565 N12 . C11 . 117.8(7)    yes
O12 . N12 . C11 . 117.8(7)    yes
N12 . C11 . N11 . 113.3(6)    yes
N12 . C11 . N11 17_565 113.3(6)    yes
N11 . C11 . N11 17_565 133.0(12)    yes
N11 . C12 . C12 17_565 107.2(3)    yes
N11 . C12 . H121 . 126.5    no
C12 17_565 C12 . H121 . 126.3    no
N11 . C13 . C13 17_565 107.4(3)    yes
N11 . C13 . H131 . 126.5    no
C13 17_565 C13 . H131 . 126.1    no
N11 17_565 C14 . N11 . 125.0(13)    yes
N11 17_565 C14 . H141 . 117.5    no
N11 . C14 . H141 . 117.5    no
C23 22_556 N21 . C21 22_556 103.2(5)    yes
C23 22_556 N21 . Zn1 . 129.8(3)    yes
C21 22_556 N21 . Zn1 . 126.7(4)    yes
C23 22_556 N21 . C21 . 98.6(5)    yes
C21 22_556 N21 . C21 . 16.1(8)    yes
Zn1 . N21 . C21 . 127.7(4)    yes
C23 22_556 N21 . C22 . 34.1(5)    yes
C21 22_556 N21 . C22 . 99.5(5)    yes
Zn1 . N21 . C22 . 126.4(4)    yes
C21 . N21 . C22 . 104.5(5)    yes
H211 22_556 C21 . N21 22_556 107.4    no
```

```
H211 22_556 C21 . N21 . 108.4    no
N21 22_556 C21 . N21 . 118.2(5)    yes
H211 22_556 C21 . H211 . 57.2    no
N21 22_556 C21 . H211 . 120.7    no
N21 . C21 . H211 . 120.9    no
N21 . C22 . C23 22_556 73.4(6)    yes
N21 . C22 . C23 . 106.4(5)    yes
C23 22_556 C22 . C23 . 88.4(10)    yes
N21 . C22 . C24 . 126.2(6)    yes
C23 22_556 C22 . C24 . 107.7(9)    yes
C23 . C22 . C24 . 127.3(5)    yes
N21 . C22 . H221 . 127.1    no
C23 22_556 C22 . H221 . 106.7    no
C23 . C22 . H221 . 126.5    no
C24 . C22 . H221 . 1.4    no
C23 22_556 C23 . N21 22_556 95.9(4)    yes
C23 22_556 C23 . C22 . 31.3(5)    yes
N21 22_556 C23 . C22 . 107.6(5)    yes
C23 22_556 C23 . C22 22_556 60.3(8)    yes
N21 22_556 C23 . C22 22_556 72.5(6)    yes
C22 . C23 . C22 22_556 91.6(10)    yes
C23 22_556 C23 . C241 . 129.9(4)    yes
N21 22_556 C23 . C241 . 126.0(6)    yes
C22 . C23 . C241 . 126.4(5)    yes
C22 22_556 C23 . C241 . 103.6(9)    yes
C23 22_556 C23 . H231 . 131.5    no
```

N21 22_556 C23 . H231 . 125.3 no

C22 . C23 . H231 . 127.0 no

C22 22_556 C23 . H231 . 105.2 no

C241 . C23 . H231 . 1.9 no

C22 . C24 . C25 . 125.4(7) yes

C22 . C24 . C26 . 126.6(7) yes

C25 . C24 . C26 . 108.0(4) yes

C24 . C25 . C28 . 108.1(5) yes

C24 . C25 . H251 . 126.6 no

C28 . C25 . H251 . 124.8 no

C24 . C26 . H293 22_556 95.2 no

C24 . C26 . C29 22_556 108.7(7) yes

H293 22_556 C26 . C29 22_556 35.6 no

C24 . C26 . S27 . 108.7(5) yes

H293 22_556 C26 . S27 . 152.1 no

C29 22_556 C26 . S27 . 138.1(8) yes

C24 . C26 . C29 . 111.3(7) yes

H293 22_556 C26 . C29 . 21.1 no

C29 22_556 C26 . C29 . 18.7(8) yes

S27 . C26 . C29 . 140.0(8) yes

C26 . S27 . C28 . 106.6(5) yes

C25 . C28 . H301 24_565 137.8 no

C25 . C28 . C30 17_565 119.8(7) yes

H301 24_565 C28 . C30 17_565 30.7 no

C25 . C28 . H303 8_555 77.0 no

H301 24_565 C28 . H303 8_555 67.3 no

C30 17_565 C28 . H303 8_555 42.8 no

C25 . C28 . S27 . 108.6(5) yes

H301 24_565 C28 . S27 . 111.0 no

C30 17_565 C28 . S27 . 130.3(8) yes

H303 8_555 C28 . S27 . 167.5 no

C25 . C28 . C30 . 111.3(8) yes

H301 24_565 C28 . C30 . 31.3 no

C30 17_565 C28 . C30 . 13.5(9) yes

H303 8_555 C28 . C30 . 36.2 no

S27 . C28 . C30 . 140.1(8) yes

H291 22_556 C29 . C26 . 97.4 no

H291 22_556 C29 . C26 22_556 90.7 no

C26 . C29 . C26 22_556 153.9(12) yes

H291 22_556 C29 . H293 22_556 139.3 no

C26 . C29 . H293 22_556 43.3 no

C26 22_556 C29 . H293 22_556 128.9 no

H291 22_556 C29 . H291 . 22.4 no

C26 . C29 . H291 . 102.1 no

C26 22_556 C29 . H291 . 94.8 no

H293 22_556 C29 . H291 . 134.8 no

H291 22_556 C29 . H292 . 129.8 no

C26 . C29 . H292 . 115.2 no

C26 22_556 C29 . H292 . 76.5 no

H293 22_556 C29 . H292 . 75.9 no

H291 . C29 . H292 . 109.5 no

H291 22_556 C29 . H293 . 91.3 no

```
C26 . C29 . H293 . 110.7    no
C26 22_556 C29 . H293 . 44.0    no
H293 22_556 C29 . H293 . 110.4    no
H291 . C29 . H293 . 109.5    no
H292 . C29 . H293 . 109.5    no
C28 8_555 C30 . C28 . 108.4(11)    yes
C28 8_555 C30 . H302 8_555 111.8    no
C28 . C30 . H302 8_555 135.2    no
C28 8_555 C30 . H301 8_555 100.7    no
C28 . C30 . H301 8_555 81.1    no
H302 8_555 C30 . H301 8_555 109.5    no
C28 8_555 C30 . H303 8_555 115.5    no
C28 . C30 . H303 8_555 32.0    no
H302 8_555 C30 . H303 8_555 109.5    no
H301 8_555 C30 . H303 8_555 109.5    no
C28 8_555 C30 . H303 24_565 155.2    no
C28 . C30 . H303 24_565 87.7    no
H302 8_555 C30 . H303 24_565 62.8    no
H301 8_555 C30 . H303 24_565 62.3    no
H303 8_555 C30 . H303 24_565 88.2    no
C28 8_555 C30 . H303 17_565 87.7    no
C28 . C30 . H303 17_565 155.2    no
H302 8_555 C30 . H303 17_565 45.5    no
H301 8_555 C30 . H303 17_565 77.4    no
H303 8_555 C30 . H303 17_565 153.0    no
C28 8_555 C30 . C28 17_565 141.6(14)    yes
```

```
C28 . C30 . C28 17_565 70.9(8)    yes
H302 8_555 C30 . C28 17_565 88.9    no
H301 8_555 C30 . C28 17_565 40.9    no
H303 8_555 C30 . C28 17_565 84.7    no
C28 8_555 C30 . C28 24_565 70.9(8)    yes
C28 . C30 . C28 24_565 141.6(14)    yes
H302 8_555 C30 . C28 24_565 72.2    no
H301 8_555 C30 . C28 24_565 62.1    no
H303 8_555 C30 . C28 24_565 171.0    no
C28 8_555 C30 . H302 24_565 94.0    no
C28 . C30 . H302 24_565 118.7    no
H302 8_555 C30 . H302 24_565 40.6    no
H301 8_555 C30 . H302 24_565 150.1    no
H303 8_555 C30 . H302 24_565 86.8    no
C28 8_555 C30 . H302 17_565 118.7    no
C28 . C30 . H302 17_565 94.0    no
H302 8_555 C30 . H302 17_565 49.2    no
H301 8_555 C30 . H302 17_565 139.5    no
H303 8_555 C30 . H302 17_565 62.9    no
C28 8_555 C30 . H301 17_565 54.6    no
C28 . C30 . H301 17_565 80.6    no
H302 8_555 C30 . H301 17_565 140.1    no
H301 8_555 C30 . H301 17_565 50.2    no
H303 8_555 C30 . H301 17_565 109.9    no
C28 8_555 C30 . H301 . 81.1    no
C28 . C30 . H301 . 100.7    no
```

```
H302 8_555 C30 . H301 . 104.2    no
H301 8_555 C30 . H301 . 24.3    no
H303 8_555 C30 . H301 . 131.7    no
C28 8_555 C30 . H302 . 135.2    no
C28 . C30 . H302 . 111.8    no
H302 8_555 C30 . H302 . 24.1    no
H301 8_555 C30 . H302 . 104.2    no
H303 8_555 C30 . H302 . 90.2    no
C28 8_555 C30 . H303 . 32.0    no
C28 . C30 . H303 . 115.5    no
H302 8_555 C30 . H303 . 90.2    no
H301 8_555 C30 . H303 . 131.7    no
H303 8_555 C30 . H303 . 104.0    no
H303 24_565 C30 . H303 17_565 71.5    no
H303 24_565 C30 . C28 17_565 26.9    no
H303 17_565 C30 . C28 17_565 84.8    no
H303 24_565 C30 . C28 24_565 84.8    no
H303 17_565 C30 . C28 24_565 26.9    no
C28 17_565 C30 . C28 24_565 86.5(14)    yes
H303 24_565 C30 . H302 24_565 94.5    no
H303 17_565 C30 . H302 24_565 77.4    no
C28 17_565 C30 . H302 24_565 120.7    no
C28 24_565 C30 . H302 24_565 99.4    no
H303 24_565 C30 . H302 17_565 77.4    no
H303 17_565 C30 . H302 17_565 94.5    no
C28 17_565 C30 . H302 17_565 99.4    no
```

```
C28 24_565 C30 . H302 17_565 120.7    no
H302 24_565 C30 . H302 17_565 29.4    no
H303 24_565 C30 . H301 17_565 112.4    no
H303 17_565 C30 . H301 17_565 94.7    no
C28 17_565 C30 . H301 17_565 88.6    no
C28 24_565 C30 . H301 17_565 67.9    no
H302 24_565 C30 . H301 17_565 148.1    no
H303 24_565 C30 . H301 . 77.4    no
H303 17_565 C30 . H301 . 62.3    no
C28 17_565 C30 . H301 . 62.1    no
C28 24_565 C30 . H301 . 40.9    no
H302 24_565 C30 . H301 . 139.5    no
H303 24_565 C30 . H302 . 45.5    no
H303 17_565 C30 . H302 . 62.8    no
C28 17_565 C30 . H302 . 72.2    no
C28 24_565 C30 . H302 . 88.9    no
H302 24_565 C30 . H302 . 49.2    no
H303 24_565 C30 . H303 . 153.0    no
H303 17_565 C30 . H303 . 88.2    no
C28 17_565 C30 . H303 . 171.0    no
C28 24_565 C30 . H303 . 84.7    no
H302 24_565 C30 . H303 . 62.9    no
H302 17_565 C30 . H301 17_565 168.4    no
H302 17_565 C30 . H301 . 150.1    no
H301 17_565 C30 . H301 . 41.5    no
H302 17_565 C30 . H302 . 40.6    no
```

```
H301 17_565 C30 . H302 . 151.0    no
H301 . C30 . H302 . 109.5    no
H302 17_565 C30 . H303 . 86.8    no
H301 17_565 C30 . H303 . 86.3    no
H301 . C30 . H303 . 109.5    no
H302 . C30 . H303 . 109.5    no
C23 . C241 . C251 . 126.8(6)    yes
C23 . C241 . C261 . 125.1(6)    yes
C251 . C241 . C261 . 108.1(4)    yes
H3011 13_655 C251 . C241 . 98.7    no
H3011 13_655 C251 . H3013 13_655 79.6    no
C241 . C251 . H3013 13_655 155.0    no
H3011 13_655 C251 . C281 . 89.5    no
C241 . C251 . C281 . 108.1(5)    yes
H3013 13_655 C251 . C281 . 96.9    no
H3011 13_655 C251 . H2511 . 78.0    no
C241 . C251 . H2511 . 129.5    no
H3013 13_655 C251 . H2511 . 25.6    no
C281 . C251 . H2511 . 122.1    no
C241 . C261 . S271 . 108.7(4)    yes
C241 . C261 . C291 . 111.0(7)    yes
S271 . C261 . C291 . 140.3(8)    yes
C261 13_655 S271 . C261 . 128.0(11)    yes
C261 13_655 S271 . C281 . 106.5(4)    yes
C261 . S271 . C281 . 106.5(4)    yes
C251 . C281 . C251 13_655 125.6(11)    yes
```

```
C251 . C281 . C301 13_655 44.8(8)    yes
C251 13_655 C281 . C301 13_655 111.2(8)    yes
C251 . C281 . S271 . 108.7(4)    yes
C251 13_655 C281 . S271 . 108.7(4)    yes
C301 13_655 C281 . S271 . 140.1(8)    yes
C251 . C281 . C301 . 111.2(8)    yes
C251 13_655 C281 . C301 . 44.8(8)    yes
C301 13_655 C281 . C301 . 74.1(15)    yes
S271 . C281 . C301 . 140.1(8)    yes
C261 . C291 . H2911 . 105.2    no
C261 . C291 . H2912 . 114.9    no
H2911 . C291 . H2912 . 109.5    no
C261 . C291 . H2913 . 108.2    no
H2911 . C291 . H2913 . 109.5    no
H2912 . C291 . H2913 . 109.5    no
H2511 13_655 C301 . C281 . 113.2    no
H2511 13_655 C301 . C301 13_655 128.6    no
C281 . C301 . C301 13_655 52.9(8)    yes
H2511 13_655 C301 . H3011 . 78.5    no
C281 . C301 . H3011 . 97.9    no
C301 13_655 C301 . H3011 . 144.4    no
H2511 13_655 C301 . H3012 . 132.8    no
C281 . C301 . H3012 . 111.6    no
C301 13_655 C301 . H3012 . 71.1    no
H3011 . C301 . H3012 . 109.5    no
H2511 13_655 C301 . H3013 . 33.0    no
```

```
C281 . C301 . H3013 . 118.2    no
C301 13_655 C301 . H3013 . 103.2    no
H3011 . C301 . H3013 . 109.5    no
H3012 . C301 . H3013 . 109.5    no
C21 22_556 H211 . C21 . 17.5    no
C301 13_655 H2511 . H3013 13_655 59.3    no
C301 13_655 H2511 . C251 . 67.3    no
H3013 13_655 H2511 . C251 . 111.6    no
C251 13_655 H3011 . C301 . 66.9    no
H2511 13_655 H3013 . C301 . 87.7    no
H2511 13_655 H3013 . C251 13_655 42.9    no
C301 . H3013 . C251 13_655 58.9    no
H301 17_565 H301 . H301 24_565 32.2    no
H301 17_565 H301 . C28 24_565 121.4    no
H301 24_565 H301 . C28 24_565 152.0    no
H301 17_565 H301 . C30 . 54.5    no
H301 24_565 H301 . C30 . 52.9    no
C28 24_565 H301 . C30 . 108.4    no
H301 17_565 H301 . H301 8_555 90.0    no
H301 24_565 H301 . H301 8_555 57.8    no
C28 24_565 H301 . H301 8_555 146.0    no
C30 . H301 . H301 8_555 77.9    no
H301 17_565 H301 . C30 17_565 84.0    no
H301 24_565 H301 . C30 17_565 76.9    no
C28 24_565 H301 . C30 17_565 94.1    no
C30 . H301 . C30 17_565 29.4    no
```

```
H301 8_555 H301 . C30 17_565 75.1    no
H302 17_565 H302 . H302 24_565 32.6    no
H302 17_565 H302 . C30 . 55.0    no
H302 24_565 H302 . C30 . 53.4    no
H302 17_565 H302 . H302 8_555 90.0    no
H302 24_565 H302 . H302 8_555 57.4    no
C30 . H302 . H302 8_555 77.9    no
H302 17_565 H302 . C30 24_565 84.4    no
H302 24_565 H302 . C30 24_565 77.4    no
C30 . H302 . C30 24_565 29.5    no
H302 8_555 H302 . C30 24_565 75.3    no
C30 . H303 . C30 24_565 17.4    no
C30 . H303 . C28 8_555 111.8    no
C30 24_565 H303 . C28 8_555 110.3    no
C29 22_556 H291 . C29 . 29.3    no
C29 22_556 H291 . H291 22_556 64.5    no
C29 . H291 . H291 22_556 93.1    no
C26 22_556 H293 . C29 . 100.3    no
C26 22_556 H293 . C29 22_556 115.6    no
C29 . H293 . C29 22_556 28.9    no

loop_
 _geom_hbond_atom_site_label_D
 _geom_hbond_site_symmetry_D
 _geom_hbond_atom_site_label_H
 _geom_hbond_site_symmetry_H
```

```
 _geom_hbond_atom_site_label_A
 _geom_hbond_site_symmetry_A
 _geom_hbond_angle_DHA
 _geom_hbond_distance_DH
 _geom_hbond_distance_HA
 _geom_hbond_distance_DA
 _geom_hbond_publ_flag
C32 . H321 . C22 . 134 0.95 2.42 3.153(15)    yes
C42 . H421 . C12 . 130 0.95 2.04 2.745(15)    yes
C12 . H121 . C42 . 137 0.95 1.97 2.745(15)    yes
C21 . H211 . O42 22_556 130 0.95 2.39 3.093(15)    yes
C21 22_556 H211 . O42 22_556 136 1.12 2.39 3.294(15)    yes
C25 . H251 . N31 . 151 0.95 1.86 2.730(15)    yes
C25 . H251 . C31 . 170 0.95 2.57 3.505(15)    yes
C25 . H251 . C32 8_555 121 0.95 2.59 3.181(15)    yes
C25 22_556 H2511 . C26 22_556 137 1.06 1.56 2.453(15)    yes
C251 . H2511 . C25 22_556 132 0.95 1.06 1.838(15)    yes
C251 . H2511 . C28 22_556 135 0.95 1.28 2.062(15)    yes
C25 22_556 H2511 . C281 . 147 1.06 2.18 3.123(15)    yes
C301 13_655 H2511 . C24 22_556 120 1.10 1.27 2.064(15)    yes
C25 22_556 H2511 . C301 13_655 157 1.06 1.10 2.123(15)    yes
C291 . H2912 . C24 . 137 0.95 2.49 3.251(15)    yes
C251 13_655 H3011 . C29 10_656 121 1.11 1.82 2.573(15)    yes
C251 13_655 H3011 . C29 13_655 129 1.11 2.00 2.838(15)    yes
C301 . H3011 . C29 10_656 158 0.95 1.82 2.725(15)    yes
C301 . H3011 . C29 13_655 162 0.95 2.00 2.914(15)    yes
```

C28 10_656 H3013 . C24 10_656 133 0.76 1.87 2.456(15) yes

C28 10_656 H3013 . C26 10_656 132 0.76 1.88 2.456(15) yes

C301 . H3013 . C25 10_656 142 0.95 1.29 2.123(15) yes

C28 10_656 H3013 . C251 13_655 178 0.76 1.30 2.062(15) yes

C28 10_656 H3013 . C281 . 133 0.76 2.11 2.688(15) yes

C28 10_656 H3013 . C301 . 120 0.76 0.95 1.490(15) yes

C301 . H3013 . C30 3_655 130 0.95 2.17 2.876(15) yes

C301 . H3013 . C30 15_555 122 0.95 2.40 3.019(15) yes

C30 . H302 . O12 17_565 123 0.95 2.44 3.061(15) yes

C30 . H303 . O12 8_555 147 0.95 2.05 2.897(15) yes

C30 . H303 . C25 8_555 162 0.95 1.56 2.483(15) yes

C30 . H303 . C251 15_554 149 0.95 2.56 3.406(15) yes

C30 . H303 . C301 11_564 124 0.95 2.23 2.876(15) yes

C29 . H292 . C261 22_556 132 0.95 1.96 2.684(15) yes

C29 . H292 . C291 22_556 160 0.95 2.54 3.443(15) yes

C26 22_556 H293 . C26 . 143 1.13 2.03 3.015(15) yes

C29 . H293 . C241 . 154 0.95 1.72 2.614(15) yes

C29 . H293 . C251 . 142 0.95 2.03 2.838(15) yes

C29 . H293 . C261 . 149 0.95 2.31 3.164(15) yes

C22 . H221 . O12 . 124 0.95 2.50 3.132(15) yes

C22 . H221 . C25 . 137 0.95 1.90 2.672(15) yes

C22 . H221 . C26 . 142 0.95 1.87 2.679(15) yes

C22 . H221 . C251 22_556 145 0.95 1.79 2.628(15) yes

C22 . H221 . C301 6_566 165 0.95 2.57 3.493(15) yes

C23 . H231 . C251 . 138 0.95 1.90 2.681(15) yes

C23 . H231 . C261 . 140 0.95 1.87 2.669(15) yes

```
_iucr_refine_instructions_details
;
#
# Punched on 20/07/17 at 19:38:36
#
#LIST     12
BLOC SCALE X'S
CONT ZN(1,U'S) UNTIL C(32)
CONT N(41,U'S) UNTIL C(44)
CONT N(11,U'S) UNTIL C(14)
CONT N(21,U'S) UNTIL C(23)
CONT C(24,U'S) UNTIL C(301)
EQUIV PART(1,OCC) PART(2,OCC)
WEIGHT -1 PART(2,OCC)
EQUIV PART(3,OCC) PART(4,OCC)
WEIGHT -1 PART(4,OCC)
EQUIV PART(5,OCC) PART(6,OCC) H(221,OCC) H(231,OCC)
WEIGHT -1 H(221,OCC) H(231,OCC)
RIDE C ( 32,X'S) H( 321,X'S)
RIDE C ( 42,X'S) H( 421,X'S)
RIDE C ( 43,X'S) H( 431,X'S)
RIDE C ( 44,X'S) H( 441,X'S)
RIDE C ( 12,X'S) H( 121,X'S)
RIDE C ( 13,X'S) H( 131,X'S)
```

```
RIDE C ( 14,X'S) H( 141,X'S)
RIDE C ( 21,X'S) H( 211,X'S)
RIDE C ( 25,X'S) H( 251,X'S)
RIDE C ( 29,X'S) H( 291,X'S) H( 292,X'S) H( 293,X'S)
RIDE C ( 30,X'S) H( 301,X'S) H( 302,X'S) H( 303,X'S)
RIDE C ( 251,X'S) H(2511,X'S)
RIDE C ( 291,X'S) H(2911,X'S) H(2912,X'S) H(2913,X'S)
RIDE C ( 301,X'S) H( 3011,X'S) H( 3012,X'S) H( 3013,X'S)
RIDE C ( 22,X'S) H( 221,X'S)
RIDE C ( 23,X'S) H( 231,X'S)
END
#
# Punched on 20/07/17 at 19:38:36
#
#LIST     16
NO
PLANAR N(11) C(12) C(11) N(12) O(12) N(11,9,1,0,1) C(12,9,1,0,1)
PLANAR N(11) C(13) C(14) C(13,9,1,0,1) N(11,9,1,0,1)
PLANAR N(41) C(41) N(42) O(42) N(42) N(41,11,1,1,1) C(42,11,1,1,1)
PLANAR N(41) C(43) C(44) C(43,11,1,1,1) N(41,11,1,1,1)
PLANAR C(21) N(21) C(22) C(23) N(21,-11,1,0,0,1) C(24) C(241)
REM NITRO RESTRAINTS
DIST 0,0.01=MEAN C(11) TO N(12),
CONT C(31) TO N(32),
CONT C(41) TO N(42)
DIST 0,0.01=MEAN N(12) TO O(12),
```

```
CONT N(32) TO O(32),
CONT N(42) TO O(42)
REM IMIDAZOLE RESTRAINTS
REM N TO C1 CARBON
DIST 0,0.01=MEAN N(11) TO C(11), N(11) TO C(14),
CONT N(21) TO C(21), N(21,-11,1,0,0,1) TO C(21)
CONT N(31) TO C(31),
CONT N(41) TO C(41), N(41) TO C(44)
REM N TO C2/C3
DIST 0,0.01=MEAN N(11) TO C(12), N(11) TO C(13),
CONT N(21) TO C(22), N(21,-11,1,0,0,1) TO C(23),
CONT N(31) TO C(32),
CONT N(41) TO C(42), N(41) TO C(43)
REM C2 TO C3 MAY NEED TO BE REMOVED
DIST 0,0.01 =MEAN C(12) TO C(12,9,1,0,1), C(13) TO C(13,9,1,0,1),
CONT  C(23) TO C(22),
CONT C(32) TO C(32,-4)
CONT C(43) TO C(43,11,1,1,1), C(42) TO C(42,11,1,1,1)
REM 1,3 RESTRAINTS FOR CARBON'S IN THIOPHENE
DIST 0,0.01 = MEAN C(21) TO C(22), C(21) TO C(23)
REM THIOPHENE RESTRAINTS
REM MAKE THE TWO RINGS PLANAR
PLANAR C(22) C(24) C(25) C(26) S(27) C(28) C(29) C(30)
PLANAR C(23) C(241) C(251) C(261) S(271) C(281) C(291) C(301)
REM MAKE THE THIOPHENE-IMIDAZOLE BONDS IDENTICAL
REM ALSO INCLUDES THE METHYL BONDS SINCE THEY ARE OF SIMLIAR LENGTH
```

```
DIST 0,0.01=MEAN C(22) TO C(24), C(23) TO C(241),
CONT C(26) TO C(29), C(28) TO C(30),
CONT C(261) TO C(291), C(281) TO C(301)
REM MAKE ALL THE C-C BONDS IN THE THIOPHENE EQUAL
DIST 0,0.01=MEAN  C(24) TO C(25), C(25) TO C(28), C(26) TO C(24),
CONT C(241) TO C(251), C(251) TO C(281), C(261) TO C(241)
REM MAKE ALL THE C-S BONDS IN THE THIOPHENE EQUAL
DIST 0,0.01=MEAN C(26) TO S(27), C(28) TO S(27),
CONT C(261) TO S(271), C(281) TO S(271)
REM 1,3 SIMILARITY RESTRAINTS FROM IMIDAZOLE TO THIOPHENE
DIST 0,0.01=MEAN C(22) TO C(25), C(22) TO C(26),
CONT C(23) TO C(251), C(23) TO C(261)
REM 1,3 SIMILARITY RESTRAINTS FOR THE METHYL GROUPS
DIST 0,0.01=MEAN C(30) TO C(25), C(29) TO C(24),
CONT C(301) TO C(251), C(291) TO C(241)
DIST 0,0.01=MEAN C(30) TO S(27), C(29) TO S(27),
CONT C(301) TO S(271), C(291) TO S(271)
REM 1,3 SIMILARITY THAT ARE LIKELY UNNECESSARY
REM DIST 0,0.01=MEAN N(21) TO C(24), C(23) TO C(24),
REM CONT N(21,-11,1,0,0,1) TO C(241), C(22) TO C(241)
REM 1,3 BOND DISTANCE RESTRAINTS IN THIOPHENE
DIST 0,0.01=MEAN C(24) TO C(28), C(26) TO C(28), C(26) TO C(25),
CONT C(241) TO C(281), C(261) TO C(281), C(261) TO C(251)
DIST 0,0.01=MEAN C(24) TO S(27), C(25) TO S(27),
CONT C(241) TO S(271), C(251) TO S(271)
REM KEEP THE THIOPHENE GEOMETRY RELATIVE TO THE IMIDAZOLE CORRECT
```

```
DIST 0,0.01 = MEAN C(24) TO C(23), C(241) TO C(22),
CONT C(24) TO N(21), C(241) TO N(21,-11,1,0,0,1)
REM THERMAL SIMILARITY RESTRAINTS FOR ONE ZN-N BOND.
REM U(IJ)'S  0.0, 0.010000 = ZN(1) TO N(31)
REM THERMAL SIMILARITY RESTRAINTS FOR IMIDAZOLE DISORDER
U(IJ)'S  0.0, 0.010000 = N(41) TO C(41)
U(IJ)'S  0.0, 0.010000 = N(42) TO C(41)
U(IJ)'S  0.0, 0.010000 = N(41) TO C(44)
U(IJ)'S  0.0, 0.010000 = N(41) TO C(43)
U(IJ)'S  0.0, 0.010000 = N(41) TO C(42)
U(IJ)'S  0.0, 0.010000 = N(11) TO C(11)
U(IJ)'S  0.0, 0.010000 = N(11) TO C(14)
U(IJ)'S  0.0, 0.010000 = N(12) TO C(11)
U(IJ)'S  0.0, 0.010000 = N(11) TO C(13)
U(IJ)'S  0.0, 0.010000 = N(11) TO C(12)
U(IJ)'S  0.0, 0.010000 = N(21) TO C(21)
U(IJ)'S  0.0, 0.010000 = N(21) TO C(22)
U(IJ)'S  0.0, 0.010000 = N(21) TO C(23)
REM SIMU AND DELU RESTRAINTS FOR THE THIOPHENE
SIMU 0.06 C(22) C(24)  C(26)  C(29)  S(27)  C(25)  C(28)  C(30)
SIMU 0.06 C(23) C(241) C(261) C(291) S(271) C(251) C(281) C(301)
DELU 0.02 C(23) C(241) C(261) C(291) S(271) C(251) C(281) C(301)
DELU 0.02 C(22) C(24)  C(26)  C(29)  S(27)  C(25)  C(28)  C(30)
END
;
```

Bibliography

(1) Swenson, H.; Stadie, N. P. *Langmuir* **2019**, *35*, 5409–5426.

(2) Rouquerol, F.; Rouquerol, J.; Sing, K. S. W., *Thermodynamics of Adsorption at the Gas/Solid Interface*, 2014, pp 25–56.

(3) Osterrieth, J. W. M. et al. *Advanced Materials*, *n/a*, 2201502.

(4) Enerdata **2020**, https://yearbook.enerdata.net/total–energy/world–consumption–statistics.html (Accessed March 27th, 2022).

(5) Van Vliet, M. T. H.; Wiberg, D.; Leduc, S.; Riahi, K. *Nature Climate Change* **2016**, *6*, 375–380.

(6) Mahajan, K.; Tomar, S. *American Journal of Agricultural Economics* **2021**, *103*, 35–52.

(7) Gill, A.; Bell, C. *QJM: An International Journal of Medicine* **2004**, *97*, 385–395.

(8) Burkhart, C. G.; Burkhart, C. N. *International Journal of Dermatology* **2014**, *53*, 1539–1541.

(9) Omi, T.; Numano, K. *Laser Therapy* **2014**, *23*, 49–60.

(10) Wiheeb, A.; Helwani, Z; Kim, J; Othman, M. *Separation Purification Reviews* **2016**, *45*, 108–121.

(11) Chakraborty, R.; K, V.; Pradhan, M.; Nayak, A. K. *Journal of Materials Chemistry A* **2022**, *10*, 6965–7005.

(12) Shi, D.; Yu, X.; Fan, W.; Wee, V.; Zhao, D. *Coordination Chemistry Reviews* **2021**, *437*, 213794.

(13) Jiang, C.; Wang, X.; Ouyang, Y.; Lu, K.; Jiang, W.; Xu, H.; Wei, X.; Wang, Z.; Dai, F.; Sun, D. *Nanoscale Advances* **2022**.

(14) Zhou, H.; Long, J. R.; Yaghi, O. M. *Chemical Reviews* **2012**, *112*, 673–674.

(15) Furukawa, H.; Cordova, K. E.; O'Keeffe, M.; Yaghi, O. M. *Science* **2013**, *341*, 1230444.

(16) Wang, Q.; Astruc, D. *Chemical Reviews* **2020**, *120*, 1438–1511.

(17) Wu, T.; Prasetya, N.; Li, K. *Journal of Membrane Science* **2020**, *615*, 118493.

(18) Mo, F.; Han, Q.; Chen, M.; Meng, H.; Guo, J.; Fu, Y. *Nanoscale* **2021**, *13*, 16244–16250.

(19) Stavila, V.; Foster, M. E.; Brown, J. W.; Davis, R. W.; Edgington, J.; Benin, A. I.; Zarkesh, R. A.; Parthasarathi, R.; Hoyt, D. W.; Walter, E. D.; Andersen, A.; Washton, N. M.; Lipton, A. S.; Allendorf, M. D. *Chemical Science* **2019**, *10*, 9880–9892.

(20) Zhang, Z.; Tian, L.; Zhang, H.; Xu, H.; Dong, P.; Zhang, Y.; Long, D. *ACS Applied Energy Materials* **2022**, DOI: 10.1021/acsaem.1c03462.

(21) Zheng, H.-Q.; Liu, C.-Y.; Zeng, X.-Y.; Chen, J.; Lü, J.; Lin, R.-G.; Cao, R.; Lin, Z.-J.; Su, J.-W. *Inorganic Chemistry* **2018**, *57*, 9096–9104.

(22) Yu, Y.; Zhang, X.-M.; Ma, J.-P.; Liu, Q.-K.; Wang, P.; Dong, Y.-B. *Chemical Communications* **2014**, *50*, 1444–1446.

(23) Lian, X.; Feng, D.; Chen, Y.-P.; Liu, T.-F.; Wang, X.; Zhou, H.-C. *Chemical Science* **2015**, *6*, 7044–7048.

(24) Ghoufi, A.; Benhamed, K.; Boukli-Hacene, L.; Maurin, G. *ACS Central Science* **2017**, *3*, 394–398.

(25) Cavka, J. H.; Jakobsen, S.; Olsbye, U.; Guillou, N.; Lamberti, C.; Bordiga, S.; Lillerud, K. P. *Journal of the American Chemical Society* **2008**, *130*, 13850–13851.

(26) Li, H.; Eddaoudi, M.; O'Keeffe, M.; Yaghi, O. M. *Nature* **1999**, *402*, 276–279.

(27) O'Keeffe, M.; Yaghi, O. M. *Chemical Reviews* **2012**, *112*, 675–702.

(28) Fu, Y.; Sun, D.; Chen, Y.; Huang, R.; Ding, Z.; Fu, X.; Li, Z. *Angewandte Chemie International Edition* **2012**, *51*, 3364–3367.

(29) Sava Gallis, D. F.; Harvey, J. A.; Pearce, C. J.; Hall, M. G.; DeCoste, J. B.; Kinnan, M. K.; Greathouse, J. A. *Journal of Materials Chemistry A* **2018**, *6*, 3038–3045.

(30) Schmidt, B. V. K. J. *Macromolecular Rapid Communications* **2020**, *41*, 1900333.

(31) Yang, D.; Gates, B. C. *ACS Catalysis* **2019**, *9*, 1779–1798.

(32) Xiao, J.-D.; Jiang, H.-L. *Accounts of Chemical Research* **2019**, *52*, 356–366.

(33) Lu, W.; Wei, Z.; Gu, Z.-Y.; Liu, T.-F.; Park, J.; Park, J.; Tian, J.; Zhang, M.; Zhang, Q.; Gentle III, T.; Bosch, M.; Zhou, H.-C. *Chemical Society Reviews* **2014**, *43*, 5561–5593.

(34) Cai, M.; Qin, L.; You, L.; Yao, Y.; Wu, H.; Zhang, Z.; Zhang, L.; Yin, X.; Ni, J. *RSC Advances* **2020**, *10*, 36862–36872.

(35) Lv, Y.; Yu, H.; Xu, P.; Xu, J.; Li, X. *Sensors and Actuators B: Chemical* **2018**, *256*, 639–647.

(36) Xiao, S.-T.; Ma, C.-T.; Di, J.-Q.; Zhang, Z.-H. *New Journal of Chemistry* **2020**, *44*, 8614–8620.

(37) Song, J.; Zhang, Z.; Hu, S.; Wu, T.; Jiang, T.; Han, B. *Green Chemistry* **2009**, *11*, 1031–1036.

(38) Zhao, Z.; Ma, X.; Kasik, A.; Li, Z.; Lin, Y. S. *Industrial Engineering Chemistry Research* **2013**, *52*, 1102–1108.

(39) Borycz, J.; Tiana, D.; Haldoupis, E.; Sung, J. C.; Farha, O. K.; Siepmann, J. I.; Gagliardi, L. *The Journal of Physical Chemistry C* **2016**, *120*, 12819–12830.

(40) Liu, J.; Lukose, B.; Shekhah, O.; Arslan, H. K.; Weidler, P.; Gliemann, H.; Bräse, S.; Grosjean, S.; Godt, A.; Feng, X.; Müllen, K.; Magdau, I.-B.; Heine, T.; Wöll, C. *Scientific Reports* **2012**, *2*, 921.

(41) Yaghi, O. M.; O'Keeffe, M.; Ockwig, N. W.; Chae, H. K.; Eddaoudi, M.; Kim, J. *Nature* **2003**, *423*, 705–714.

(42) Cordova, K. E.; Yaghi, O. M. *Materials Chemistry Frontiers* **2017**, *1*, 1304–1309.

(43) Gropp, C.; Canossa, S.; Wuttke, S.; Gándara, F.; Li, Q.; Gagliardi, L.; Yaghi, O. M. *ACS Central Science* **2020**, *6*, 1255–1273.

(44) Moosavi, S. M.; Nandy, A.; Jablonka, K. M.; Ongari, D.; Janet, J. P.; Boyd, P. G.; Lee, Y.; Smit, B.; Kulik, H. J. *Nature Communications* **2020**, *11*, 4068.

(45) Wang, L. J.; Deng, H.; Furukawa, H.; Gándara, F.; Cordova, K. E.; Peri, D.; Yaghi, O. M. *Inorganic Chemistry* **2014**, *53*, 5881–5883.

(46) Trickett, C. A.; Helal, A.; Al-Maythalony, B. A.; Yamani, Z. H.; Cordova, K. E.; Yaghi, O. M. *Nature Reviews Materials* **2017**, *2*, 17045.

(47) Jiang, H.; Alezi, D.; Eddaoudi, M. *Nature Reviews Materials* **2021**, *6*, 466–487.

(48) Kang, Z.; Fan, L.; Sun, D. *Journal of Materials Chemistry A* **2017**, *5*, 10073–10091.

(49) Zhang, X.; Zhou, T.; Sundmacher, K. *AIChE Journal* **2022**, *68*, e17524.

(50) Rallapalli, P.; Prasanth, K. P.; Patil, D.; Somani, R. S.; Jasra, R. V.; Bajaj, H. C. *Journal of Porous Materials* **2011**, *18*, 205–210.

(51) Suh, M. P.; Park, H. J.; Prasad, T. K.; Lim, D.-W. *Chemical Reviews* **2012**, *112*, 782–835.

(52) Gándara, F.; Furukawa, H.; Lee, S.; Yaghi, O. M. *Journal of the American Chemical Society* **2014**, *136*, 5271–5274.

(53) Kapelewski, M. T.; Runčevski, T.; Tarver, J. D.; Jiang, H. Z. H.; Hurst, K. E.; Parilla, P. A.; Ayala, A.; Gennett, T.; FitzGerald, S. A.; Brown, C. M.; Long, J. R. *Chemistry of Materials* **2018**, *30*, 8179–8189.

(54) Gándara, F.; Furukawa, H.; Lee, S.; Yaghi, O. M. *Journal of the American Chemical Society* **2014**, *136*, 5271–5274.

(55) Li, Y.; Wen, G. *European Journal of Inorganic Chemistry* **2020**, *2020*, 2303–2311.

(56) Wang, S.; Zhang, Y.; Tang, Y.; Wen, Y.; Lv, Z.; Liu, S.; Li, X.; Zhou, X. *Chemical Engineering Science* **2020**, *219*, 115604.

(57) Martínez-Ahumada, E.; López-Olvera, A.; Jancik, V.; Sánchez-Bautista, J. E.; González-Zamora, E.; Martis, V.; Williams, D. R.; Ibarra, I. A. *Organometallics* **2020**, *39*, 883–915.

(58) McGrath, D. T.; Ryan, M. D.; MacInnis, J. J.; VandenBoer, T. C.; Young, C. J.; Katz, M. J. *Chemical Science* **2019**, *10*, 5576–5581.

(59) Rieth, A. J.; Tulchinsky, Y.; Dincă, M. *Journal of the American Chemical Society* **2016**, *138*, 9401–9404.

(60) Hamon, L.; Serre, C.; Devic, T.; Loiseau, T.; Millange, F.; Férey, G.; Weireld, G. D. *Journal of the American Chemical Society* **2009**, *131*, 8775–8777.

(61) Martínez-Ahumada, E.; Díaz-Ramírez, M. L.; Velásquez-Hernández, M. d. J.; Jancik, V.; Ibarra, I. A. *Chemical Science* **2021**, *12*, 6772–6799.

(62) Li, J.-R.; Kuppler, R. J.; Zhou, H.-C. *Chemical Society Reviews* **2009**, *38*, 1477–1504.

(63) Zou, Y.-H.; Huang, Y.-B.; Si, D.-H.; Yin, Q.; Wu, Q.-J.; Weng, Z.; Cao, R. *Angewandte Chemie International Edition* **2021**, *60*, 20915–20920.

(64) Wang, Z.-J.; Han, L.-J.; Gao, X.-J.; Zheng, H.-G. *Inorganic Chemistry* **2018**, *57*, 5232–5239.

(65) Avci, G.; Velioglu, S.; Keskin, S. *ACS Applied Materials Interfaces* **2018**, *10*, 33693–33706.

(66) Knebel, A. et al. *Nature Materials* **2020**, *19*, 1346–1353.

(67) Rahimi, A.; García, J. M. *Nature Reviews Chemistry* **2017**, *1*, 0046.

(68) Knebel, A.; Zhou, C.; Huang, A.; Zhang, J.; Kustov, L.; Caro, J. *Chemical Engineering Technology* **2018**, *41*, 224–234.

(69) Danaci, D.; Bui, M.; Mac Dowell, N.; Petit, C. *Molecular Systems Design Engineering* **2020**, *5*, 212–231.

(70) Sarkisov, L.; Martin, R. L.; Haranczyk, M.; Smit, B. *Journal of the American Chemical Society* **2014**, *136*, 2228–2231.

(71) Schneemann, A.; Bon, V.; Schwedler, I.; Senkovska, I.; Kaskel, S.; Fischer, R. A. *Chemical Society Reviews* **2014**, *43*, 6062–6096.

(72) Kriesten, M.; Vargas Schmitz, J.; Siegel, J.; Smith, C. E.; Kaspereit, M.; Hartmann, M. *European Journal of Inorganic Chemistry* **2019**, *2019*, 4700–4709.

(73) Lee, J. H.; Jeoung, S.; Chung, Y. G.; Moon, H. R. *Coordination Chemistry Reviews* **2019**, *389*, 161–188.

(74) Liu, Z.; Zhang, L.; Sun, D. *Chemical Communications* **2020**, *56*, 9416–9432.

(75) Zhang, S.; Zhang, S.; Yin, N.; Huang, Z.; Xu, W.; Yue, K.; Li, X.; Li, D. *ACS Applied Materials Interfaces* **2021**, *13*, 6430–6441.

(76) Jiang, Y.; Heinke, L. *Langmuir* **2021**, *37*, 2–15.

(77) Liu, W.; Pan, Y.; Xiao, W.; Xu, H.; Liu, D.; Ren, F.; Peng, X.; Liu, J. *MedChemComm* **2019**, *10*, 2038–2051.

(78) Yao, Z.; Pan, L.; Liu, L.; Zhang, J.; Lin, Q.; Ye, Y.; Zhang, Z.; Xiang, S.; Chen, B. *Science Advances* **2019**, *5*, 1–7.

(79) Liu, F.; Pan, Q. *Journal of Materials Chemistry A* **2018**, *6*, 11288–11295.

(80) Elsaidi, S. K.; Mohamed, M. H.; Banerjee, D.; Thallapally, P. K. *Coordination Chemistry Reviews* **2018**, *358*, 125–152.

(81) Serre, C.; Millange, F.; Thouvenot, C.; Noguès, M.; Marsolier, G.; Louër, D.; Férey, G. *Journal of the American Chemical Society* **2002**, *124*, 13519–13526.

(82) Loiseau, T.; Serre, C.; Huguenard, C.; Fink, G.; Taulelle, F.; Henry, M.; Bataille, T.; Férey, G. *Chemistry – A European Journal* **2004**, *10*, 1373–1382.

(83) Couck, S.; Denayer, J. F. M.; Baron, G. V.; Rémy, T.; Gascon, J.; Kapteijn, F. *Journal of the American Chemical Society* **2009**, *131*, 6326–6327.

(84) Hamon, L.; Llewellyn, P. L.; Devic, T.; Ghoufi, A.; Clet, G.; Guillerm, V.; Pirngruber, G. D.; Maurin, G.; Serre, C.; Driver, G.; van Beek, W.; Jolimaître, E.; Vimont, A.; Daturi, M.; Férey, G. *Journal of the American Chemical Society* **2009**, *131*, 17490–17499.

(85) Boutin, A.; Coudert, F.-X.; Springuel-Huet, M.-A.; Neimark, A. V.; Férey, G.; Fuchs, A. H. *The Journal of Physical Chemistry C* **2010**, *114*, 22237–22244.

(86) Zornoza, B.; Martinez-Joaristi, A.; Serra-Crespo, P.; Tellez, C.; Coronas, J.; Gascon, J.; Kapteijn, F. *Chemical Communications* **2011**, *47*, 9522–9524.

(87) Angeli, G. K.; Loukopoulos, E.; Kouvidis, K.; Bosveli, A.; Tsangarakis, C.; Tylianakis, E.; Froudakis, G.; Trikalitis, P. N. *Journal of the American Chemical Society* **2021**, *143*, 10250–10260.

(88) Qiu, Q.-F.; Chen, C.-X.; Wei, Z.-W.; Cao, C.-C.; Zhu, N.-X.; Wang, H.-P.; Wang, D.; Jiang, J.-J.; Su, C.-Y. *Inorganic Chemistry* **2019**, *58*, 61–64.

(89) Krause, S.; Bon, V.; Stoeck, U.; Senkovska, I.; Többens, D. M.; Wallacher, D.; Kaskel, S. *Angewandte Chemie International Edition* **2017**, *56*, 10676–10680.

(90) Shi, Y.-X.; Li, W.-X.; Zhang, W.-H.; Lang, J.-P. *Inorganic Chemistry* **2018**, *57*, 8627–8633.

(91) Danowski, W.; van Leeuwen, T.; Browne, W. R.; Feringa, B. L. *Nanoscale Advances* **2021**, *3*, 24–40.

(92) Galangau, O.; Norel, L.; Rigaut, S. *Dalton Transactions* **2021**, *50*, 17879–17891.

(93) Huang, X.; Li, T. *Journal of Materials Chemistry C* **2020**, *8*, 821–848.

(94) Goulet-Hanssens, A.; Eisenreich, F.; Hecht, S. *Advanced Materials* **2020**, *32*, 1905966.

(95) Bigdeli, F.; Lollar, C. T.; Morsali, A.; Zhou, H. C. *Angewandte Chemie International Edition* **2020**, *59*, 4652–4669.

(96) Tan, P.; Jiang, Y.; Liu, X. Q.; Sun, L. B. *ACS Energy Letters* **2019**, *4*, 2656–2667.

(97) Balmond, E. I.; Tautges, B. K.; Faulkner, A. L.; Or, V. W.; Hodur, B. M.; Shaw, J. T.; Louie, A. Y. *The Journal of Organic Chemistry* **2016**, *81*, 8744–8758.

(98) Minkin, V. I. *Chemical Reviews* **2004**, *104*, 2751–2776.

(99) Schwartz, H. A.; Olthof, S.; Schaniel, D.; Meerholz, K.; Ruschewitz, U. *Inorganic Chemistry* **2017**, *56*, 13100–13110.

(100) Healey, K.; Liang, W.; Southon, P. D.; Church, T. L.; D'Alessandro, D. M. *Journal of Materials Chemistry A* **2016**, *4*, 10816–10819.

(101) Garg, S.; Schwartz, H.; Kozlowska, M.; Kanj, A. B.; Müller, K.; Wenzel, W.; Ruschewitz, U.; Heinke, L. *Angewandte Chemie International Edition* **2019**, *58*, 1193–1197.

(102) Ou, R.; Zhang, H.; Truong, V. X.; Zhang, L.; Hegab, H. M.; Han, L.; Hou, J.; Zhang, X.; Deletic, A.; Jiang, L.; Simon, G. P.; Wang, H. *Nature Sustainability* **2020**, 1052–1058.

(103) Schultz, T.; Quenneville, J.; Levine, B.; Toniolo, A.; Martínez, T. J.; Lochbrunner, S.; Schmitt, M.; Shaffer, J. P.; Zgierski, M. Z.; Stolow, A. *Journal of the American Chemical Society* **2003**, *125*, 8098–8099.

(104) Koshima, H.; Ojima, N.; Uchimoto, H. *Journal of the American Chemical Society* **2009**, *131*, 6890–6891.

(105) Bandara, H. M. D.; Burdette, S. C. *Chemical Society Reviews* **2012**, *41*, 1809–1825.

(106) Park, J.; Yuan, D.; Pham, K. T.; Li, J.-R.; Yakovenko, A.; Zhou, H.-C. *Journal of the American Chemical Society* **2012**, *134*, 99–102.

(107) Brown, J. W.; Henderson, B. L.; Kiesz, M. D.; Whalley, A. C.; Morris, W.; Grunder, S.; Deng, H.; Furukawa, H.; Zink, J. I.; Stoddart, J. F.; Yaghi, O. M. *Chemical Science* **2013**, *4*, 2858–2864.

(108) Mutruc, D.; Goulet-Hanssens, A.; Fairman, S.; Wahl, S.; Zimathies, A.; Knie, C.; Hecht, S. *Angewandte Chemie International Edition* **2019**, *58*, 12862–12867.

(109) Yanai, N.; Uemura, T.; Inoue, M.; Matsuda, R.; Fukushima, T.; Tsujimoto, M.; Isoda, S.; Kitagawa, S. *Journal of the American Chemical Society* **2012**, *134*, 4501–4504.

(110) Zeleňák, V.; Vargová, Z.; Almáši, M.; Zeleňáková, A.; Kuchár, J. *Microporous and Mesoporous Materials* **2010**, *129*, 354–359.

(111) Epley, C. C.; Love, M. D.; Morris, A. J. *Inorganic Chemistry* **2017**, *56*, 13777–13784.

(112) Modrow, A.; Zargarani, D.; Herges, R.; Stock, N. *Dalton Transactions* **2011**, *40*, 4217–4222.

(113) Woodward, R. B.; Hoffmann, R. *Angewandte Chemie International Edition* **1969**, *8*, 781–853.

(114) Anslyn, E.; Dougherty, D.; Dougherty, E., *Modern Physical Organic Chemistry*, 2006, pp 875–934.

(115) Roberts, M. N.; Carling, C.-J.; Nagle, J. K.; Branda, N. R.; Wolf, M. O. *Journal of the American Chemical Society* **2009**, *131*, 16644–16645.

(116) Irie, M., *Molecular Design of Photochromic Diarylethenes for Photonics*, 1994, pp 319–322.

(117) Tani, K.; Ishibashi, Y.; Miyasaka, H.; Kobatake, S.; Irie, M. *The Journal of Physical Chemistry C* **2008**, *112*, 11150–11157.

(118) Irie, M.; Fukaminato, T.; Matsuda, K.; Kobatake, S. *Chemical Reviews* **2014**, *114*, 12174–12277.

(119) Herder, M.; Schmidt, B. M.; Grubert, L.; Pätzel, M.; Schwarz, J.; Hecht, S. *Journal of the American Chemical Society* **2015**, *137*, 2738–2747.

(120) Irie, M. *Molecular Crystals and Liquid Crystals Science and Technology. Section A. Molecular Crystals and Liquid Crystals* **1993**, *227*, 263–270.

(121) Zhang, J.; Tian, H. *Advanced Optical Materials* **2018**, *6*, 1701278.

(122) Ai, Q.; Ahn, K.-H. *RSC Advances* **2016**, *6*, 43000–43006.

(123) Moriyama, Y.; Matsuda, K.; Tanifuji, N.; Irie, S.; Irie, M. *Organic Letters* **2005**, *7*, 3315–3318.

(124) Logtenberg, H.; Browne, W. R. *Organic Biomolecular Chemistry* **2013**, *11*, 233–243.

(125) Pu, S.-Z.; Sun, Q.; Fan, C.-B.; Wang, R.-J.; Liu, G. *Journal of Materials Chemistry C* **2016**, *4*, 3075–3093.

(126) Majee, D.; Presolski, S. *ACS Catalysis* **2021**, *11*, 2244–2252.

(127) Wilson, D.; Branda, N. R. *Angewandte Chemie International Edition* **2012**, *51*, 5431–5434.

(128) Samachetty, H. D.; Lemieux, V.; Branda, N. R. *Tetrahedron* **2008**, *64*, 8292–8300.

(129) Lemieux, V.; Spantulescu, M.; Baldridge, K. K.; Branda, N. R. *Angewandte Chemie International Edition* **2008**, *47*, 5034–5037.

(130) Sud, D.; Wigglesworth, T. J.; Branda, N. R. *Angewandte Chemie International Edition* **2007**, *46*, 8017–8019.

(131) Samachetty, H. D.; Branda, N. R. *Chemical Communications* **2005**, 2840–2842.

(132) Shibata, K.; Muto, K.; Kobatake, S.; Irie, M. *The Journal of Physical Chemistry A* **2002**, *106*, 209–214.

(133) Irie, M. *Photochemical Photobiological Sciences* **2010**, *9*, 1535–1542.

(134) Walton, I. M.; Cox, J. M.; Coppin, J. A.; Linderman, C. M.; Patel, D. G.; Benedict, J. B. *Chemical Communications* **2013**, *49*, 8012–8014.

(135) Park, J.; Feng, D.; Yuan, S.; Zhou, H. C. *Angewandte Chemie International Edition* **2015**, *54*, 430–435.

(136) Fan, C. B.; Le Gong, L.; Huang, L.; Luo, F.; Krishna, R.; Yi, X. F.; Zheng, A. M.; Zhang, L.; Pu, S. Z.; Feng, X. F.; Luo, M. B.; Guo, G. C. *Angewandte Chemie International Edition* **2017**, *56*, 7900–7906.

(137) Luo, F.; Fan, C. B.; Luo, M. B.; Wu, X. L.; Zhu, Y.; Pu, S. Z.; Xu, W. Y.; Guo, G. C. *Angewandte Chemie International Edition* **2014**, *53*, 9298–9301.

(138) Nikolayenko, V. I.; Herbert, S. A.; Barbour, L. J. *Chemical Communications* **2017**, *53*, 11142–11145.

(139) Patel, D. G.; Walton, I. M.; Cox, J. M.; Gleason, C. J.; Butzer, D. R.; Benedict, J. B. *Chemical Communications* **2014**, *50*, 2653–2656.

(140) Walton, I. M.; Cox, J. M.; Mitchell, T. B.; Bizier, N. P.; Benedict, J. B. *CrystEngComm* **2016**, *18*, 7972–7977.

(141) Cox, J. M.; Walton, I. M.; Benedict, J. B. *Journal of Materials Chemistry C* **2016**, *4*, 4028–4033.

(142) Duan, G.; Yam, V. W. W. *Chemistry – A European Journal* **2010**, *16*, 12642–12649.

(143) Yaghi, O.; Kalmutzki, M.; Diercks, C., *Introduction to Reticular Chemistry: Zeolitic Imidazolate Frameworks*, 2019, pp 463–479.

(144) Banerjee, R.; Phan, A.; Wang, B.; Knobler, C.; Furukawa, H.; O'Keeffe, M.; Yaghi, O. M. *Science* **2008**, *319*, 939–943.

(145) Yaghi, O.; Kalmutzki, M.; Diercks, C., *Introduction to Reticular Chemistry: Functionalization of MOFs*, 2019, pp 145–176.

(146) Lalonde, M. B.; Mondloch, J. E.; Deria, P.; Sarjeant, A. A.; Al-Juaid, S. S.; Osman, O. I.; Farha, O. K.; Hupp, J. T. *Inorganic Chemistry* **2015**, *54*, 7142–7144.

(147) Burnett, B. J.; Barron, P. M.; Hu, C.; Choe, W. *Journal of the American Chemical Society* **2011**, *133*, 9984–9987.

(148) Karagiaridi, O.; Bury, W.; Mondloch, J. E.; Hupp, J. T.; Farha, O. K. *Angewandte Chemie International Edition* **2014**, *53*, 4530–4540.

(149) Yang, J.; Zhang, Y.-B.; Liu, Q.; Trickett, C. A.; Gutiérrez-Puebla, E.; Monge, M.; Cong, H.; Aldossary, A.; Deng, H.; Yaghi, O. M. *Journal of the American Chemical Society* **2017**, *139*, 6448–6455.

(150) Jayachandrababu, K. C.; Sholl, D. S.; Nair, S. *Journal of the American Chemical Society* **2017**, *139*, 5906–5915.

(151) Neilson, B. M.; Lynch, V. M.; Bielawski, C. W. *Angewandte Chemie International Edition* **2011**, *50*, 10322–10326.

(152) Banerjee, R.; Furukawa, H.; Britt, D.; Knobler, C.; O'Keeffe, M.; Yaghi, O. M. *Journal of the American Chemical Society* **2009**, *131*, 3875–3877.

(153) Karagiaridi, O.; Bury, W.; Sarjeant, A. A.; Stern, C. L.; Farha, O. K.; Hupp, J. T. *Chemical Science* **2012**, *3*, 3256–3260.

(154) Xu, M.-M.; Chen, Q.; Xie, L.-H.; Li, J.-R. *Coordination Chemistry Reviews* **2020**, *421*, 213421.

(155) Irie, M.; Lifka, T.; Uchida, K.; Kobatake, S.; Shindo, Y. *Chemical Communications* **1999**, 747–750.

(156) Moon, S.-Y.; Liu, Y.; Hupp, J. T.; Farha, O. K. *Angewandte Chemie International Edition* **2015**, *54*, 6795–6799.

(157) Huang, H.; Sato, H.; Aida, T. *Journal of the American Chemical Society* **2017**, *139*, 8784–8787.

(158) Furlong, B. J.; Katz, M. J. *Journal of the American Chemical Society* **2017**, *139*, 13280–13283.

(159) Ortica, F. *Dyes and Pigments* **2012**, *92*, 807–816.

(160) Shoji, H.; Kitagawa, D.; Kobatake, S. *Research on Chemical Intermediates* **2013**, *39*, 279–289.

(161) Kitagawa, D.; Kobatake, S. *Chem Rec* **2016**, *16*, 2005–15.

(162) Xiong, K.-T.; Li, M.-L.; Jiang, Y.; Xu, H.-B.; Zeng, M.-H. *New Journal of Chemistry* **2020**, *44*, 8061–8067.

(163) Zhang, J.-Q.; Wang, Q.-C.; Zou, L.; Jia, C.-Y. *Chinese Chemical Letters* **2014**, *25*, 762–766.

(164) Peng, X.; Deng, J.-G.; Xu, H.-B. *RSC Advances* **2013**, *3*, 24146–24153.

(165) Huang, S.; Li, Z.; Li, S.; Yin, J.; Liu, S. *Dyes and Pigments* **2012**, *92*, 961–966.

(166) Tshepelevitsh, S.; Kütt, A.; Lõkov, M.; Kaljurand, I.; Saame, J.; Heering, A.; Plieger, P. G.; Vianello, R.; Leito, I. *European Journal of Organic Chemistry* **2019**, *40*, 6735–6748.

(167) Omar M. Yaghi Markus J. Kalmutzki, C. S. D., *Building Units of MOFs*, 2019, pp 57–81.

(168) Dhakshinamoorthy, A.; Santiago-Portillo, A.; Asiri, A. M.; Garcia, H. *ChemCatChem* **2019**, *11*, 899–923.

(169) Chen, Z.; Hanna, S. L.; Redfern, L. R.; Alezi, D.; Islamoglu, T.; Farha, O. K. *Coordination Chemistry Reviews* **2019**, *386*, 32–49.

(170) Deng, H.; Grunder, S.; Cordova, K. E.; Valente, C.; Furukawa, H.; Hmadeh, M.; Gándara, F.; Whalley, A. C.; Liu, Z.; Asahina, S.; Kazumori, H.; O'Keeffe, M.; Terasaki, O.; Stoddart, J. F.; Yaghi, O. M. *Science* **2012**, *336*, 1018–1023.

(171) Banerjee, R.; Phan, A.; Wang, B.; Knobler, C.; Furukawa, H.; O'Keeffe, M.; Yaghi, O. M. *Science* **2008**, *319*, 939–943.

(172) Redfern, L. R.; Farha, O. K. *Chemical Science* **2019**, *10*, 10666–10679.

(173) Vahabi, A. H.; Norouzi, F.; Sheibani, E.; Rahimi-Nasrabadi, M. *Coordination Chemistry Reviews* **2021**, *445*, 214050.

(174) Zhong, G.; Liu, D.; Zhang, J. *ChemistrySelect* **2018**, *3*, 7066–7080.

(175) Marshall, R. J.; Forgan, R. S. *European Journal of Inorganic Chemistry* **2016**, *2016*, 4310–4331.

(176) Kutzscher, C.; Nickerl, G.; Senkovska, I.; Bon, V.; Kaskel, S. *Chemistry of Materials* **2016**, *28*, 2573–2580.

(177) McGuirk, C. M.; Katz, M. J.; Stern, C. L.; Sarjeant, A. A.; Hupp, J. T.; Farha, O. K.; Mirkin, C. A. *Journal of the American Chemical Society* **2015**, *137*, 919–925.

(178) Garg, S.; Schwartz, H.; Kozlowska, M.; Kanj, A. B.; Müller, K.; Wenzel, W.; Ruschewitz, U.; Heinke, L. *Angewandte Chemie International Edition* **2019**, *58*, 1193–1197.

(179) Mutruc, D.; Goulet-Hanssens, A.; Fairman, S.; Wahl, S.; Zimathies, A.; Knie, C.; Hecht, S. *Angewandte Chemie International Edition* **2019**, *58*, 12862–12867.

(180) Granchi, C.; Caligiuri, I.; Bertelli, E.; Poli, G.; Rizzolio, F.; Macchia, M.; Martinelli, A.; Minutolo, F.; Tuccinardi, T. *Journal of Enzyme Inhibition and Medicinal Chemistry* **2017**, *32*, 1240–1252.

(181) Lawrence, M. C.; Katz, M. J. *The Journal of Physical Chemistry C* **2022**, *126*, 1107–1114.

(182) Marshall, R. J.; Kalinovskyy, Y.; Griffin, S. L.; Wilson, C.; Blight, B. A.; Forgan, R. S. *Journal of the American Chemical Society* **2017**, *139*, 6253–6260.

(183) Katz, M. J.; Brown, Z. J.; Colón, Y. J.; Siu, P. W.; Scheidt, K. A.; Snurr, R. Q.; Hupp, J. T.; Farha, O. K. *Chemical Communications* **2013**, *49*, 9449–9451.

(184) Vahabi, A. H.; Norouzi, F.; Sheibani, E.; Rahimi-Nasrabadi, M. *Coordination Chemistry Reviews* **2021**, *445*, 214050.

(185) Xi, F.-G.; Liu, H.; Yang, N.-N.; Gao, E.-Q. *Inorganic Chemistry* **2016**, *55*, 4701–4703.

(186) Baggi, G.; Casimiro, L.; Baroncini, M.; Silvi, S.; Credi, A.; Loeb, S. J. *Chemical Science* **2019**, *10*, 5104–5113.

(187) Dolgopolova, E. A.; Galitskiy, V. A.; Martin, C. R.; Gregory, H. N.; Yarbrough, B. J.; Rice, A. M.; Berseneva, A. A.; Ejegbavwo, O. A.; Stephenson, K. S.; Kittikhunnatham, P.; Karakalos, S. G.; Smith, M. D.; Greytak, A. B.; Garashchuk, S.; Shustova, N. B. *Journal of the American Chemical Society* **2019**, *141*, 5350–5358.